UNIVERSITY OF TASMANIA

THEORETICAL DESIGN AND DEVELOPMENT OF CATALYST SYSTEMS

by

Katrina Ellen Frankcombe, B. Sc. (Hons.)

Being a thesis submitted in fulfilment of the requirements

for the degree of

Doctor of Philosophy

at the University of Tasmania

The Department of Chemistry

University of Tasmania

June, 1997

DECLARATION

This thesis contains no material which has been accepted for a degree or diploma by the University or any other institution, except in the way of background information, and duly acknowledged in the thesis. To the best of my knowledge, this thesis contains no copy or paraphrase of any material previously published or written, except when due reference is made.

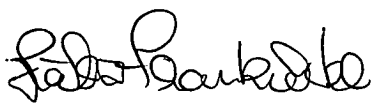

K. E. Frankcombe

June, 1997

Katrina E Frankcombe
June 1997

ABSTRACT

Wave function based *ab initio* and nonlocal density functional methods have been employed to impart a unique insight into the competing mechanisms operating in the carbonylation of alkyl-palladium(II) complexes of bidentate ligands. The theoretical methods employed were established by two benchmark studies. Geometries of physically meaningful accuracy were obtained using second-order Møller-Plesset (MP2) methods or nonlocal density functional theory (DFT) with a small-core pseudopotential on palladium and double-ζ basis sets with polarisation functions on the ligands. Reliable reaction energies required a higher level of correlation (such as CCSD(T)) together with large basis sets incorporating diffuse functions and polarisation functions.

For every system investigated, the lowest energy pathway proceeded *via* novel five-coordinate intermediates and transition structures. This is in contrast to the generally assumed four-coordinate pathways and has important ramifications in the context of rationalising experimentally observed CO/olefin copolymerisation activities. The competing carbonylation mechanisms for the model neutral and cationic palladium(II) systems $Pd(N\text{-}O)(CH_3)(PH_3) + CO \rightarrow Pd(N\text{-}O)(COCH_3)(PH_3)$ (N-O = $NHCHCOO^-$ (**1**), NHCHCHO (**21**)) have been investigated in detail. Despite marked differences in the lowest energy mechanisms, variation in the overall energetics for the neutral and cationic systems was found to be less than 15 kJ/mol. Furthermore, it has been unequivocally demonstrated that differences in CO/ethylene copolymerisation activity of neutral and cationic palladium(II) complexes of bidentate N-O ligand can be attributed to the activation energy of ethylene insertion (a variation of 55.4 kJ/mol). This is the first theoretical investigation to reproduce the distinct CO/ethylene copolymerisation rates of cationic and neutral complexes, thereby allowing clear elucidation of this important phenomenon.

Ligand influences have been assessed by modelling the carbonylation reaction for a range of complexes: $Pd(X\text{-}Y)(CH_3)(L)$ (X-Y = NHCHCHO, L = PF_3 (**41**),

$P(CH_3)_3$ (**51**); X-Y = NHCHCHNH, L = PH_3 (**61**), CH_3 (**71**)). With the exception of the neutral diimine complex (**71**) variations in the activation energy for the methyl migration step are surprisingly small. Values ranged from 39.5 kJ/mol for **41** to 55.6 kJ/mol for **1**. Conversely, it was shown that differences in carbonylation reactivity typically arise in the ligand substitution and isomerisation steps. The high migration barrier associated with **71** (67.5 kJ/mol) is due to a reduction in σ-donation by the migrating methyl group and an increase in metal-carbonyl π back-donation.

The study provides the most definitive theoretical evidence to date for the participation of five-coordinate species in the migratory insertion reactions of alkyl-palladium(II) complexes. In particular, a novel transition structure has been identified which accounts for the isomerisation of square-pyramidal d^8 complexes. The integral rôle proposed for five-coordinate species in the carbonyl and olefin migratory insertion reactions has led to the formulation of novel rationale to account for several ambiguous experimental trends.

In summary, all of the theoretical results presented exhibit outstanding agreement with all available experimental structural and kinetic data. This study clearly demonstrates that computational chemistry is now mature and can make a significant contribution at the leading edge of catalyst design and development.

Acknowledgements

I would like to thank everyone who offered or gave their help and support throughout my PhD. In particular, I would like to thank:

My supervisor, Dr Brian Yates, who has been unfailing in his assistance, encouragement and enthusiasm. His concern for the success and happiness of his students is exceptional.

My associate supervisor, Professor Kingsley Cavell who provided the original initiative of the work as well as continuing advice.

My associate supervisor at ANSTO, Dr Robert Knott, who always seems to working hard to secure more computing power for me (and doesn't mind relinquishing the odd cherry ripe).

Dr George Heard and Dr George Britovsek for their help and advice (not to mention patience).

Dr Trevor Hambley for performing the X-ray crystal structure presented.

The Australian Institute of Nuclear Science and Engineering (AINSE) for financial support, and their grant of computing time.

The ARC for the grant of supercomputer time at the ANU.

Jason Hoare and Mel Green for critically reading parts of my thesis.

I would finally like to thank my family and friends who have made the last three years of my life the best so far.

List of Publications

Heard, G. L.; Frankcombe, K. E.; Yates, B. F. "A Theoretical Study of the Stevens Rearrangement of Methylammonium Methylide and Methylammonium Formylmethylide" *Aust. J. Chem.* **1993**, *46*, 1375.

Frankcombe, K. E.; Cavell, K. J.; Knott, R. B.; Yates, B. F. "Large Basis Set Calculations of Model Zerovalent Palladium Complexes" *J. Phys. Chem.* **1995**, *99*, 14316.

Frankcombe, K. E.; Cavell, K. J.; Knott, R. B.; Yates, B. F. "Competing Mechanisms in the Carbonylation of Neutral Palladium(II) Complexes Containing Bidentate Ligands: Theoretical Insights"
J. Chem. Soc., Chem. Commun., **1996**, 781

Frankcombe, K. E.; Cavell, K. J.; Knott, R. B.; Yates, B. F. "Ligand Substitution: An Assessment of the Reliability of *ab Initio* Calculations" *J. Phys. Chem.* **1996**, *100*, 18363.

Frankcombe, K. E.; Cavell, K. J.; Knott, R. B.; Yates, B. F. "Competing Reaction Mechanisms for the Carbonylation of Neutral Palladium(II) Complexes Containing Bidentate Ligands: A Theoretical Study" *Organometallics*, **1997**, in press.

Glossary of Abbreviations

Pyridinecarboxylic acid	pyca
Bipyr	bpy
1,10-phenanthroline	phen
Molecular Orbital	MO
Trigonal bipyramidal	TBP
Square pyramidal	SQP
Lowest Unoccupied Molecular Orbital	LUMO
Restricted Hartree-Fock	RHF
Møller Plesset	MP
Potential Energy Surface	PES
Extended Hückel Theory	EHT
Effective Core Potential	ECP
Relativistic Effective Core Potential	RECP
Basis Set Superposition Error	BSSE
Density Functional Theory	DFT
Local Density Approximation	LDA
Natural Bond Orbital	NBO
Natural Population Analysis	NPA

Graphical Key

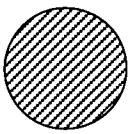

Palladium

Phosphorus

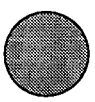

Carbon

Nitrogen

Oxygen

Hydrogen

Table of Contents

Chapter 1	**Introduction**	**1**
1.1	Catalysis and Polyketones	1
1.2	Stepwise Copolymerisation	2
1.3	Mechanistic Studies	3
1.4	Carbonylation	9
1.4.1	*Experimental Studies*	10
1.4.2	*Theoretical Studies*	16
1.5	Olefin Insertion	19
1.6	Five-Coordination in d^8 Species	22
1.7	The Project	25
Chapter 2	**Theoretical Methods**	**27**
2.1	Introduction	27
2.2	General Molecular Orbital Theory	29
2.2.1	*The Electronic Problem and Hartree–Fock (HF) Theory*	30
2.3	Post-Hartree-Fock Methods: the inclusion of dynamic electron correlation	33
2.3.1	*Configuration Interaction (CI)*	33
2.3.2	*Coupled Cluster (CC) Methods*	35
2.3.3	*Møller-Plesset Perturbation Theory*	36
2.4	The Basis Set	37
2.5	Density Functional Theory (DFT)	40
2.5.1	*The General Formalism*	40
2.5.2	*Approximations to E_{XC}*	41
2.6	Relativistic Effects and Effective Core Potentials (ECP's)	48

Chapter 2 (continued):

2.7	Geometry Optimisation	50
2.8	Computational Methods Stategy	52
2.9	Conclusions	54
Chapter 3	**Evaluation of the Available Theoretical Methods**	**56**
3.1	Introduction	56
3.2	Additional Computational Methods	58
3.3	Geometries	63
3.4	Reaction Energies	69
3.5	Conclusions	75
Chapter 4	**Ligand Substitution and the Application of *ab Initio* Methods to Potential Energy Surfaces**	**77**
4.1	Introduction	77
4.2	Additional Computational Methods	80
4.3	Calculations on the Reactant Pd(N-O)(CH_3)(PH_3) (**1a**)	81
4.4	Calculations on the Product Pd(N-O)(CH_3)(CO) (**2a**)	87
4.5	Geometry of the Transition Structure (**TS(1'a-2'a)**)	87
4.6	Pseudo Five-coordinate Intermediates (**1'a** and **2'a**)	92
4.7	Reaction and Activation Energies	94
4.8	Conclusions	99
Chapter 5	**Competing Reaction Mechanisms for the Carbonylation of Neutral Palladium(II) Complexes Containing Bidentate (N-O) Ligands**	**101**
5.1	Introduction	101
5.2	Overview of the Theoretical Methods	103

Chapter 5 (continued):

5.3	Ligand Substitution Reactions and Isomerisation	104
5.3.1	*Replacement of the phosphine ligand by carbon monoxide*	104
5.3.2	*Replacement of the donor nitrogen by the phosphine for* ***2'b***	108
5.3.3	*Ligand substitution and isomerisation of* ***2'a***	111
5.4	Methyl Migration	112
5.5	Conclusions	118
Chapter 6	**Comparison of the Competing Reaction Mechanisms and Energetics for Carbonylation of Neutral and Cationic Palladium(II) Complexes Containing Bidentate (N-O) Ligands**	**119**
6.1	Introduction	119
6.2	Overview of the Theoretical Methods	122
6.3	Coordination of Carbon Monoxide	127
6.4	Rearrangements and Isomerisation	130
6.5	Methyl Migration	131
6.6	Comparison of the Neutral and Cationic Complexes	137
6.7	Conclusions	140
Chapter 7	**Olefin Insertion**	**141**
7.1	Introduction	141
7.2	Overview of the Theoretical Methods	143
7.3	Comparison of Ethylene Insertion in the Neutral and Cationic Systems	145
7.4	Conclusions	154
Chapter 8	**Ligand Effects in the Carbonylation Step**	**155**
8.1	Introduction	155
8.2	Overview of the Theoretical Methods	157

Chapter 8 (continued):

8.3	Carbonylation of $[Pd(N\text{-}O)(CH_3)(PF_3)]^+$ (**41**)	158
8.4	Carbonylation of $[Pd(N\text{-}O)(CH_3)(P(CH_3)_3)]^+$ (**51**)	165
8.5	Carbonylation of the Diimine Complexes $[Pd(N\text{-}N)(CH_3)(PH_3)]^+$ (**61**) and $Pd(N\text{-}N)(CH_3)_2$ (**71**)	169
8.6	Comparison of the Energetics of Carbonylation for Systems **1 - 71**	178
8.7	Conclusions	182
Chapter 9	**Summary and Conclusions**	**184**
References		**187**

Appendical Data is Presented in Volume II. (Supplementary Material)

CHAPTER 1

Introduction

Chapter 1

Introduction

The use of palladium complexes in catalytic chemistry is now well established with processes such as carbonyl insertion at a palladium centre being employed in the production of CO/ethylene copolymers[1] and optically active polyketones,[2-6] and very recently in the highly selective formation of methylmethacrylate.[7] Traditionally, catalyst design has relied upon the skilful use of experimental methods to identify intermediates and mechanistic steps.[1,8-12] However, such methods have often been unsuccessful in elucidating details of the various transformations involved. As a result, the rapid advances in computational techniques have facilitated an increased interest in the theoretical modelling of catalytic processes.[13]

The following sections will provide a foundation for the importance of polyketones, their catalytic synthesis and the unique rôle of Group 10 complexes as catalysts.

1.1 Catalysis and Polyketones

Catalysis may be divided into three categories; heterogeneous, homogeneous and enzymatic. The current study is primarily concerned with the production of polyketones by *homogeneous* catalysis,[14] a process in which the catalyst and reactants occupy the same phase. With a seemingly large range of polymers and methods of polymer preparation currently available, the question arises "why are we seeking new routes to the formation of polyketones?"

Polyketones afford several advantages over the currently available polymers:

• An alternating polyketone is highly crystalline, therefore possessing a high melting point and high mechanical strength.[15]

• The presence of carbonyl groups in the chain provide sites for functionalisation yielding polymers with specific properties.[16,17] They also act as a chromophore assisting photodegradability, and may provide a site for enzymatic attack promoting biodegradability.[15]

• Carbon monoxide is relatively inexpensive, particularly in comparison with ethylene. Hence, the more carbon monoxide which can be incorporated into the polymer, the less expensive the resulting product.

Catalytic syntheses of polyketones are favoured over free radical and gamma ray induced processes as they require milder conditions and possess higher product selectivity and reaction rates. They are also the only method known to produce strictly alternating polyketones. Palladium(II) catalysts are attractive due to their relatively high stability and subsequently lower susceptibility to poisoning by nitrogen, oxygen or halogens in the solvent. Although the manufacture of polyketones *via* a palladium catalysed reaction has now reached the commercial production stage,[7,18] the demand for unique and improved catalytic processes is high. Development of novel catalysts allow "new industrial players" to enter the copolymerisation field.

1.2 Stepwise Copolymerisation

The potential and scope of palladium complexes in catalytic CO/olefin copolymerisation is highlighted in a recent review by Drent.[19] Although the catalytic conversion of CO and ethylene into copolymers was noted prior to the 1980's, reaction rates, yields and selectivities were low. Two important discoveries are responsible for the recent interest in this area. Firstly, polyketones were shown to possess thermoplastic properties. Secondly, the use of palladium

complexes of bidentate ligands with weakly coordinating anions was found to markedly increase the rate and selectivity of the reaction. This permitted more flexible reaction conditions and the use of a larger range of olefins. In addition, retention of the stereochemistry allows the synthesis of optically active polymers.[5]

A general pathway for the CO/olefin copolymerisation to yield polyketones is illustrated in Scheme 1.1. The propagation process consists of alternating insertions of carbon monoxide and ethylene into a metal-carbon bond, terminating with β-hydride elimination. Clearly, this cycle is simplistic and other initiation/termination steps operate in competition to yield a range of products with different end groups. Replacement of monodentate ligands by a bidentate ligand has been demonstrated to shift the propagation/termination equilibrium from the formation of methylpropionate toward production of high molecular weight copolymers.[19]

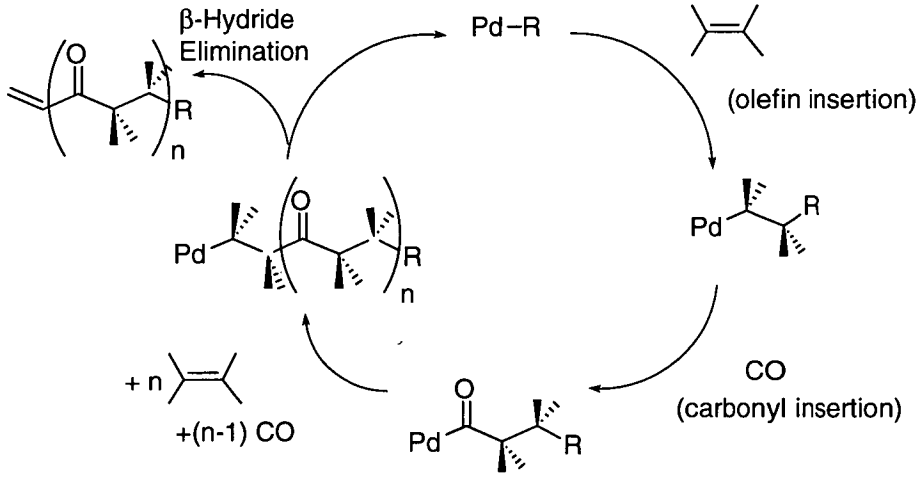

Scheme 1.1: *The general catalytic cycle for CO/olefin copolymerisation.*

1.3 Mechanistic Studies

There has been considerable interest in the mechanism of stepwise copolymerisation. Initially, palladium catalysed stepwise CO/olefin insertions were only observed for sterically bulky ligands (such as tert-butyl styrene[20]) with low

reaction rates. Van Koten *et al.* achieved stepwise insertions of CO and norbornene using $Pd(CH_3)Cl(bpy)$.[12,21] Olefin insertion proceeded following the abstraction of the halide by AgOTf, and subsequent stabilisation of the active cationic species by CH_3CN. Subsequent insertion of CO required low temperatures (-30°C), and the addition of NaCl or NaI. Vrieze and coworkers have reported stepwise insertions of CO and norbornadiene under mild conditions employing a complex of a rigid bidentate N-N ligand.[11] In this case, halide abstraction was unnecessary, possibly indicating the participation of five-coordinate species.

The optimum catalyst to date was developed by Drent,[18,22] and is currently being implemented in the commercial production of CO/ethylene polyketones.[23] The catalytic species is formed *in situ* in a methanolic solution of palladium acetate, a diphosphine ligand such as dppp, and a Brønsted or Lewis acid. Variation of the diphosphine ligand permits manipulation of the reaction rate and the product molecular weight distribution. The reaction is also accelerated by very weakly or non-coordinating Brønsted acids, such as OTf^- and BF_4^-. This is considered to be due to displacement of the acetate ligands by the anion, providing an accessible coordination site to which the olefin or CO can bind prior to insertion. The catalytically active species is therefore believed to be of the type $[Pd(L_2)P']^+$ (P' = growing polymer chain) in which the fourth coordination position is occupied by the Brønsted acid or a solvent molecule, and is often called a "vacant" coordination site.

A number of groups have recently studied the influence of the ligands on the copolymerisation reaction rate in order to gain some insight into the discrete transformations involved; a review of these studies is given by Cavell.[24] A series of papers have appeared in the literature investigating the microscopic insertion steps responsible for copolymerisation using organopalladium complexes of bidentate N-N,[11,12,20,25-29] N-P[30,31] and P-P[32-34] ligands and tridentate N-N-N[28,35-38] ligands. Not only was the rate of CO and olefin insertion shown to

decrease in the order N-N > P-P » N-P, but the rate dependence on steric and electronic properties of the ligands also varied. In the case of dinitrogen ligands, insertion was facilitated by a more rigid chelate with a small bite angle,[11] whereas the reverse was observed for the diphosphine ligand,[34] and no correlation between chelate flexibility and migration rate is exhibited by the trinitrogen ligands.[38] The contrasting rate dependencies suggest that different mechanisms are operating in the different systems. In agreement with the studies by Drent,[18] the insertion rate is generally enhanced in complexes incorporating a weakly coordinating anionic ligand irrespective of the chelate ligand.

The kinetics of insertion reactions of complexes incorporating N-N and N-P ligands indicate that the chelate may be bonded in a monodentate fashion in some cases.[29,31,39,40] Chelate ligands which display such behaviour are called *hemilabile*. That is, at least one "arm" of the chelate ligand has the potential to dissociate to permit the coordination of another ligand. Complexes incorporating hemilabile ligands are attracting considerable interest as catalysts as they may offer increased control over the course of the reaction. As opposed to systems incorporating weakly bound monodentate ligands, restraining the dissociated chelate arm to remain in the vicinity of the metal favours stabilisation of the product against chain-termination processes by recoordination of the ligand.

Cavell *et al.* have investigated the copolymerisation activity of a range of neutral and cationic alkyl- and allyl-palladium complexes of hemilabile P-O,[41] N-O[42] and P-O-N ligands.[43] The cationic complexes were shown to be catalytically active towards CO/ethylene insertions with rates considerably lower than those observed for diphosphine ligands.[43] The reduced activity may be associated with the hemilabile behaviour of the ligands such that they resemble monodentate ligands which are known to yield less active catalysts. While the neutral complexes (**I**) displayed CO insertion rates similar to their cationic counterparts (**II**), they were inactive towards copolymerisation. Similar results have been reported by van Leeuwen *et al.*[29,38] which together imply that the CO

insertion step is not responsible for the dramatic differences in copolymerisation activity of cationic and neutral complexes.

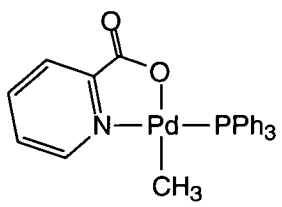

(I)

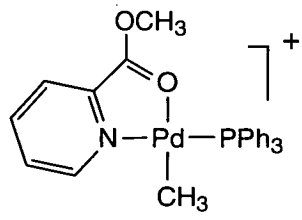

(II)

An elegant mechanistic study by Rix *et al.*[44] has provided rate constants for the microscopic steps in CO/ethylene copolymerisation catalysed by $[(phen)Pd(P')(L)]^+Ar'B^-$ (Ar'=3,5-$(CF_3)_2C_6H_3$; L=CO, C_2H_4 and P' denotes the growing polymer chain). The insertion barriers were shown to increase in the order

$$\Delta G^{\ddagger}_{P'\rightarrow CO} < \Delta G^{\ddagger}_{Ac\rightarrow C2H4} < \Delta G^{\ddagger}_{P'\rightarrow C2H4}$$ (refer to Table 1.1).

In agreement with theoretical studies,[45,46] consecutive insertions (denoted "misinsertions") of either CO or ethylene are unfavourable. Ethylene misinsertions were shown to be inhibited due to the low binding affinity of ethylene relative to CO (as they compete for coordination), and the increased insertion barrier. The collective results are consistent with the mechanism illustrated in Scheme 1.2.

Coordination of an alkyl carbonyl oxygen of the growing polymer chain to the metal, as shown in Scheme 1.2, is characteristic of intermediates isolated between insertions. Four-coordinate species of this type have been characterised in a number of investigations.[11,12,47] Very recently, Cavell *et al.* presented an X-ray structure of a square–pyramidal intermediate (refer to Figure 1.1) in which the oxygen of the chelate ligand is weakly associated to the metal in the apical position.[16]

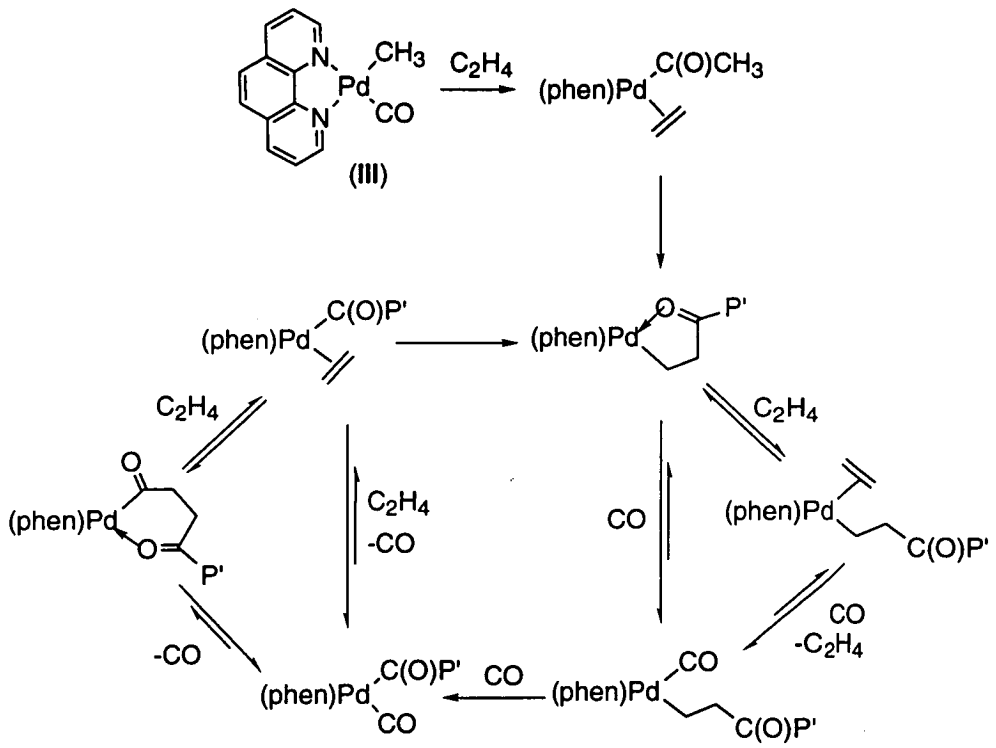

Scheme 1.2: *The proposed mechanism for CO/ethylene copolymerisation catalysed by [Pd(phen)(CH3)(CO)]+ (phen = 1,10-phenanthroline).*[44] *P' denotes the growing polymer chain. Note that all species illustrated possess a formal charge of 1+.*

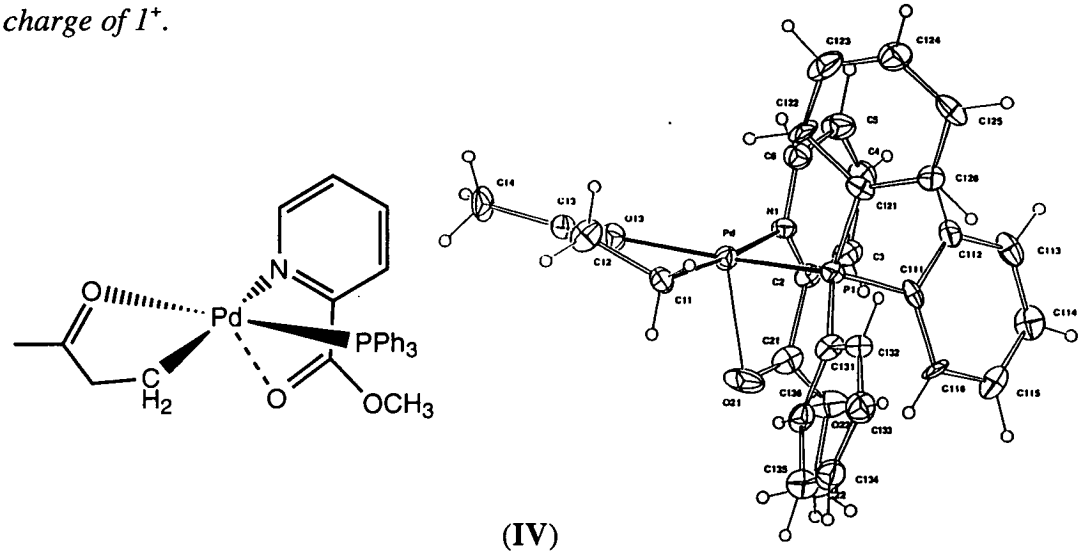

(IV)

Figure 1.1: *Pseudo five-coordinate intermediate resulting from successive insertions of CO and ethylene in the complex Pd(N-O)(CH3)(PPh3) (N-O = 6-methyl picolinate).*[48] *Selected bond lengths (Å); Pd-P 2.215(6), Pd-N 2.19(1), Pd-C(11) 2.00(1), Pd-O(13) 2.16(2), Pd-O(21) 2.78(1).*

The application of theoretical methods to the copolymerisation process has been a particularly active area since 1996. Morokuma *et al.*[46] have investigated copolymerisation by the systems $[(HN{=}CHCH{=}NH)M(CH_3)]^+$ (M = Pd,Ni) as models of the 1,10-phenanthroline complexes of Rix *et al.*[44] Ziegler *et al.*[45,49] have performed a similar study for the model diphosphine system $[(H_2PCH{=}CHPH_2)PdH]^+$. The results of both studies compared well with experiment (refer to Table 1.1). Aside from the choice of model system, the two studies differ in the mechanism investigated. Morokuma and coworkers considered only insertions from four-coordinate intermediates such as those proposed by Rix *et al.* in Scheme 1.2. Conversely, Ziegler allowed the carbonyl groups of the growing polymer chain to coordinate to the metal resulting in five-coordinate intermediates (see, for example, Scheme 1.3).[45] Both investigations determined the energetics associated with CO and ethylene misinsertions with similar findings. It was found that CO possesses a higher binding affinity for the metal than ethylene, thus inhibiting ethylene homopolymerisation, even though the latter is thermodynamically favoured. Multiple insertions of CO are unfavourable due to the high activation energy, and the instability of the carbon-carbon bond formed. Finally, Morokuma found that copolymerisation is more facile in Ni complexes, but proceeds with lower selectivity towards strict alternation of CO and ethylene units.

Table 1.1: *Theoretical and experimental activation energies (kJ/mol) for CO and ethylene insertions into Pd-carbon bonds. Note that the experimental values are Gibbs free energies and therefore include entropic contributions, but these are assumed to be relatively small.*

	Experimental[44]	Morokuma *et al.*[46]	Ziegler *et al.*[45]
$\Delta E_{Me\text{->}CO}$	63 (at -66°C)	62.3	48
$\Delta E_{Me\text{->}C2H4}$	79 (at -25°C)	67.8	65
$\Delta E_{Ac\text{->}C2H4}$	71 (at -45°C)	76.1	58
$\Delta E_{Ac\text{->}CO}$	not observed	118.0	109

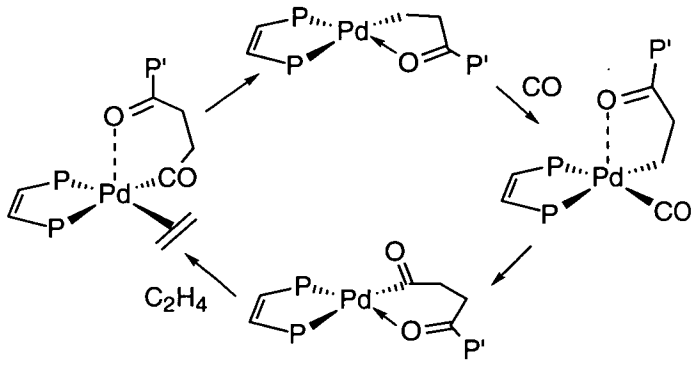

Scheme 1.3: *The catalytic cycle studied by Margl and Ziegler.*[49]

The remaining sections of this chapter will focus on mechanistic aspects of the rate-determining CO and olefin insertion steps and the possible rôle of five-coordinate transition metal geometries in the catalytic cycle.

1.4 Carbonylation

The carbonyl group is one of the most versatile functionalities available due mainly to its reactivity and its polarising effect on neighbouring atoms and groups. Insertion of carbon monoxide into a metal-carbon bond (formally referred to as carbonylation) may be employed to produce carbonyl-containing compounds under mild conditions with a high selectivity. Although the major interest in this area involves the synthesis of polyketones, such methods are also potentially useful in the synthesis of stereochemically pure pharmaceuticals and fine chemicals.

Due to its integral role in CO/olefin copolymerisation, the mechanism of carbonylation has been the focus of several experimental[9,10,31,44,50-54] and theoretical studies.[55] A main emphasis of investigation has been whether to view the reaction as *carbonyl insertion* or *methyl migration* (refer to Figure 1.2). Although the reaction is typically referred to as "carbonyl insertion", the weight of available evidence supports methyl migration[56] with few exceptions,[10] and will be referred to thus, hereafter. Migration reactions of 16 electron square–planar

complexes are of particular interest as there are potentially more reaction pathways available than for octahedral or tetrahedral complexes. The reaction may take place spontaneously in the square plane, or may be facilitated by coordination of a nucleophile yielding a five-coordinate 18 electron species.

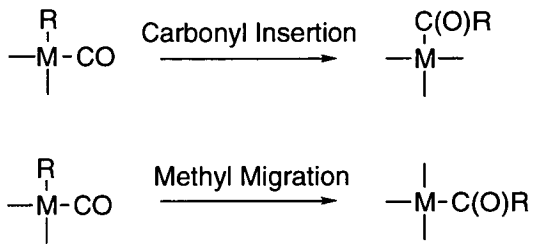

Figure 1.2: *Carbonyl insertion and methyl migration processes.*

1.4.1 *Experimental Studies*

Since the prototype migration reaction (1) was reported in 1957,[57] experimental interest in this process has been widespread.

$$RMn(CO)_5 + L \longrightarrow R{-}\overset{O}{\overset{\|}{C}}{-}Mn(CO)_4L \qquad (1)$$

The majority of experimental work on Group 10 complexes has focused on platinum, mainly due to the relative stability of the reactive intermediates involved.[51,58,59] Palladium complexes generally react *via* the same pathways but exhibit higher reaction rates and are therefore more suitable for industrial application.

The factors controlling spontaneous migration in square–planar carbonyl complexes are relatively well understood and are consistent with the simple mechanism in Scheme 1.4.[51,55] This pathway reflects the observations that the carbonyl group should be *cis* to the organic R^- group and the reaction is facilitated by bulky substituents *cis* to R^-, the addition of excess L (or other nucleophile) and a more highly basic R^-. The presence of a ligand with a high trans influence, *trans* to R^-, also increases the migration capacity provided it is not sterically bulky. The importance of the size of L has not been clearly explained but may be due to

unfavourable steric crowding in either the three- or four-coordinate intermediates following migration.[51]

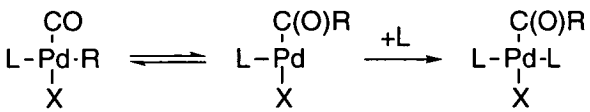

L = a neutral ligand; X = an anion

Scheme 1.4: *Mechanism for spontaneous migration in complexes of the type Pd(L)(X)(CO)(R).*

The pathways involved in carbonylation when the carbonyl group is not initially coordinated to the metal centre are less easily explained. Early kinetic studies by Garrou and Heck[50] on the carbonylation of complexes ML_2RX (M = Pt, Pd, Ni; R = organic group; X = halide; L = PR'_3) supported the initial formation of a five-coordinate intermediate $ML_2RX(CO)$ (**A** in Scheme 1.5). For each complex, the dominant carbonylation mechanism appeared to involve the subsequent dissociation of a labile ligand (L) to form MLRX(CO) from which isomerisation and migration proceeds (route 1 in Scheme 1.5). This route is in competition with direct migration from a five-coordinate intermediate to form $ML_2X(COR)$ (route 2). More recent work has indicated that the latter mechanism is dominant in cases such as those involving $SnCl_3$ as a "nonparticipating anion" (X^-) and more basic (i.e., less labile) phosphine ligands.[51]

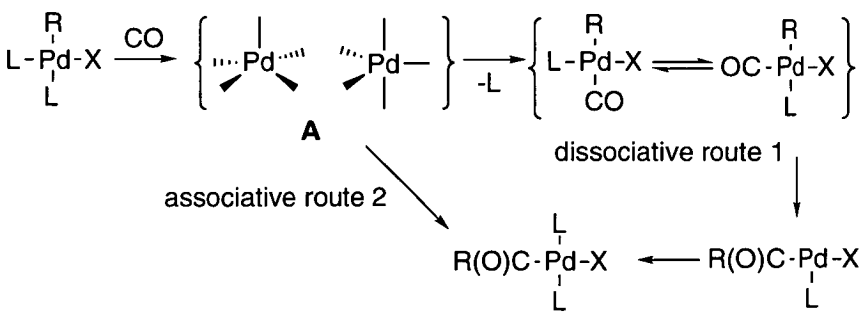

Scheme 1.5: *The competing carbonylation mechanisms proposed by Garrou and Heck.*[50] *Both pathways proceed via a five-coordinate intermediate (**A**) of unknown geometry.*

Reports of carbonylation of palladium and platinum complexes incorporating multidentate ligands are fairly recent. In 1984, Anderson and Cross suggested that such complexes did not support carbonylation, presumably due to geometrical constraints placed on five-coordinate species by the chelate (in the case of route 2 in Scheme 1.5) or the increased barrier of phosphine displacement (in the case of route 1).[51] A possible exception was noted for hemilabile bidentate ligands which could behave in a monodentate fashion throughout the reaction. A year later, Anderson and Lumetta reported slow CO insertions in complexes (L-L')Pt(Ph)Cl (where L-L' = P-P, P-S, P-N).[30] They proposed that the P-N and P-S complexes reacted *via* partial dissociation of the chelate, whereas the diphosphine ligands remained bidentate. Subsequently, a number of investigations have appeared in the literature reporting facile carbonylation of chelate complexes.[8,10-12,27,29,31,33,34,43,60-62]

Several possible carbonylation mechanisms for square–planar complexes of bidentate ligands have been proposed and are illustrated in Figure 1.3. Migration may proceed from a five-coordinate intermediate (**A**), or from a four-coordinate intermediate following the displacement of a monodentate ligand (intermediate **B**) or one "arm" of the bidentate ligand (intermediate **C**). The *direct* insertion of a CO molecule into a metal-carbon bond appears unlikely. Four-coordinate intermediates have been detected by NMR and IR techniques in the carbonylation of complexes incorporating a weakly associated ligand. Intermediates in the carbonylation of complexes which have no weakly bound ligands have not been detected, but have been suggested to be five-coordinate.[36,37,63] In particular, Vrieze *et al.*[36] have reported rapid carbonylation of a palladium(II) complex incorporating a rigid tridentate N-N-N ligand for which dissociation of a donor nitrogen to allow a four-coordinate mechanism is unlikely. Despite evidence of this type, migration in palladium and platinum complexes *via* a five-coordinate transition structure is often disregarded with little justification. Note that nickel complexes exhibit distinct

reaction behaviour, and the participation of five-coordinate species is commonly implicated.

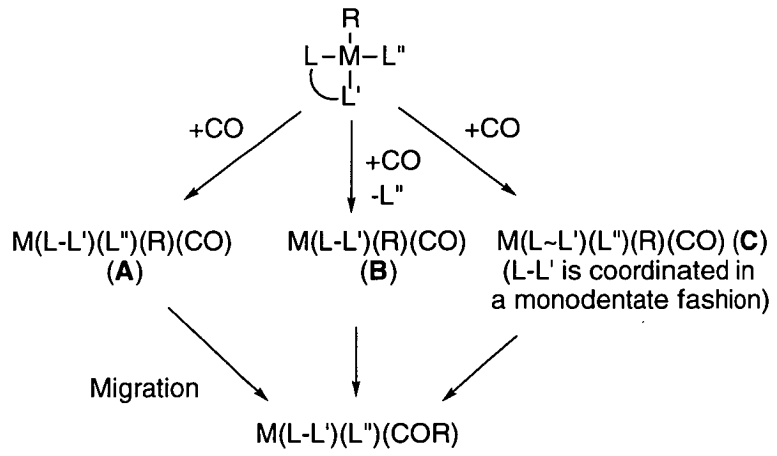

Figure 1.3: *Proposed carbonylation routes in square–planar complexes containing bidentate ligands.*

As discussed in Section 1.2, Vrieze *et al.* have examined the carbonylation of neutral and cationic organopalladium complexes of N-N,[11] N-P[31] and P-P[34] ligands. Acceleration of insertions by more flexible P-P ligands with larger bite angles has been attributed to decreased barriers of pseudorotations and migration, or to the ease of the bidentate ligand in adopting monodentate coordination.[34] Early theoretical studies reported an increase in the angle between the ancillary ligands in the four-coordinate migration transition structure (refer to Figure 1.4).[64] The transition structure would therefore be favoured by P-P ligands which are more able to effect larger P-M-P angles. It should be noted, however, that similar *trans*-angle opening has not been observed in subsequent, more rigorous theoretical studies.[56,65]

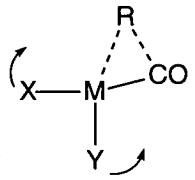

Figure 1.4: *Opening of the X-Pd-Y angle in the migration transition structure.*[64]

The reverse trends reported for the N-N ligands are difficult to rationalise. Elsevier *et al.* considered partial dissociation of the rigid N-N ligands unlikely, and proposed a mechanism *via* dissociation of the halide.[11] Partial dissociation of one of the nitrogens of the rigid N-N ligand, bis(*p*-anisylimino)acenaphthene (*p*-An-BIAN), was reported by Vrieze *et al.* for allene insertions into palladium-carbon bonds of neutral and cationic Pd(R)X(*p*-An-BIAN) complexes (**V**).[39] An X-ray crystal structure of an isolated intermediate displayed a distorted square–pyramidal geometry with an elongated apical Pd-N bond (2.600 Å). Subsequent work on N-N complexes has shown that carbonylation is aided by steric bulk close to one of the nitrogen donors.[29] They speculated that steric interactions would favour displacement of the nitrogen, providing a site susceptible to attack by CO. Following coordination of CO two possible schemes were proposed: (i) migration from an intermediate of type **C** (in Figure 1.3), or (ii) recoordination of the nitrogen to form a square–pyramidal five-coordinate species (**A**) and subsequent migration. However, neither pathway satisfactorily accounts for all of the observed ligand effects. Although they considered the existence of a trigonal–bipyramidal intermediate in which the halide and methyl groups occupy axial positions, migration from such an intermediate was viewed to be unlikely.

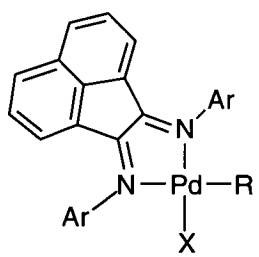

(**V**)

(Ar = *p*-$CH_3OC_6H_4$ (*p*-An))

The *p*-An-BIAN complexes investigated by Vrieze *et al.* displayed unusual reactivities towards CO insertions.[40] Whilst the cationic complexes possessed

allene insertion rates higher than the neutral complexes, subsequent insertion of CO was only observed for the neutral complexes. This is contrary to the generally reported higher reactivity of cationic *versus* neutral organopalladium(II) complexes.[1,5,7,19,31,33,34,41,66] The absence of carbonylation activity was attributed to the inability of the weakly coordinating $SO_3CF_3^-$ ion to stabilise the insertion product. In contrast to other CO insertion products, stabilisation by coordination of an alkyl carbonyl oxygen to form a six-membered palladacycle does not appear to take place. An explanation for this is not obvious, but it is consistent with previous findings.[11]

Recent experimental studies have shown platinum(II),[60] and palladium(II)-alkyl[61,62] complexes of pyridinecarboxylic acid (pyca) derivatives (**I**) undergo rapid carbonylation. From the early experimental work the mechanistic proposals illustrated in Scheme 1.6 were postulated as possible reaction pathways. These encapsulated the observed importance of the lability of the nitrogen donor, and the lability and trans influence of the phosphine ligand. A similar dependence of the reactivity on the ligands was noted for the corresponding cationic complexes, $[Pd(N\text{-}O)(L)(CH_3)]^+ BF_4^-$ (N-O = methylpicolinate).[42,43] The carbonylation rate decreases with increasing basicity of the phosphine ligand (L). However, in the case of the neutral complexes if L is replaced by a ligand with a low binding affinity and low trans influence (such as pyridine), the reaction terminates following displacement of this ligand. Modification of the chelating pyca ligand has been shown to increase the carbonylation rate in the series:[62]

pyca < 4-NO_2-pyca < 6-CH_3-pyca < 6-CH_3-4-NO_2-pyca

The increase in reactivity with the addition of substituents on the pyridyl ring has been attributed to an increase in the lability of the donor nitrogen due to electronic and/or steric effects. Finally, the carbonylation reactivity of the substituted-pyca complexes exhibits a strong solvent dependence. The reaction is facilitated by a strongly coordinating solvent, such as THF, but fails to proceed in aromatic solvents which suggests that a ligand-solvent exchange equilibrium is integral to the

reaction. This effect is reversed in the case of the non-substituted pyca ligand, implying the involvement of different mechanisms.

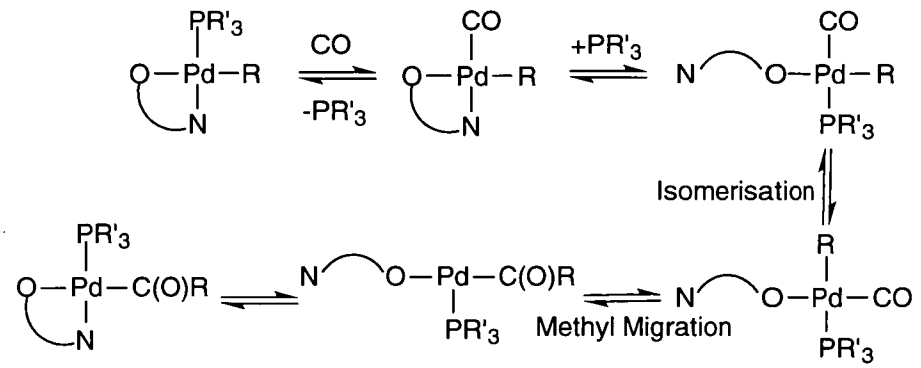

Scheme 1.6: *Mechanism consistent with experimental kinetic observations for the carbonylation of organopalladium complexes of potentially hemilabile N-O ligands.*[61]

1.4.2 *Theoretical Studies*

A number of theoretical studies on CO insertion/methyl migration have appeared in the literature.[55] Possibly the earliest and most notable of these was published by Berke and Hoffmann in 1978.[67] They applied Extended Hückel theory (EHT) to the reaction $CH_3Mn(CO)_5 \rightarrow CH_3(CO)\text{-}Mn(CO)_4$ assuming that the process took place by methyl migration. The main contributions to the activation energy were postulated to include:

- a four-electron destabilising interaction between the occupied methyl σ orbital and the CO lone pair σ orbital. This is partially relieved by interaction between the former methyl σ orbital and the CO π^* orbital.
- a rise in energy of the orbital which is the Mn-CH_3 σ-bond of the reactant, and is transformed primarily into the Mn-acyl bond of the five-coordinate intermediate, and
- the loss of one π-type overlap during the migration.

Some compensation is supplied by stabilisation of the σ-type acyl orbital.

In the mid 1980's, Morokuma and coworkers performed a series of *ab initio* calculations on the "carbonyl insertion" step in four-coordinate platinum and palladium complexes.[56,65,68] The group compared the energetics of formal carbonyl insertion, methyl migration and a concerted process in which the angle between the non-participatory ligands opens. They concluded that methyl migration was preferred and examined the paired interactive hybrid molecular orbitals (IHMO's) to rationalise this result. It was proposed that the transition structure for formal CO insertion was destabilised due to repulsion between the two carbonyl lone pair electrons and the metal d_{xy} electrons (refer to II in Figure 1.5). In the methyl migration process the carbonyl lone pair is no longer directed toward the metal d_{xy} orbital, and the repulsion between the singly occupied methyl sp^3 orbital and the metal d_{xy} orbital is low (III in Figure 1.5).

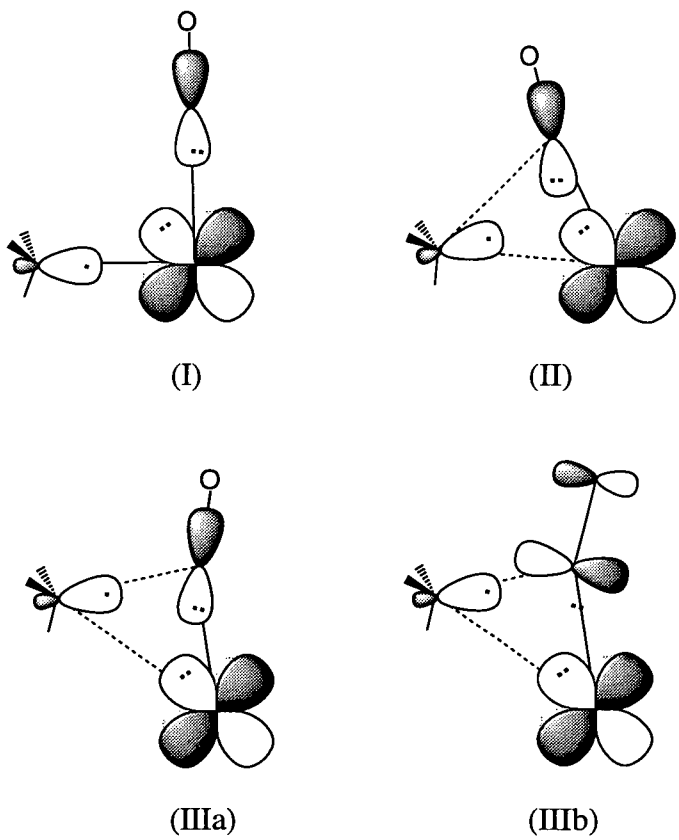

Figure 1.5: *IHMO's for the reactant (I), formal carbonyl insertion transition structure (II), and the methyl migration transition structure (IIIa,b).*

Tchougreeff *et al.*[69] applied a qualitative configuration interaction (CI) method to the general carbonylation reaction to provide insight into factors controlling the activation energy of the methyl migration step. The group adopted the proposal that the four-electron destabilising interaction between the methyl lone pair σ-orbital and the CO lone pair σ-orbital is the main contribution to the activation energy. They argued that as the extent of σ-donation from the methyl group to the metal is increased, this repulsive interaction decreases accordingly. Consequently, the crucial factors controlling the migration capacity of a complex are the effective ionisation potential, or basicity, of the migrating R^- group, and the electron affinity, or acidity, of the rest of the complex. In general, they proposed that migration is more facile when involving a basic R^- group and occurring in the ligand sphere of a stronger acid.

Although the methyl migration step has been extensively studied, little attention has been paid to reactions in which the carbonyl group is initially uncoordinated or to complexes containing chelating ligands. Van Koten *et al.* recently compared the reaction mechanisms operating in the carbonylation of the systems $[Pd(CH_3)(NH_3)_3]^+$ and $Pd(CH_3)_2(NH_3)_2$, models of complexes containing tridentate and bidentate nitrogen donor ligands.[28] Clearly, predictions made using NH_3 groups to replace a chelate ligand, particularly one in which the nitrogen donor is a pyridyl nitrogen, are of dubious value. Geometries were optimised at the RHF level, and improved energies were generated including electron correlation. The lowest energy pathway for carbonylation of both systems involved the initial coordination of carbon monoxide *via* associative replacement of one of the NH_3 groups followed by methyl migration and re-association of the NH_3 ligand. Although the results precluded the formation of *strongly* bound five-coordinate intermediates, the transition structure for methyl migration in the cationic species was observed to be stabilised by the presence of the dissociated NH_3 in the vicinity of the coordination sphere. A similar stabilisation was not found for the neutral species.

Only two theoretical investigations have considered carbonylation of organopalladium complexes incorporating bidentate ligands.[45,46,49] The initial reactant in each study was a three-coordinate complex assumed to be formed following the dissociation of a labile ligand, resulting in substantial simplification of the reaction pathway. No previous work has modelled the reaction of stable four-coordinate complexes incorporating potentially hemilabile bidentate ligands.

1.5 Olefin Insertion

In contrast to the carbonylation step, there have been relatively few mechanistic studies of insertions of olefins into palladium(II)-acyl bonds. The latter has only recently been recognised as an elementary transformation in many catalytic reactions.[33,70] A number of experimental studies have subsequently appeared in the literature regarding olefin insertion of palladium(II) complexes of bidentate N-N,[11,12,26,44] P-P,[32,34] and N-O ligands,[16,43] and tridentate N-N-N[38] ligands. The transformation is also gaining attention by theoreticians[71] as it appears to be rate-determining in CO/olefin copolymerisation.[44,46,49]

Experimental studies of olefin insertion into a metal-acyl bond have been problematic due to the low stability of the intermediates and products. The insertion product possesses a β-hydrogen, providing a low-energy decomposition pathway to yield palladium hydride and an alkene. The susceptibility of the inserted complex towards β-hydrogen elimination has typically limited the insertion process to strained alkenes, for which the β-hydrogen is in a position inaccessible to nucleophilic attack by the metal.[11,12,21,47] Attempts to generate a stable product generally inhibit the reaction. Brumbaugh and Sen were the first to characterise a palladium alkene-inserted product.[47] The stability of the complex was attributed to coordination of the acyl oxygen as discussed in Section 1.2. The first *direct* observation of olefin insertion into a metal-acyl bond has recently been

accomplished by Brookhart and coworkers for the catalytic cycle illustrated in Scheme 1.2.[44]

The dependence of the reaction rate and mechanism on the coordinated ligands displays similar trends to those observed for carbonylation (Section 1.3). In general, as for "carbonyl insertion", "olefin insertion" is more accurately described as R-group migration.[71] As it is a nucleophilic attack by the olefin, the rate is enhanced by low-lying LUMO's on the olefin and/or a partial positive charge on the migrating group. However, in the case of the diphosphine ligands, Vrieze and coworkers believe that electronic factors are less important than the availability of a coordination site.[33] For example, the insertion rate increased in the series:

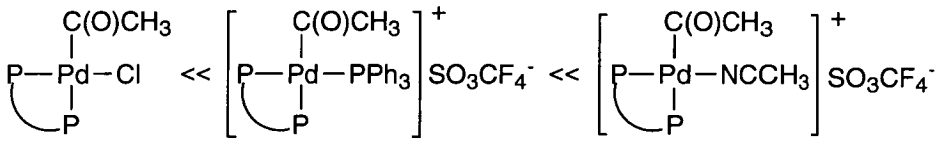

Kinetic studies suggest that the insertion rate in a neutral complex is enhanced by the dissociation of an anionic ligand to yield a cationic species with a vacant coordination site, facilitating the coordination of the olefin and ensuing transformations.[9,11,12,20,47]

An early EHT study by Thorn and Hoffmann[72] compared the reaction barriers for ethylene insertion into a Pt-H bond of four- and five-coordinate systems $PtH(PH_3)_2(C_2H_4)Cl_n$ (n=0-1). They concluded that the five-coordinate route was unfavourable, olefin insertion in $PtH(PH_3)_2X$ being facilitated by a more labile X^- which may be displaced by ethylene prior to insertion. Subsequent experimental work has provided support for the four-coordinate insertion mechanism.[44,73] Kinetic measurements by Sen *et al.* indicated that olefin insertion into the palladium-acyl bond of neutral complexes, $Pd(PPh_3)_2(Cl)(COR)$, could be accounted for by phosphine dissociation followed by olefin coordination and insertion from a four-coordinate intermediate.[47] However, the reaction of the corresponding cationic complexes ($[Pd(PPh_3)_2(CH_3CN)(COR)]^+BF_4^-$) proved to

be more complex, kinetic results being inconsistent with either the basic four- or five-coordinate pathways.

The concept of a vacant coordination site has been challenged by a number of research groups who have suggested the participation of five-coordinate intermediates and transition structures.[11,12,28,29,40] A very recent study by Vrieze *et al.* on norbornadiene insertion into the Pd-acyl bond of complexes $[Pd(C_7H_8C(O)R)(Ar\text{-}BIAN)]^+X^-$ has implicated the existence of competing four- and five-coordinate routes.[40] They put forward several possible mechanisms accounting for the reaction kinetics, including dissociation of the halide (X^-) or of one of the nitrogen donors, however further clarification is required.

A number of *ab initio* studies have been performed on ethylene insertion; a comprehensive review of these is provided by Koga and Morokuma.[71] These authors investigated olefin insertion from $M(H)_2(PH_3)(C_2H_4)$ (M=Ni, Pd, Pt) at the RHF level.[74] The transition structure is stabilised by orbital interactions between the occupied σ_{MH} and vacant σ_{MH}* orbitals and alkene π* and π orbitals respectively (refer to Figure 1.6). If the metal $d_{x^2-y^2}$ orbital is vacant (which is the case for d^8 metals) the σ_{MH} and σ_{MH}* MO's have high degrees of metal d character which favours the above interactions. An occupied $d_{x^2-y^2}$ orbital does not play a major role in the σ_{MH} MO, resulting in a higher activation energy.

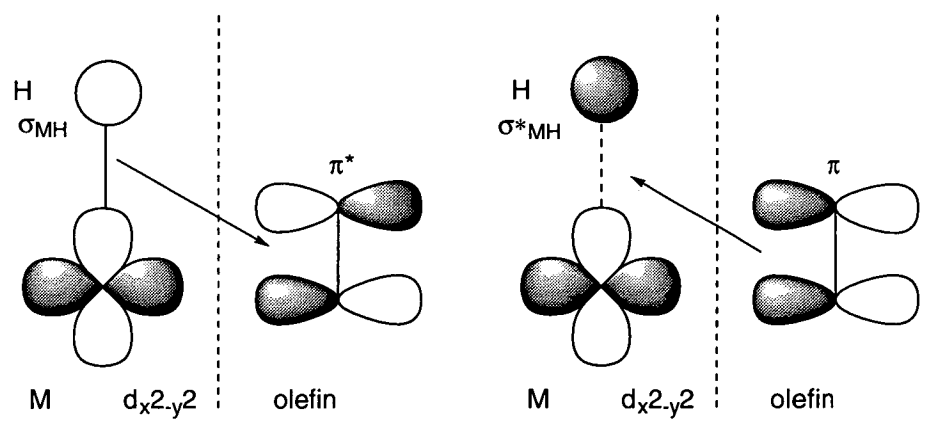

Figure 1.6: *IHMO's dominant in the insertion of ethylene into a M-H bond.*

More recently, Siegbahn *et al.*[75] have performed density functional calculations on ethylene coordination, insertion and β-hydrogen elimination in the complexes PdR^+, $Pd(NH_3)_2R^+$, and $Pd(NH{=}CH_2CH_2{=}NH)R^+$ ($R{=}CH_3$, CH_2CH_3). The variation in the insertion activation energy with different ancillary ligands was surprisingly small and compared well to the experimental value. This indicates that the solvent and ligands have little influence on the reaction barrier, rather its magnitude may be intrinsic to the metal. Small decreases in the insertion activation energy in the presence of ancillary ligands can be correlated with increases in the metal-olefin bond strength. The ligands influence the binding energy of the olefin, and the exothermicity of insertion.

1.6 Five-Coordination in d^8 Species

The chemistry of d^8 complexes is largely dominated by coordinatively unsaturated 16 electron square–planar structures. Only recently have stable five-coordinate Pt(II) and Pd(II) complexes been isolated, most of these conforming to the general formula [M(N-N)(olefin)XY] where N-N = bidentate N-donor ligand and X, Y = monodentate anionic ligands (refer to Figure 1.7).[76] Five-coordinate Pd(II) complexes are less stable than the corresponding Pt(II) complexes by approximately four orders of magnitude, explaining their comparative rarity. In contrast, five-coordination in Ni(II) chemistry is known to be fairly prevalent.

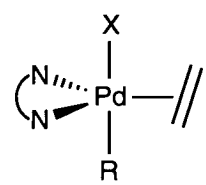

Figure 1.7: *Structure of typical five-coordinate palladium(II) and platinum(II) complexes with the formula [M(N-N)(olefin)XY].*[76]

Several studies have appeared this decade investigating the influence of ligands on the stability of five-coordinate Pd(II)[77] and Pt(II)[78-80] complexes. Paccioni and coworkers have isolated and obtained X-ray crystal structures of a series of Pt(II) complexes exhibiting coordination between four and five.[80] Consistent with other studies, formal five-coordinate Pt(II) complexes possess a trigonal–bipyramidal (TBP) geometry. However, with a weakening of the coordination of the fifth ligand, the geometry distorts away from TBP towards a flattened square–pyramidal (f-SQP) geometry (refer to Figure 1.8) with the more weakly bound ligand in the apical position.

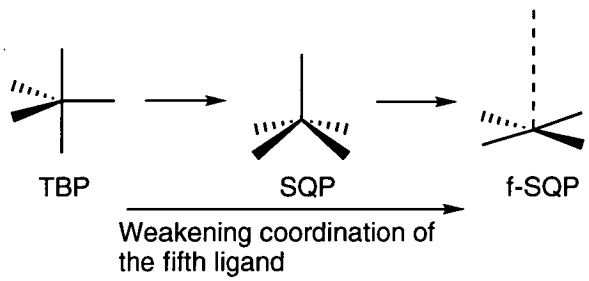

Figure 1.8: *Distortion of the geometry away from trigonal–bipyramidal (TBP) towards flattened-square–pyramidal (f-SQP).*

The equilibrium between four- and five-coordination is governed by the metal p_z and d_{z^2} orbitals lying above and below the plane of the square–planar geometry.[81] For five-coordination to be favoured, the empty metal p_z orbital must be able to accept an electron pair from the fifth ligand, and the repulsion between the ligand orbitals and the occupied metal d_{z^2} orbital minimised. It has been found that the ability of ligands to stabilise five-coordination is dependent on their ability to reduce the electron density on the metal. A strong π-acceptor in the square plane reduces the electron density in the metal d_{z^2} orbital, thereby lowering the electronic repulsion with the occupied orbitals of the fifth ligand. This explains why the majority of five-coordinate Pd(II) complexes isolated to date incorporate an olefin

ligand. In contrast, strong σ-donors favour four-coordination due to the higher electrophilicity of the metal in this state.

In general, five-coordination is observed in cases where there is strong destabilisation of the four-coordinate square–planar geometry.[76] Steric effects are therefore important, as bulky ligands induce distortion of the square–planar geometry. The participation of five-coordinate species in the copolymerisation reaction may therefore offer an alternative explanation for the increase in carbonylation activity with ligands of higher steric bulk.[29] Previously, this observation has been attributed to a destabilisation of the four-coordinate intermediate such that migration proceeds to minimise the steric interactions.

Isomerisation of square–planar d^8 complexes is generally thought to proceed via pseudorotations and TBP intermediates.[58] The Berry intramolecular rearrangement illustrated in Figure 1.9 is often invoked to account for isomerisation of TBP or SQP intermediates. However, such a mechanism cannot account for isomerisation of f-SQP five-coordinate palladium and platinum complexes unless they first undergo significant distortion to an elevated-SQP geometry.[82]

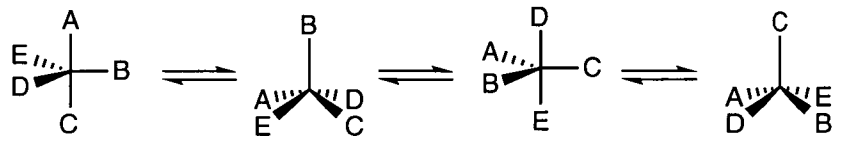

Figure 1.9: *The Berry pseudorotation, accounting for the isomerisation of many five-coordinate SQP intermediates (via TBP transition structures) and TBP intermediates (via SQP transition structures).*

Evidence for the participation of five-coordinate intermediates and transition structures in the fundamental transformations of d^8 complexes has been provided by a number of studies. Garrou and Heck isolated a five-coordinate reactive intermediate in the carbonylation of an organoplatinum(II) complex (as mentioned in Section 1.4.1).[50] Theoretical investigations have considered the rôle of

five-coordinate species in ligand substitutions,[83,84] carbonylation[28] and olefin insertions[49] of d^8 square–planar complexes. These have supported ligand susbstitution *via* five-coordinate transition structures, however the existence of five-coordinate species in insertion reactions remains unconfirmed.

1.7 The Project

Experimental studies on the carbonylation of platinum- and palladium-alkyl complexes of picolinic acid derivatives (**I**) have indicated that coordination and subsequent insertion of CO may proceed *via* a number of competing pathways. Despite elegant kinetic measurements, a fundamental understanding of the details of the various transformations involved remains elusive. Theoretical methods have the potential to provide significant contributions towards the understanding of reaction mechanisms, hence there is growing interest in combining theoretical and experimental methods to study carbonylation reactions. The initial objective of the current project was to employ accurate theoretical methods to identify low energy reaction mechanisms for carbonylation of **I**, and provide some insight into how these may be manipulated to achieve greater reactivity.

The CO/olefin copolymerisation activity of alkyl-palladium(II) complexes has been shown to be highly dependent on the coordinated ligands. For example, cationic palladium(II) chelate complexes are, in general, significantly more active towards CO/olefin copolymerisation than their neutral counterparts. Although there are several theoretical studies of carbonylation in the literature, no clear rationale has been provided for these contrasting reactivities. Against this background, we have aimed to assess the influence of a range of coordinated ligands on the mechanism and activation energy of carbonylation. Furthermore, the olefin insertion step in the copolymerisation reaction for neutral and cationic palladium-acyl complexes of N-O ligands will be compared.

In the course of this research, interest in palladium(II) catalysed copolymerisation by theoreticians has been considerable and a number of investigations have recently appeared in the literature. Only two studies relating to carbonylation of complexes incorporating bidentate ligands have been performed to date, both of which initiate from a three-coordinate reacting species. As discussed in Section 1.4, carbonylation of four-coordinate chelate complexes is complex, involving a number of competitive pathways which are yet to be clearly delineated. The present work represents the first theoretical investigation of carbonylation of four-coordinate chelate complexes. The rôle of novel five-coordinate intermediates and transition structures in ligand substitutions, isomerisation and migratory insertions will be closely examined. Finally, we will demonstrate the exceptional strength of quantum chemistry in the reproduction and elucidation of experimental trends which have previously been enigmatic, thereby potentially enabling more efficient catalyst design.

CHAPTER 2

Theoretical Modelling of Organometallic Systems

Chapter 2

Theoretical Modelling of Organometallic Systems

2.1 Introduction

Although theoretical techniques have been employed in the examination of bonding in organic molecules since early this century, their application to systems containing transition metals has developed only recently. Computational modelling of real chemical problems originated in the form of the quantum mechanical Hückel method in the 1930's which was used to calculate π-orbital energies.[85] It was generalised in the 1950's to include σ-bonds creating the extended Hückel theory (EHT).[86-89] Subsequently, between 1960 and 1980 three classes of computational methods arose. The most rigorous, and consequently the most computationally demanding, is *ab initio* theory. As the name implies, *ab initio* methods are derived from first principles quantum mechanics. Parameterisation of the most time consuming components of the Schrödinger equation gave rise to semi-empirical methods. Although not as reliable and versatile as *ab initio* techniques, such algorithms can be applied to much larger systems. The third theoretical model is the most empirical method, molecular mechanics, and is based on a classical "ball and spring" picture of the chemical bond.

Organometallic chemistry is a fairly recent field. The first structural characterisation of an organometallic complex (ferrocene) appeared in 1951[90,91] and led to the Dewar-Chatt-Duncanson model explaining the interaction between the metal and ligands.[92,93] In the early 1970's EHT was first applied to organometallic compounds.[94] However, due to the diversity of transition metals, the subsequent development of the field was slow. The ability of transition metals to adopt a range of oxidation states and coordination geometries coupled with a relative lack of experimental data makes parameterisation of these systems problematical. A few

semiempirical algorithms are now available for transition metals,[95] but their reliability does not compare to the organic semiempirical methods.

Ab initio theory is clearly suited to transition metal compounds except for the following problems:

• The number of electrons in transition metals is high making even simple systems computationally demanding;

• Electron correlation effects in transition metal compounds are important;[55,71]

• Relativistic effects become significant for the late first-row transition metals, and cannot be ignored in the treatment of second- and third-row transition metals.[96]

Such problems have limited the routine modelling of transition metal complexes until the last decade. Rapid advances in computational power coupled with the development of effective core potentials (ECP's), incorporating relativistic effects for the second- and third-row metals, and density functional methods has prompted a plethora of recent publications dealing with transition metals and their reactivities.

This chapter will provide a brief overview of the *ab initio* molecular orbital methods employed in the present work, their advantages and drawbacks. More detailed derivations and discussions can be obtained in the references for Hartree–Fock based methods,[97] ECP's,[98-100] and density functional theory[101-103] and references therein.

2.2 General Molecular Orbital Theory

The foundation of quantum chemistry is the relativistic time-independent Schrödinger equation (Equation 2.1) to which an approximate solution is determined.

$$\mathcal{H}\Psi = E\Psi \tag{2.1}$$

where $\mathcal{H}$= the Hamiltonian operator for a system of nuclei and electrons
E = the energy of the system
Ψ = the wavefunction.

The Hamiltonian is a Hermitian operator. For N electrons and M nuclei:

$$\mathcal{H} = -\sum_{i}^{N}\frac{1}{2}\nabla_i^2 - \sum_{A}^{M}\frac{1}{2M_A}\nabla_A^2 - \sum_{i}^{N}\sum_{A}^{M}\frac{Z_A}{r_{iA}} + \sum_{i}^{N}\sum_{j>i}^{N}\frac{1}{r_{ij}} + \sum_{A}^{M}\sum_{B>A}^{M}\frac{Z_A Z_B}{R_{AB}} \tag{2.2}$$

where M_A = ratio of the mass of nucleus A of atomic number Z_A to the mass of an electron and ∇_i^2 and ∇_A^2 are Laplacian operators involving differentiation with respect to the coordinates of the ith electron and Ath nucleus.

The first two terms in Equation 2.2 are the operators for the kinetic energy of the electrons and nuclei respectively. The remaining terms describe the coulombic interactions: the attraction between electrons and nuclei, repulsion between the electrons, and repulsion between the nuclei in that order.

In order to solve the Schrödinger equation, several approximations are invoked. The principal approximation is the Born-Oppenheimer approximation in which we assume that the motion of the nuclei is negligible compared to the motion of the electrons. Under this assumption, the kinetic energy of the nuclei can be approximated as zero, and the final term of Equation 2.2 is constant. The Hamiltonian can be subsequently partitioned into an electronic and a nuclear component:

$$\mathcal{H} = \mathcal{H}_{elec} + \mathcal{H}_{nucl} \tag{2.3}$$

Molecular orbital theory is primarily interested with solutions to the electronic problem

$$\mathcal{H}_{elec}\Phi_{elec} = E_{elec}\Phi_{elec} \tag{2.4}$$

where E_{elec} is the electronic energy and Φ_{elec} is the electronic wavefunction.

In the following sections the symbol $\mathcal{H}$ will denote the electronic Hamiltonian.

2.2.1 *The Electronic Problem and Hartree–Fock (HF) Theory*

An electron is completely described by a *spin orbital*, χ, which is a wave function dependent on both the spacial coordinate, $\mathbf{r}$, and spin, ω. These coordinates are denoted by $\mathbf{x} = \{\mathbf{r},\omega\}$, such that the wave function for an N-electron system can be written as $\Phi(\mathbf{x}_1,\mathbf{x}_2,...,\mathbf{x}_N)$. The simplest ground-state wavefunction satisfying the Pauli Exclusion principle is the single determinant constructed from the set of spin orbitals $\{\chi j\}$ (a *Slater determinant*).

$$\begin{aligned}\Psi_0(\mathbf{x}_1,\mathbf{x}_2,...,\mathbf{x}_N) &= (N!)^{-1/2}\begin{vmatrix} \chi_i(\mathbf{x}_1) & \chi_j(\mathbf{x}_1) & \cdots & \chi_k(\mathbf{x}_1) \\ \chi_i(\mathbf{x}_2) & \chi_j(\mathbf{x}_2) & \cdots & \chi_k(\mathbf{x}_2) \\ \vdots & \vdots & & \vdots \\ \chi_i(\mathbf{x}_N) & \chi_j(\mathbf{x}_N) & \cdots & \chi_k(\mathbf{x}_N) \end{vmatrix} \\ &= |\chi_i\ \chi_j\ \cdots\ \chi_k\rangle\end{aligned} \tag{2.5}$$

Such a solution describes N electrons in N spin orbitals without explicitly defining which electron occupies each particular orbital, and therefore incorporates *exchange correlation.* However, as the motion of electrons with unparallel spins remain independent, the wavefunction is termed *uncorrelated.*

The energy associated with a wave function, Ψ, is given by its expectation value.

$$E = \langle\Psi|\mathcal{H}|\Psi\rangle \tag{2.6}$$

The variation principle states that the best approximation to the ground-state wave function, $\Psi_0(\mathbf{x}_1,\mathbf{x}_2,...,\mathbf{x}_N)$, is obtained by minimising the energy with respect to the choice of spin orbitals, $\{\chi j\}$. In the Hartree–Fock (HF) approximation the

wave function is a single determinant (Equation 2.5), such that the minimum energy is given by Equation 2.7.

$$E_o = \langle \Psi_o | \mathcal{H} | \Psi_o \rangle = \sum_a \langle \chi_a | h | \chi_a \rangle + \frac{1}{2} \sum_{ab} \langle \chi_a \chi_b \| \chi_a \chi_b \rangle \tag{2.7}$$

where $\mathcal{H}$ represents the electronic Hamiltonian, and h is an operator describing the kinetic energy and potential energy of a single electron.

The ground-state wave function is obtained by systematically varying the choice of spin orbitals *via* a self consistent procedure. This yields what is known as the HF integro-differential equation.

$$h(1)\chi_a(1) + \sum_b [\mathcal{J}_b(1) - \mathcal{K}_b(1)]\chi_a(1) = \varepsilon_a \chi_a(1)$$

$$\text{or} \tag{2.8}$$

$$f(1)\chi_a(1) = \varepsilon_a \chi_a(1)$$

where

$$\begin{aligned} f(1) &= h(1) + \sum_b [\mathcal{J}_b(1) - \mathcal{K}_b(1)] \\ &= h(1) + \upsilon^{HF}(1) \end{aligned} \tag{2.9}$$

$$\mathcal{J}_b(1) = \int d\mathbf{x}_2 |\chi_b(2)|^2 r_{12}^{-1} \tag{2.10}$$

$$\mathcal{K}_b(1) = \int d\mathbf{x}_2 \chi_b^*(2) r_{12}^{-1} \chi_a(2) \tag{2.11}$$

Hence, the many-electron problem in Equation 2.4 is reduced to an effective one-electron problem in which we have introduced the *Fock Operator, f*. The first term of Equation 2.9 is denoted the *core-Hamiltonian operator*. Equations 2.10 and 2.11 define the *local* coulomb operator and *nonlocal* exchange operator respectively which, together, constitute the effective one-electron potential operator (or HF potential) υ^{HF}. The eigenfunctions of Equation 2.8 define the spin orbitals, and the eigenvalues, ε_a, equate to the orbital energies.

For closed-shell systems it is often convenient and reasonable to adopt a restricted wavefunction. That is, the spin orbitals are required to have the same spatial function for each spin function ("spin up" and "spin down"), giving rise to the restricted HF (RHF) equations. Spin can subsequently be eliminated from the HF equations by integration to yield spatial equations.

$$f(\mathbf{r}_1)\psi_i(\mathbf{r}_1) = \varepsilon_i\psi_i(\mathbf{r}_1) \tag{2.12}$$

Roothaan proposed expanding the spatial molecular orbitals ψ_i as a linear expansion of a set of known basis functions $\{\phi_\mu(\mathbf{r}_1)|\mu=1,2,...K\}$:

$$\psi_i = \sum_{\mu=1}^{K} \mathbf{C}_{\mu i}\phi_\mu \qquad i=1,2,...K \tag{2.13}$$

such that the integro-differential equation (Equation 2.12) is converted to a set of algebraic equations solvable by matrix techniques.

$$\sum_\upsilon F_{\mu\upsilon} C_{\upsilon i} = \varepsilon_i \sum_\upsilon S_{\mu\upsilon} C_{\upsilon i} \qquad i=1,2,...,K \tag{2.14a}$$

or

$$\mathbf{FC} = \mathbf{SC}\varepsilon \tag{2.14b}$$

where

$$\mathbf{C} = \begin{pmatrix} C_{11} & \cdots & C_{1K} \\ \vdots & & \vdots \\ C_{K1} & \cdots & C_{KK} \end{pmatrix} \qquad \varepsilon = \begin{pmatrix} \varepsilon_1 & & \mathbf{O} \\ & \varepsilon_2 & \ddots \\ \mathbf{O} & & \varepsilon_K \end{pmatrix}$$

We have introduced the overlap matrix **S**

$$S_{\mu\upsilon} = \int d\mathbf{r}_1 \phi_\mu^*(1)\phi_\upsilon(1) \tag{2.15}$$

and the matrix representation of the Fock operator within the set of basis functions $\{\phi_\mu\}$: the Fock matrix **F**

$$\begin{aligned} F_{\mu\upsilon} &= \int d\mathbf{r}_1 \phi_\mu^*(1) f(1)\phi_\upsilon(1) \\ &= H_{\mu\upsilon}^{\text{core}} + \sum_a^{N/2} \sum_{\lambda\sigma} C_{\lambda a} C_{\sigma a}^* \left[2(\mu\upsilon|\sigma\lambda) - (\mu\lambda|\sigma\upsilon)\right] \end{aligned} \tag{2.16}$$

in which

$$H_{\mu\upsilon}^{\text{core}} = \int d\mathbf{r}_1 \phi_\mu^*(1) h(1)\phi_\upsilon(1) \tag{2.17}$$

is the core-Hamiltonian matrix. The second term in Equation 2.16 is often replaced by $G_{\mu\upsilon}$ which contains the two-electron terms. Equations 2.14-2.17 are known as the Roothaan equations and can be solved iteratively.

In many cases, including open-shell systems, the 'restricted' picture of molecular orbitals is inappropriate. In such instances the Pople-Nesbit equations

are often employed in which the spatial orbitals form two sets, $\{\psi^{\alpha}\}$ and $\{\psi^{\beta}\}$, each expanded in $\{\phi_{\mu}\}$.

$$\mathbf{F}^{\alpha}\mathbf{C}^{\alpha} = \mathbf{S}\mathbf{C}^{\alpha}\varepsilon^{\alpha}$$
$$\mathbf{F}^{\beta}\mathbf{C}^{\beta} = \mathbf{S}\mathbf{C}^{\beta}\varepsilon^{\beta} \qquad (2.18)$$

where

$$F^{\alpha}_{\mu\upsilon} = H^{\text{core}}_{\mu\upsilon} + \sum_{\lambda}\sum_{\sigma}\sum_{a}^{N^{\alpha}} C^{\alpha}_{\lambda a}(C^{\alpha}_{\sigma a})^{*}\left[(\mu\upsilon|\sigma\lambda) - (\mu\lambda|\sigma\upsilon)\right] + \sum_{\lambda}\sum_{\sigma}\sum_{a}^{N^{\beta}} C^{\beta}_{\lambda a}(C^{\beta}_{\sigma a})^{*}(\mu\upsilon|\sigma\lambda) \qquad (2.19)$$

These equations are analogous to the Roothaan equations and constitute *unrestricted* Hartree–Fock (UHF) theory. A deficiency of this method is that it does not produce a pure spin state.

HF methods often yield remarkably good qualitative potential energy surfaces even when the absolute energies are poor. This can be attributed to the Hartree–Fock and correlated PES's being close to parallel in regions around stationary points.

2.3 Post-Hartree–Fock Methods: the Inclusion of Dynamic Electron Correlation

2.3.1 *Configuration Interaction (CI)*

The limitations of HF theory are particularly evident in transition metal complexes for which the orbitals are often very close in energy. Generation of reliable reaction energetics for organometallic reactions requires the inclusion of electron correlation energy.[99] On its own, HF theory represents the simplest *ab initio* approximation, but it also acts as a starting point for a range of more accurate calculations incorporating electron correlation. Electron correlation is defined as the difference between the exact non-relativistic energy of the system, $\mathcal{E}_o$, and the HF energy, E_o.

$$E_{corr} = \mathcal{E}_o - E_o \qquad (2.20)$$

As the HF energy is an upper bound to the exact energy, E_{corr} is always negative.

Conceptually, the simplest post-HF method is configuration interaction (CI). In this approximation the many-electron wave function, $|\Phi_0\rangle$, is expanded as a linear combination of the ground-state HF slater determinant, $|\Psi_0\rangle$, and excited determinants $|\Psi_a^r\rangle$, $|\Psi_{ab}^{rs}\rangle$, $|\Psi_{abc}^{rst}\rangle$ etc.

$$|\Phi_0\rangle = |\Psi_0\rangle + \sum_{ar} c_a^r |\Psi_a^r\rangle + \sum_{\substack{a<b \\ r<s}} c_{ab}^{rs} |\Psi_{ab}^{rs}\rangle + \sum_{\substack{a<b<c \\ r<s<t}} c_{abc}^{rst} |\Psi_{abc}^{rst}\rangle + \ldots \qquad (2.21)$$

where, for example, the determinant $|\Psi_a^r\rangle$ represents a wave function in which an electron of $|\Psi_0\rangle$ is excited from spin orbital χ_a to a virtual orbital χ_r. The linear variation method is employed to determine the corresponding energies by constructing a matrix representation of the Hamiltonian in the basis of the N-electron functions in Equation 2.21 and finding the eigenvalues. This method is called *full CI* and generates the exact energy of the ground-state and all excited states in the subspace spanned by the basis set. However, full CI calculations are rarely tractable in practice. A solution is to truncate Equation 2.21. For example, CISD denotes a calculation in which Equation 2.21 is truncated at the third term such that only single and double excitations are considered.

$$|\Phi_{CISD}\rangle = |\Psi_0\rangle + \sum_{ar} c_a^r |\Psi_a^r\rangle + \sum_{\substack{a<b \\ r<s}} c_{ab}^{rs} |\Psi_{ab}^{rs}\rangle \qquad (2.22)$$

This approach is somewhat justified as wave functions which differ by more than two spin orbitals do not mix directly (note that they mix *indirectly via* coupling with other wavefunctions).

A drawback of truncated CI is known as the size-consistency problem. Size-consistency means that the energy of a many particle system is proportional to the number of particles as $N \rightarrow \infty$. Although full CI and RHF theories are size-consistent, truncated CI is not, and the approximation becomes less accurate as the number of electrons increases.

2.3.2 *Coupled Cluster (CC) Methods*

Coupled cluster (CC) methods achieve size-consistency while sacrificing the variational property of the CI method (i.e., the resulting energy is not an upper bound to the exact energy). Consider the intermediate normalised CI wave function where we have ignored the single excitations due to symmetry, and the triple, quintuple etc. excitations which do not mix directly with $|\Psi_o\rangle$.

$$|\Phi_o\rangle = |\Psi_o\rangle + \sum_{\substack{a<b \\ r<s}} c_{ab}^{rs} |\Psi_{ab}^{rs}\rangle + \sum_{\substack{a<b<c<d \\ r<s<t<u}} c_{abcd}^{rstu} |\Psi_{abcd}^{rstu}\rangle + \ldots \tag{2.23}$$

One method of simplifying the Hamiltonian matrix is to consider each electron pair independently of all other electrons. This is the basis of the Independent Electron Pair Approximation (IEPA) which reduces the N-electron problem to N(N-1)/2 two-electron problems. The coupled cluster approximation extends the IEPA by incorporating coupling between the electron pairs. The coefficients of the quadruple excitations are expressed as products of the coefficients of the double excitations.

$$\begin{aligned} c_{abcd}^{rstu} &\cong c_{ab}^{rs} * c_{cd}^{tu} = c_{ab}^{rs} c_{cd}^{tu} - \langle c_{ab}^{rs} * c_{cd}^{tu} \rangle \\ &= c_{ab}^{rs} c_{cd}^{tu} - c_{ac}^{rs} c_{bd}^{tu} + c_{ad}^{rs} c_{bc}^{tu} - c_{ab}^{rt} c_{cd}^{su} + c_{ac}^{rt} c_{bd}^{su} - c_{ad}^{rt} c_{bc}^{su} \\ &+ c_{ab}^{ru} c_{cd}^{st} - c_{ac}^{ru} c_{bd}^{st} + c_{ad}^{ru} c_{bc}^{st} + c_{ab}^{tu} c_{cd}^{rs} - c_{ac}^{tu} c_{bd}^{rs} + c_{ad}^{tu} c_{bc}^{rs} \\ &- c_{ab}^{su} c_{cd}^{rt} + c_{ac}^{su} c_{bd}^{rt} - c_{ad}^{su} c_{bc}^{rt} + c_{ab}^{st} c_{cd}^{ru} - c_{ac}^{st} c_{bd}^{ru} + c_{ad}^{st} c_{bc}^{ru} \end{aligned} \tag{2.24}$$

That is, c_{abcd}^{rstu} is the sum of all possible products of double excitations which yield the particular quadruple excitation. Substituting this expression into Equation 2.23 and solving the eigenvalue problem

$$(\mathcal{H} - E_o)|\Phi_o\rangle = E_{corr}|\Phi_o\rangle \tag{2.25}$$

we obtain the coupled cluster doubles (CCD) equations (Equation 2.26) which only include the double excitations.

$$\sum_{\substack{c<d \\ t<u}} \left\langle \Psi_o \middle| \mathcal{H} \middle| \Psi_{cd}^{tu} \right\rangle c_{cd}^{tu} = E_{corr} \left| \Phi_o \right\rangle \tag{2.26a}$$

$$\left\langle \Psi_{ab}^{rs} \middle| \mathcal{H} \middle| \Psi_o \right\rangle + \sum_{\substack{c<d \\ t<u}} \left\langle \Psi_{ab}^{rs} \middle| \mathcal{H} - E_o \middle| \Psi_{cd}^{tu} \right\rangle c_{cd}^{tu} - \sum_{\substack{c<d \\ t<u}} \left\langle \Psi_o \middle| \mathcal{H} \middle| \Psi_{cd}^{tu} \right\rangle \left\langle c_{ab}^{rs} * c_{cd}^{tu} \right\rangle = 0 \tag{2.26b}$$

Although single excitations have little effect on the correlation energy, they are typically incorporated due to their small number. A popular approach is CCSD(T) which includes single and double excitations, and a perturbative treatment of triple excitations. Coupled cluster theory produces better results than CI or the many-body perturbation methods (which will be discussed in Section 2.3.3), however the computational demands are extensive. For example, CCSD(T) scales with N^7 (where N is the number of basis functions).

A more recent method involves adding quadratic terms to the truncated CI equation to achieve size-consistency.[104] This method is termed quadratic CI (QCI) and can be considered a simplified coupled cluster method that does not contain the cubic and quartic terms, thereby facilitating its implementation. However, the QCI wave function is not well defined and some dramatic failings have been identified.[105]

2.3.3 *Møller-Plesset Perturbation Theory*

Møller-Plesset methods improve the Hartree–Fock energy of an N-electron system by employing perturbation theory. The Hamiltonian is partitioned into the Hartree–Fock Hamiltonian, $\mathcal{H}_o$, and a perturbation term $\mathcal{V}$.

$$\mathcal{H} = \mathcal{H}_o + \mathcal{V} \tag{2.27}$$

where

$$\mathcal{V} = \sum_{i<j} r_{ij}^{-1} - \mathcal{V}^{HF} = \sum_{i<j} r_{ij}^{-1} - \sum_i v^{HF}(i) \tag{2.28}$$

The total energy of the system is given by

$$E_o = E_o^{(0)} + E_o^{(1)} + E_{corr} \cdots \tag{2.29}$$

where the first two terms (the zeroth and first-order perturbations) constitute the HF energy. The electron correlation energy (E_{corr}) can be expanded as a Taylor series

$$E_{corr} = E_o^{(2)} + E_o^{(3)} + \cdots \tag{2.30a}$$

where

$$E_o^{(2)} = \frac{1}{4}\sum_{abrs}\frac{\left|\left\langle \Psi_o \left| \sum_{i<j} r_{ij}^{-1} \right| \Psi_{ab}^{rs} \right\rangle\right|^2}{\varepsilon_a + \varepsilon_b - \varepsilon_r - \varepsilon_s} = \frac{1}{4}\sum_{abrs}\frac{|\langle ab \| rs \rangle|^2}{\varepsilon_a + \varepsilon_b - \varepsilon_r - \varepsilon_s} \tag{2.30b}$$

$$\begin{aligned} E_o^{(3)} = & \frac{1}{8}\sum_{abcdrs}\frac{\langle ab\|rs\rangle\langle cd\|ab\rangle\langle rs\|cd\rangle}{(\varepsilon_a + \varepsilon_b - \varepsilon_r - \varepsilon_s)(\varepsilon_c + \varepsilon_d - \varepsilon_r - \varepsilon_s)} \\ & + \frac{1}{8}\sum_{abrstu}\frac{\langle ab\|rs\rangle\langle rs\|tu\rangle\langle tu\|ab\rangle}{(\varepsilon_a + \varepsilon_b - \varepsilon_r - \varepsilon_s)(\varepsilon_a + \varepsilon_b - \varepsilon_t - \varepsilon_u)} \\ & + \sum_{abcrst}\frac{\langle ab\|rs\rangle\langle cs\|tb\rangle\langle rt\|ac\rangle}{(\varepsilon_a + \varepsilon_b - \varepsilon_r - \varepsilon_s)(\varepsilon_a + \varepsilon_c - \varepsilon_r - \varepsilon_t)} \end{aligned} \tag{3.30c}$$

Equation 2.30a is truncated after n-order perturbations to give nth-order Møller-Plesset perturbation theory, or MPn. Perturbation theory is size-consistent, but unfortunately does not improve monotonically as higher-order perturbations are added. Instead it tends to exhibit oscillatory behaviour. In particular, MP2 theory often generates parameters remarkably close to experiment, whereas MP3 is often poor, MP4 gets closer to experiment and so on.[105-108]

2.4 The Basis Set[109,110]

The linear expansion of the spatial molecular orbitals in Equation 2.13 is exact for any complete (ie. infinite) set of basis functions $\{\phi_\mu\}$. However, the set is restricted to be finite for tractability, and hence a careful choice of basis functions is crucial for an accurate calculation. There are two main types of basis function commonly in use: *Slater*-type functions and *Gaussian*-type functions. The latter are normally adopted for molecular calculations as the evaluation of two-electron integrals is less time consuming, although more functions are required to accurately represent a given orbital. A Gaussian-Type Orbital (GTO) has the form

$$g_p(\alpha_{p\mu}, \mathbf{r} - \mathbf{R}_p) = (2\alpha_{p\mu}/\pi)^{3/4} \, e^{-\alpha|\mathbf{r}-\mathbf{R}_p|^2} \tag{2.31}$$

For molecular calculations these functions (termed primitives) are normally grouped together in a fixed linear combination, or contraction.

$$\phi_\mu^{\mathrm{CGF}}(\mathbf{r} - \mathbf{R}_\mathrm{A}) = \sum_{p=1}^{L} d_{p\mu} \, g_p(\alpha_{p\mu}, \mathbf{r} - \mathbf{R}_p) \tag{2.32}$$

The primitives are typically derived from atomic self-consistent field (SCF) calculations using large sets of uncontracted gaussians. Contraction coefficients and exponents can then be obtained. Normally, a set of standard exponents optimised over a set of small molecules are used, as those resulting from atomic calculations are often inappropriate for the treatment of molecular orbitals.

One method of contraction is to fit a set of GTO's to a Slater-Type Orbital (STO) by minimising the sum of the squares of the deviations between the GTO and fitted STO. This method was used to derive the STO-LG series of basis sets, where L denotes the number of primitive gaussians per basis function.[111] These sets are called *minimal* (meaning that each atomic orbital is described by a single basis function) and cannot yield quantitatively reliable results.[109]

An improvement on the minimal basis set is to describe each valence orbital by two basis functions. Such basis sets are termed *split-valence* or double-ζ basis sets, and allow additional flexibility in the valence region which is important for the calculation of molecular properties. The optimum exponents for double-ζ basis sets are slightly above and below the optimal exponents of the minimal basis functions, such that the resulting functions are dubbed 'inner' and 'outer' functions. This effectively allows expansion or contraction of the orbitals in the molecular environment by varying the relative weights of the functions in the SCF calculation. For example, the K-LMG basis sets of Pople and co-workers[112] denote a set in which the core orbitals are described by a single contraction of K primitive gaussians, and the valence orbitals are described by an 'inner' contraction of L primitives, and an 'outer' contraction of M primitives.

Accurate molecular calculations require polarisation functions to allow for charge concentrations away from the nucleus, such as in a chemical bond. These are basis functions of higher angular momentum number. For example, d-type functions are usually added to the main group elements. Basis functions with very small exponents (diffuse functions) are often required, particularly for the description of Rydberg and other diffuse molecular orbitals. In this study we will use the notation of Pople and coworkers to define the basis set. For example, 6-31+G(2d,p) defines the 6-31G basis set augmented by two d-type polarisation functions and a set of diffuse s and p functions (indicated by the '+' sign) on the main group elements, and one p-type polarisation function on hydrogen. Recent work has indicated that determination of reliable reaction energies for organometallic systems requires the use of relatively large basis sets including at least one f-type polarisation function and a diffuse d function on the metal.

A "balanced" basis set is essential for meaningful results in molecular calculations. A basis set is said to be balanced when the relative error is approximately the same for all of the valence orbitals such that there is uniform emphasis over all of the electron distribution.[110] Associated with the use of an incomplete basis set is the *basis set superposition error* (BSSE). The definition of the BSSE is controversial and, consequently, so is the validity of the methodologies currently employed to estimate or to reduce the error.[113] The BSSE results from a non-physical lowering in energy of a system caused by the presence of additional neighbouring basis functions. For example, a molecular system may utilise the basis functions of a second molecule to compensate for inadequacies in its own basis set and thereby lower its energy. This can result in an apparent interaction between the two molecules, an effect particularly obvious in weakly bound systems. The most commonly used method for estimating the BSSE is the counterpoise correction scheme.[114,115] This involves a calculation of the two molecular fragments separately and in the vicinity of the basis functions of the other molecular fragments. The artificial lowering in energy resulting from the additional

basis functions can therefore be estimated. In principle, the BSSE can alternatively be eliminated by systematically augmenting the basis set in a balanced fashion such that a limit can be determined as the number of basis functions, $N \rightarrow \infty$ (and $BSSE \rightarrow 0$). However, application of this method is clearly unsuited to systems containing more than a few atoms due to high computational demands.

2.5 Density Functional Theory (DFT)

2.5.1 *The General Formalism*[116]

Conventional HF-based *ab initio* methods express the energy of a system of N-interacting electrons as a function of spin orbitals; $E=E[\chi]$. An alternative formalism which is rapidly growing in popularity, particularly for extended systems, is density functional theory (DFT). In contrast to the conventional methods, the energy of the N-electron system is written as a functional of the electron density at point **r**; $E=E[n(\mathbf{r})]$.

The theoretical foundation of DFT was developed by Hohenberg and Kohn,[117] and is established by two fundamental theorems:

(1) The external potential, $V(\mathbf{r})$, of a non-degenerate ground-state wave function, Ψ, is defined uniquely by the electron density $n(\mathbf{r})$.

(2) For a given $V(\mathbf{r})$ the non-degenerate ground-state energy is also a unique function of $n(\mathbf{r})$.

From the Adiabatic approximation, the electronic Hamiltonian can be partitioned as

$$\mathcal{H}=T+U+V_{ext} \tag{2.33}$$

where T denotes the kinetic energy operator of electrons, and U and V_{ext} describe the electron-electron and electron-nuclear interactions respectively. V_{ext} is considered external to the system of electrons. Hence, the ground-state energy can be expressed by Equation 2.34.

$$\begin{aligned} E[n] &= \min\langle \Psi_n | \mathcal{H} | \Psi_n \rangle \\ &= \min\langle \Psi_n | T + U + V_{ext} | \Psi_n \rangle \\ &= F[n] + \min\langle \Psi_n | V_{ext} | \Psi_n \rangle \end{aligned} \tag{2.34}$$

It can be further shown that the electron-electron interaction energy, $U[n] = \min\langle \Psi_n | U | \Psi_n \rangle$, may be written as

$$U[n] = E_C[n] + E_{XC}[n] \tag{2.35}$$

so that

$$F[n] = T[n] + E_C[n] + E_{XC}[n] \tag{2.36}$$

where $E_C[n]$ denotes the classical Coulomb-Hartree energy, and $E_{XC}[n]$ accounts for the explicit many-body effects which include correlation beyond the Hartree approximation due to the Pauli Exclusion Principle, and coulomb correlation.

Note that the above equations can be solved iteratively in a manner similar to that of conventional *ab initio* methods. Although it has been shown that the generation of accurate energetics often requires density functional-optimised basis sets, the use of conventional basis sets is common and yields reasonable geometries.

In order to determine the ground-state energy, the form of the Hohenberg-Kohn functional, F[n], is required. However, as this functional includes complicated many-body effects in $E_{XC}[n]$, its exact form is not known and must be approximated.

2.5.2 *Approximations to E_{XC}*

The correct form of the Exchange-Correlation energy, $E_{XC}[n]$, involves integrals of the density functions from different space points, and is therefore nonlocal. For an interacting system, E_{XC} can be exactly expressed by

$$E_{XC}[n] = \frac{1}{2} \int\int d\mathbf{r}\, d\mathbf{r}'\, n(\mathbf{r}) V(\mathbf{r} - \mathbf{r}') n_{XC}(\mathbf{r}, \mathbf{r}') \tag{2.37}$$

where $n_{XC}(\mathbf{r},\mathbf{r}') = n(\mathbf{r}')\int_0^1 d\lambda[g_\lambda(\mathbf{r},\mathbf{r}') - 1]$ is a conditional particle density at $\mathbf{r}$ given the presence of a particle at $\mathbf{r}'$, and is referred to as the exchange-correlation (XC) hole. $g_\lambda(\mathbf{r},\mathbf{r}')$ is the pair correlation functional of the system of density $n(\mathbf{r})$ and coulomb interaction $\lambda V(\mathbf{r})$. The spherical symmetry of the coulomb potential allows the XC energy to be expressed in terms of the spherical average of the XC hole. This has important consequences with respect to the success of various approximations to the XC energy and will be discussed below.

The simplest approximation to the XC functional is the *local density approximation (LDA).* In this formalism, the electron density is assumed to vary slowly in space such that the system can be divided into discrete 'cells' of constant electron density. $E_{XC}[n]$ can then be obtained by summation over the cells or, in the continuous limit, by integration:

$$E_{XC}^{LDA}[n] = \int d\mathbf{r}\, n(\mathbf{r})\varepsilon_{XC}[n(\mathbf{r})] \tag{2.38}$$

where $\varepsilon_{XC}[n(\mathbf{r})]$ represents the exchange-correlation energy per particle of a strictly homogeneous system of density n.

The remarkable success of the LDA is mainly due to a cancellation of errors, and can be attributed to the independence of the exact XC energy (Equation 2.37) to the non-spherical parts of n_{XC}. Although the description of the XC hole may be poorly represented by the LDA, its spherical average is surprisingly good. Experience has demonstrated that LDA performs better than HF-based methods with very few exceptions.[118] Geometries, physical trends and charge densities are typically well reproduced. Binding energies are often reliable with the exception of some s-d bonded systems. However, total energies are usually poor due to near-degeneracy effects and non-spherical, rapidly varying densities. The prediction of reaction energetics has also been shown to be unreliable for a number of organometallic potential energy surfaces (PES's).[119]

Gradient Corrections[118]

An improvement to the LDA is to allow the energy to depend also on the various gradients of the density, $\frac{\delta V_{XC}(\mathbf{r})}{\delta n(\mathbf{r})}$, by the addition of so-called gradient corrections to the LDA exchange-correlation energy. As the main function of gradient corrections is to include some nonlocal effects in the calculation, they are also called *nonlocal corrections.* A drawback of such methods is that, unlike HF-based methods, there is no logical scheme by which the result can be systematically improved by the inclusion of additional terms.

Consider a variation in the external potential, δw, then the change in ground-state density is defined as

$$\delta n = \chi \delta w \tag{2.39}$$

where $\chi(\mathbf{r},\mathbf{r}')$ is the static linear density response function of the system. It can be shown that

$$\chi = \chi_o + \chi_o(V + K_{XC})\chi \tag{2.40}$$

where χ_o is the static linear response function for a non-interacting system, and we have introduced the Kernel, K_{XC}.

$$K_{XC}(\mathbf{r},\mathbf{r}') = \frac{\delta V_{XC}(\mathbf{r})}{\delta n(\mathbf{r}')} = \frac{\delta^2 E_{XC}[n]}{\delta n(\mathbf{r})\delta n(\mathbf{r}')} \tag{2.41}$$

Therefore, χ for the interacting system can be determined given the second derivative of the XC energy, K_{XC}, and vice versa. A gradient expansion for E_{XC} can now be constructed by determining the change in E_{XC} when the homogeneous electron density is perturbed by δn by a weak external potential. To second-order:

$$\begin{aligned} E_{XC}[n] &= E_{XC}[n_o] + \int d\mathbf{r} \frac{\delta E_{XC}}{\delta n} \delta n + \tfrac{1}{2} \int d\mathbf{r} \delta n \frac{\delta^2 E_{XC}}{\delta n \delta n'} \delta n' \\ &= \int d\mathbf{r}\, n_o\, \varepsilon_{XC}(n_o) + \int d\mathbf{r} \mu_{XC}(n_o)\delta n + \tfrac{1}{2} \int d\mathbf{r} \delta n K_{XC} \delta n' \\ &= E_{XC}^{LDA}[n] + \tfrac{1}{2} \int d\mathbf{r} \delta n \{K_{XC} - \mu'_{XC} \delta(\mathbf{r} - \mathbf{r}')\} \delta n' \end{aligned} \tag{2.42}$$

where $\mu_{XC} = \frac{\partial(n\varepsilon_{XC})}{\partial n}$, and the subscript 'o' defines the homogeneous limit for which the LSDA is exact. Taking the Fourier transform of Equation 2.42 we get

$$E_{XC}[n] = E_{XC}^{LDA}[n] + \tfrac{1}{2}\int \frac{d^3\mathbf{q}}{(2\pi)^3}\{K_{XC}(\mathbf{q}) - K_{XC}(0)\}\left|\delta n_{\mathbf{q}}\right|^2 \qquad (2.43)$$

where $K_{XC}(0) = \frac{\partial \mu_{XC}}{\partial n}$ from the compressibility sum rule of the electron gas. If it is further assumed that the Fourier components of the perturbed density are insignificant at large $\mathbf{q}$, such that K_{XC} can be expanded as a small-$\mathbf{q}$ Taylor series, then in real space

$$E_{XC}[n] = E_{XC}^{LDA}[n] + \int B_{XC}(n_o)|\nabla n|^2 \, d^3\mathbf{r} \qquad (2.44)$$

where B_{XC} is the second-order coefficient of the Taylor expansion of K_{XC}.

A range of different gradient corrections have appeared in the literature in the past decade. Langreth, Perdew, Mehl and Hu developed a gradient correction based on the Random Phase Approximation (RPA) denoted the LPM functional.[120,121] To minimise computational cost, and to avoid overestimation of the XC energy at small $\mathbf{q}$, they proposed the full inclusion of gradient corrections down to a cut-off $\mathbf{q}$ below which the corrections are neglected. This yielded the expression:

$$E_{XC}^{LPM}[n] = E_{XC}^{LDA}[n] + a\int [n(\mathbf{r})]^{-4/3}[\nabla n(\mathbf{r})]^2\{e^{-F} - \tfrac{7}{18}\}d^3\mathbf{r} \qquad (2.45)$$

where

$$F^{LPM} = b\cdot|\nabla n(\mathbf{r})|\cdot[n(\mathbf{r})]^{-7/6} \qquad (2.46)$$

$a = \frac{\pi}{8}(3\pi^2)^{-4/3}$; $b = (9\pi)^{1/6} f$, and f is a 'fudge factor', the choice of which is relatively insensitive between the range 0.15-0.17.

In general, the LDA is valid when

$$\frac{|\nabla n(\mathbf{r})|}{k_F(\mathbf{r})n(\mathbf{r})} << 6 \qquad (2.47a)$$

and gradient corrections are required when

$$\frac{|\nabla n(\mathbf{r})|}{k_{TF}(\mathbf{r})n(\mathbf{r})} << 1 \qquad (2.47b)$$

where $k_F(\mathbf{r}) = \sqrt[3]{3\pi^2 n(\mathbf{r})}$ (the local Fermi momentum) and $k_{TF}(\mathbf{r}) = 2\sqrt{k_F(\mathbf{r})/\pi}$ (the Thomas-Fermi wave vector).

The largest errors in the LPM scheme are associated with an incorrect treatment of exchange. Perdew[122] developed a gradient correction for exchange only which incorporated a certain degree of parameterisation to simplify its use

$$E_{XC}^{PW}[n] = A_X \int [n(\mathbf{r})]^{4/3} F_X^{PW}(s) d^3\mathbf{r} \qquad (2.48)$$

where $A_X = -\frac{3}{4\pi}(3\pi^2)^{1/3}$ (a constant determined by the electron gas limit), and

$$F_X^{PW}(s) = (1 + \frac{as^2}{m} + bs^4 + cs^6)^m \qquad (2.49)$$

a=7/81; b=14; c=1/5; m=1/15 and s is the dimensionless density gradient, $s = \frac{|\nabla n(\mathbf{r})|}{2k_F(\mathbf{r})n(\mathbf{r})}$. Note that $F_X^{PW}(s) = 1$ corresponds to the LDA result for exchange only. Perdew then removed the exchange contribution from the LPM scheme and rescaled the formula to obtain a nonlocal correction for the correlation energy (denoted P86). The latter functional significantly reduced the overbinding associated with LDA calculations, but has a tendency to over-correct these errors particularly for weakly bound systems. More recently, Perdew and Wang modified Equation 2.49 to give the correct limits at large and small s, yielding the functional denoted PW91.[123]

An alternative method was employed by Becke.[124-126] He designed a functional based on the electron density, its gradients and different integrals which incorporates a number of parameters. These parameters were selected such that the experimental properties based on exchange and correlation were reproduced for a range of different systems. The form of these corrections is identical to Equation 2.48. Becke focused on the exchange energy, noting that gradient

corrections become insignificant at large density gradients, and later introduced modifications to yield the correct contributions to the energy at large radii. The resulting functional (Equation 2.50) is denoted Becke88.[126]

$$F_X^{B88}(s) = 1 + \frac{\beta s^2}{1 + (2.25/\pi)\beta s \, \mathrm{arsinh}(\gamma s)} \tag{2.50}$$

where $\gamma = 2(6\pi^2)^{1/3}$, and β is the only adjustable parameter.

The resulting exchange energy exhibits the correct inverse dependence on $\mathbf{r}$ at large distances.

The Becke88 functional was found to produce poor results for electron-nonconserving processes, such as ionisation, unless used in conjunction with a nonlocal correction for correlation. A commonly used gradient correction for correlation energy is that of Lee, Yang and Parr (denoted "LYP").[127] This was developed by conversion of the Colle-Salvetti formula for correlation energy based on the HF second-order electron density matrix into a functional based on the local kinetic energy density.

$$E_C^{LYP} = -a\int \frac{1}{1+dn^{-1/3}}\{n + bn^{-2/3}[C_F - 2t_W + (\frac{1}{9}t_W + \frac{1}{18}\nabla^2 n)]e^{-cn^{-1/3}}\}d\mathbf{r} \tag{2.51}$$

where $t_W(\mathbf{r}) = \frac{1}{8}\frac{|\nabla n(\mathbf{r})|^2}{n(\mathbf{r})} - \frac{1}{8}\nabla^2 n(\mathbf{r})$, $C_F = \frac{3}{10}(3\pi^2)^{2/3}$, a=0.049, b=0.132, c=0.2533, and d=0.349.

As exchange energies are considerably larger than correlation energies, it appears logical to treat exchange exactly as do HF-based methods. However, part of the success of the above functionals is attributed to a cancellation of error associated with the combined treatment of exchange and correlation, such that attempts to treat exchange separately have been unsuccessful. Becke has developed a so-called 'Hybrid' method (B3) in which half of the exchange contribution is treated exactly and the other half is recovered with the correlation energy through generalised gradient approximations.[128]

$$E_{XC}^{B3}[n] = E_{XC}^{LSDA}[n] + a_o \cdot (E_X^{HF}[n] - E_X^{LSDA}[n]) + a_X \cdot E_X^{B88} + a_C E_C \tag{2.53}$$

where a_0, a_X, and a_C are semi-empirical coefficients determined by fitting the functional to the G1 data base,[129,130] E_X^{B88} is the Becke88 gradient correction, E_C is a gradient correction for correlation such as PW91, and E_X is the exact exchange energy functional (the HF exchange energy expression determined using density functional orbitals).

The reliability of the PW91, Becke88, B3 and LYP gradient corrections have been assessed in a number of studies.[119,131-136] They display an accuracy approaching that of CI-type *ab initio* methods for a wide range of molecules including the G2[137] data base. However, their comparable performance is not consistent and it is generally recommended that a range of functionals be compared when studying new systems in order to select an appropriate method. Calibrative DFT studies on organometallic systems have identified a number of errors inherent to the density functionals. LDA methods tend to overestimate metal-ligand binding energies (by up to 100%) resulting in short metal-ligand bond lengths.[134,138] This error is slightly overcorrected by the inclusion of nonlocal corrections. In contrast, the LDA description of metal-carbonyl π back-donation is superior to nonlocal LDA or CCSD(T).[134] DFT is typically not accurate enough to distinguish between low-lying electronic states, such that the use of spin-unrestricted wavefunctions is suggested. In general, LDA and gradient-corrected LDA methods are not appropriate for atoms or small molecules which are strongly homogeneous.[118] Weakly bound systems, such as those involving hydrogen-bonding or van der Waals interactions, are also poorly represented. A consequence of defining the energy as a functional of the one-electron density is that there is no formal way to describe proper spin or excited states. This may limit the applicability of DFT to open-shell transition metal complexes.

Although the B3 functional has been reported to often correct a number of the failures of other density functionals,[139-141] inaccuracies persist[136,142] and further benchmark calculations are required. In general, the results are considerably more sensitive to the basis set than those generated by other density

functionals, such that parameters generated using the B3 functional with small to medium basis sets are often of lower quality.[135]

2.6 Relativistic Effects and Effective Core Potentials (ECP's)

There are two main difficulties associated with the treatment of molecules containing heavy atoms; the large number of two electron integrals to be evaluated and the increased importance of relativistic effects. For example, the number of two-electron integrals scales with N^4, N^5 and N^7 for RHF, MP2 and CCSD(T) methods respectively, where N is the number of basis functions.

One method in common use which reduces the number of two-electron integrals in the calculation is to replace the chemically-inert core electrons with a linear combination of gaussian functions called a pseudopotential. There are two types of pseudopotential: the *ab initio* model potential (AIMP) in which the valence orbitals retain the correct nodal structure, and the effective core potential (ECP) in which the valence orbitals are "smoothed out" in the core region. In practice, there is little difference in reliability between the two methods, however smaller valence basis sets may be used with ECP's. The parameters for the ECP are typically derived from numerical all-electron calculations on the chemically relevant atomic ion by a fit procedure. The ECP's of Hay and Wadt were generated on an analytical grid by inverting the Fock equations for pseudo orbitals derived from numerical atomic wave functions. The numerically tabulated potentials are then fitted with analytical gaussian functions by a least-squares fit. As the least-squares fitting procedure may require a large number of gaussians, Stevens *et al.* instead generated compact analytic expansions to yield "compact ECP's".[143]

Relativistic effects arise due to the high velocity of electrons close to the nucleus which is directly proportional to the nuclear charge (or atomic number).[144,145] They become important for the late first-row transition metals, their neglect resulting in overestimated bond lengths and low binding energies. The

dominant relativistic effects are described by the mass-velocity, Darwin and spin-orbit coupling terms. The mass-velocity term accounts for the increase in effective mass of an electron as it approaches the speed of light. A consequence of this is a contraction of the core orbitals due to the inverse relation between the effective mass of an electron and its orbital extent. This indirectly affects the valence region, generally contracting the s and p orbitals, while the d and f orbitals become more diffuse due to increased screening of the nuclear charge. The Darwin term corrects the point charge description of the electron to a finite charge distribution. This results in a reduction in nuclear-electron attractions and electron-electron repulsions. The spin-orbit term describes the coupling between the electron spin and orbital angular momentum, an effect which is less important and is typically averaged out.

If relativistic effects are included in the underlying all-electron calculation (by employing the Dirac-Hartree–Fock equation) the resulting ECP is termed *quasirelativistic*. This relies on the assumption that the major relativistic effects can be included in a calculation as a constant which is independent of the molecular environment of the atom. The ECP's of Hay and Wadt[146-148] and Stevens *et al.*[143] incorporate the Darwin and mass-velocity terms for the second- and third-row transition metals (and first-row transition metals in the case of the ECP's by Stevens *et al.*). Dolg and coworkers have introduced a series of similar relativistic ECP's (RECP's) which can be used with a spin-orbit coupling perturbation.[149,150]

The applicability of various ECP's to organometallic systems has been investigated by a number of groups.[99,151] Experience has shown that the error associated with the replacement of the core electrons by a "well-parameterised" potential function is insignificant compared to the error introduced by basis set truncation and the incomplete recovery of electron correlation. The most important consideration is the definition of the core region (which orbitals should be replaced by the pseudopotential) and the flexibility of the valence basis set. As the orbital extent of the outer-core s and p orbitals of transition metals is similar to that of the

valence d orbitals, the former should be included in the valence space. ECP's of this type have been developed by Hay and Wadt,[148] Stevens *et al.*[143] and Dolg *et al.*[149,150] and are referred to as *small-core* ECP's. *Large-core* ECP's describe those in which only the valence orbitals are explicitly considered.[146]

2.7 Geometry Optimisation

One of the most common uses of theoretical calculations to date has been the generation of structural parameters. The methods discussed in the previous sections produce an energy which is a function of internuclear coordinates, R_{AB} (refer to Equation 2.2). The dependence of the energy on the nuclear coordinates is described by a (3N-6)-dimensional *potential energy surface* (PES) (where 3N-6 is the number of degrees of freedom of a non-linear system of N atoms). A stationary point on the PES is defined as a point at which the energy gradient in Equation 2.53 equals zero.

$$f_i = \frac{\partial E(\mathbf{x}_e)}{\partial x_i} \quad i = 1,2,...,(3N-6) \tag{2.53}$$

Consider a small variation, $\mathbf{q}$, in the nuclear coordinates $\mathbf{x}^\dagger=(x_1,x_2,...,x_{3N})$, such that the new coordinates $\mathbf{x}_1=\mathbf{x}+\mathbf{q}$. The energy, E[**x**], may be expressed as a Taylor expansion

$$E(\mathbf{x}_1) = E(\mathbf{x}) + \mathbf{q}^\dagger\mathbf{f}(\mathbf{x}) + \frac{1}{2}\mathbf{q}^\dagger\mathbf{H}(\mathbf{x})\mathbf{q} + ... \tag{2.54}$$

where the Hessian $H_{ij} = \dfrac{\partial E(\mathbf{x})}{\partial x_i \partial x_j}$

Close to a stationary point Equation 2.54 may be approximated by the first three terms. Therefore, if **x** corresponds to a stationary point (for which $\mathbf{f}(\mathbf{x}_e)=0$) and the Hessian is non-singular, it can be shown that

$$\mathbf{q} = -\mathbf{H}^{-1}(\mathbf{x}_1)\mathbf{f}(\mathbf{x}_1) \tag{2.55}$$

$\mathbf{x}_e$ can be determined provided $\mathbf{x}_1$ is a point close enough on the PES.

We are typically interested in stationary points corresponding to equilibrium structures (local minima) for which all of the eigenvalues of the Hessian matrix are positive, or transition structures (saddle points) for which one (and only one) of the eigenvalues of the Hessian is negative. There are a variety of algorithms currently available for locating stationary points on the PES ranging from methods without gradients to those which analytically generate gradients and second derivatives. As analytic second derivatives for pseudopotentials were not available to us, PES searches in the present work were performed using analytic gradients and numerically estimated second derivatives. These are quasi-Newton update procedures.

An optimisation requires an initial input "guess" geometry defined by the user. The gradient at this geometry indicates the direction along the PES in which the energy decreases most rapidly (the direction of steepest descent) and the nuclear coordinates are subsequently varied in this direction by an amount determined by the estimated Hessian. The energy and gradients at the new coordinates are calculated such that the PES is traced step-wise towards a local minimum. Clearly the nature of the local minimum and the efficiency of the optimisation (the number of iterations required to reach a stationary point) will be highly dependent on the initial "guess". The choice of coordinate system for optimisations also has a bearing on the efficiency of the calculation and has been controversial for a number of years. Internal coordinates (or Z-matrices) have traditionally been employed. However, Cartesian coordinates or mixed internal and Cartesian coordinates have been reported to be superior in some cases.[152,153] More recently, Pulay[154-156] and Baker[157] have advocated the use of redundant internal coordinate systems which is now integrated into the GAUSSIAN 94 suite of programs.[158]

2.8 Computational Methods Strategy

All of the calculations presented were performed using GAUSSIAN 92 version F[159] (which includes the DFT package) or GAUSSIAN 94 revision B.3[158] on Sparc 690 and SGI R4400 workstations, Fujitsu VP2200/10, Fujitsu VPP400 and CRAY J90 high performance computers. Full geometry optimisations were carried out using the Berny gradient optimisation algorithm, or, in the case of calculations including f-functions or high levels of theory, the Fletcher-Powell energy-based method. For systems with 50 variables or less, transition structures were located using the eigenvector-following optimisation method[160,161] which updates the Hessian at each step of the optimisation. Transition structures with more than 50 variables were located using the Berny optimisation algorithm. The PES was followed "downhill" by gradient optimisation on either side of the saddle point to the intermediates.

Three transition metal pseudopotentials were used: Hay and Wadt's large- and small-core RECP's (denoted LANL1[146] and LANL2[148] respectively), and the small-core RECP of Stevens *et al.*[143] (SKBJ). For the calibrative studies (in Chapters 3 and 4) a range of different metal valence basis sets were used in conjunction with various ligand basis sets which will be described in the appropriate chapters.

Density functional calculations were carried out using the DFT algorithm incorporated in GAUSSIAN 92 and GAUSSIAN 94 with and without nonlocal corrections. The local density functional employed the Slater exchange functional[162] with the correlation functional of Vosko, Wilk and Nusair[163] (S-VWN). Nonlocal corrections were included using Becke's 1988 exchange functional[126] with the correlation functional of Perdew and Wang[123] (denoted B-PW91) or the correlation functional of Lee, Yang and Parr[127] (denoted B-LYP). The three-term hybrid functional of Becke[128] was also examined with the Lee, Yang and Parr correlation functional (denoted B3-LYP). For all DFT calculations

an unpruned fine (75,302) grid was employed for integration (75 radial shells around each atom, and 302 angular points in each shell). The same RECP's and basis sets were used for DFT calculations as for the conventional *ab initio* calculations for convenient comparison.[133]

In Chapters 5 through to 8, the PES was probed at the RHF level of theory using the LANL1 RECP. The corresponding minimal valence basis set (3s/3p/4d)/[3/3/4][146] was used for the metal valence, and STO-3G on the main group elements. The geometries and force constants calculated at this level of theory were used as starting points for high level calculations. As analytic second derivatives for RECP's were not available to us,[164] frequency calculations were performed (numerically) only at this lowest level of theory. These calculations confirmed the correct nature of each of the stationary points on the PES. Improved geometries were obtained using the B-LYP functional and, in some cases, MP2 methods. For correlated optimisations, the LANL2 RECP was employed for the metal with the (8s/6p/4d)/[341/321/31][148] contraction for the valence region. The 6-31G(d) basis set was adopted for the main group elements. This RECP and basis set will be referred to as "basis set A". Natural bond orbital (NBO)[165,166] and natural population analyses (NPA)[167,168] were performed on selected stationary points at MP2/[basis set A]. These calculations included a search for highly delocalised structures,[169] and the 5s and 5p orbitals are defined as Rydberg orbitals (default in GAUSSIAN 94).

For further refined energies, single-point MP2 calculations were performed employing the LANL2 RECP with the (9s/6p/5d/4f)/[33111/3111/2111/211] valence basis set of Bauschlicher *et al.*[170] and 6-311+G(2d,p) on the main group elements. This basis set will be denoted "basis set B".

In general, C_S symmetry was adopted for the three- and four-coordinate species, and C_1 symmetry for the five-coordinate intermediates and transition structures.

The following notation will be employed throughout this study to define the RECP, basis set and level of theory:

level of theory/metal RECP and basis set:ligand basis set

For example, MP2/LANL2:6-31G(d) describes an MP2 calculation employing the LANL2 RECP on the metal and the 6-31G(d) basis set on the ligands. Unless otherwise stated the metal valence basis set for the LANL2 RECP is the valence double-ζ basis set incorporated in GAUSSIAN 92. For single-point calculations '//' will be used to mean 'at the structure optimised with'. For instance, MP2/LANL2:6-31G(d)//B-LYP/LANL2:6-31G(d) indicates that a single-point MP2 calculation has been performed using the B-LYP geometry, both with the LANL2 RECP and 6-31G(d) basis set.

2.9 Conclusions

As a consequence of the rapid advances in computational techniques, significant contribution from the theoretical modelling of transition metal complexes and their reactions is becoming possible. However, the area of computational organometallic chemistry is relatively new due to the difficulty associated with modelling transition metals. Until the last decade, organometallic calculations were limited to *ab initio* calculations on systems containing only a few atoms, or semi-empirical methods on well-parameterised groups of complexes. The development of pseudopotentials for transition metals has significantly reduced the computational expense involved in *ab initio* calculations of these complexes. In addition, a range of density functional methods appear to offer viable alternatives to conventional *ab initio* methods. Given the variety of methods available, and the relative lack of extensive testing, a theoretical study of organometallic reactions must be preceded by calibrative studies.

The reliability of a particular theoretical method is dependent on the organometallic system. For example, a number of studies have demonstrated that

metal-ligand bonds with significant π-contribution require correlated levels of theory for a correct description of the π-interaction.[171-175] The oxidation state of the transition metal is also important. Complexes of transition metals in low oxidation states require higher levels of theory and larger basis sets than complexes of high oxidation state metals to obtain results of the same quality.[176]

The accuracy of calculations are normally judged by one of two methods:

(i) comparison to experimental data

or (ii) by investigating the convergence of the generated parameters with increasing computational sophistication.

As structural parameters and reaction energies for the systems considered in the present study are scarce, the benchmark calculations performed in Chapters 3 and 4 rely heavily on the second method of assessment. This work provides a basis from which to select a theoretical method that offers an appropriate compromise between accuracy and computational demands, which can then be utilised in the study of reaction mechanisms (Chapters 5-8). It is important to note that the calculations performed in this study represent the molecules isolated in a vacuum. The majority of experimental reactions considered are performed in chloroform which is generally regarded as non-coordinating. Therefore, the neglect of solvent effects is not considered to affect the qualitative conclusions.

CHAPTER 3

Evaluation of the Available Theoretical Methods

(Frankcombe, K. E.; Cavell, K. J.; Yates, B. F.; Knott, R. B.

J. Phys. Chem., **1995**, *99*, 14316.)

Chapter 3

Evaluation of the Available Theoretical Methods

3.1 Introduction

In the following chapters we will discuss calculations of medium-sized three-, four-, and five-coordinate model palladium(II) complexes. In the initial stages of the investigation of these systems[177] it was observed that metal-ligand bonds which involve π back-donation (in particular Pd-P and Pd-CO bonds) are highly dependent on the basis set and level of theory. This has been previously reported by a number of research groups.[171-175] Furthermore, assessment of the reliability of calculated Pd-P and Pd-CO bond lengths and energies is made particularly difficult by the lack of experimental information against which theory can be compared.

In the absence of experimental benchmarks, theoretical methods are often tested by studying the convergence of calculated parameters with increasing levels of theory. For model systems of experimental interest, the use of high levels of theory or large basis sets is currently limited due to the sharp rise in computational requirements with the number of atoms or basis functions. The objective of the work presented in this chapter was to obtain an estimation of the quality of the metal-ligand bond lengths and reaction energies generated by various theoretical methods employing the fragments PdCO and $PdPH_3$. The use of these simple molecules has allowed the results generated by methods tractable for larger systems to be compared to those obtained employing both large basis sets and including high levels of electron correlation.

The bonding in PdCO has been theoretically investigated by a number of research groups over the last ten years.[171,173,178-181] Possibly the most elegant of

these studies is one by Siegbahn and coworkers[178] which looked at the metal-ligand bond length and dissociation energy using relativistic *ab initio* methods. Large all-electron basis sets were employed and geometry optimisations were performed at SCF, CASSCF, multi-reference contracted CI (CCI) and modified CPF (MCPF). The importance of relativistic effects and electron correlation on the bonding properties was illustrated. Relatively few such studies have been performed on $PdPH_3$. A recent paper by Pacchioni and Bagus looked at the nature of the Pd-P bond with a variety of different phosphines.[172] This *ab initio* study adopted the small-core RECP of Hay and Wadt[148] for palladium and looked at the effect of adding d functions to phosphorus and the inclusion of electron correlation. Both polarisation functions and electron correlation were found to be necessary in order to correctly describe the metal-ligand π back-donation. It was also shown that the phosphorus d functions act as polarisation functions which can combine with the phosphine antibonding orbitals to form hybridised π-acceptor orbitals, rather than acting as orbitals involved directly with the bonding.

Against this background, the present calculations have been performed using three different RECP's for palladium.[143,146,148] The effects of dynamic electron correlation were examined using MPn (n=2-4), CISD, QCISD(T), CCSD and CCSD(T) methods. Different basis sets were studied at both RHF and correlated levels, including different basis set contractions, polarisation functions and diffuse functions. A range of density functionals were also investigated using the same RECP's and basis sets. The main emphasis of the investigation was on the metal-ligand bond lengths and the reaction energy for the model reaction:

$$Pd\text{-}PH_3 + CO \longrightarrow PH_3 + Pd\text{-}CO.$$

The metal-ligand bond lengths (Å) and reaction energies (kJ/mol) generated at each level of theory and basis set are given in Tables 3.1-3.3, 3.5 and 3.6. Refer to Appendix 1 for the complete set of geometrical data and total energies.

3.2 Additional Computational Methods

In addition to the computational methods outlined in Section 2.8, the following basis sets and levels of theory were employed in the current chapter. To investigate the influence of the basis set on the metal-ligand bonds a range of different metal valence basis sets were used in conjunction with various ligand basis sets at the RHF and MP2 levels. The different basis sets and contractions are listed in Tables 3.1 to 3.3. At the RHF level, a range of small basis sets were studied from the minimal basis LANL1MB as implemented in GAUSSIAN 92, which employs the fully contracted (3s/3p/4d) valence basis set for palladium,[146] an ECP for phosphorus[147] and STO-3G for the first-row atoms, to the double-ζ quality metal valence basis sets given by Hay and Wadt[146,148] or Stevens *et al.*[143] with the 6-31G(d) basis set on the ligands.

At the MP2 level, the palladium valence basis set of Hay and Wadt was augmented with an energy-optimised diffuse d function (0.0618) which was optimised in the present study at CCSD(T) for the $4d^{10}$ state of the palladium atom. An f-type polarisation function was added (exponent 1.472[182]) and was split into two functions (exponents 2.944 and 0.736) and three functions (4.416, 1.472 and 0.4907). The valence basis set was also systematically uncontracted by splitting off the outermost s, p, and d functions to generate basis sets of triple-ζ quality in the valence region (5s, 5p and 4d atomic orbitals) and a double-ζ description of the outer core orbitals (4s and 4p). These extensions are summarised in Table 3.4. The (9s/6p/5d/4f)/[33111/3111/2111/211] valence basis set of Bauschlicher *et al.*[170] developed for use with the Hay and Wadt small-core RECP was employed as a comparison (basis sets 24-26 in Table 3.3). The influence on the reaction energy of uncontracting the four f-type polarisation functions, and adding diffuse functions to the ligand basis set was also investigated. Ligand basis sets from 3-21G (with a set of d-type polarisation functions on phosphorus) to

6-311G(3df,p) were used for geometry optimisations and up to 6-311+G(2d,p) for the single-point calculations of the reaction energy. For comparison, the fully optimised triple-ζ plus polarisation basis sets of Ahlrichs *et al.*[183] (denoted TZ2P) were employed on the ligands. Some of these basis sets were also employed for density functional calculations (refer to Table 3.5).

Dynamic electron correlation was introduced through the Møller-Plesset methods (MPn, n=2-4), CISD, QCISD(T), CCSD and CCSD(T). The core electrons were frozen at all correlated levels. BSSE's were ignored as it is thought that at the correlated levels of theory the basis sets used were flexible enough and the reaction energies large enough to minimise these errors.

Unlike many previous studies of these systems,[171,178,179] all geometrical parameters in the molecules were optimised. Only the metal-ligand bond lengths are discussed here in detail as the bond lengths between ligand atoms and the bond angles did not change significantly with varying levels of theory, basis sets or pseudopotentials.

C_{3V} and C_{∞} symmetries were assumed for $PdPH_3$ and PdCO, respectively. The latter symmetry allocation was tested by relaxing the symmetry constraints to C_S symmetry.

Table 3.1: *Effects of the basis set and pseudopotential at the RHF level.*

Basis set			Pd-PH_3 Bond length (Å)		Pd-CO Bond length (Å)		Reaction energy (kJ/mol)	
Metal valence[a]	Ligand C,O,H	Ligand P	LANL1	LANL2	LANL1	LANL2	LANL1	LANL2
minimal	STO-3G	minimal[b]	2.741	2.536	1.960	1.954	-169	-137
minimal	STO-3G	STO-3G	2.315	2.364	1.960	1.954	-2.16	-5.12
double-ζ	D95V	double-ζ[b]	2.491	2.524	1.958	2.014	-44.2	-25.7
double-ζ	3-21G	3-21G	2.467	2.522	2.002	2.072	-32.0	-25.7
double-ζ	3-21G	3-21G(d)	2.304	2.516	2.002	2.072	-15.5	-13.7
double-ζ	6-31G	6-31G	2.453	2.383	1.935	2.022	-36.3	-19.6
double-ζ	6-31G(d)	6-31G(d)	2.311	2.381	1.943	2.036	-13.1	-3.37
All Electron[c]			2.01 Å (Non-Relativistic: 2.18 Å)					

[a] As implemented in GAUSSIAN 92: minimal refers to the contraction (3s/3p/4d)/[3/3/4] and double-ζ to (3s/3p/4d)/[21/21/31] for the LANL1 pseudopotential[146] and to (8s/6p/4d)/[35/33/4] and (8s/6p/4d)/[341/321/31] respectively for the LANL2 pseudopotential.[148]

[b] The phosphorus core orbitals are represented by a pseudopotential[147] as implemented in GAUSSIAN 92.

[c] RHF relativistic calculation.[178] The basis sets were as follows:

Palladium: (17s/13p/10d)/[11s/8p/4d]; C, O: (9s/5p/1d)/[4s/3p/1d].

Table 3.2: *Effect of increasing the level of theory*[a] *on the metal-ligand bond lengths (Å) and energy (kJ/mol) for the model reaction:*

$$Pd\text{-}PH_3 + CO \rightarrow Pd\text{-}CO + PH_3$$

	Pseudopotential and basis set on palladium								
Level of	LANL1[21/21/31][b]			LANL2[341/321/31][b]			SKBJ[4121/4121/311]		
theory	$Pd\text{-}PH_3$	Pd-CO	ΔE	$Pd\text{-}PH_3$	Pd-CO	ΔE	$Pd\text{-}PH_3$	Pd-CO	ΔE
RHF	2.311	1.943	-13.1	2.381	2.036	-3.4	2.360	2.034	-1.5
MP2	2.204	1.801	-53.4	2.259	1.856	-35.0	2.201	1.858	-24.0
MP3	2.234	1.848	-25.1	2.302	1.916	-10.5			
MP4	2.186	1.812	-68.5	2.249	1.851	-54.9	2.200	1.860	-39.3
CISD	2.233	1.851	-6.4	2.297	1.915	+5.2			
CCSD	2.219	1.837	-3.4	2.288	1.898	-19.2			
QCISD(T)	2.200	1.827	-46.1	2.258	1.879	-32.3			
CCSD(T)	2.200	1.828	-43.2	2.276	1.883	-28.2	2.225	1.887	-17.1
S-VWN	2.234	1.883	-36.2	2.120	1.794	-61.7			
B-LYP	2.381	1.984	-32.3	2.198	1.856	-57.5	2.208	1.870	-54.5
B-PW91				2.171	1.837	-54.0			
B3-LYP	2.349	1.965	-26.4	2.208	1.867	-41.9	2.213	1.879	-38.8

[a] The 6-31G(d) basis set is employed for the ligands.

[b] As implemented in GAUSSIAN 92.

Table 3.3: *Effect of the basis set on the metal-ligand bond lengths (Å) and reaction energies (kJ/mol) at the MP2 level of theory.*

	Basis set				Bond lengths		ΔE
	Metal valence	ECP	Ligand	Basis set size[a]	Pd-PH_3	Pd-CO	
1	(8s/6p/4d)/[341/321/31]	lanl2	6-31G(d)	46 (50)	2.259	1.856	-35.0
2	(8s/6p/4d)/[341/321/31]	lanl2	6-31G(2d)	51 (60)	2.207	1.824	-47.9
3	(8s/6p/4d)/[341/321/31]	lanl2	6-31G(2d,p)	60 (60)	2.203	1.824	-45.4
4	(8s/6p/4d)/[341/321/31]	lanl2	6-31+G(2d,p)	64 (68)	2.201	1.822	-39.2
5	(8s/6p/4d)/[341/321/211]	lanl2	6-311G(d)	62 (63)	2.243	1.839	-34.4
6	(8s/6p/4d)/[341/321/211]	lanl2	6-311G(2d)	67 (73)	2.191	1.819	-41.1
7	(8s/6p/4d)/[3311/321/211]	lanl2	6-311G(d)	63 (64)	2.211	1.832	-28.0
8	(8s/6p/4d)/[3311/3111/211]	lanl2	6-311G(d)	66 (67)	2.202	1.843	-27.7
9	(8s/6p/4d)/[3311/3111/211]	lanl2	6-311G(2d)	71 (77)	2.190	1.833	-32.8
10	(8s/6p/5d)/[341/321/311]	lanl2	6-31G(d)	51 (55)	2.281	1.866	-25.5
11	(8s/8p/5d)/[4121/4121/311]	SKBJ	6-31G(d)	55 (59)	2.201	1.858	-24.0
12	(8s/6p/5d)/[341/321/311]	lanl2	6-31G(2d)	56 (65)	2.225	1.832	-42.5
13	(8s/6p/4d/1f)/[341/321/31/1]	lanl2	6-31G(d)	53 (57)	2.219	1.817	-44.2
14	(8s/6p/5d/1f)/[341/321/311/1]	lanl2	6-31G(d)	58 (62)	2.243	1.827	-34.7
15	(8s/6p/5d/2f)/[341/321/311/11]	lanl2	6-31G(2d)	70 (79)	2.170	1.800	-43.3
16	(8s/8p/5d)/[4121/4121/311]	SKBJ	6-31G(2d,p)	69 (69)	2.194	1.846	-35.0
17	(8s/6p/5d/2f)/[341/321/311/11]	lanl2	6-31G(2d,p)	79 (79)	2.167	1.800	-39.9
18	(8s/6p/5d/3f)/[341/321/311/111]	lanl2	6-31G(2d,p)	86 (86)	2.167	1.804	-33.1
19	(8s/6p/4d/1f)/[3311/3111/211/1]	lanl2	6-311G(2d,p)	87 (84)	2.143	1.798	-36.0
20	(8s/6p/4d/2f)/[3311/3111/211/11]	lanl2	6-311G(2d,p)	94 (91)	2.132	1.808	-23.1
21	(8s/6p/5d/1f)/[3311/3111/311/1]	lanl2	6-311G(2d,p)	92 (89)	2.154	1.807	-30.7
22	(8s/6p/5d/2f)/[3311/3111/311/11]	lanl2	6-311G(2d,p)	99 (96)	2.142	1.814	-18.4
23	(8s/6p/5d/2f)/[21311/21111/311/11]	lanl2	6-311G(2d,p)	103 (100)	2.131	1.808	-14.8
24	(9s/6p/5d/4f)/[33111/3111/2111/211]	lanl2	6-311G(2d,p)	107 (104)	2.138	1.817	-8.0
25	(9s/6p/5d/4f)/[33111/3111/2111/211]	lanl2	TZ2P[c]	108 (108)	2.125	1.814	-7.2
26	(9s/6p/5d/4f)/[33111/3111/2111/211]	lanl2	6-311G(2df,p)	114 (118)	2.114	1.792	-10.8
27	(9s/6p/5d/4f)/[33111/3111/2111/211]	lanl2	6-311G(3df,p)	119 (128)	2.104	1.780	-23.2
	all electron (relativistic)[b] (17s/13p/10d)/[11s/8p/4d]	-	(9s/5p/1d)/ [4/3/1]			1.86	

[a] Number of basis functions for $PdPH_3$ and, in parentheses, PdCO. [b] CPF20 calculation.[178]

[c] Contraction scheme: P: [5121111/51111/11]; C, O: [511111/411/11]; H: [311/1].[183]

Table 3.4: *Summary of extensions to the (8s/6p/4d)/[341/321/31] basis set accompanying the LANL2 pseudopotential for palladium.*

Extension	Basis sets in Table 3.3
Uncontract s functions [341] -> [3311]	7-9, 19-22
-> [21311]	23
Uncontract p functions [321] -> [3111]	8-9, 19-22
-> [21111]	23
Uncontract d functions [31] -> [211]	5-9, 19-20
Add diffuse d function	10-12, 14-18, 21-23
Add f polarisation function	13-14, 19, 21
Add two f polarisation functions	15, 17, 20, 22-23
Add three f polarisation functions	18

3.3 Geometries

The Pd-CO and Pd-PH_3 bond lengths calculated at the RHF level are displayed in Table 3.1. It is clear that RHF theory overestimates these metal-ligand bond lengths. For example, for $PdPH_3$ the metal-ligand distances were greater than 2.3 Å which is the upper bound for experimental palladium-phosphine bond lengths with a few rare exceptions.[1] It should also be noted that the replacement of an ECP for phosphorus with an all-electron basis set led to a substantial improvement in the metal-phosphine bond lenth for the minimal basis calculations, but no significant variation for the calculations employing a valence double-ζ basis set. The bond lengths obtained with the large-core LANL1 pseudopotential were generally shorter than those generated by LANL2. This can be attributed to the neglect of the electron-electron repulsion between the valence electrons and the outer core electrons in the LANL1 pseudopotential. The inclusion of the outer core electrons in the valence space, however, results in a weaker treatment of relativistic effects for these electrons. This effect is expected to be negligible which is

supported by the agreement between the Pd-CO bond length calculated at RHF/LANL2:6-31G(d) (2.036 Å) and the relativistic calculations of Siegbahn *et al.*[178] (2.01 Å) employing all-electron basis sets of similar quality to LANL2:6-31G(d).

Comparing the bond lengths calculated at RHF to those at MP2, it can be seen that the addition of electron correlation significantly contracts the metal-ligand bond lengths, illustrating that RHF is inadequate for geometries of transition metal complexes that include metal-ligand π back-donation. This effect has been reported by various groups including Pacchioni *et al.*[172] and Dedieu *et al.*[174]

The variation in geometry with the level of theory is displayed in Table 3.2. The results obtained using the SKBJ pseudopotential and accompanying basis set are also included. The geometries generated by MP2, MP4, CCSD(T) and QCISD(T) were very close with only a small variation between MP2 and CCSD(T). The good agreement between CCSD(T) and QCISD(T) illustrates the similarity between the two methods for this system, although recent studies have highlighted areas where QCISD(T) fails.[105] In contrast, the MP3 and CISD metal-ligand bonds were longer than those calculated at other correlated levels but were very close (within 0.005 Å) to each other. This latter trend was also reported in a non-relativistic pseudopotential study on PdCO by Schwerdtfeger and coworkers.[181]

Although there is relatively little difference between the results obtained using the LANL2 or SKBJ pseudopotentials at the RHF level of theory, at correlated levels the metal-phosphine bond lengths become distinct. These differences may be due to the additional basis functions present in the SKBJ basis set which result in variations in the bonding description which are more obvious when electronic excitations are considered. Similar trends were observed for both pseudopotentials; there is a moderate increase in the metal-ligand bond length on going from MP2 to CCSD(T) of approximately 0.02 Å, a variation which can be

ignored for the present purposes given the sizeable increase in computational effort from MP2 to CCSD(T).

Table 3.3 summarises the dependence of the geometries and reaction energetics on the basis set size at a correlated level (MP2). The major changes in metal-ligand bond length were observed when a diffuse d function and an f-type polarisation function were added to the metal valence space (although these effects somewhat cancelled each other), and when the ligand basis set was augmented with a second set of d polarisation functions. A summary of the effects on the metal-ligand bond length when various functions were added to the basis sets is given below:

Addition of:

• an f-type polarisation function to the metal contracted the bonds by approximately 0.04 Å,

• a diffuse d function to the metal valence basis set lengthened the bonds by 0.02 Å and 0.01 Å for $PdPH_3$ and PdCO respectively,

• a second set of d-type polarisation functions on the ligands contracted the bonds by 0.05 Å and 0.02-0.03 Å for $PdPH_3$ and PdCO respectively,

• a second f-type polarisation function on the metal contracted the Pd-PH_3 bond by about 0.01 Å but extended the Pd-CO bond by approximately 0.01 Å,

• a set of f-type polarisation functions of the ligands contracted the bonds by about 0.024 Å, and

• a third set of d-type polarisation functions on the ligands contracted the bonds by a further 0.01 Å.

Adding a third f-type polarisation function to the metal, p-type polarisation functions to the hydrogens or a set of s and p diffuse functions to the ligands, had little influence on the geometries. Uncontracting the metal and ligand valence basis sets to triple-ζ quality had a significant effect on the $PdPH_3$ metal-ligand bond length (an 0.05 Å contraction) but only a minor influence on the Pd-CO bond length (approximately -0.01 Å). Splitting the metal outer core orbitals to double-ζ

quality resulted in only a small change (about -0.01 Å). It may be noted that the Pd-CO metal-ligand bond length converged faster than the Pd-PH_3 bond length.

The results obtained employing the metal valence basis set of Hay and Wadt[148] uncontracted and augmented with polarisation functions and diffuse functions (basis set 23) were very close to those obtained using the previously optimised valence basis set of Bauschlicher and coworkers[170] (basis set 24), thus justifying the polarisation and diffuse exponents employed in this study. The results generated by the SKBJ pseudopotential and basis set appear to be very good given that there are only 9 additional metal basis functions. This basis set is optimised with three 4d functions, including a diffuse function, and a double-ζ description of the 4s, 4p, 5s and 5p orbitals. The sharing of exponents between the s and p orbitals of the same principal quantum number also improves the computational efficiency.

In summary, an overall contraction of approximately 0.15 Å for Pd-PH_3 and 0.05 Å for Pd-CO was obtained on enlarging the basis set. This variation is not expected to be important for qualitative studies on these types of systems, particularly at the MP2 level, as there will be a certain amount of cancellation of the error from using a smaller basis set (such as the standard double-ζ metal valence basis set[148] together with 6-31G(d) on the ligands) due to the observed increase in bond length on going from MP2 to CCSD(T). The Pd-CO bond length calculated using basis set 8 at the MP2 level can be compared to the result obtained by Siegbahn *et al.*[178] employing an almost equivalent all-electron basis set at the CPF20 level of theory with relativistic effects included by first-order perturbation theory. The comparison is good, 1.843 Å using basis set 8 and 1.86 Å for the all-electron relativistic study, particularly if we note that there may be a small increase in bond length on going from the MP2 to CPF20 level of theory, as noted earlier for the transition from the MP2 to CCSD(T) level of theory. The small-core RECP method for calculations of transition metal complexes can therefore be justified.

A study on PdCO by Schwerdtfeger and coworkers generated a metal-ligand bond length at MP2 of 1.909 Å.[181] This calculation employed the small-core nonrelativistic ECP of Dolg *et al.*[150] with a triple-ζ valence basis set and 6-311+G(d) on carbon and oxygen. Comparing this bond length to that obtained by Rohlfing and Hay (1.882 Å),[173] in which an RECP was employed, it was concluded that the influence of relativistic effects on the geometry were negligible. Although there is only a small difference in the bond lengths, this can be explained in terms of differing methods of calculation rather than the insignificance of relativistic effects. The Hay and Wadt study employed a large-core ECP for Pd with only a minimal basis description of the valence region, and 4-31G for the ligand. If the value of 1.909 Å of Schwerdtfeger is instead compared to 1.843 Å obtained using basis set 8 at the MP2 level (Table 3.3), a significant contraction due to relativistic effects may be inferred.

The nonlocal density functionals, B-LYP, B-PW91 and B3-LYP, produced metal-ligand bond lengths which compared well to those generated at the MP2 level with the LANL2:6-31G(d) basis set (refer to Table 3.2). The LANL1 pseudopotential gave spurious results; the S-VWN bonds were slightly longer than those generated at MP2, which is unusual given the tendency of local approximations to underestimate bond lengths, and the B-LYP functional produced bonds which were far too long (outside the experimental limits). This indicates that it is important in DFT calculations to explicitly treat the outer core electrons in order to obtain reasonable results. The LANL2 and SKBJ results were very close, although the Pd-PH_3 bond length was significantly contracted from the MP2 result calculated using LANL2. This may indicate the relative independence of density functional methods on the basis set size. To test this hypothesis, calculations were performed using the LANL2 pseudopotential with larger basis sets using the B-LYP and B3-LYP functionals (Table 3.5). Very little variation in the metal-ligand bond lengths was observed, indicating that smaller basis sets could be employed with nonlocal DFT methods to give results comparable to those obtained

with large basis sets at the MP2 level. The computational expense of B-LYP is significantly less than that of MP2, particularly as the number of basis functions increases; hence, nonlocal DFT appears to be a viable alternative for obtaining the geometries of transition metal complexes.

Table 3.5: *Effect of the basis set and pseudopotential on the metal-ligand bond lengths using the B-LYP and B3-LYP functionals*

Basis set				Bond lengths (Å)	
Metal valence	ECP	Ligand	Basis set size[a]	$Pd-PH_3$	Pd-CO
B-LYP					
(3s/3p/4d)/[21/21/31]	lanl1	6-31G(d)	42 (46)	2.381	1.984
(8s/6p/4d)/[341/321/31]	lanl2	6-31G(d)	46 (50)	2.198	1.856
(8s/8p/5d)/[4121/4121/311]	SKBJ	6-31G(d)	55 (59)	2.208	1.870
(8s/6p/5d/2f)/[341/321/311/11]	lanl2	6-31G(2d,p)	79 (79)	2.199	1.856
(9s/7p/5d/4f)/[33111/3111/2111/211]	lanl2	6-311G(2d,p)	107 (104)	2.193	1.859
B3-LYP					
(8s/6p/4d)/[341/321/31]	lanl2	6-31G(d)	46 (50)	2.208	1.867
(8s/6p/5d/2f)/[341/321/311/11]	lanl2	6-31G(2d,p)	79 (79)	2.205	1.867
(9s/7p/5d/4f)/[33111/3111/2111/211]	lanl2	6-311+G(2d,p)	111 (112)	2.197	1.870

[a] Number of basis functions for $PdPH_3$ and, in parentheses, PdCO.

Although this study focuses on the metal-ligand interactions, a brief mention may be made of the ligand geometries. We observed that the C-O bond length in PdCO varied from 1.12 Å to 1.15 Å at the RHF level of theory and 1.14 Å to 1.18 Å at correlated levels. The P-H bond length in $PdPH_3$ was 1.37-1.46 Å and 1.40-1.43 Å at the RHF and correlated levels respectively, while the Pd-P-H angle varied from 119° to 121° and 120° to 123° at the RHF and correlated levels respectively (Appendix 1).

3.4 Reaction Energies

The calculated energies for the process

$$Pd\text{-}PH_3 + CO \longrightarrow Pd\text{-}CO + PH_3$$

were less consistent than the geometries (see Tables 3.1-3.3) and varied more with the level of theory used. In particular, the reaction energies calculated employing the B-LYP and B-PW91 functionals with small-core pseudopotentials were larger than those obtained using post-Hartree–Fock methods. This difference may, in part, be a result of using wave function based *ab initio* rather than density functional optimised basis sets. Single-point energy calculations at MP2 and CCSD(T) using the B-LYP geometries yielded energies within a few kJ/mol of the energies obtained by full geometry optimisations at these levels. Using the LANL2:6-31G(d) pseudopotential and basis set, the single-point energies at the B-LYP geometry were -35.8 kJ/mol and -30.0 kJ/mol, which can be compared to the geometry-optimised values of -35.0 kJ/mol and -28.2 kJ/mol at MP2 and CCSD(T) respectively (refer to Table 3.6). This illustrates the independence of reaction energies on small variations (up to 0.06 Å) in geometries; that is, the potential surface is relatively flat in the region of the equilibrium metal-ligand bond lengths. The B-LYP energies obtained using the LANL2 and SKBJ pseudopotentials were very close such that the additional expense of the SKBJ pseudopotential and basis set is not warranted for density functional calculations.

The reaction energies determined using the B3-LYP density functional display a marked improvement over the other nonlocal density functionals. The agreement between B3-LYP and CCSD(T) is improved further by increasing the flexibility of the basis set (refer to Table 3.6).

Table 3.6: *Single-point energy calculations for the reaction:*

$$Pd\text{-}PH_3 + CO \rightarrow Pd\text{-}CO + PH_3.$$

Level of Theory	Reaction Energy (kJ/mol)
MP2 // B-LYP[a]	-35.8
CCSD(T) // B-LYP[a]	-30.0
CCSD(T) // MP2[a]	-27.8
[21311/21111/311/111]: 6-311+G(2d,p) // basis set 23[b]	-11.7
basis set 24+[d] // basis set 24[b]	-13.7
[33111/3111/2111/1111]: 6-311+G(2d,p) // basis set 24[b]	-13.8
[33111/3111/2111/211]: 6-311++G(2d,p) // basis set 24[b]	-12.1
basis set 24+ // basis set 1[b]	-21.2
basis set 24+ // basis set 11[b]	-14.3
MP2/basis set 24+ // B-LYP/basis set 1	-14.4
B3-LYP/basis set 24+ // B3-LYP/basis set 24+	-23.3
CCSD(T)/basis set 24+ // MP2/basis set 24[c]	-8.4

[a] These calculations performed with theLANL2[341/321/31]: 6-31G(d) basis set (basis set A).

[b] These calculations performed at the MP2 level with the LANL2 pseudopotential.

[c] These calculations performed with the LANL2 pseudopotential.

[d] Basis set 24+ refers to LANL2[33111/3111/2111/211]: 6-311+G(2d,p) (basis set B).

The reaction energies obtained at CCSD(T) and QCISD(T) were within 5 kJ/mol of each other but differed from those at lower levels of theory by more than 7 kJ/mol, with the MP2 energies being the closest probably due to some fortuitous cancellation of error. Although the geometries varied slightly on going from MP2 to CCSD(T), single-point CCSD(T) energy calculations at the MP2 geometries yielded reaction energies which were very close to those resulting from full geometry optimisation at CCSD(T). For the LANL2 pseudopotential the CCSD(T) single-point reaction energy was -27.8 kJ/mol which is very close to the CCSD(T) geometry optimised value of -28.2 kJ/mol.

Convergence which is close to uniform was only obtained for the energies when very large basis sets were used for the ligands and metal valence (refer to Table 3.3). The use of a triple-ζ description of the valence region (for example basis sets 7, 8 and 9) raised the reaction energy by about 7 kJ/mol, where splitting the unoccupied 5p functions on the metal appeared to have the least effect. It is difficult to directly compare the reaction energies obtained using the LANL2 and SKBJ pseudopotentials given the differences in the valence basis sets, but it appears at the MP2 level that the SKBJ pseudopotential and basis set give superior energetics and geometries for a particular number of basis functions (contrary to our findings for density functional theory described above). Adding polarisation functions to the metal resulted in an increase in the reaction energy, whereas the addition of polarisation functions to the first- and second-row atoms decreased the energy. This latter effect may result from the relative ability of the palladium centre to reduce its negative charge by employing the CO basis functions, thus favouring the formation of PdCO and decreasing the reaction energy.

Although a third f-type polarisation function on the metal, p-type polarisation functions on the hydrogens, and diffuse s and p functions on the first- and second-row atoms were shown not to be important for determining the geometries, the influence of these functions on the energy was significant. Single-point energy calculations at the basis 23 geometries using a modification of

this basis set (with three f-type functions and a set of diffuse functions on C, O and P) changed the reaction energy by 3 kJ/mol to give -11.7 kJ/mol (Table 3.6). This is very close to the equivalent single-point reaction energy of -13.7 kJ/mol calculated at the basis 24 geometries using basis set 24 augmented by a set of diffuse s and p functions on the ligands (denoted basis set 24+). A set of diffuse s functions on the hydrogens or a fourth f-type polarisation function on palladium caused a further small energy variation of +1.6 kJ/mol and -0.1 kJ/mol respectively (Table 3.6). The calculations employing the basis sets of Ahlrichs *et al.*[183] on the ligands (basis set 25) produced geometries and energies which varied little from those determined using the Pople basis sets (6-311G(2d,p)).

A balanced description of the metal and ligands appears to be highly important in this case.[184] Other research groups typically use a small-core pseudopotential with a valence double-ζ basis set (such as the LANL2 pseudopotential with the (8s/6p/4d)/[341/321/31] valence basis set) on the metal, which includes the unoccupied 5p orbitals, with 3-21G(*) or 6-31G(d) on the ligands.[185] One to three f functions are often added to the metal valence basis with no additional functions on the ligands,[178] such that it is rare to add more polarisation functions to the ligands than to the metal. Taking this information into account the largest basis set (27) is probably unbalanced toward the ligands (explaining the sharp drop in the reaction energy between calculation 26 and 27), as are those with two sets of d-type polarisation functions on the ligands but no f functions on the metal (basis sets 6, 12 and 16). We should also ignore the calculations which have an f function on the metal but not the more important diffuse d function (basis sets 13, 19 and 20). When the above caveats are taken into account the information in Tables 3.3 and 3.6 suggests that the reaction energies at MP2 with balanced basis sets converge to a value between -11 and -15 kJ/mol.

Given the relative independence of the reaction energy on small changes in geometry, single-point energy calculations with large basis sets using geometries

calculated with modest basis sets may be appropriate. Single-point MP2 energy calculations using the MP2/SKBJ:6-31G(d) and B-LYP/LANL2:6-31G(d) geometries at basis set 24+ gave reaction energies of -14.3 kJ/mol and -14.4 kJ/mol respectively. These are very close to the single-point value of -13.7 kJ/mol obtained using the basis set 24 geometry (refer to Table 3.6), indicating the validity of such an approach to obtaining reaction energies. A similar single-point calculation using the MP2/LANL2:6-31G(d) geometry generated a reaction energy of -21.2 kJ/mol, which deviates significantly from the single-point value of -13.7 kJ/mol. It is, however, an improvement on the MP2/LANL2:6-31G(d) fully optimised value of -35.0 kJ/mol and within 10 kJ/mol of -13.7 kJ/mol.

The variation in the reaction energy on going from MP2 to CCSD(T) precludes employing just the MP2 level (even with large basis sets and full geometry optimisation) to obtain quantitative energies. However, at present CCSD(T) calculations with large basis sets are not routinely possible for "real" systems using the current algorithms, which require several gigabytes of disk space. It may be noted from Table 3.2 that the variation in reaction energy on increasing the level of theory from MP2 to CCSD(T) is approximately 7 kJ/mol for both the LANL2 description of the metal and the SKBJ pseudopotential with the larger valence basis set. A correction to the MP2 energy similar to that proposed by Pople *et al.* for first-row elements[130,137,186] may therefore be appropriate. Applying this scheme to the approximate MP2 basis set limit of -14 kJ/mol we can predict a CCSD(T) reaction energy close to -7 kJ/mol. A single-point CCSD(T) energy calculation utilising basis set 24+ and employing the MP2 geometry generated by basis set 24, gave a reaction energy of -8.4 kJ/mol (refer to Table 3.6), providing some justification for the use of such a scheme. For larger systems we therefore propose the following procedure for obtaining approximate reaction energies from single-point calculations:

$$E[\text{CCSD(T)/large basis set}] \approx E[\text{MP2/large basis set}] + \Delta E \qquad (3.1a)$$

where ΔE is a correction for correlation effects beyond MP2.

$$\Delta E = E[CCSD(T)/modest\ basis\ set] - E[MP2/modest\ basis\ set]. \quad (3.1b)$$

The modest basis set refers to basis set 1 (basis set A in Chapters 5-8) or 11; the large basis set, to basis set 24+ (basis set B).

As discussed in Section 3.3 the level of theory used for determining the geometry is not critical. In particular, we have shown that single-point energy calculations employing large basis sets at the geometries generated by MP2/SKBJ:6-31G(d) and B-LYP/LANL2:6-31G(d) are very close to those resulting from the MP2/basis set 24 geometries. To test our scheme, the following calculations were performed:

$$\begin{aligned} E[CCSD(T)/large\ basis\ set] \approx\ & E[MP2/basis\ set\ 24+\ //\ B\text{-}LYP/basis\ set\ 1] + \\ & \{E[CCSD(T)/basis\ set\ 1\ //\ B\text{-}LYP/basis\ set\ 1] - \\ & E[MP2/basis\ set\ 1\ //\ B\text{-}LYP/basis\ set\ 1]\} \end{aligned} \quad (3.2a)$$

$$\approx -14.4 + \{-30.0 + 35.8\}$$

$$\approx -8.6\ kJ/mol$$

$$\begin{aligned} E[CCSD(T)/large\ basis\ set] \approx\ & E[MP2/basis\ set\ 24+\ //\ MP2/basis\ set\ 11] + \\ & \{E[CCSD(T)/basis\ set\ 11\ //\ MP2/basis\ set\ 11] - \\ & E[MP2/basis\ set\ 11\ //\ MP2/basis\ set\ 11]\} \end{aligned} \quad (3.2b)$$

$$\approx -14.3 + \{-16.5 + 24.0\}$$

$$\approx -6.8\ kJ/mol$$

Both results are close to the CCSD(T) calculation of -8.4 kJ/mol. Clearly this method will only provide an estimate of the reaction energy, and further calculations are required to assess its applicability to other systems.

The validity of using pseudopotential calculations to generate accurate reaction energies is difficult to determine due to the lack of experimental information and relativistic all-electron calculations for this process. The similarity between the LANL2 and SKBJ reaction energies with equivalent basis sets, however, encourages the use of the RECP approximation as the two

pseudopotentials were derived using different schemes. The SKBJ pseudopotential offers a good compromise between accuracy of the energies and geometries and the demand on computational resources.

3.5 Conclusions

For the investigation of metal-ligand bonds which have a π back-donation contribution to the bonding, a set of d-type polarisation functions on the ligands and the inclusion of correlation are essential. Both the LANL2 and SKBJ pseudopotentials produced geometries which compared well with all-electron results, although in post-Hartree–Fock calculations for a given number of basis functions the results obtained using the SKBJ description for the metal appeared to be superior. The metal-ligand bond lengths varied little when levels of theory higher than MP2 were employed. Larger basis sets on the metal and ligands contracted the metal-ligand bond length moderately, an effect more noticeable for the metal-phosphine than for the metal-carbonyl bond; however, such variations had little effect on the reaction energies. Nonlocal DFT with a small-core pseudopotential provided geometries of at least comparable quality to MP2 calculations with considerable computational savings; hence, geometry optimisations using nonlocal DFT with the LANL2 pseudopotential on the metal and 6-31G(d) on the ligands are advised.

The calculation of reliable reaction energies was more problematical, particularly given the lack of experimental information with which to compare. For results of quantitative accuracy at least CCSD(T) or QCISD(T) methods are required in addition to large basis sets, in agreement with the recent findings of Frenking *et al.* for the low oxidation state Group VIa transition metals.[176] Reaction energies calculated using DFT compared poorly with those obtained using conventional methods such as CCSD(T), but single-point post-Hartree–Fock calculations using B-LYP geometries produced reaction energies which varied little

from those resulting from post-Hartree–Fock geometries. As the potential surface in the region of the equilibrium metal-ligand bond length appears to be reasonably flat, large basis set single-point calculations using geometries calculated with modest size basis sets using either MP2 or nonlocal DFT methods produce reaction energies within 5 kJ/mol of values resulting from full geometry optimisations. It may also be valid to apply a correction for correlation effects beyond MP2 level to the reaction energies of large systems. The energies obtained at MP2/LANL2:6-31G(d) (or MP2/SKBJ:6-31G(d)) appear to be of qualitative value only.

In summary, we suggest the following scheme for calculating reliable reaction energies for palladium species similar to those described in this paper:

(i) Optimise the geometries at B-LYP/LANL2:6-31G(d).

(ii) Perform single-point calculations at CCSD(T) with a large basis set, using the geometries obtained in (i).

(iii) If the calculations in (ii) are not feasible, obtain an estimate for the energy from the additivity scheme (Equation 3.2a) proposed in this paper (which involves doing two smaller single-point calculations for each species).

CHAPTER 4

Ligand Substitution and the Application of ab Initio Methods to Potential Energy Surfaces

(Frankcombe, K. E.; Cavell, K. J.; Yates, B. F.; Knott, R. B.

J. Phys. Chem., **1996**, *100*, 18363)

Chapter 4

Ligand Substitution and the Application of ab Initio Methods to Potential Energy Surfaces

4.1 Introduction

The previous chapter has investigated the reliability of various *ab initio* methods with respect to the description of equilibrium metal-ligand bonds incorporating π-interactions. We will now apply these methods to a potential energy surface (PES), thereby gauging their accuracy with respect to the description of saddle points and reactive intermediates.

As discussed in Section 1.4.1, experimental studies on the carbonylation of alkyl-palladium(II) complexes of pyridinecarboxylic acid derivatives have led to the proposal of the mechanism illustrated in Scheme 4.1 as a possible reaction mechanism.[61] The first step of this pathway involves the replacement of the phosphine ligand in the coordination sphere by carbon monoxide and will be the focus of the present chapter (refer to Scheme 4.2). The complete PES for the carbonylation process will be considered in Chapter 5.

The mechanism for ligand substitution reactions of square-planar d^8 complexes has been a subject of conjecture for many years. Garrou and Heck[50] investigated the carbonylation of a series of square-planar platinum, palladium, and nickel complexes with monodentate ligands in an attempt to discern the mechanisms involved. From experimental data only, they proposed the participation of five-coordinate transition structures and intermediates. In fact, they were able to isolate an intermediate with the formula $\{(p\text{-}Me_2NC_6H_4)_3P\}_2PtPhI(CO)$, the structure of which was uncertain.

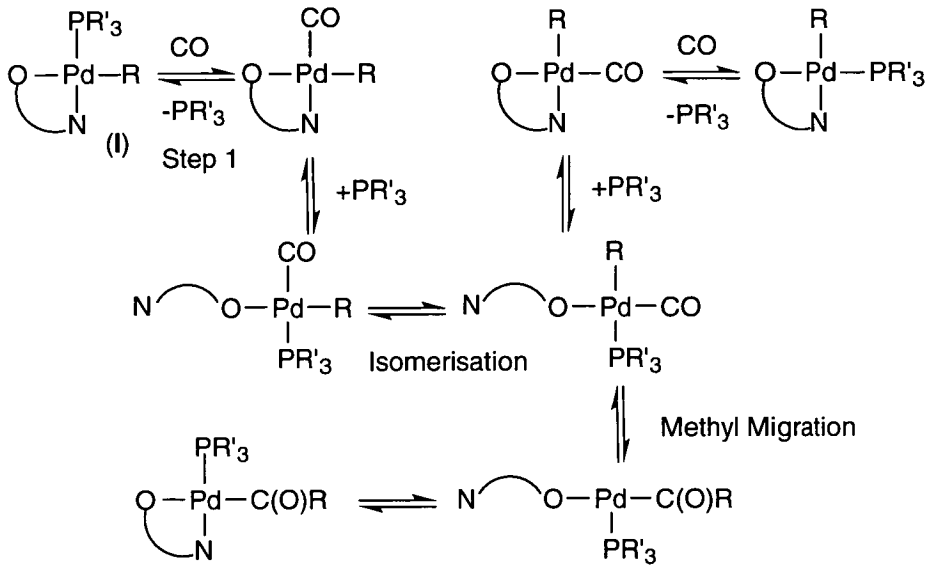

Scheme 4.1 *One of the possible mechanisms for the carbonylation of alkyl-palladium complexes of pyridinecarboxylic acid derivatives based on experimental evidence.*

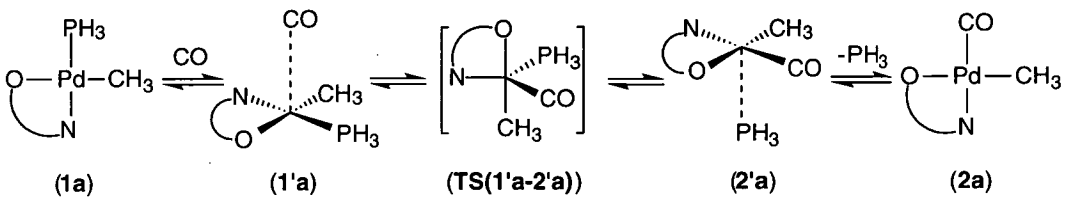

Scheme 4.2 *Possible intermediates and transition structure (TS(1'a-2'a)) participating in the associative ligand replacement mechanism of the model complex (1a).*

More recently, theoretical studies on square-planar palladium[28] and platinum[83,84] complexes with monodentate ligands have provided evidence that their substitution reactions proceed *via* a pseudo trigonal–bipyramidal transition structure. Although Markies *et al.* located shallow potential wells corresponding to the weak association of a fifth ligand to the metal centre, the binding energy was very low (in the order of 8 kJ/mol) and no strongly bound five-coordinate intermediates could be located.[28] Similar weakly bound states were located by

Muguruma *et al.* in the investigation of ligand exchange reactions of a cationic platinum(II) complex with H_2O.[84] Even less is known about the mechanisms associated with ligand replacement in d^8 complexes incorporating chelate ligands such as the postulated first step of the mechanism outlined in Scheme 4.1 (Step 1).

The reliability of various theoretical methods in the description of transition metal complexes is still unpredictable. This is particularly true of density functional methods for which the relative accuracy of each functional varies with the system under consideration. Calibrative studies have shown that the accuracy of a particular *ab initio* method is dependent on the transition metal, its oxidation state and the ligands involved.[171-176,187] In this light, the catalytic process shown in Scheme 4.1 presents a major challenge; π-accepting phosphine and carbonyl ligands are intimately involved in the transformations thought to take place, and the metal possesses a formal charge of plus 2. In addition, palladium is a second-row transition metal for which relativistic effects cannot be ignored.[178] Assessment of the accuracy of a given calculation by studying the convergence of geometries and energies with respect to the level of theory and basis set size, is restricted by the high computational demands associated with post-Hartree–Fock methods. We will compare the results obtained for the model reaction in Scheme 4.2 with those presented in Chapter 3 at levels tractable for the former model. This will allow us to estimate the validity of the conclusions formulated in the previous chapter with respect to the treatment of large systems.

Therefore, the present investigation serves a dual purpose. We provide, to our knowledge, the first theoretical investigation of ligand substitution of a model square-planar palladium complex containing a chelate ligand. This reaction is employed as a model for which to compare geometries and reaction energetics determined using various basis sets and levels of theory, including an assessment of density functional methods. For computational ease the experimental system (**I**) has been simplified to the model complex (**1a**). This model is not far removed from the experimental one; the simplification of the picolinic acid ligand to

NHCHCOO$^-$ retains the planar chelate backbone and the π-accepting ability of the nitrogen donor. The validity of the replacement of triphenylphosphine by PH_3 is, however, debatable and we remain aware of its inadequacies.[188,189]

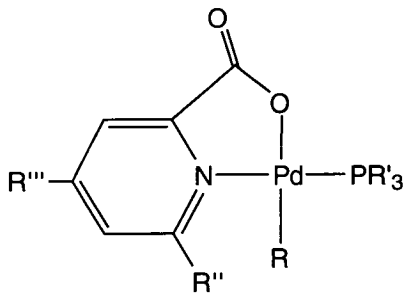

(I)

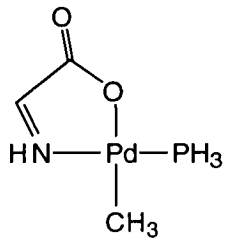

(1a)

Metal-ligand bond lengths (Å), selected bond angles (deg) and energies relative to **1a** + CO (kJ/mol) generated at each level of theory and basis set are given in Tables 4.1 - 4.8. Refer to Appendix 2 for the complete set of geometrical data and total energies. Appendix 3 contains the crystallographic data for $Pd(C_5H_4NCOO^-2\text{-}N,O)(CH_3)(PPh_3)$ and the synthesis method employed.

4.2 Additional Computational Methods

In addition to the computational methods outlined in Section 2.8, the following basis sets and levels of theory have been employed. A range of basis sets were assessed at the RHF level of theory. Both the minimal and double-ζ metal valence basis sets of Hay and Wadt were employed with the corresponding RECP's.[146,148] The (8s/8p/5d)/[4121/4121/311] double-ζ valence basis set of Stevens and coworkers was used in conjunction with the SKBJ RECP.[143] The ligands were described by an ECP and a minimal valence basis set on phosphorus[147] and the STO-3G basis set on the remaining atoms to 6-31G(d) on all main group elements (refer to Table 4.1).

For improved energies, single-point calculations were performed using the CCSD(T) method. These calculations were carried out using the LANL2 RECP

with the corresponding double-ζ valence basis set, and 6-31G(d) on the ligands (basis set A) at the geometries determined at the MP2 level with the same RECP and basis set.

The stability of wavefunctions obtained at the B-LYP level of theory were tested with respect to relaxing various constraints. The counterpoise correction method incorporated into GAUSSIAN 94 was employed to determine the BSSE's at the MP2 and B-LYP levels for weakly bound species. C_S symmetry was adopted for the four-coordinate species, and C_1 symmetry for the five-coordinate intermediates and transition structures. The former symmetry allocation was tested by relaxing the symmetry to C_1 symmetry.

4.3 Calculations on the Reactant Pd(N-O)(CH_3)(PH_3) (1a)

An X-ray crystal structure of Pd(N-O)(CH_3)(PPh_3) (N-O = pyridine carboxylate (pyca)) was obtained,[190] providing an experimental benchmark for comparison with the calculated geometric parameters (refer to Table 4.1 and Figure 4.1). The variation in metal-ligand bond lengths and bond angles with increasing basis set size and different levels of theory for Pd(N-O)(CH_3)(PH_3) (N-O = $NHCHCOO^-$) is displayed in Table 4.1. The trends in metal-phosphine bond length are similar to those discussed in Chapter 3 for the zerovalent $PdPH_3$ fragment. In agreement with previous studies[172,178,187] it can be seen that polarisation functions on the main group elements and electron correlation are essential for a correct description of metal-ligand bonds which involve π-back donation, in this case the Pd-PH_3 and Pd-N bonds. The influence of these factors on the other metal-ligand bond lengths was significantly less. The bond angles were relatively insensitive to the basis set or level of theory.

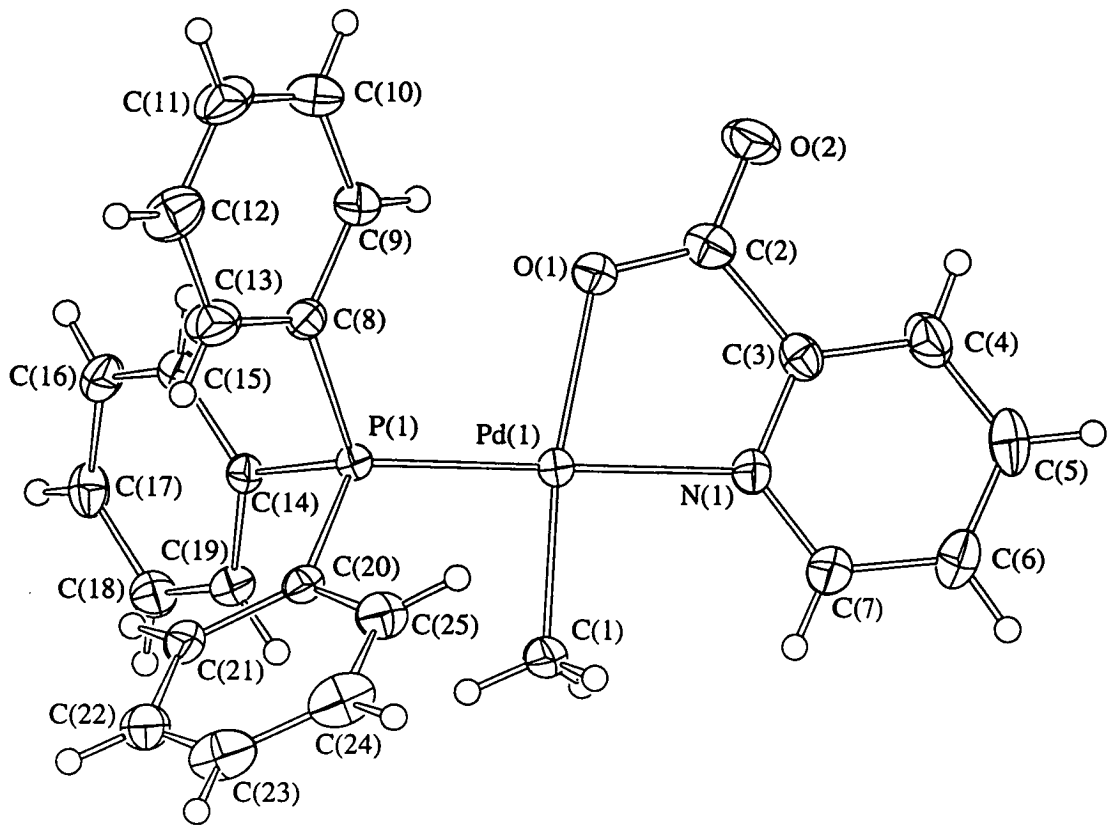

Figure 4.1: *ORTEP structure of $Pd(N\text{-}O)(CH_3)(PPh_3)$ (N-O = pyridine carboxylate (pyca)).*[190] *All atoms are drawn at 30% probability ellipsoids except for hydrogens which have been assigned the isotropic thermal parameters of the atom to which they are bound.*

Table 4.1: *Effects of the RECP and basis set on the geometry of Pd(N-O)(CH_3)(PH_3) (**1a**) employing conventional ab initio methods.*

Basis set and RECP			Metal-ligand bond lengths (Å)				Metal ligand bond angles (deg)		
RECP	Metal basis set	Ligand basis set	Pd-PH_3	Pd-CH_3	Pd-N	Pd-O	Pd-C (P)	Pd-N (C)	Pd-O (N)
	RHF Calculations								
LANL1	[3/3/4]	STO-3G	2.399	2.011	2.024	1.925	92.4	92.8	82.8
LANL2	[341/321/31]	3-21G	2.438	2.078	2.102	2.082	91.1	94.6	78.8
SKBJ	[4121/4121/311]	3-21G	2.441	2.066	2.111	2.082	91.8	94.8	78.8
LANL1	[21/21/31]	3-21G(*)[a]	2.260	2.039	2.077	2.013	88.0	94.6	79.8
LANL2	[341/321/31]	3-21G(*)[a]	2.355	2.083	2.111	2.078	88.7	95.0	78.8
SKBJ	[4121/4121/311]	3-21G(*)[a]	2.347	2.070	2.123	2.078	89.3	95.3	78.7
LANL2	[341/321/31]	6-31G	2.445	2.054	2.134	2.128	93.2	95.2	77.4
SKBJ	[4121/4121/311]	6-31G	2.451	2.046	2.136	2.128	92.9	97.4	77.3
LANL1	[21/21/31]	6-31G(d)	2.285	1.986	2.093	2.052	90.1	94.6	79.2
LANL2	[341/321/31]	6-31G(d)	2.375	2.046	2.146	2.126	90.9	95.4	77.7
SKBJ	[4121/4121/311]	6-31G(d)	2.368	2.045	2.146	2.127	91.0	95.4	77.7
	MP2 Calculations								
LANL1	[21/21/31]	6-31G(d)	2.184	1.972	2.062	2.073	89.5	93.3	80.5
LANL2	[341/321/31]	6-31G(d)	2.261	2.051	2.101	2.139	89.1	93.4	79.4
SKBJ	[4121/4121/311]	6-31G(d)	2.214	2.036	2.091	2.125	89.3	93.3	79.5
	Experimental results for Pd(pyca)(CH_3)(PPh_3)[b] (**I**)		2.230	2.021(3)	2.114(2)	2.134(2)	87.7	92.2(1)	78.2

[a] The phosphorus basis set was augmented with a single d-type polarisation function (exponent 0.55).[191]

[b] Refer to Appendix 3 for the experimental method and full set of positional parameters, bond lengths and angles.

Table 4.2: *Geometry of Pd(N-O)(CH_3)(PH_3) (**1a**) calculated employing density functional methods.*

		Metal-ligand bond lengths (Å)				Bond angles (deg)		
Functional	RECP[a]	Pd-PH_3	Pd-CH_3	Pd-N	Pd-O	C-Pd-P	N-Pd-C	O-Pd-N
S-VWN	LANL1	2.191	1.990	2.070	2.078	87.5	94.8	80.4
S-VWN	LANL2	2.192	2.081	2.020	2.083	89.3	92.9	80.0
B-LYP	LANL1	2.325	2.047	2.163	2.167	91.7	95.2	78.8
B-LYP	LANL2	2.274	2.088	2.107	2.174	91.6	93.7	78.6
B-LYP	SKBJ	2.273	2.087	2.108	2.165	91.7	93.7	78.6
B-PW91	LANL2	2.242	2.067	2.083	2.152	90.9	93.7	78.9
B3-LYP	LANL2	2.273	2.059	2.100	2.146	90.8	94.0	78.7

[a] The double-ζ valence basis sets were employed for the metal as described in the text, and 6-31G(d) on the ligands.

Table 4.3: *Effects of the level of theory, RECP, and basis set on the geometry of Pd(N-O)(CH_3)(CO) (**2a**) and the reaction energy.*

Level of theory, basis set and RECP				Metal-ligand bond lengths (Å)				Reaction energy
Level of theory	RECP	Metal basis set	Ligand basis set	Pd-CO	Pd-CH_3	Pd-N	Pd-O	(kJ/mol)
RHF	LANL1	[3/3/4]	STO-3G	2.070	2.011	2.000	1.925	+32.3
RHF	LANL1	[21/21/31]	3-21G	2.005	2.024	2.054	2.011	+7.0[a]
RHF	LANL2	[341/321/31]	6-31G	2.052	2.059	2.105	2.117	+13.7
RHF	LANL1	[21/21/31]	6-31G(d)	1.961	1.985	2.062	2.053	+10.2
RHF	LANL2	[341/321/31]	6-31G(d)	2.064	2.046	2.105	2.123	+20.7
RHF	SKBJ	[4121/4121/311]	6-31G(d)	2.052	2.045	2.111	2.121	+19.7
MP2	LANL1	[21/21/31]	6-31G(d)	1.799	2.000	2.066	2.075	-7.8
MP2	LANL2	[341/321/31]	6-31G(d)	1.860	2.068	2.095	2.133	+5.1
MP2	SKBJ	[4121/4121/311]	6-31G(d)	1.846	2.051	2.076	2.124	+2.7
S-VWN	LANL1	[21/21/31]	6-31G(d)	1.860	2.004	2.063	2.081	-13.6
S-VWN	LANL2	[341/321/31]	6-31G(d)	1.834	2.028	2.025	2.083	-43.2
B-LYP	LANL1	[21/21/31]	6-31G(d)	1.958	2.064	2.144	2.167	-12.9
B-LYP	LANL2	[341/321/31]	6-31G(d)	1.891	2.102	2.106	2.174	-36.9
B-PW91	LANL2	[341/321/31]	6-31G(d)	1.871	2.079	2.082	2.151	-34.4
B3-LYP	LANL2	[341/321/31]	6-31G(d)	1.897	2.070	2.088	2.143	-18.7

[a] The phosphorus basis set was augmented with a single d-type polarisation function (exponent 0.55).[191]

Bond lengths calculated utilising the large-core RECP of Hay and Wadt were consistently shorter than those generated using the small-core RECP's. This is due to the neglect of electron-electron repulsion between the outer core electrons of the metal and valence electrons of the ligands in molecular calculations. The small-core RECP's of Stevens *et al.* and Hay and Wadt produced similar geometries at the RHF level, but at the MP2 level of theory differences became evident. Such trends were discussed in Chapter 3 and may be due to the increased flexibility in the outer core orbitals of the SKBJ valence basis set. Comparing the calculated geometries with the experimental parameters for $Pd(N\text{-}O)(CH_3)(PPh_3)$ (N-O = pyridine carboxylate (pyca))[190] it can be seen that MP2/SKBJ:6-31G(d) and MP2/LANL2:6-31G(d) satisfactorily reproduced bond lengths and angles (to within 0.031 Å and 2°).

Table 4.2 displays the geometries determined employing local and nonlocal density functional methods. The tendency of local DFT to overestimate metal-ligand bond strengths[118] was reflected by the contracted bonds generated by the S-VWN functional. In contrast, geometries calculated using nonlocal density functional methods were close to those obtained at the MP2 level with the LANL2 RECP. The extension in metal-ligand bond length when the metal outer core orbitals were included in the valence space was not so evident for density functional calculations. This is consistent with the unreliability of density functional calculations employing the large-core LANL1 pseudopotential observed in Chapter 3.[187] The B3-LYP functional produced bond lengths and angles which were slightly closer to experiment than those generated using the B-LYP functional. The B-PW91 functional, however, was less consistent, improving some parameters while others were made worse. The geometry determined at B-LYP/SKBJ:6-31G(d) was virtually indistinguishable from the B-LYP/LANL2:6-31G(d) geometry.

4.4 Calculations on the Product Pd(N-O)(CH_3)(CO) (2a)

Table 4.3 displays the dependence of the geometry of **2a** and the reaction energy on the level of theory, RECP, and basis set. Unfortunately, no experimental values of closely related systems were available as palladium complexes with CO ligands are typically highly unstable. Like the Pd-PH_3 bond, calculation of the Pd-CO bond parameters are problematical due to the π back-donation interaction. The trends in metal-ligand bond length were similar for both bonds. Again, for most parameters the B3-LYP method yielded geometrical parameters slightly closer to the MP2 values than those determined using the B-LYP or B-PW91 methods.

4.5 Geometry of the Transition Structure (TS(1'a-2'a))

The transition structure geometries determined at various levels of theory are displayed in Table 4.4. It is clear that for the determination of reasonable transition structures, the RHF level of theory is unsuitable. In particular, the Pd-PH_3 bond length is approximately 0.7 Å longer than that calculated at correlated levels with the same RECP. Extending the basis set from the minimal description to double-ζ valence basis sets and augmenting the basis sets on the main group elements had little influence on the poor performance of RHF theory. In contrast, the introduction of electron correlation had a dramatic effect on the geometry, yielding a more symmetric pseudo trigonal–bipyramidal structure (Figure 4.2). The Pd-PH_3 and Pd-CO bonds were contracted, and conversely the *trans* Pd-N bond weakened.

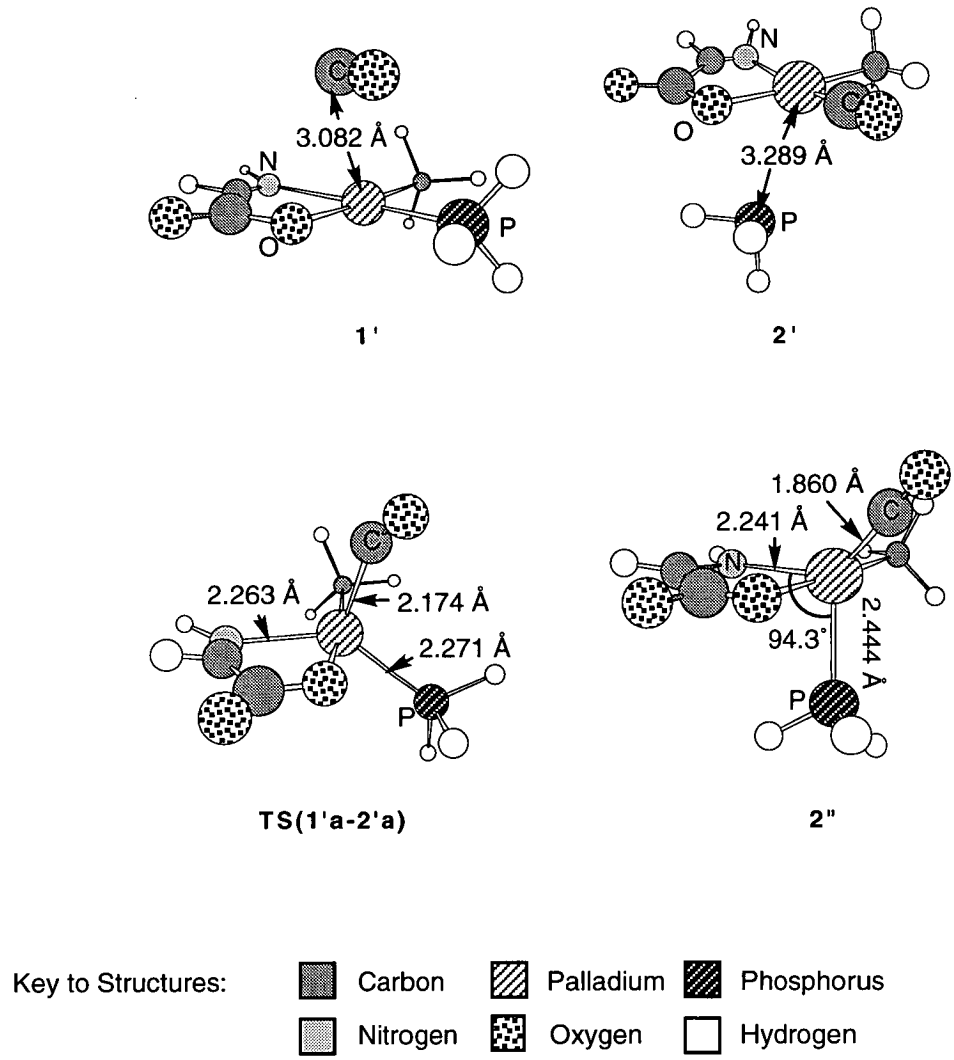

Figure 4.2: *MP2-optimised structures. Intermediates **1'a** and **2'a** and transition structure **TS(1'a-2'a)** were optimised at MP2/LANL2:6-31G(d), and intermediate **2"a** was optimised at MP2/SKBJ:6-31G(d). Note the nonlinear coordination of the carbonyl group in **TS(1'a-2'a)**, reflecting the transitional nature of the structure whereby the bonding is midway between mainly π-accepting (**1'a**) and the synergic σ-donating/π-accepting character of a typical palladium-carbonyl bond (**2'a**).*

Table 4.4: *Effects of the level of theory, RECP and basis set on the transition structure geometries (**TS(1'a-2'a)**).*

Level of theory, RECP and basis set	r(Pd-PH_3) Å	r(Pd-CO) Å	r(Pd-N) Å	r(C-O) Å	PH_3 DA,[a] deg	CO DA,[a] deg
RHF						
LANL1[3/3/4]:STO-3G	2.781	2.398	2.108	1.145	49.7	45.2
LANL1[21/21/31]:3-21G(*)[b]	2.710	2.395	2.140	1.125	49.8	47.4
LANL1[21/21/31]:6-31G(d)	2.752	2.370	2.185	1.110	54.6	45.5
LANL2[341/321/31]:6-31G(d)	2.961	2.548	2.019	1.110	51.8	37.8
MP2						
LANL1[21/21/31]:6-31G(d)	2.207	2.139	2.173	1.156	40.3	75.6
LANL2[341/321/31]:6-31G(d)	2.271	2.174	2.263	1.153	44.6	81.2
SKBJ[4121/4121/311]:6-31G(d)	2.218	2.208	2.188	1.156	36.3	79.0
B-LYP						
LANL2[341/321/31]:6-31G(d)	2.322	2.157	2.249	1.159	41.4	70.2
B3-LYP[c]						
LANL2[341/321/31]:6-31G(d)	2.306	2.185	2.282	1.142	44.8	73.3

[a] The dihedral angle (DA) between this group and the plane of the complex.

[b] The phosphorus basis set was augmented with a single d-type polarisation function (exponent 0.55).[191]

[c] This transition structure was not for the carbonyl replacing the phosphine, but rather the carbonyl replacing the nitrogen donor (refer to the text).

Table 4.5: *Geometries of the intermediate located on the reactant side of the transition structure (**1'a**).*

Level of theory, RECP and basis set	r(Pd-PH_3) Å	r(Pd-CO) Å	r(Pd-N) Å	r(C-O) Å	CO DA,[a] deg
RHF					
LANL1[3/3/4]:STO-3G	2.409	3.307	2.028	1.148	83.9
LANL1[21/21/31]:3-21G(*)[b]	2.269	3.584	2.077	1.127	49.2
LANL1[21/21/31]:6-31G(d)	2.287	3.992	2.094	1.113	57.6
LANL2[341/321/31]:6-31G(d)	2.383	4.113	2.147	1.112	47.4
MP2					
LANL1[21/21/31]:6-31G(d)	2.180	2.880	2.064	1.154	92.2
LANL2[341/321/31]:6-31G(d)	2.259	3.082	2.102	1.153	92.5
SKBJ[4121/4121/311]:6-31G(d)	2.215	3.274	2.090	1.153	93
B-LYP					
LANL2[341/321/31]:6-31G(d)	2.281	3.025	2.110	1.153	90.9

[a] The dihedral angle (DA) between CO and the plane of the complex.

[b] The phosphorus basis set was augmented with a single d-type polarisation function (exponent 0.55).[191]

Table 4.6: *Geometries of the intermediate located on the product side of the transition structure (2'a).*

Level of theory, RECP and basis set	r(Pd-PH_3) Å	r(Pd-CO) Å	r(Pd-N) Å	r(C-O) Å	PH_3 DA,[a] deg
RHF					
LANL1[3/3/4]:STO-3G	3.385	2.086	2.017	1.144	86.5
LANL1[21/21/31]:3-21G(*)[b]	4.236	2.027	2.056	1.123	0.7
LANL1[21/21/31]:6-31G(d)	4.635	1.968	2.064	1.108	15.2
LANL2[341/321/31]:6-31G(d)	4.562	2.069	2.107	1.106	25.9
MP2					
LANL1[21/21/31]:6-31G(d)	3.192	1.795	2.078	1.159	92.3
LANL2[341/321/31]:6-31G(d)	3.289	1.855	2.107	1.158	91.4
SKBJ[4121/4121/311]:6-31G(d)	3.344	1.842	2.084	1.160	88.7
(**2"a** in parentheses)	(2.444)	(1.860)	(2.241)	(1.166)	(85.0)

[a] The dihedral angle (DA) between PH_3 and the plane of the complex.

[b] The phosphorus basis set was augmented with a single d-type polarisation function (exponent 0.55).[191]

Nonlocal density functional theory appeared to perform well, producing bond lengths only marginally longer than those determined at the MP2 level. At a glance the B3-LYP functional generated geometrical parameters closer to the MP2 values than the B-LYP functional, but closer inspection of the character of the transition structure revealed an inconsistency. Optimisation from the transition structure on the side of the products indicated that this corresponds to replacement of the chelate nitrogen rather than the phosphine. It is likely that there would be little difference between the transition structure for replacement of the phosphine or replacement of the nitrogen donor. We can see in Figure 4.2 that both of these ligands and the entering carbonyl ligand are approximately evenly spaced in the equatorial plane. Small variations in the relative strengths of the palladium-phosphine and palladium-nitrogen bonds may therefore alter the outcome of the transformation. A transition structure corresponding to substitution of the phosphine could not be located using the B3-LYP functional.

4.6 Pseudo Five-coordinate Intermediates (1'a and 2'a)

Intermediate geometries resulting from following the PES "downhill" from the transition structure are displayed in Tables 4.5 and 4.6. The lowest level of theory studied, RHF/LANL1[3/3/4]:STO-3G, performed remarkably well, probably due to fortuitous cancellation of errors, such as a large BSSE counteracting the inadequate treatment of π-interactions. When the basis sets were uncontracted to double-ζ valence basis sets at the RHF level, the weak interaction with the metal was no longer observed. Instead, the uncoordinated ligand participated in a weak electrostatic interaction with the bidentate ligand similar to that observed by Muguruma *et al.* for the interaction between a cationic platinum complex and H_2O.[84]

Electron correlation strengthened the interaction between the fifth ligand and the metal producing a flattened-square–pyramidal geometry in which the CO or PH_3

were weakly bound at approximately 3 Å for the Hay and Wadt RECP's (Figure 4.2). This effect has also been reported very recently by Markies *et al.*[28] It has been proposed that the ability of a fifth ligand to bind to a d^8 metal, such as palladium or platinum, is enhanced if the coordinated ligands are strong π-acceptors.[77,80,192] This may explain why such an interaction was observed only when electron correlation was considered, as RHF theory does not adequately describe the π back-donation interactions. The orientation of the weakly coordinated carbon monoxide parallel to the plane is consistent with such a postulate, indicating that the interaction is mainly π in character (refer to Figure 4.2).[193] Similar nonlinear coordination of CO has been reported in an *ab initio* study of CO addition to four-coordinate iridium complexes.[194]

Following the PES "downhill" from the transition structure using the SKBJ pseudopotential produced very interesting results. A structure where carbon monoxide was weakly bound at 3.274 Å similar to that determined utilising the Hay and Wadt RECP's was located. However, a shallow potential well was located on the product side, corresponding to a distorted trigonal–bipyramidal intermediate (**2"a**) with marginally elongated Pd-PH_3, Pd-N and Pd-CO bonds (illustrated in Figure 4.2). This structure was a mere 2.2 kJ/mol higher in energy than the structure involving the phosphine weakly bound at 3.344 Å (refer to Table 4.6). For the Hay and Wadt pseudopotentials a flattening in the PES was observed during the optimisation in the region of a similar structure.

The weak coordination of the carbonyl to the metal was reproduced by the B-LYP density functional calculations, although the binding energy was reduced to 3 kJ/mol. A similar interaction between the metal and unbound phosphine ligand was not observed using density functional methods. Optimisation from the transition structure proceeded smoothly "downhill" toward **2a** plus uncoordinated PH_3. This inconsistency may be a consequence of the unrealistic favouring of the Pd-CO bond over the Pd-PH_3 bond reflected by the large exothermicity of the reaction (an effect also noted in Chapter 3),[187] or the reduced importance of

BSSE's.[135] In addition, the description of weakly bound structures has been known to present a challenge to DFT.[118]

4.7 Reaction and Activation Energies

Energies of the intermediates (**1'a**, **2'a** and **2a** + PH_3) and the transition structure (**TS(1'a-2'a)**) relative to the separated reactants (**1a** plus CO) are given in Tables 4.3 and 4.7. The trends in bond lengths, electron densities, and reaction energies reported in Chapter 3 compare well with those presented for the current model at the levels considered. We therefore feel justified in extending the conclusions outlined in the previous chapter to the present system. In particular, we will apply the additivity scheme (Equation 3.1) to the determination of improved reaction energetics. For the following discussion we have employed the MP2/LANL2:6-31G(d) geometries.

The potential well associated with the interaction of the four-coordinate complexes with a fifth ligand was very small (-9.3 kJ/mol and -10.2 kJ/mol at MP2/LANL2:6-31G(d) for **1'a** and **2'a**, respectively), and as a result BSSE's cannot be ignored. We approached the problem of reducing the BSSE using two methods: the counterpoise correction method at MP2/LANL2:6-31G(d) and by performing single-point calculations employing an extended basis set (basis set B, defined in Section 2.8). The counterpoise correction method predicted a potential well associated with **2'a** of -5.2 kJ/mol, indicating that the weakly bound structure was not merely a result of BSSE. In contrast, for **1'a** a counterpoise correction of 10.4 kJ/mol was calculated, cancelling the potential well. Using the second method, however, single-point MP2/[basis set B]//MP2/LANL2:6-31G(d) calculations predicted a large stabilisation of the five-coordinate species with respect to the four-coordinate intermediates (refer to Figure 4.3). The energies of **1'a**, **TS(1'a-2'a)**, **2'a**, and **2a** + PH_3 with respect to **1a** + CO were -18.8, -4.5, -22.1 and +4.1 kJ/mol respectively.

Table 4.7: *Effect of the level of theory, RECP and basis set on the energies (kJ/mol) of intermediates and transition structures relative to the separated reactants (**1a** + CO).*

Level of theory and basis set		Relative energies (kJ/mol)			
Metal RECP and basis set	Ligand basis set	Intermediate **1'a**	**TS(1'a-2'a)**	Intermediate **2'a**	Products (**2a** + PH_3)
RHF Calculations					
LANL1[3/3/4]	STO-3G	-34.4	+13.6	-10.2	+32.2
LANL1[21/21/31]	3-21G(*)[a]	-21.1	+28.7	-14.4	+7.0
LANL1[21/21/31]	6-31G(d)	-7.3	+50.6	+3.6	+10.1
LANL2[341/321/31]	6-31G(d)	-8.5	+51.7	+13.1	+20.7
MP2 Calculations					
LANL1[21/21/31]	6-31G(d)	-14.8	+2.1	-27.1	-7.8
LANL2[341/321/31]	6-31G(d)	-9.3	+15.0	-10.2	+5.1
SKBJ[4121/4121/311]	6-31G(d)	-6.1	+13.8	-10.3 (-8.1[b])	+2.7
B-LYP					
LANL2[341/321/31]	6-31G(d)	-3.0	+7.9	c	-36.9
B3-LYP					
LANL2[341/321/31]	6-31G(d)	c	+21.3	c	-18.7

[a] The phosphorus basis set was augmented with a single d-type polarisation function (exponent 0.55).[191]

[b] This value corresponds to the pseudo trigonal–bipyramidal intermediate located (**2"a**).

[c] No intermediate was located at these levels of theory and basis set.

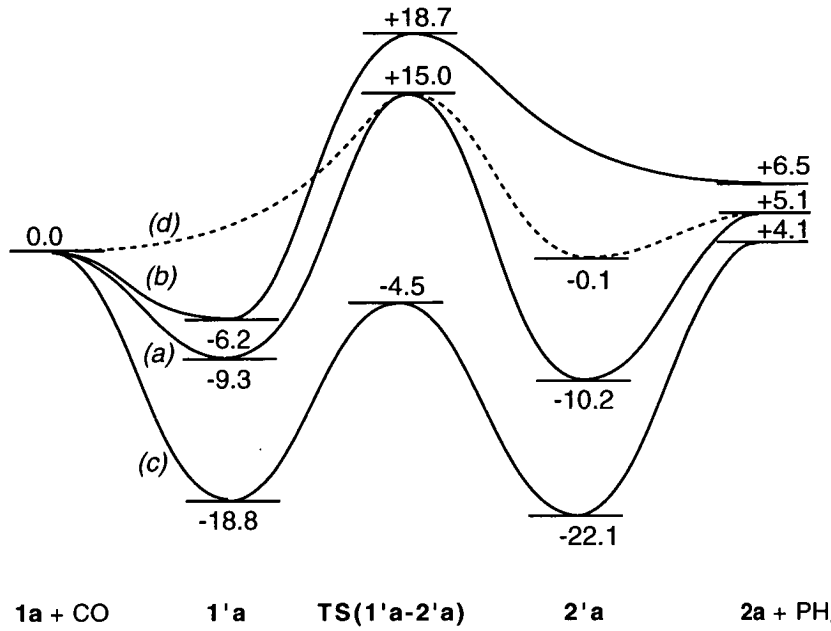

Figure 4.3: *The potential energy surfaces (energies in kJ/mol) determined at*

(a) MP2/LANL2:6-31G(d) (MP2/[basis set A]),

(b) MP2/LANL2:6-31G(d)//B-LYP/LANL2:6-31G(d),

(c) MP2/[basis set B]//MP2/LANL2:6-31G(d),

(d) counterpoise corrected MP2/LANL2:6-31G(d) (dashed).

Table 4.8: *Single-point energy calculations.*

	Energies relative to the reactants 1a + CO (kJ/mol)	
	Activation energy	Reaction energy
MP2/LANL2:6-31G(d)//B-LYP/LANL2:6-31G(d)	+18.7	+6.5
MP2/[basis set B]//MP2/LANL2:6-31G(d)	-4.5	+4.1
MP2/[basis set B]//MP2/SKBJ:6-31G(d)	-6.4	+8.5
MP2/[basis set B]//B-LYP/LANL2:6-31G(d)	+1.2	+6.9
CCSD(T)/LANL2:6-31G(d)//MP2/LANL2:6-31G(d)	+24.4	+9.9
Approximate CCSD(T)/[basis set B]// MP2/LANL2:6-31G(d)	+4.9	+8.9
B3-LYP/[basis set B]//B3-LYP/LANL2:6-31G(d)	+28.9[a]	-7.5

[a] The energy corresponding to the transition structure for CO replacing the nitrogen donor.

Expansion of the metal and ligand basis sets at the MP2 level for the fragment systems resulted in small contractions in the metal-ligand bonds involving π back-donation.[187] There may therefore be additional stabilisation of the five-coordinate species when a large basis set is employed due to an improved description of the π back-donation from the metal, as discussed in Section 4.6. The counterpoise correction calculations were repeated with the large basis set (B) and predicted BSSE's of 10.8 and 9.9 kJ/mol for **1'a** and **2'a**, respectively. Why the BSSE was not reduced in spite of the expansion of the basis set is unclear, but we note that the counterpoise correction provides only an estimate of the BSSE and its validity is controversial.[113]

Calculations at MP2/[basis set B]//MP2/SKBJ:6-31G(d) produced energies very close to those obtained with the MP2/LANL2:6-31G(d) geometries regardless of the small variations in geometry (refer to Table 4.8). An energy of -24.1 kJ/mol was calculated for the distorted trigonal–bipyramidal intermediate (**2''a**), slightly lower in energy than the flattened-square–pyramidal intermediate **2'a** (-17.4 kJ/mol) at this level. It appears likely that subsequent steps in the reaction would proceed directly from a structure similar to **2''a** rather than from **2a** or **2'a**. The contrast between this work and the results of previous theoretical investigations[28,83] may be due to a number of factors, including the presence of a number of π-acceptors in the present system. This is the most rigorous investigation to date on ligand substitution reactions of d^8 palladium complexes, and we have shown that lower levels of theory are inadequate for the treatment of five-coordinate species.

Single-point CCSD(T)/LANL2:6-31G(d) calculations on the present system are given in Table 4.8. The error in energetics due to incomplete inclusion of electron correlation was small, the main result being to reduce the stability of the five-coordinate transition structure with respect to the four-coordinate intermediates. Given the other approximations that have been made in this work, in particular the replacement of triphenylphosphine with PH_3 and the use of an RECP, the

additional expense of routine CCSD(T) calculations cannot be justified. Single-point CCSD(T)/LANL2:6-31G(d) energies of the pseudo five-coordinate intermediates were not determined as values neglecting BSSE's would be misleading, and the calculation of such errors at this level of theory is currently too computationally demanding. It is possible that CCSD(T) corrections would result in a reduction of the stability of these species. Using the additivity scheme outlined above we have obtained an approximation to the CCSD(T) energies;

Reaction energy[CCSD(T)/[basis set B]] $\approx$ +4.1 + [9.9 - 5.1]
= +8.9 kJ/mol

Activation energy[CCSD(T)/[basis set B]] $\approx$ -4.5 + [24.4 - 15.0]
= +4.9 kJ/mol

These values will be employed throughout the remainder of this chapter as a benchmark against which other methods can be compared.

The reaction energies determined using the B-LYP and B-PW91 functionals were too exothermic, a result also observed in our previous investigation (Chapter 3).[187] This error was partially corrected employing the B3-LYP functional, producing an error of -27.6 kJ/mol with the LANL2:6-31G(d) basis set with respect to our benchmark. Single-point calculations at B3-LYP/[basis set B]//B3-LYP/LANL2:6-31G(d) yielded a reaction energy closer to the benchmark value but not an improvement on the MP2/LANL2:6-31G(d) energy (refer to Table 4.8). MP2 single-point calculations at the nonlocal DFT geometries produced energies which compared favourably to those resulting from MP2-optimised geometries (Table 4.8).

As noted earlier, the nature of the transition structure located employing the B3-LYP functional was inconsistent with all of the other levels of theory investigated. Single-point calculations at B3-LYP/[basis set B] produced a barrier of +28.9 kJ/mol, much higher than our benchmark for the "true" transition structure of +4.9 kJ/mol. It appears that the description of some transition structures may present a challenge to the B3-LYP density functional.

The wavefunctions generated at the stationary points (including the transition structure) employing the B-LYP functional were shown to have very small restricted to unrestricted instabilities. However, single-point calculations allowing the wavefunction to become unrestricted did not vary the energy significantly, and the unrestricted wavefunctions were found to have no internal instabilities and expectation values $\langle S^2 \rangle = 0.00$. Thus, our closed-shell treatment is justified. The zero-point vibrational energies of the weakly bound species may also influence their stability. However, without analytic second derivatives such calculations are currently too computationally demanding.

4.8 Conclusions

For the calculations of geometries, electron correlation and polarised basis sets in combination with a small-core RECP are essential. Geometries determined at MP2/SKBJ:6-31G(d) or MP2/LANL2:6-31G(d) (MP2/[basis set A]) display the closest agreement with available experimental data (an average error of ±0.02 Å and ±1.3°). For substantially less computational effort, the nonlocal DFT geometries with small-core RECP's were also close to experiment (an average error of ±0.04 Å and ±2° for the B-LYP functional) and are similar to those produced at MP2/[basis set A]. The B3-LYP functional performed well for geometries at the end-points of the reaction but generated a transition structure inconsistent with other methods.

Single-point MP2 calculations at the B-LYP geometries produced energies which agreed well with those determined using the MP2 geometries. The inconsistency between the transition structures located using B3-LYP and other methods highlights the need for caution in the study of such processes. We advise that if the transition structure is "near degenerate" (at least two possible transition structures lie very closely together), more than one method should be employed to ensure consistency. In general, in our own work we propose to perform geometry

optimisations at B-LYP/[basis set A] with the exception of structures incorporating weakly bound species. Improved energies will then be obtained at MP2/[basis set B]. Geometry optimisations will be performed at MP2/[basis set A] for the weakly bound structures and, within the limit of available computational resources, for refined geometries.

Finally, the results presented in this chapter demonstrate that for our model system the exchange of CO for PH_3 is an endothermic process that should proceed with only a small activation energy. The stabilisation of the five-coordinate intermediates with respect to the four-coordinate species may preclude the formation of four-coordinate species such as **2a** in the reaction process. From the present results it is more likely that further transformations would proceed from five-coordinate intermediates such as **2'a** or a more tightly bound distorted trigonal–bipyramidal intermediate **2''a**. We do not exclude the possibility that other carbonylation mechanisms may operate which do not involve the ligand substitution on which this study is based, such as the direct insertion of carbon monoxide into the metal-ligand bond;[195] these will be considered in the following chapter.[196,197] Finally, we note that the replacement of triphenylphosphine with PH_3 has both electronic and steric consequences. The weaker π-accepting ability of triphenylphosphine would result in a destabilisation of the five-coordinate species and this will be considered in Chapter 8.

CHAPTER 5

Competing Reaction Mechanisms for the Carbonylation of Neutral Palladium Complexes Containing Bidentate (N-O) Ligands

(Frankcombe, K. E.; Cavell, K. J.; Knott, R. B.; Yates, B. F.

J. Chem. Soc, Chem. Commun. **1996**, 781.

Frankcombe, K. E.; Cavell, K. J.; Yates, B. F.; Knott, R. B.

Organometallics **1997**, in press.)

Chapter 5

Competing Reaction Mechanisms for the Carbonylation of Neutral Palladium(II) Complexes Containing Bidentate (N-O) Ligands

5.1 Introduction

Despite elegant kinetic work, the mechanisms operating in the carbonylation of square-planar d^8 complexes are yet to be clearly defined. The carbonylation pathways of complexes containing chelate ligands are particularly uncertain. Recent experimental studies have shown palladium(II)-alkyl complexes of pyridine carboxylic acid derivatives (**I**) undergo rapid carbonylation.[60-62] Based on kinetic data,[60,61] the mechanistic proposals illustrated in Scheme 5.1 have been postulated as possible reaction pathways. Note that an isomeric mixture of the reacting complex is used, but only one isomer of the final acyl complex (N *trans* to P, **5a**) is obtained. In addition, the possibility of direct insertion of uncoordinated carbon monoxide into the metal-methyl bond must not be excluded.

The theoretical methods recommended in the previous chapter have been adopted to investigate each of the possible mechanisms in Scheme 5.1, allowing us to predict the dominant pathways and rate-determining steps for the carbonylation reaction. The system introduced in Chapter 4 (**1**) has been used to model the experimental system (**I**). To our knowledge, this study represents the first investigation of the carbonylation of palladium(II) complexes containing hemilabile chelate ligands. In addition, we provide new and tangible evidence for the participation of five-coordinate intermediates and transition structures in the fundamental transformations of d^8 palladium complexes.

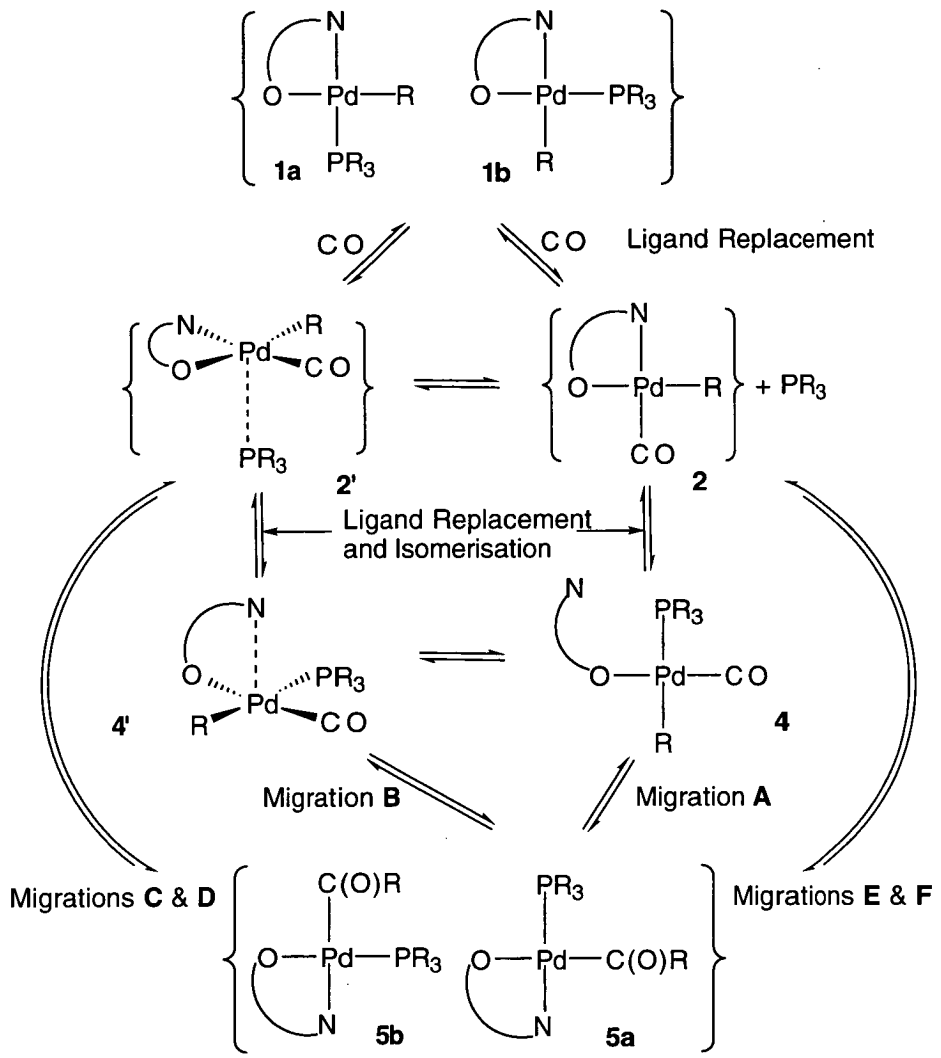

Scheme 5.1: *Proposed reaction pathways for the carbonylation of neutral palladium(II)-alkyl complexes of pyridine carboxylic acid (pyca). Species in parentheses may exist as an isomeric mixture although, for simplicity, the second isomer is not always shown. Different isomers are distinguished by the letters* ***a*** *and* ***b****.*

The metal-ligand bond lengths (Å), selected bond angles (deg) and relative energies (kJ/mol) from the correlated calculations are presented in Tables 5.1 - 5.5. The complete set of geometrical data and total energies generated at correlated and RHF levels of theory are listed in Appendix 4.

5.2 Overview of the Theoretical Methods

The theoretical methods employed are introduced in Section 2.8. MP2 geometry optimisations have been performed for the key transformations of the competitive pathways. In the majority of cases there is excellent agreement between the energies determined at the MP2 level with the MP2 or B-LYP geometries. Where this agreement deviates, the apparent contradiction can be attributed to differences in geometry and becomes more pronounced for the single-point MP2 calculations employing basis set B. It is worth noting that, while the energies of the five-coordinate species with respect to the four-coordinate intermediates are poorly estimated at MP2/[basis set B]//B-LYP/[basis set A], energies relative to species of the same coordination number are close to those based on the MP2 geometries. Unless otherwise stated, in the following discussion the geometries and energetics were determined at MP2/[basis set A] and MP2/[basis set B]//MP2/[basis set A], respectively, and relative energies have been determined with respect to **1a** + CO. The complete PES at MP2/[basis set B]//MP2/[basis set A] for the lowest energy reaction pathway is depicted in Figure 5.1.

We have identified four possible reaction mechanisms for carbonylation in which alkyl migration is the rate-determining step. In the first section, we will discuss the possible ligand substitution and isomerisation steps which may occur prior to methyl migration. In the second section, we will present a comparison of the possible methyl migration paths and an overview of the entire pathway. Experimentally, the reaction is carried out in chloroform which is generally regarded as a non-coordinating solvent. Preliminary calculations introducing a single solvent molecule at the RHF level with a large-core RECP[146] and a minimal basis set indicated that discrete solvent-solute interactions would not significantly influence the reaction pathway.

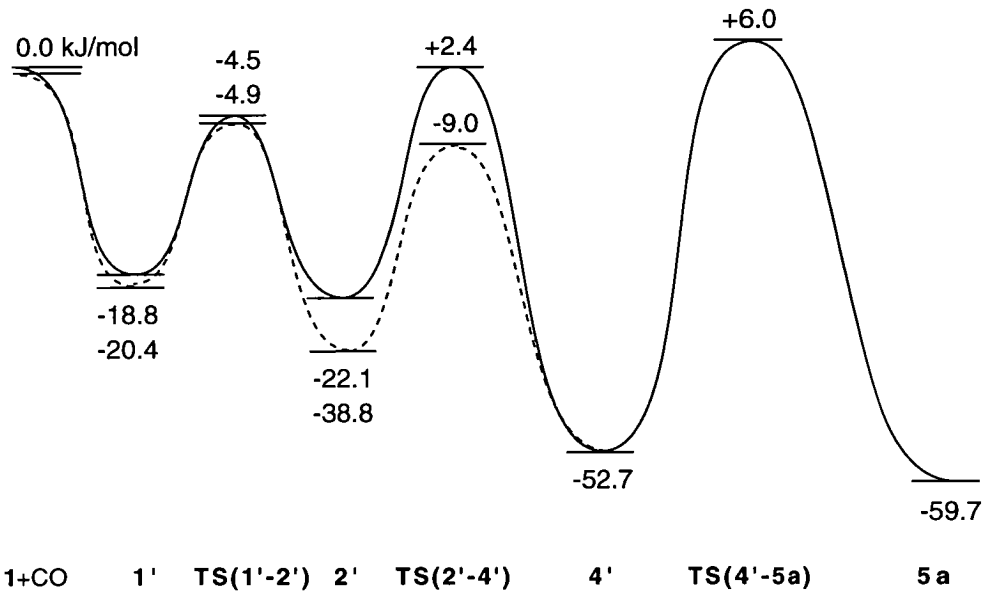

Figure 5.1: *Potential energy surface for the lowest energy pathway (via Migration **B**, **TS(4'-5a)**) at MP2//[basis set B]//MP2[basis set A].*

5.3 Ligand Substitution Reactions and Isomerisation

5.3.1 *Replacement of the phosphine ligand by carbon monoxide*

Here, we extend our previous investigation of the ligand substitution reaction of **1a**,[177] discussed in Chapter 4, to include the corresponding associative mechanism of the *cis*(N,P) isomer, **1b**, and the dissociative mechanism for both isomers (refer to Figure 5.2). The metal-ligand bond lengths and relative energies of the species involved in the associative and dissociative mechanism are displayed in Tables 5.1 and 5.2 respectively.

Irrespective of the level of theory used, there was found to be less than 3 kJ/mol difference in energy between the two isomers **1a** and **1b**. This is consistent with the experimental observation that the initial complex (**I**) is obtained as an isomeric mixture.[60,62] The associative ligand substitution of **1b** is similar to that of **1a**, proceeding *via* a trigonal–bipyramidal transition structure (**TS(1'b-2'b)** in Figure 5.2) with a barrier of +15.5 kJ/mol with respect to the preceding intermediate, **1'b**.

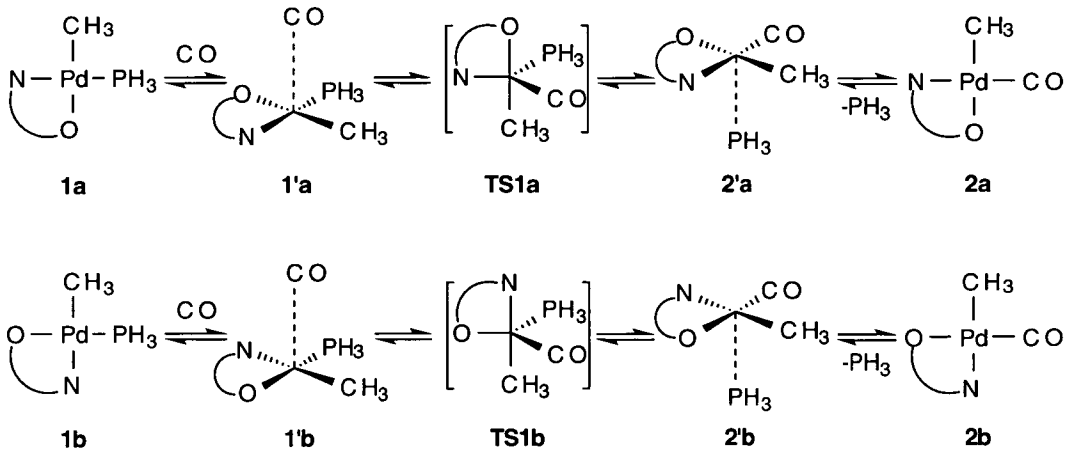

Associative

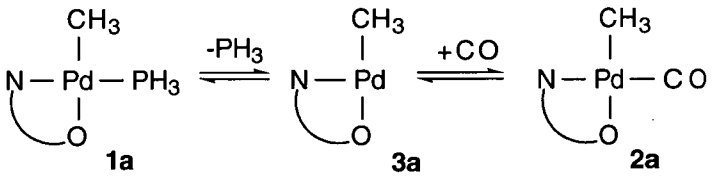

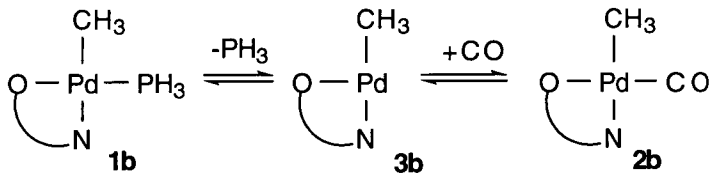

Dissociative

Figure 5.2: *Replacement of the phosphine ligand in* ***1a*** *and* ***1b*** *by carbon monoxide* .[177]

In the absence of solvent effects, it is clear from the energies given in Table 5.2 that the dissociative mechanism is unfavourable. Expansion of the basis set at the MP2 level decreased the possibility of a competitive dissociative mechanism, generating a reaction barrier of +232.4 kJ/mol. Hence, the effect of increasing the basis set size can be summarised as follows: the relative energy of the five-coordinate species decreases, the stability of four-coordinate intermediates does not vary greatly, and three-coordinate species become less stable.

Table 5.1: *Metal-ligand bond lengths of the reactants, intermediates and transition structures involved in the replacement of phosphine with carbon monoxide, calculated at B-LYP/[basis set A]. The results for both isomers are included. Parameters calculated at MP2/[basis set A] are in parentheses.*

Structure	Bond lengths (Å)				
	Pd-PH_3	Pd-CO	Pd-N	Pd-O	Pd-CH_3
1a	2.274 (2.261)	-	2.107 (2.101)	2.174 (2.139)	2.088 (2.051)
1b	2.276 (2.265)	-	2.213 (2.211)	2.109 (2.073)	2.074 (2.048)
1'a	2.281 (2.259)	3.025 (3.082)	2.110 (2.102)	2.179 (2.144)	2.088 (2.051)
1'b[a]	(2.254)	(3.012)	(2.197)	(2.082)	(2.055)
TS(1'a-2'a)	2.322 (2.271)	2.157 (2.174)	2.249 (2.263)	2.185 (2.153)	2.104 (2.071)
TS(1'b-2'b)	2.370 (2.288)	2.106 (2.123)	2.209 (2.201)	2.221 (2.200)	2.100 (2.080)
2'a[a]	(3.289)	(1.855)	(2.107)	(2.150)	(2.067)
2'b[a]	(3.368)	(1.841)	(2.202)	(2.077)	(2.073)
2a	-	1.891 (1.860)	2.105 (2.095)	2.174 (2.133)	2.102 (2.068)
2b	-	1.886	2.220	2.082	2.091
3a	-	-	2.015	2.167	2.048
3b	-	-	2.203	2.071	2.024

[a] Corresponding structures could not be located at B-LYP/[basis set A], as discussed in Chapter 4.[177]

Table 5.2: *Relative energies of the reactants, intermediates and transition structures involved in transformations prior to methyl migration (kJ/mol).*

Energies:	B-LYP/Basis A	MP2/Basis A	MP2/Basis A	MP2/Basis B	MP2/Basis B
Geometries:	B-LYP/Basis A	B-LYP/Basis A	MP2/Basis A	B-LYP/Basis A	MP2/Basis A
1a	0	0	0	0	0
1b	2.33	1.3	1.6	-0.6	+0.9
1'a	-3.0	-6.2	-9.3	-14.2	-18.8
1'b[a]	-	-	-10.2	-	-20.4
TS(1'a-2'a)	7.9	18.7	15.0	1.2	-4.5
TS(1'b-2'b)	18.6	27.3	23.0	6.3	-4.9
2'a[a]	-	-	-10.2	-	-22.1
2'b[a]	-	-	-23.6	-	-38.8
2a	-36.9	6.5	5.1	6.9	4.1
2b	-44.9	-7.9		-11.9	
3a	132.4	171.0		238.5	
3b	124.6	169.1		232.4	
TS(2'b-4')	-2.1	7.9	3.1	0.1	-9.0
TS(2'a-4')	9.25	17.6	14.7	6.3	2.4
4'	-18.5	-14.5	-23.0	-36.1	-52.7
TS(4'-4)	-1.4	7.5		-15.2	
4	-35.9	-23.1	-23.3	-44.0	-46.4

[a] Corresponding structures could not be located at B-LYP/[basis set A].

A search for a transition structure corresponding to replacement of the donor nitrogen by carbon monoxide was unsuccessful. The calculations are therefore consistent with experimental results. Replacement of triphenylphosphine in **I** with the less labile (but stronger trans influencing) tricyclohexylphosphine inhibits carbonylation.[60] This indicates that partial or full dissociation of the phosphine must take place.

5.3.2 *Replacement of the donor nitrogen by the phosphine for 2'b*

The substitution is illustrated in Figure 5.3. Tables 5.2 and 5.3 display the energies and geometries of the intermediates and transition structures involved. As for the substitution of PH_3 by CO, the reaction proceeds *via* a five-coordinate pseudo trigonal–bipyramidal transition structure (**TS(2'b-4')** in Figure 5.4) in which the nitrogen, phosphine, and methyl groups occupy positions in the equatorial plane. The activation energy was calculated to be 29.8 kJ/mol with respect to **2'b**, higher than the activation energy for the substitution of PH_3 by CO (13.4 and 15.5 kJ/mol from intermediates **1'a** and **1'b** respectively). Refer to Figure 5.1, which includes these steps as part of the complete PES.

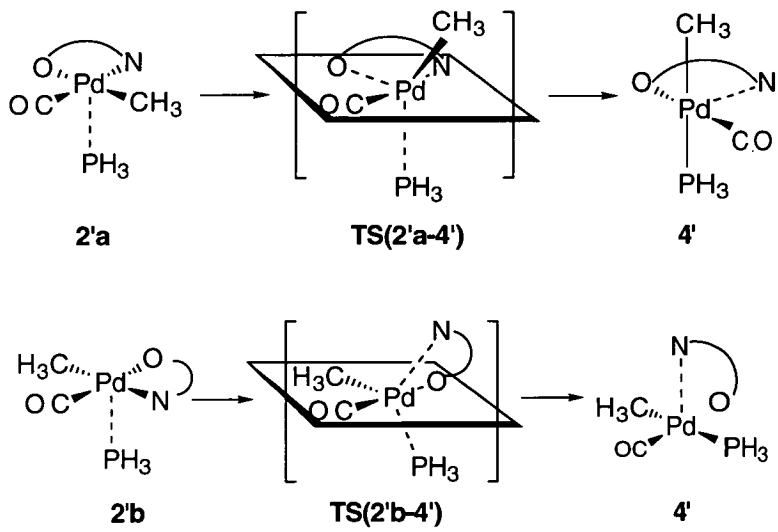

Figure 5.3: *Replacement of the donor nitrogen by the phosphine ligand, incorporating isomerisation for 2'a.*

The product of this step is of particular interest (**4'** in Figures 5.3 and 5.4). In contrast to previous five-coordinate intermediates which have been challenging for density functional methods, the B-LYP functional located an intermediate in which the nitrogen-metal bond was lengthened from a typical equilibrium value of 2.1-2.2 Å to 2.722 Å. Refinement of the geometry at MP2/[basis set A] generated a strengthened Pd-N bond of 2.351 Å. The geometry of the intermediate closely resembles the crystal structures of similar five-coordinate platinum intermediates incorporating bidentate ligands obtained by Pacchioni and coworkers.[80] Furthermore, this is the first theoretical investigation of the carbonylation of square-planar palladium(II) complexes in which a *strongly* bound five-coordinate intermediate has been located. Markies *et al.*[28] located a neutral intermediate in which an NH_3 group was weakly associated to the metal with a bond length of 3.11 Å, which is most likely an artifact of BSSE. The stronger bond in the present study may be a result of ligands with increased π back-donating ability or the inclusion of electron correlation in the geometry optimisations. Large basis set single-point calculations reinforce the stability of this intermediate, yielding an energy relative to **1a** + CO of -52.7 kJ/mol.

Table 5.3: *Selected bond lengths (Å) and bond angles (deg) of the species involved in the replacement of the donor nitrogen by the phosphine ligand at B-LYP/[basis set A]. MP2/[basis set A] parameters are in parentheses.*

	TS(2'b-4')	TS(2'a-4')	4'	TS(4'-4)	4
Pd-PH_3	2.863 (2.746)	2.810 (2.747)	2.514 (2.482)	2.526	2.516 (2.491)
Pd-CO	1.881 (1.833)	1.885 (1.847)	1.887 (1.827)	1.882	1.888 (1.850)
Pd-CH_3	2.115 (2.106)	2.120 (2.093)	2.120 (2.089)	2.120	2.124 (2.095)
Pd-O	2.094 (2.096)	2.482 (2.357)	2.127 (2.191)	2.073	2.080 (2.057)
Pd-N	2.535 (2.407)	2.120 (2.115)	2.722 (2.351)	3.615	4.848 (4.789)
CO-Pd-CH_3	89.4 (83.6)	90.8 (84.8)	87.7 (84.9)	88.0	88.9 (86.0)

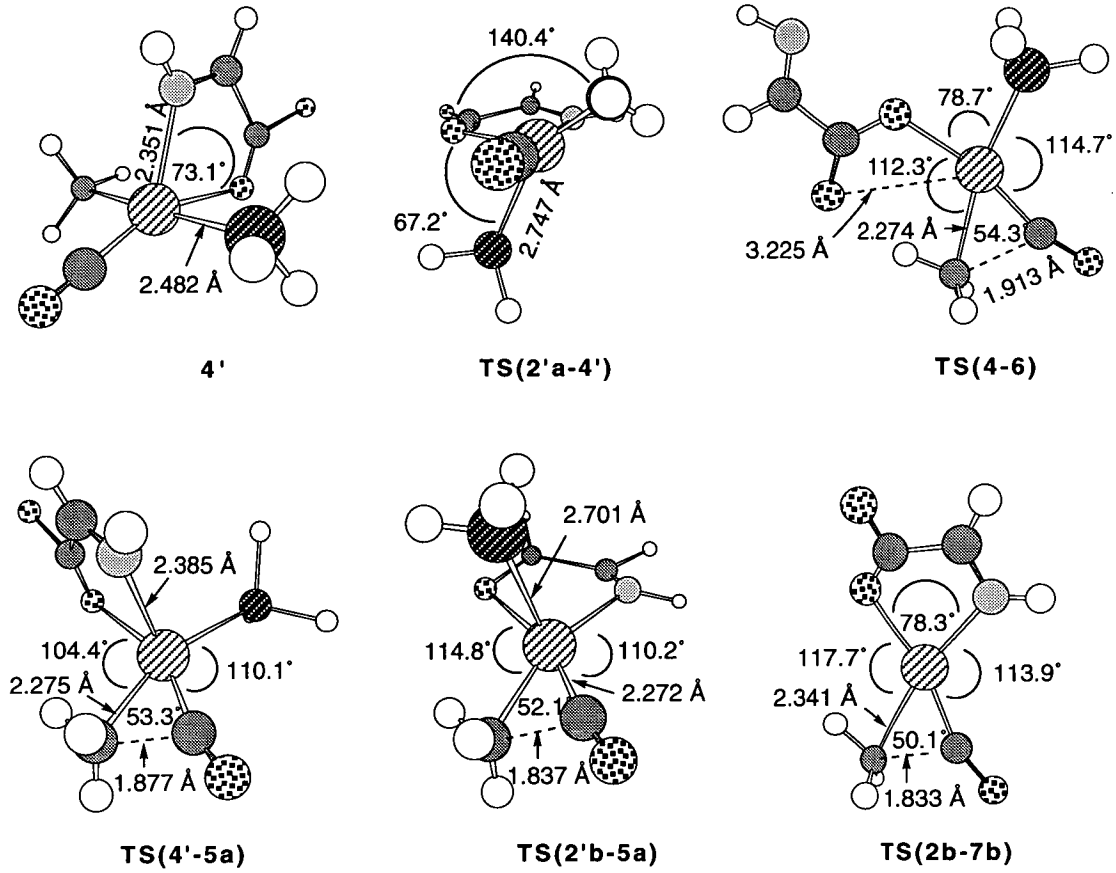

Figure 5.4: *Selected structures optimised at MP2/[basis set A], with the exception of* ***TS(2b-7b)*** *which was optimised at B-LYP/[basis set A].*

5.3.3 *Ligand substitution and Isomerisation of 2'a*

The energies and geometries of the transition structure and intermediates involved are given in Tables 5.2 and 5.3 respectively. The transformation is illustrated in Figure 5.3. It was surprising that the relative energy of **5a** is higher than that of **5b** by 17.1 kJ/mol (at MP2/[basis set B]//B-LYP/[basis set A]), and yet experimentally only the *trans*(N,P) isomer is observed.[60,62] This indicates a number of possibilities the most likely of which is that the *trans*(N,P) product is formed and is stable towards isomerisation. As NMR studies of the experimental product demonstrate that isomerisation is not facile and previous work has indicated that to promote methyl migration the highly trans influencing phosphine should be *trans* to the methyl group, the weight of available evidence strongly supports that possibility. In this case, isomerisation must occur *prior* to methyl migration.

The well known Berry pseudorotations cannot account for the isomerisation of d^8 complexes unless there is a significant distortion of the flattened-square–pyramidal geometry, typical of pentacoordinate palladium and platinum complexes, to an elevated square–pyramidal geometry prior to isomerisation.[82] We have proposed[196] a novel pathway for isomerisation with concomitant ligand substitution *via* the distorted transition structure (**TS(2'a-4')**) illustrated in Figures 5.3 and 5.4. Essentially, the methyl group moves out of the plane of the flattened-square–pyramidal intermediate **2'a** toward a position *trans* to the phosphine. This causes a lengthening in the relatively strong palladium-oxygen bond, a result which provides the driving force for isomerisation. In a single step, the carbonyl group moves to a position *trans* to the oxygen, transferring the elongation from the metal-oxygen to the more labile metal-nitrogen bond, and the metal-phosphine bond strengthens. The process occurs with a barrier of +24.6 kJ/mol relative to **2'a**. The resulting structure, **4'**, is identical to that obtained in the previous section for ligand substitution from **2'b** (refer to Figure 5.3).

5.4 Methyl Migration

The geometries and relative energies of each of the species involved are displayed in Tables 5.4 and 5.5 respectively. We were unable to locate a transition structure which yielded a product consistent with a true carbonyl insertion process (i.e., one in which the resulting acyl group occupies the coordination position previously occupied by the methyl group).

It was previously suggested that methyl migration may proceed from a four-coordinate intermediate in which the donor nitrogen was unbound.[60] We will refer to this path as Migration **A** (Figure 5.5). The transition structure (**TS(4-6)** in Figures 5.4 and 5.5) for this process was found to be stabilised by a weak interaction between the metal and the carbonyl group of the bidentate ligand, such that the product of this step is the four-coordinate complex **6**. The activation energy for this step of the reaction was calculated to be +71.2 kJ/mol with respect to **4** (or +24.8 kJ/mol with respect to **1a** + CO). Two further transformations are required to generate the final product, **5a**. It is therefore more likely that migration will take place from an intermediate in which the nitrogen is in a position to recoordinate directly in the migration step.

Migration **B** refers to methyl migration from **4'** (Figure 5.5) in which the nitrogen recoordinates during the transformation to yield the *trans*(N,P) product, **5a**. The transition structure (**TS(4'-5a)** in Figures 5.4 and 5.5) is stabilised by the interaction between the metal and the donor nitrogen. Markies *et al.*[28] observed a weaker stabilising interaction for the cationic species $[Pd(NH_3)_2(CH_3)(CO)\cdots(NH_3)]^+$; however, no stabilisation was observed for their neutral model. The activation energy for Migration **B** is +58.7 kJ/mol with respect to **4'** (or +6.0 kJ/mol with respect to **1a** + CO). The full PES for this mechanism is given in Figure 5.1, which is in excellent qualitative agreement with our PES previously presented employing medium basis sets.[196]

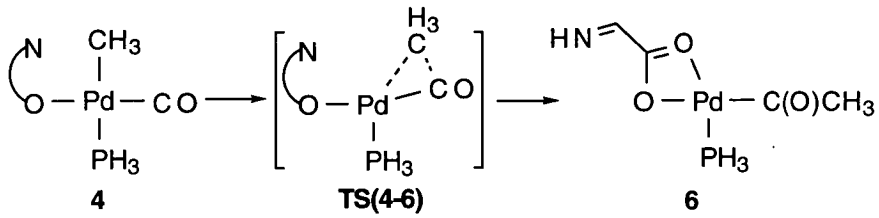

Migration **A**

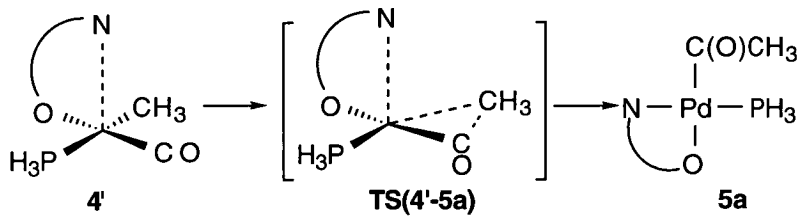

Migration **B**

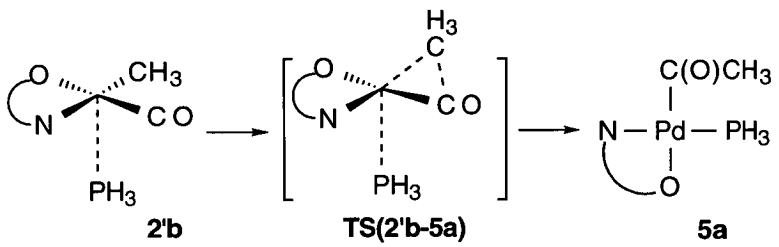

Migration **D**

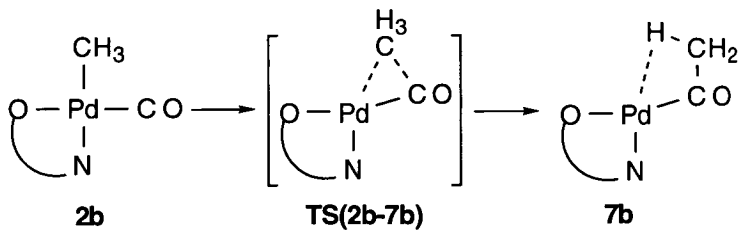

Migration **F**

Figure 5.5: *Methyl migration steps.*

Table 5.4: *Selected geometrical parameters of the methyl migration transition structures and products at B-LYP/[basis set A]. MP2/[basis set A] values are in parentheses.*

	Bond lengths Å					Angle deg
	Pd-CH_3	Pd-CO	Pd-PH_3	Pd-N	Pd-O	C-Pd-C
TS(4-6)	2.363 (2.275)	1.875 (1.828)	2.372 (2.389)	-	2.130/3.265 (2.129/3.225)	54.7 (54.3)
TS(4'-5a)	2.334 (2.274)	1.868 (1.807)	2.354 (2.363)	2.563 (2.385)	2.182 (2.210)	54.7 (53.3)
TS(2'a-5b)[a]	(2.276)	(1.805)	(2.732)	(2.269)	(2.146)	(51.7)
TS(2'b-5a)[a]	(2.272)	(1.801)	(2.701)	(2.155)	(2.221)	(52.1)
TS(2a-7a)	2.358	1.863	-	2.208	2.111	51.1
TS(2b-7b)	2.341	1.869	-	2.104	2.157	50.1
5a	-	2.044 (1.969)	2.321 (2.293)	2.106 (2.129)	2.206 (2.179)	-
5b	-	2.033	2.320	2.293	2.133	-
6	-	2.013	2.313	-	2.178/2.362	-
7a	2.562	1.916	-	2.255	2.114	38.0
7b	2.536	1.916	-	2.088	2.191	38.5

[a] Corresponding structures could not be located at B-LYP/[basis set A].

Table 5.5: *Relative energies of the transition structures and products of the migration steps (kJ/mol).*

Energies:	B-LYP/Basis A	MP2/Basis A	MP2/Basis A	MP2/Basis B	MP2/Basis B	Step
Geometries:	B-LYP/Basis A	B-LYP/Basis A	MP2/Basis A	B-LYP/Basis A	MP2/Basis A	
TS(4-6)	+28.2	+43.1	+42.1	+25.4	+24.8	**A**
TS(4'-5a)	+30.9	+38.3	+30.9	+19.5	+6.0	**B**
TS(2'a-5b)[a]	-	-	+58.5	-	+56.0	**C**
TS(2'b-5a)[a]	-	-	+43.9	-	+35.3	**D**
TS(2a-7a)	+34.0	+83.6		+101.6		**E**
TS(2b-7b)	+29.1	+73.0		+84.9		**F**
5a	-79.0	-41.9	-51.6	-40.0	-59.7	
5b	-88.8	-63.5		-57.1		
6	-65.8	-29.9		-15.3		
7a	+18.7	+96.7[b]				
7b	+18.7	+77.1[b]				

[a] Corresponding structures could not be located at B-LYP/[basis set A].

[b] Note that the single-point MP2 energies for these intermediates are higher than the single-point energies of the transition structures corresponding to their formation (**TS(2a-7a)** and **TS(2b-7b)** for **7a** and **7b** respectively). As single-point MP2 calculations using [basis set B] appear not to significantly vary the relative energy of four-coordinate structures, such calculations were not performed on **7a** and **7b**.

Migrations **C** and **D** take place from the intermediates incorporating weakly bound phosphines (**2'a** and **2'b** respectively). Migration **D** and the corresponding transition structure (**TS(2'b-5a)**) are illustrated in Figures 5.4 and 5.5 respectively. As these structures could not be successfully treated using DFT, geometries were optimised only at the MP2 level. The transition structures are five-coordinate with methyl migration occurring concomitantly with the phosphine ligand re-establishing a normal coordination (**TS(2'a-5b)** and **TS(2'b-5a)** for Migrations **C** and **D** respectively). Migration **D** produces the correct *trans*(N,P) acyl product (**5a**). This process has an energy of +35.3 kJ/mol with respect to **1a** + CO. Conversely, Migration **C** yields the *cis*(N,P) product (**5b**), which is not observed experimentally. The higher activation energy of Migration **C** (+56.0 kJ/mol) compared to Migration **D** is therefore consistent with experimental observations that only **5a** is formed.

Migrations **E** and **F** take place from the four-coordinate intermediates **2a** and **2b** respectively, where the phosphine ligand has completely dissociated. Migration **F** is illustrated in Figure 5.5. In this case, the transition structures are four-coordinate (**TS(2a-7a)** and **TS(2b-7b)** for Migrations **E** and **F** respectively, the latter is depicted in Figure 5.4). The resulting intermediates (**7a** and **7b**) are pseudo four-coordinate as the palladium-methyl bond does not fully break; instead a hydrogen of the methyl group attempts to accommodate the vacant coordination site prior to recoordination of the phosphine. This agostic interaction was only observed at the B-LYP level and provides minimal stabilisation, hence activating the C-C bond toward the reverse reaction. Note also that the barrier of Migration **E** is higher than the barrier of Migration **F** by 10.6 kJ/mol at MP2/[basis set A]//B-LYP[basis set A], *the latter migration yielding the correct product isomer.* The activation energies of these transformations are more than 29 kJ/mol higher than those of Migrations **A**, **B**, and **D**, a difference which solvent effects are unlikely to offset. We can therefore conclude that

the transition structure for methyl migration must be stabilised by an "incoming" fifth ligand, such that the product is truly four-coordinate.

Comparing all of these mechanisms, we observe little difference between the energies for Migrations **A**, **B**, and **D** employing basis set A (Table 5.5). In fact, in the absence of more rigorous calculations we may be tempted to predict that Migration **D** would be favourable due to the lower number of transformations involved. The importance of increasing the flexibility of the basis set is therefore clear. With basis set B, Migration **D** is significantly less favourable than Migrations **A** and **B**, indicating that migration proceeds *via* either partial or full dissociation of the donor nitrogen. The lower activation energy of Migration **B** compared to Migration **A**, coupled with the direct formation of the final product, **5a**, indicates that the former migration pathway will be preferred.

The results of Chapter 4 suggest that the errors arising from an incomplete inclusion of electron correlation for the present system are in the range of 5-8 kJ/mol,[177] so that we do not expect such errors to vary the qualitative conclusions of this work. More important are the consequences of employing PH_3 as a model for triphenylphosphine.[188,189] The weaker π-accepting ability triphenylphosphine would result in a destabilisation of the five-coordinate relative to the four-coordinate species,[77,80,82] and this issue will be considered further in Chapter 8. Conversely, the larger steric bulk of triphenylphosphine would lower the stability of square-planar four—coordinate geometries relative to the less sterically crowded five-coordinate structures. This consequence of the steric bulk of triphenylphosphine is demonstrated experimentally by the deformation of $Pd(C_5H_4NCOO^-\text{-}2\text{-}N,O)(CH_3)(PPh_3)$ away from square-planar (refer to the ORTEP diagram in Figure 4.1).

5.5 Conclusions

The present work has identified the lowest energy pathway for the carbonylation of the model system $Pd(CH_3)(PH_3)(N\text{-}O)$ (Figure 5.1). The rate-determining step is methyl migration, the transition structure for which is stabilised by the approach of the partially dissociated donor nitrogen thus producing a four-coordinate product. The reaction proceeds *via* a modest barrier and is exothermic overall. The lowest-energy pathway reflects well the experimentally found importance of the lability and trans influence of the phosphine ligand and the lability of the palladium-nitrogen bond. In addition, isomerisation has been shown to occur prior to migration such that only the product isolated experimentally is obtained. Extending our conclusions to the experimental system (**I**), it is possible that the additional steric bulk and reduced π-accepting ability of triphenylphosphine will favour the full dissociation of the donor nitrogen.

Finally, investigation of the dissociative ligand exchange mechanism indicates that the commonly discussed intermediates possessing a vacant coordination site (three-coordinate)[19,60] are not energetically feasible.

CHAPTER 6

Comparison of the Competing Reaction Mechanisms and Energetics for Carbonylation of Neutral and Cationic Palladium Complexes

Chapter 6

Comparison of the Competing Reaction Mechanisms and Energetics for Carbonylation of Neutral and Cationic Palladium(II) Complexes Containing Bidentate (N-O) ligands

6.1 Introduction

The marked differences in reaction behaviour between neutral and cationic complexes has been a topic of conjecture for a number of years.[7,31,33,34,41,66,198-200] Nowhere is this more evident than in palladium(II) chelate catalysed polyketone formation, where neutral complexes show little or no activity in this reaction, whilst their cationic counterparts are generally significantly more active.[1,5,12,19,43,48,62] However, experimental investigations of the individual migratory insertion steps indicate that the relative rates of carbonylation for neutral and cationic systems depend on the structure of the chelating ligand.[29,31,34,39,66] Cationic alkyl- or aryl-complexes appear to only exhibit *consistently* higher carbonylation reactivities than neutral complexes when the bidentate ligand is symmetrical (N-N or P-P).[12,29,31,34,66]

Experimental studies performed concurrently with the present work found that cationic complexes of N-O ligands possessed similar carbonylation reaction rates to the neutral systems under equivalent reaction conditions.[43] Similar observations have been made by Vrieze *et al.* for palladium(II) complexes of asymmetric N-N ligands,[29] although the use of different solvents precluded unambiguous comparison of reaction rates between the neutral and cationic complexes. More recently, Vrieze *et al.*[39] reported a *lack* of carbonylation reactivity for cationic allyl-palladium complexes incorporating the *p*-An-BIAN ligand (**VI**), while the neutral complexes readily insert

CO. A possible explanation is the inability of the weakly coordinating anion in the former system to stabilise particular reaction intermediates.

Despite the publication of a number of studies aimed at the elucidation of mechanisms, little insight into the conflicting behaviour of cationic and neutral complexes has been gained. A recent theoretical investigation by Markies *et al.* compared the carbonylation of the cationic complex $[Pd(NH_3)_3(CH_3)]^+$ to that of the neutral complex $[Pd(NH_3)_2(CH_3)_2]$.[28] Negligible variation in the reaction mechanism or energetics was reported. They concluded that the enhanced reactivity of the cationic system did not appear to be intrinsic to the cationic character, and may instead arise from solvent effects.

Experimental mechanistic studies of carbonylation of the cationic system (**II**) have not been able to clearly elucidate the transformations taking place. In contrast to the corresponding neutral system (**I**),[61,62] phosphine dissociation is not indicated.[42,43] The oxygen donor has been observed to exhibit some hemilability, evidence of which is provided by an X-ray crystal structure obtained of the novel pseudo five-coordinate intermediate $[Pd(CH_2CH_2C(O)CH_3\text{-}C,O)(C_5H_4N(CO_2CH_3)\text{-}1\text{-}N)(PPh_3)]^+BF_4^-$[48] (refer to Figure 1.1).

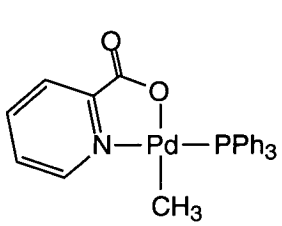

(**I**)

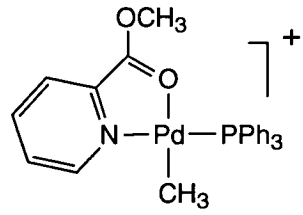

(**II**)

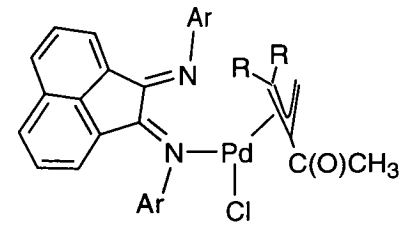

(**VI**) Ar = *p*-$CH_3OC_6H_4$ (*p*-An)

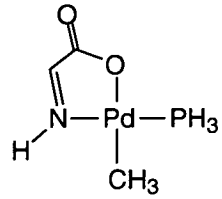

(**1**)

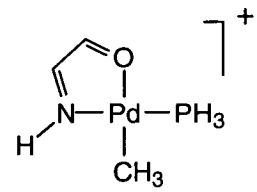

(**21**)

As a result of the current interest in this area of catalysis, this chapter aims to confront two problems: first, to investigate the possible reaction mechanisms for the model cationic complex **21** (Scheme 6.1); second, to compare the lowest energy pathway for the cationic model to the lowest energy pathway defined in Chapter 5 for the neutral model **1** (illustrated in Scheme 6.2). For qualitative purposes the cationic model (**21**) is similar to the experimental system (**II**); the model chelate ligand retains the backbone of methyl picolinate including some delocalisation effects and the π-accepting ability of the imino nitrogen donor.

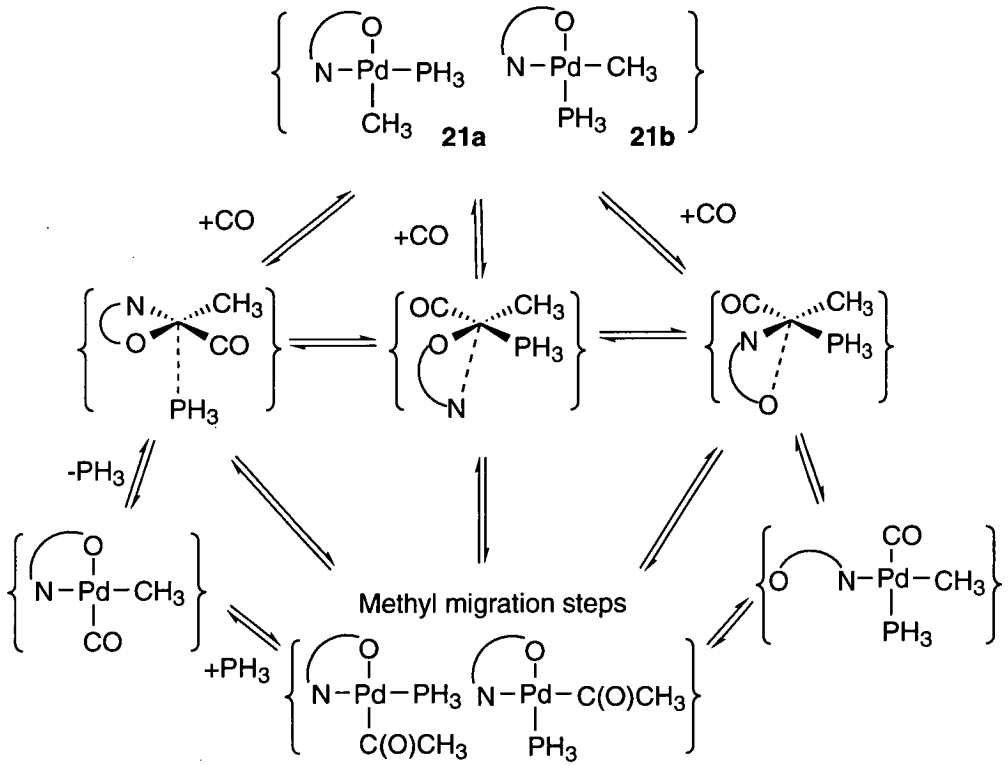

Scheme 6.1: *Carbonylation mechanisms investigated for the model system **21**. Note that all species are cationic. The brackets indicate a possible isomeric mixture although, for simplicity, the second isomer is not always shown.*

The metal-ligand bond lengths (Å), selected bond angles (deg) and relative energies (kJ/mol) from the correlated calculations are presented in Tables 6.1 and 6.2

and Figures 6.1 - 6.3. The complete set of geometrical data and total energies generated at correlated and RHF levels of theory are listed in Appendix 5.

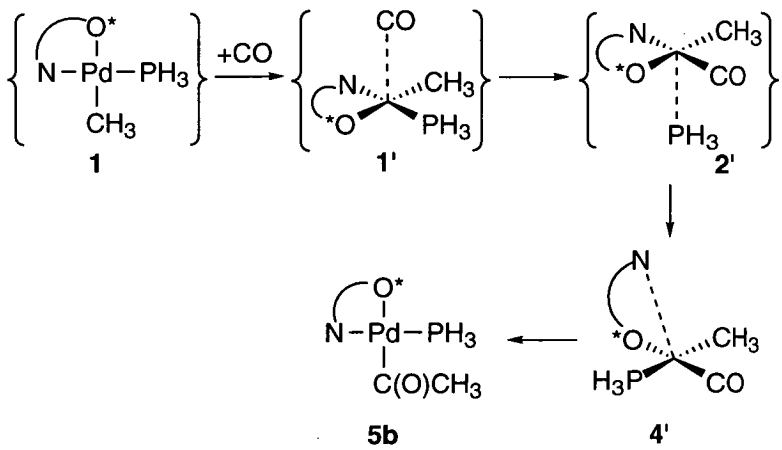

Scheme 6.2: *The lowest energy pathway for carbonylation of the neutral model* ***1*** *(refer to Chapter 5). The asterix on the chelate oxygen distinguishes it as a hydroxyl group, and the brackets indicate a mixture of trans(CH_3,O) and cis(CH_3,O) isomers.*

6.2 Overview of the Theoretical Methods

C_S symmetry was adopted for the four-coordinate reactants and C_1 symmetry was used for all other intermediates and transition structures. Various methyl migration steps were investigated at the B-LYP/[basis set A] level of theory. Refined geometries for the mechanism associated with the lowest energy migration were obtained at MP2/[basis set A]. In all cases, the energies determined using the MP2 geometries and the B-LYP geometries agree to within 5 kJ/mol. The only discrepancy between the two theories arose when dealing with the trigonal–bipyramidal intermediate **22'a**. This structure was not located at the MP2 level, and a single-point energy at MP2/[basis set B]//MP2/[basis set A] indicated that the structure is unfavourable and, therefore, that the B-LYP PES is unreliable in this region. Unless otherwise stated, the geometries discussed will be those determined at the B-LYP level of theory, and

energies have been determined at MP2/[basis set B] with respect to the separated reactants, **21a** + CO.

The first sections will consider coordination of CO to the four-coordinate reactant and the subsequent ligand substitution processes. Eight possible migratory insertion steps were investigated and will be discussed in Section 6.5. Section 6.6 will present a comparison between the MP2/[basis set B]//MP2/[basis set A] potential energy surfaces for the cationic system of the present study and the neutral system investigated in Chapter 5.

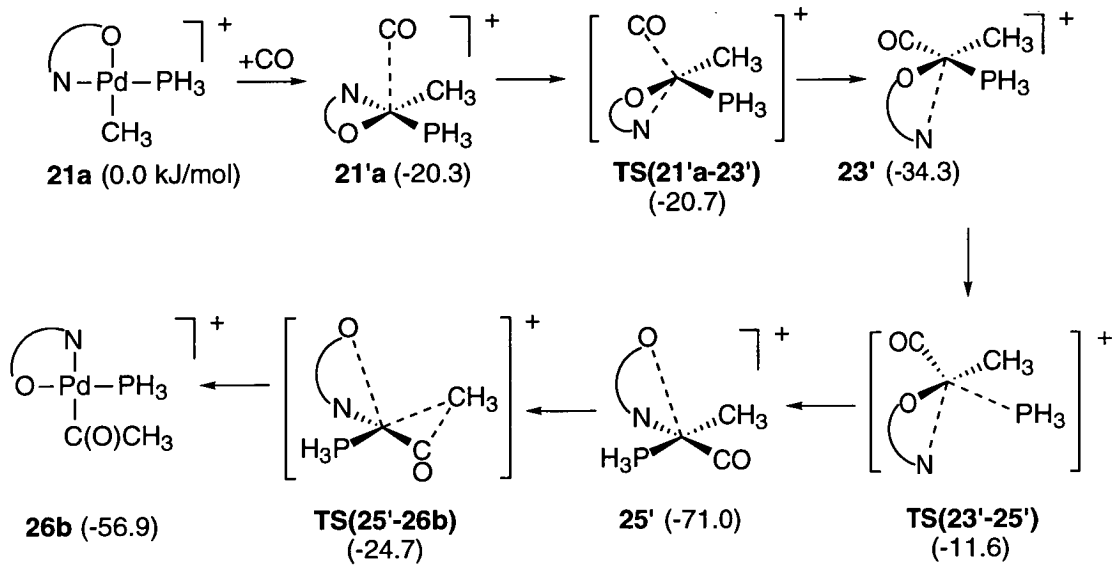

Scheme 6.3: *The lowest energy reaction mechanism for carbonylation of* ***(i) 21a****, and* ***(ii) 21b****.*

Table 6.1: *Metal-ligand bond lengths for the Reactants, Intermediates, Transition Structures, and Products of the lowest energy reaction Mechanism. Optimised with the B-LYP/[basis set A] method, MP2/[basis set A] values are in parentheses.*

	Metal-ligand bond lengths (Å)				
	Pd-P	Pd-CH_3	Pd-N	Pd-O	Pd-CO
21a	2.314 (2.298)	2.068 (2.049)	2.131 (2.155)	2.338 (2.332)	-
21'a	2.315 (2.292)	2.073 (2.052)	2.143 (2.161)	2.345 (2.328)	2.909 (2.950)
TS(21'a-22'a)[†]	2.353 (2.302)	2.092 (2.079)	2.164 (2.292)	2.326 (2.319)	2.304 (2.267)
22'a	2.698	2.101	2.138	2.310	1.959
23'	2.409 (2.404)	(2.103)	2.853 (2.603)	2.352 (2.333)	1.967 (1.957)
TS(22'a-25')[†]	2.865 (2.730)	2.118 (2.107)	2.102 (2.160)	2.491 (2.453)	1.925 (1.889)
25'	2.530 (2.502)	2.141 (2.113)	2.146 (2.154)	2.918 (2.710)	1.912 (1.882)
TS(25'-26b)	2.402 (2.401)	2.356 (2.282)	2.216 (2.256)	2.829 (2.643)	1.881 (1.845)
26b	2.341 (2.327)	3.003 (2.917)	2.320 (2.332)	2.297 (2.302)	2.034(2.023)
21b	2.284 (2.276)	2.069 (2.058)	2.241 (2.263)	2.244 (2.241)	-
24'	2.414 (2.405)	2.128 (2.110)	2.259 (2.229)	3.006 (2.785)	1.960 (1.939)
TS(24'-23')	2.406 (2.397)	2.127 (2.113)	2.671 (2.569)	2.538 (2.431)	1.958 (1.954)

[†] Intermediate **22'a** was not located at the MP2 level of theory. Otimisation of the transition structures generated **23'**.

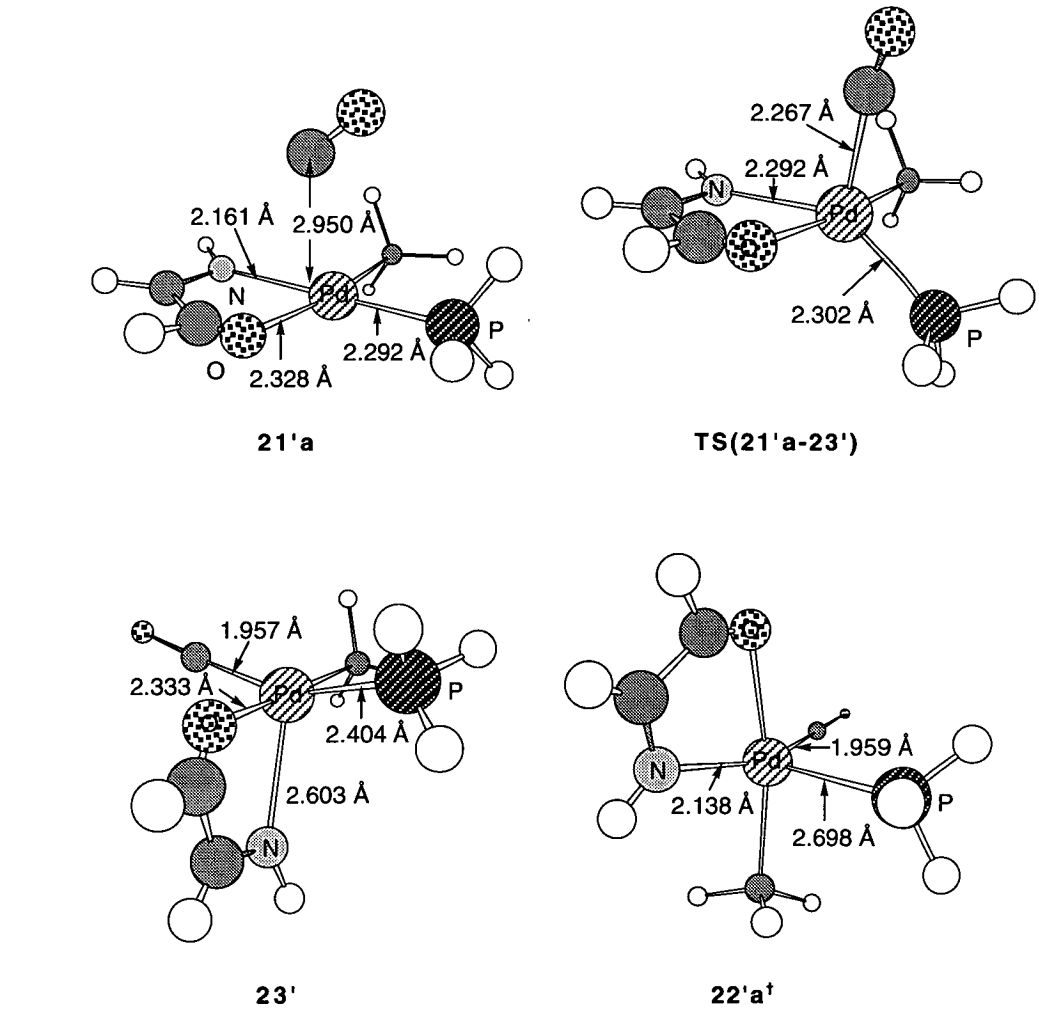

Figure 6.1: *Selected structures optimised at MP2/[basis set A] with the exception of* ***22'a*** *(†A trigonal–bipyramidal intermediate optimised at B-LYP/[basis set A]).*

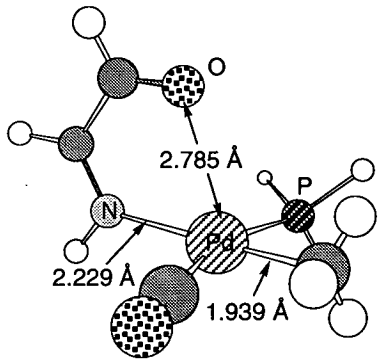

24'

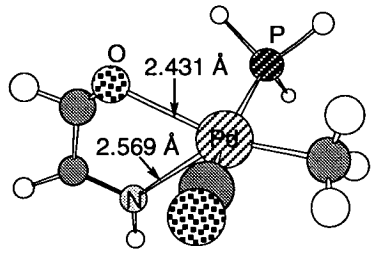

TS(24'-23')

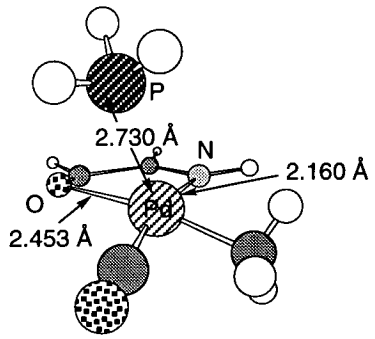

TS(23'-25')

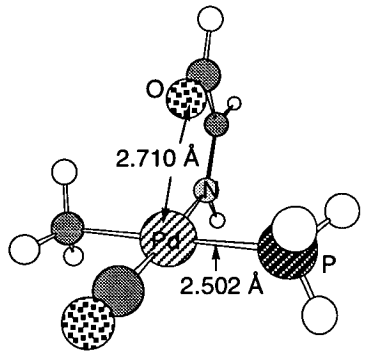

25'

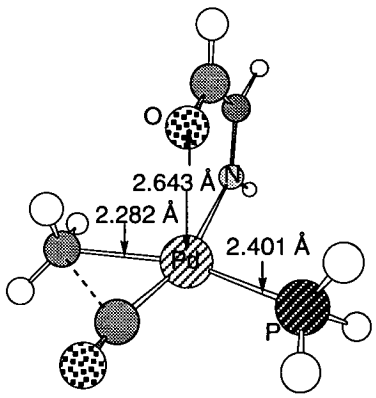

TS(25'-26b)

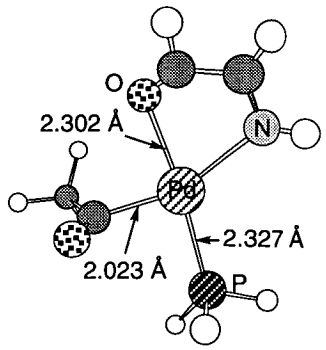

26b

Figure 6.1 (continued).

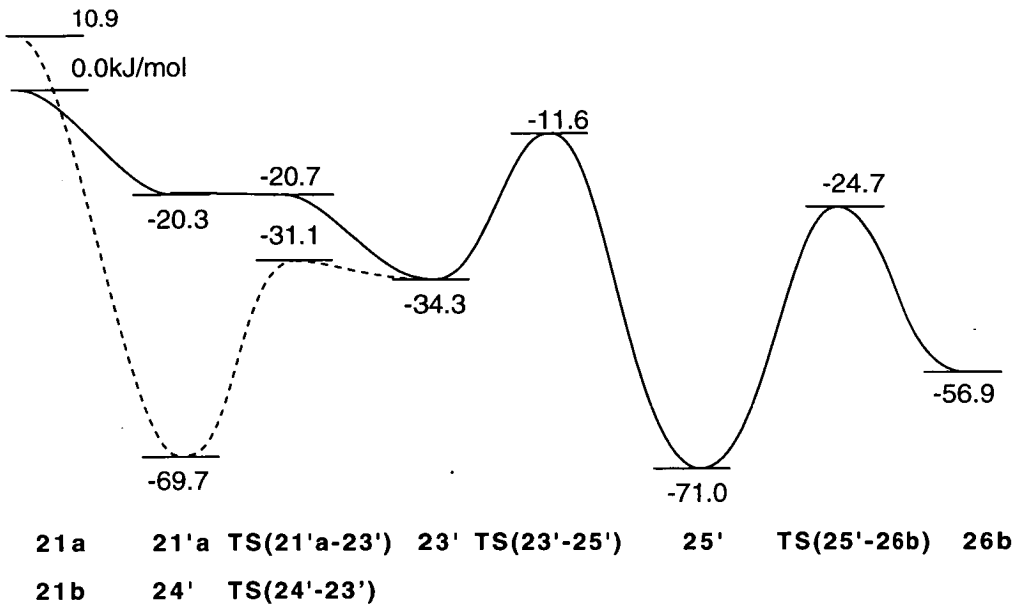

Figure 6.2: *The potential energy surface for the lowest energy pathway (via **TS(25'-26b)**) at MP2/[basis set B]//MP2/[basis set A] for carbonylation of **21a** (—) and **21b** (---).*

6.3 Coordination of Carbon Monoxide

The geometries of the reactants, intermediates and transition structures are displayed in Table 6.1. Selected structures are illustrated in Figure 6.1. The *trans*(N,P) reactant (**21a**) was found to be lower in energy than the *cis* isomer (**21b**) by 10.9 kJ/mol. This is due to the favourable alignment of the highly trans influencing methyl group and the weak donor oxygen in the *trans* isomer. In contrast, the *cis* and *trans* isomers of the neutral reactant (**1**) were within 3kJ/mol in energy. The difference concurs with the experimental isolation of only the *trans* isomer of the cationic reactant,[43] while the neutral reactant is typically obtained as an isomeric mixture.[61,62] Initially, consider the coordination of carbon monoxide to the *trans*(N,P) isomer **21a** (refer to Scheme 6.3). An intermediate in which CO is weakly interacting with the metal was located with a metal-carbonyl separation of 2.950 Å and an energy of

-20.3 kJ/mol (**21'a** in Figure 6.1). Single-point energies at MP2/[basis set B] indicate that *if* such an intermediate exists it is unstable, undergoing ligand substitution with a negligible barrier (refer to the PES in Figure 6.2).

The transition structures located for ligand substitution of **21'a** employing MP2 and B-LYP methods exhibited subtle differences. In particular, the MP2-optimised metal-nitrogen bond length (2.292 Å) was elongated from that determined by B-LYP (2.164 Å). This seems unusual given the tendency of nonlocal B-LYP to *overestimate* metal-ligand bond lengths,[118] and MP2 methods to *underestimate* them.[134] Optimisation downhill from the transition structures at each level of theory showed that they corresponded to different points on the PES. The diverging paths are illustrated in Figure 6.3. The B-LYP transition structure corresponds to coordination of CO with simultaneous weakening of the Pd-PH_3 bond to form a trigonal–bipyramidal intermediate (**22'a** in Figure 6.1). Conversely, the MP2 transition structure corresponds to replacement of the donor nitrogen to yield **23'** explaining the elongated metal-nitrogen bond length in the transition structure. The single-point MP2 energy of B-LYP-optimised **22'a** is high in comparison to **23'**, supporting formation of the latter.[†] A similar variation in transition structures between MP2 methods and DFT when the transition structure is near-degenerate has been highlighted in Chapter 4. A transition structure linking **22'a** and **23'** at the B-LYP level of theory could not be located. However, intuitively we can predict that the deformation of the PH_3-Pd-CO angle of **22'a** towards 180° yielding **23'** is likely to be facile. Experimental mechanistic work has demonstrated a rate enhancement with an increase in steric bulk on the donor nitrogen,[42] consistent with partial dissociation of the nitrogen predicted at the MP2 level of theory.

[†] The well depth associated with the formation of **22'a** at B-LYP/[basis set A] was 10.0 kJ/mol with respect to the transition structure **TS(21'a-22'a)**, and +0.6 kJ/mol with respect to **23'**. The B-LYP PES therefore appears to be fairly flat in this region.

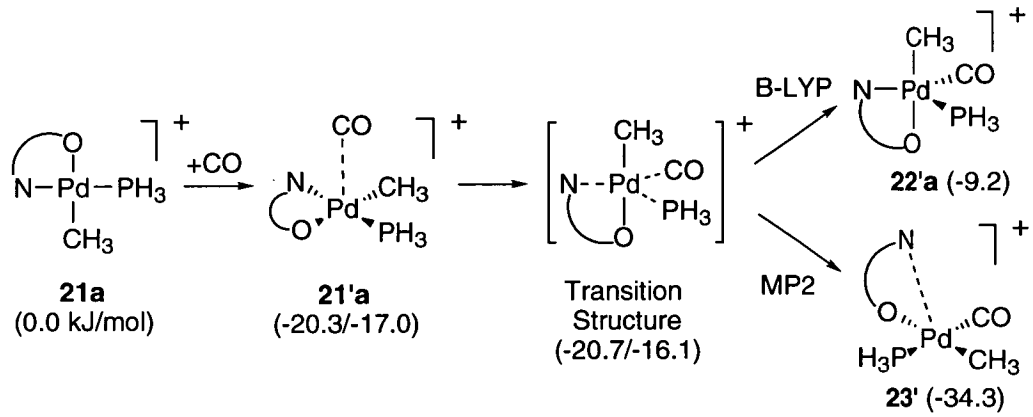

Figure 6.3: *Coordination of CO to* ***21a*** *illustrating the differing results of the MP2 and B-LYP calculations. Single-point MP2/[basis set B] energies are given at the MP2 / B-LYP geometries.*

Although we have considered coordination of CO *via* partial dissociation of PH_3 or of the donor nitrogen, displacement of the donor oxygen is also possible. Such a transformation for **21a** would be expected to be relatively facile due to the position of the highly trans influencing methyl group. However, the resulting *trans*(CH_3,CO) intermediate will be an unproductive species. We have also considered the coordination of CO to **21a** *via* a three-coordinate intermediate (**27a**) following the complete dissociation of PH_3. The high barrier generated for this process (196.1 kJ/mol at MP2/[basis set A]//B-LYP/[basis set A]) is similar to the corresponding reaction of **1a** presented in Section 5.3.1.

Coordination of carbon monoxide to the *cis*(N,P) isomer **21b** proceeded without a barrier to yield an intermediate in which the oxygen is weakly bound (**24'** in Figure 6.1). No intermediate in which the carbonyl is weakly bound was located (refer to Scheme 6.3). Similar processes have been reported by Ziegler *et al.*[45,49] for coordination of CO to model cationic complexes incorporating a non-labile P-P ligand. The relative energy of **24'** is very low (-69.7 kJ/mol), consistent with its direct

formation. The low strength of the Pd-O bond, and high exothermicity of formation of **24'** precludes observation of competing rearrangements.

6.4 Rearrangements and Isomerisation

The rearrangements considered are illustrated in Scheme 6.3. Selected geometrical parameters are listed in Table 6.1, and structures are illustrated in Figure 6.1. The replacement of the donor nitrogen of **24'** in the metal coordination sphere by the oxygen is straight forward and proceeds *via* a trigonal–bipyramidal transition structure (**TS(24'-23')** in Figure 6.1) to yield **23'**. As illustrated by the PES in Figure 6.2, the reaction from the two isomers **21a** and **21b** merges at this point. The substitution has a moderately high activation energy of 38.6 kJ/mol with respect to **24'**. Furthermore, rearrangement of **23'** to yield **24'** possesses a negligible barrier (3.2 kJ/mol) thereby creating a "thermodynamic sink" in the PES. We can therefore surmise that increasing the lability of the donor oxygen or decreasing the lability of the nitrogen would terminate the reaction at this point yielding a potentially isolable carbonyl complex. Vrieze *et al.* previously postulated the formation of such intermediates to rationalise the experimentally monitored reduction of carbonylation reactivity of alkyl-palladium complexes of N-P chelate ligands relative to their N-N and P-P counterparts.[31]

Isomerisation and concomitant ligand substitution takes place from **23'** *via* a distorted transition structure (**TS(23'-25')** in Figure 6.1) with a modest activation energy (22.7 kJ/mol). A similar process was presented in Section 5.3.3 for isomerisation in the neutral system. The product is the pseudo five-coordinate intermediate (**25'** in Figure 6.1) in which the metal-oxygen bond is elongated (2.710 Å at MP2/[basis set A]). The prediction of such an intermediate has been reinforced by subsequent experimental work in which a similar intermediate has been

isolated and analysed by X-ray crystallography (refer to Figure 1.1).[48] The experimental metal-oxygen distance (2.78(1) Å) is midway between the MP2 and DFT values.

It is interesting to note the significant elongation of the Pd-PH_3 bond in **TS(23'-25')** (refer to Table 6.1 and Figure 6.4). This results from competition for σ-donation and π back-donation due to the carbonyl and donor nitrogen groups in the equatorial plane. Although no evidence of phosphine *dissociation* has been observed experimentally, replacement of PPh_3 with the more basic PCy_3 dramatically reduces the carbonylation rate of the complex.[42] This trend can therefore be rationalised by inhibition of isomerisation by a less labile phosphine and will be discussed further in Chapter 8.

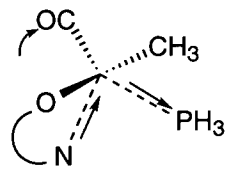

Figure 6.4: *Isomerisation transition structure **TS(23'-25')**, illustrating the elongation in the palladium-phosphorus bond.*

6.5 Methyl Migration

Migration was investigated from each of the intermediates illustrated in Figure 6.5. Relative energies of the transition structures, intermediates and products are included in Figure 6.5. Selected bond lengths and angles for the transition structures and the activation energies for each migration step are given in Table 6.2. Although transition structures corresponding to migration from intermediates in which the donor nitrogen is weakly bound were optimised at the RHF level of theory, reoptimisation at correlated levels produced lower-energy migration transition structures.

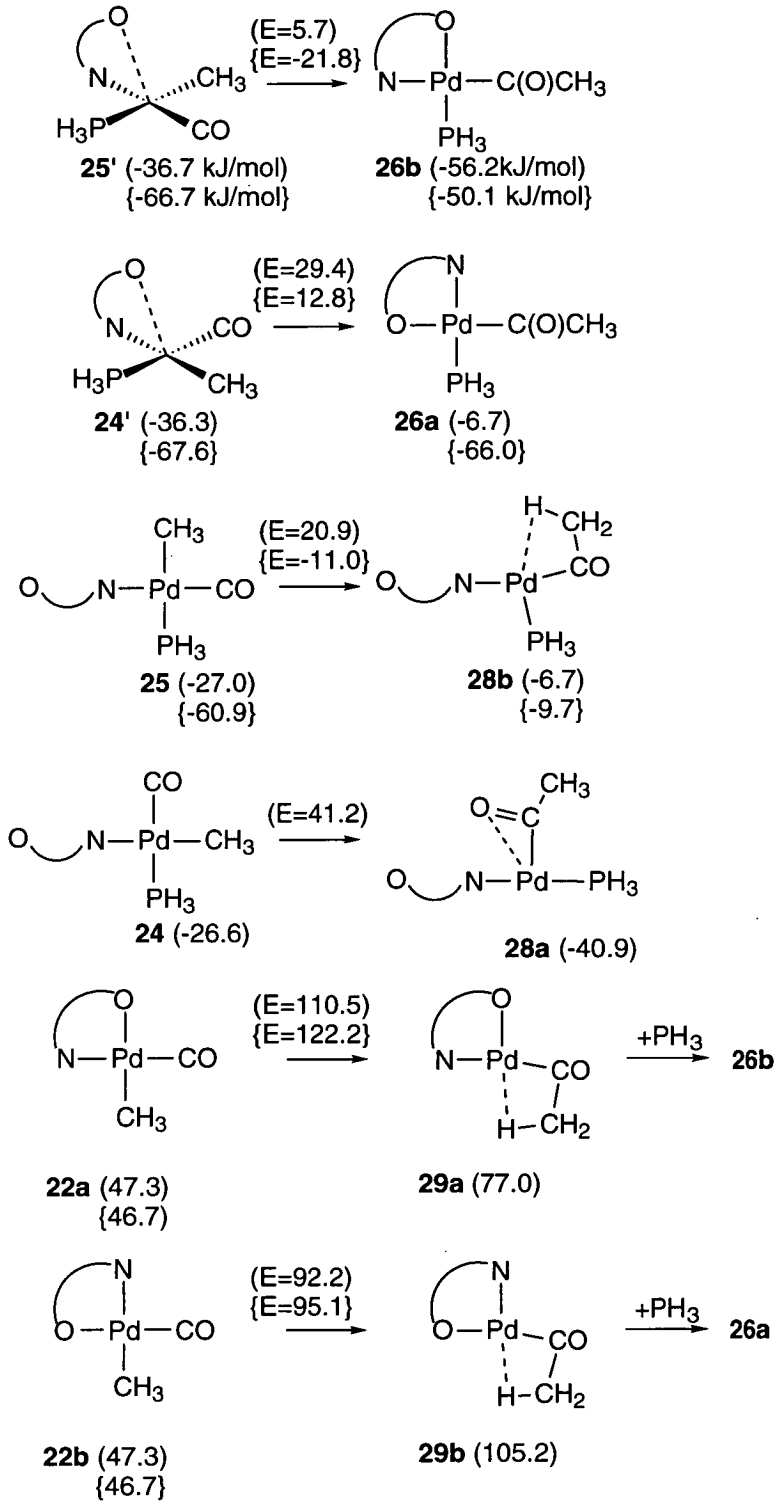

Figure 6.5: *Methyl migration steps considered. Relative energies have been determined at (MP2/[basis set A]//B-LYP[basis set A]), and {MP2/[basis set B]//B-LYP/[basis set A]}. The barrier, E, associated with each step is also indicated.*

Migration from **25'** possessed the lowest activation energy at every level of theory considered (refer to Table 6.2). This is in agreement with the previous speculation that migration is more likely to proceed from an intermediate in which the CO is *trans* to a donor nitrogen,[31] and the phosphine is *trans* to the alkyl group.[201,202] The transition structure and product for this step are illustrated in Figure 6.1.

Table 6.2: *Activation energies and selected geometric parameters for the methyl migration steps considered. Geometries have been optimised at the B-LYP level of theory, activation energies have been determined at MP2/[basis set A]//B-LYP/[basis set A] and MP2/[basis set B]//B-LYP/[basis set A] in parentheses.*

	Metal-ligand bond lengths (Å)					Angle (deg)	Activation energy
	Pd-CH_3	Pd-CO	Pd-PH_3	Pd-N	Pd-O	C-Pd-C	(kJ/mol)
TS(25'-26b)	2.356	1.881	2.402	2.216	2.829	55.3	42.4 (44.9)
TS(24'-26a)	2.351	1.892	2.532	2.160	2.856	53.2	65.7 (80.4)
TS(25-28b)	2.359	1.888	2.401	2.187	-	54.6	47.9 (49.9)
TS(24-28a)	2.353	1.898	2.532	2.134	-	52.9	67.8
TS(22a-29a)	2.321	1.874	-	2.258	2.266	51.4	70.5 (84.6)
TS(22b-29b)	2.297	1.867	-	2.146	2.353	54.3	44.9 (48.4)
TS(4'-5a)[a]	2.334	1.868	2.354	2.563	2.182	54.7	55.6 (58.7)

[a] The lowest energy methyl migration transition structure for the neutral complex (refer to Chapter 5).

The barrier to migration from **25**, in which the oxygen is completely dissociated from the metal centre (49.9 kJ/mol), is only marginally higher than the barrier to migration from **25'** (44.9 kJ/mol). The preceding intermediate (**25**) is also close in energy to **25'**. Analogous results were obtained for migration from the neutral intermediates **4** and **4'** (refer to Chapter 5). However, while the product of migration from **4** was stabilised by coordination of the carboxyl oxygen of the chelate, similar stabilisation could not be imparted by the chelate ligand of the cationic system. The product of the latter migration is a pseudo four-coordinate intermediate (**28b**), which is high in energy and therefore activated towards decarbonylation or β-hydride elimination. Partial stabilisation is provided by an agostic interaction with a hydrogen of the methyl group of the acyl ligand. Interestingly, the corresponding reaction of the *cis*(CH_3,P) isomer (**24** in Figure 6.5) yields a T-shaped product involving a more stable agostic interaction with the carbonyl oxygen of the acyl ligand (**28a**). Note that solvent-stabilisation of the agostic product (**28b**) may occur in the experimental medium, so that migration from **25** competes with migration from **25'**.

Migration from the *cis*(CH_3,P) intermediates (**24'** and **24**) is significantly higher in energy than migration from the related *trans*(CH_3,P) intermediates (**25'** and **25** respectively). Such trends are typically attributed to a weakening of the Pd-CH_3 bond *trans* to the highly trans influencing phosphine, activating the bond towards migration.[201,202] However, the Pd-CH_3 bond lengths and natural charges on the methyl groups determined for each migration precursor are similar (refer to Tables 6.1 and 6.3). Natural population analyses in Table 6.3 suggest that the variation between isomers can instead be attributed to differences in the degree of metal-carbonyl π back-donation. This is illustrated by a lower positive charge on the carbonyl carbon of the *cis*(P,CH_3) intermediates together with a decrease in the Pd d_{xy} population. Positioning the phosphine *trans* to CO rather than *trans* to CH_3 induces an increase in σ-donation from PH_3 and a reduction in metal-phosphorus π back-donation. A

subsequent increase in electron density on the metal results in enlargement of the d-orbitals (enhancing orbital overlap) and facilitates metal-carbonyl π back-donation. As discussed in Section 1.4.2, the increase in the carbonyl π* orbital population reduces stabilisation of the migration transition structure, explaining the increased barrier for migration from the *cis*(P,CH_3) isomers.

Table 6.3: *Charges on palladium and selected ligands for migration precursors from natural population analyses.*[a]

	Molecular fragments					Pd d-orbital population (Pd–CO / CH_3; X, Y, Z)	
	Pd	CH_3	PH_3	carbonyl C	carbonyl O	$d_{x^2-y^2}$	d_{xy}
25'	0.462	-0.021	0.217	0.472	-0.306	1.426	1.897
25	0.442	-0.016	0.209	0.480	-0.297	1.372	1.892
24'	0.426	-0.014	0.293	0.454	-0.304	1.575	1.835
24	0.405	-0.013	0.301	0.466	-0.296	1.375	1.913
22a	0.508	0.066	-	0.478	-0.286	1.406	1.822
22b	0.542	0.068	-	0.472	-0.292	1.358	1.870
4'[b]	0.555	-0.008	0.182	0.387	-0.387	1.438	1.863

[a]Note that the validity of natural orbital population analyses applied to transition metals when treating the empty p orbitals as Rydberg rather than valence orbitals has been questioned.[203]

[b]Intermediate preceding the lowest energy methyl migration step for the neutral system (Chapter 5).

Finally, rearrangement must occur to allow the donor oxygen in **24'** and **24** to re-establish normal (i.e., strong) coordination and to yield a stable product. These results reinforce the earlier prediction that intermediates of the type **24'** will be isolable for some systems.

Migration from four-coordinate intermediates formed by dissociation of the phosphine ligand were shown to be high in energy for the neutral system (Chapter 5). While the barrier to the corresponding migration from the *cis*(CO,O) cationic intermediate (**22a**) was similarly large, migration from the *trans*(CO,O) intermediate (**22b**) proceeded with a barrier comparable to migration from **25'** or **25** (refer to Table 6.2). Natural population analyses of **22a** and **22b** indicate that the marked difference between the isomers is again due to reduced in-plane Pd-CO π back-donation in the *trans*(CO,O) isomer. The lower Pd $d_{x^2-y^2}$ orbital population of **22b** relative to **22a** indicates a drop in σ-donation to the metal. This is due to the *trans* alignment of the methyl and imine groups resulting in reduced σ-donation by the imine nitrogen. The relative magnitude of the corresponding increase in σ-donation from the oxygen in the *trans*(O,CO) arrangement is small due to the low σ-donor capacity of the oxygen. Consequently, the palladium d-orbitals of **22b** are contracted and less electron density is available for π back-donation. Again, note that there is little variation in the Pd-CH_3 bond between the *cis* and *trans* isomers (Tables 6.2 and 6.3). The reduced σ-donation by the donor nitrogen in the *trans*(O,CO) neutral intermediate (**2b**) is balanced by an increase in the strength of the covalent Pd-O bond relative to **2a**, explaining the high migration barrier in this case.

Vrieze *et al.* suggested that increased polarisation of the C-O bond *trans* to an imine nitrogen may be partially responsible for the high carbonylation reactivity of alkylpalladium complexes of rigid N-N ligands.[11] The natural charges on the carbonyl C and O listed in Table 6.3 illustrate that there is negligible variation in CO charge polarisation between *cis* and *trans* isomers considered in this study.

Although the activation energy associated with migration from **22b** is low, the high relative energy of **22b** indicates that full dissociation of the phosphine is energetically unfavourable and such a pathway is not competitive.

The lowest energy pathway for carbonylation of the cationic system therefore involves migration from **25'**. The PES in Figure 6.2 for this mechanism illustrates the existence of two high-energy transformations: ligand substitution of **24'** (38.6 kJ.mol) and methyl migration (46.3 kJ/mol). The product of the reaction is the *cis*(N,P) isomer, **26b**. Experimental studies on (**II**)[42,43] have been unable to unambiguously identify the stereochemistry of the cationic acyl product which has previously been assumed to be the *trans*(N,P) isomer in agreement with studies on the neutral system (**I**).[61,62] However, characterisation of the intermediate following alkene insertion (**IV** in Figure 1.1) showed this insertion product to be the unexpected *cis*(N,P) isomer! NMR studies on the product of carbonylation of **II** have indicated that isomerisation between the product isomers is facile.[43] The *trans*(N,P) isomer, **26a**, was found to be lower in energy than **26b** suggesting that isomerisation of the products may occur.

6.6 Comparison of the Neutral and Cationic Complexes

The competing mechanisms operating in the carbonylation of the neutral complex are presented in Chapter 5, and the lowest energy pathway is illustrated in Scheme 6.2. There are several obvious differences in the reaction mechanism of carbonylation of the neutral and cationic systems which are primarily due to replacement of the strong covalent Pd-O bond in **1** with a dative Pd-O bond in **21**. Consequently, there is an additional potentially labile metal-ligand bond in the cationic system yielding a complex more flexible towards rearrangements.

The coordination behaviour of the phosphine varies between the neutral and cationic systems. Partial dissociation of PH_3 has been demonstrated in the rearrangements of the neutral system required to yield an intermediate activated

The coordination behaviour of the phosphine varies between the neutral and cationic systems. Partial dissociation of PH_3 has been demonstrated in the rearrangements of the neutral system required to yield an intermediate activated towards methyl migration (Section 5.3.1). Similar dissociation is not observed for the cationic system, however the phosphine must possess a certain degree of lability to allow isomerisation. This effect is observed only in the transition structure, highlighting the power of theoretical calculations which provide a unique insight into transformations and can elucidate experimental trends that are otherwise not obvious.

A superposition of the cationic and neutral PES's is given in Figure 6.6. It can be seen that the energies of intermediates **24'** and **25'** relative to the four-coordinate reactants and products are lower than the relative energy of the neutral migration precursor **4'**. This can be attributed to the low strength of the Pd-O bond in the cationic complex relative to the other metal-ligand bonds, resulting in its facile cleavage.

There is very little difference in the overall reaction energy, carbonylation of the neutral complex being more exothermic than that of the cationic complex by 2.8 kJ/mol. There is a small decrease of 12.4 kJ/mol in the barrier of the methyl migration step for the cationic system compared to the neutral system which will be rationalised in Chapter 8. The main contrast is that carbonylation of the cationic complex proceeds with no overall barrier, whereas a very modest barrier of +6.0 kJ/mol is associated with carbonylation of the neutral complex. It should also be noted that there are two moderately high barriers associated with carbonylation of the cationic complex, whereas only the methyl migration step in the neutral system has a high activation energy. Following the completion of this work experimental studies have shown that the reaction rates of the neutral and cationic systems (**I** and **II** respectively) are very similar,[43] consistent with our findings.

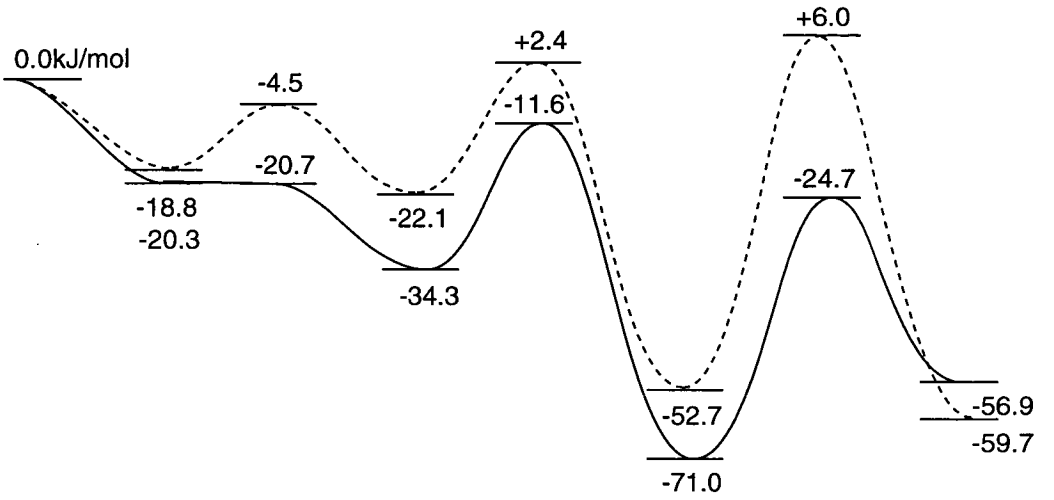

(i) The *trans*(N,P) isomers **1a** and **21a**

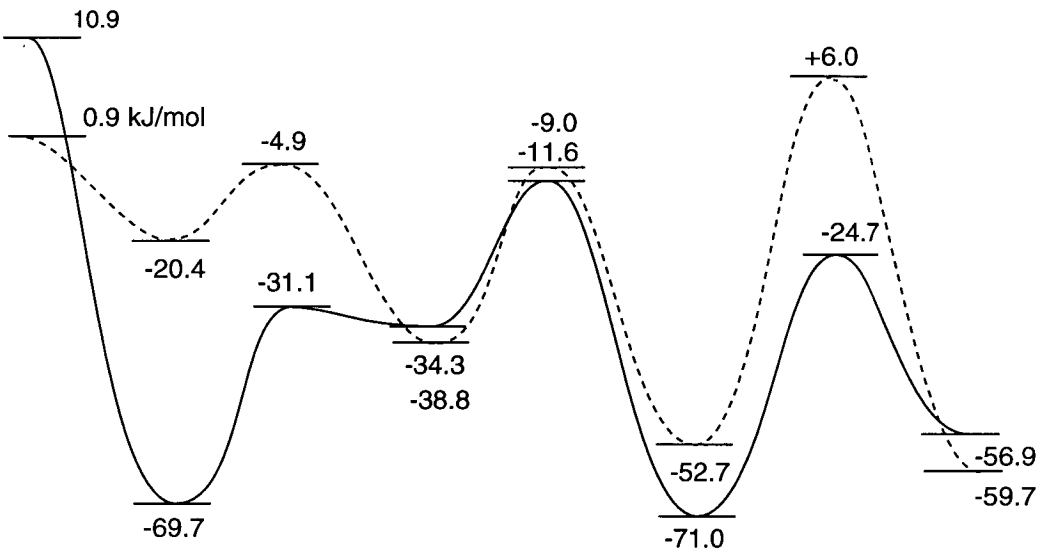

(ii) The *cis*(N,P) isomers **1b** and **21b**

Figure 6.6: *Overlays of the PES's for the lowest energy carbonylation mechanisms for the cationic system (—) and the neutral system (---). Energies were generated at MP2/[basis set B]//MP2/[basis set A].*

6.7 Conclusions

The lowest energy pathway for carbonylation of the model cationic complex $Pd(N\text{-}O)(CH_3)(PH_3)$ (N-O = NHCHCHO) involves methyl migration from a pseudo five-coordinate intermediate in which the donor oxygen is weakly bound (**25'** in Figure 6.1). Rearrangements to generate **25'** proceed *via* square–pyramidal pseudo five-coordinate intermediates and trigonal–bipyramidal transition structures. The agreement between the theoretically predicted mechanism and experimental mechanistic results is exceptional. We have implicated the participation of partial dissociation of the donor nitrogen, and shown that the phosphine must possess some lability. Variations in activation energies for methyl migration from *cis* and *trans*(CO,N) isomers can be rationalised by changes in metal-carbonyl π back-donation rather than changes in the metal-methyl bond strength, or CO charge polarisation.

The barrier associated with the rate-determining migration step was not significantly different from that determined for the neutral model in Chapter 5. However, while this step is the only high energy transformation for the neutral model, there are two high-energy steps in the carbonylation of the cationic complex. The results are consistent with experimental kinetic measurements which have shown that the rate constants for carbonylation of the cationic and neutral N-O complexes are similar. Therefore, the differences in copolymerisation activities between cationic and neutral N-O complexes appear to arise from the olefin insertion step rather than carbonylation. A comparative study of the ethylene insertion step will be presented in Chapter 7.

CHAPTER 7

Olefin Insertion

Chapter 7

Olefin Insertion

7.1 Introduction

The enhanced CO/olefin copolymerisation activity of cationic complexes compared to their neutral counterparts has been demonstrated experimentally.[1,5,19,42,43,62] In many cases, neutral complexes are only observed to catalyse copolymerisation following dissociation of a weakly bound anionic ligand to generate an active cationic species.[19,66] A commonly cited explanation involves the increased ease of displacement of a ligand from the cationic catalyst species by the reacting substrate (either CO or the olefin). However, unambiguous evidence for this rationale has not been provided.

The results presented in Chapter 6 together with kinetic studies indicate that the relative rates of carbonylation of cationic and neutral N-O complexes are similar.[43] This suggests that the olefin insertion step is responsible for the inactivity of the latter towards the copolymerisation of CO and ethylene. Although this has been suggested previously by others,[29,43] the present study is the first to apply theoretical methods to this problem of fundamental interest.

Stepwise insertions of CO and ethylene into a palladium-hydride bond has been theoretically investigated by Morokuma *et al.*[46] and Ziegler *et al.*[45,49] The catalytic species in both studies was of the type $[L_2PdH]^+$, where L_2 represents a bidentate ligand (N-N[46] or P-P[45,49]). The bearing of the fourth ligand of a "real" catalyst on the reaction energetics was neglected. Ziegler *et al.* considered the effect on the CO/ethylene coordination and insertion energies by chelation of carbonyl groups of the

growing polymer chain.[49] The barrier of the insertion step was shown to be insensitive to the weak association of a fifth ligand, the latter having more influence on the ethylene binding energy and on the stability of the product. The activation energies determined by each group compared well to the experimental results of Rix *et al.*,[44] and showed the olefin insertion step to be rate-determining.

Siegbahn and coworkers investigated ethylene binding energies and barriers for insertion into palladium-*alkyl* bonds for a range of model one-, two-, and three-coordinate cationic palladium(II) complexes.[75] Again, ligand displacement and rearrangement transformations were neglected. They found that although alkene coordination energies were sensitive to coordinated ligands, the insertion barrier appears to be intrinsic to the metal. The dependence of copolymerisation activity on the nonparticipatory ligands was suggested to be due to variations in olefin coordination energies and the susceptibility of the product towards β-hydride elimination, rather than the insertion barrier. Agreement between the calculated insertion barrier and experiment[9] led to the proposal that the influence of the counterion or solvent was minimal.

Although olefin insertion is generally hindered for neutral N-O and N-N complexes, Sen and coworkers have reported the insertion of norbornylene into the palladium-acyl bond of $Pd(PPh_3)_2(Cl)(COR)$.[47] The reaction was observed to be accelerated by the presence of a phosphine "sponge", which led them to postulate a four-coordinate mechanism following olefin-assisted displacement of a phosphine ligand. However, the reaction kinetics could not be unambiguously explained by a single mechanism. Evidence for the formation of bridged species was also obtained which may afford an alternative explanation for the rate-dependence on the phosphine "sponge".

In the present work, we therefore aim to delineate the increased olefin insertion reactivity of cationic complexes relative to their neutral counterparts. In Chapters 5

and 6 we have discussed carbonylation of model N-O complexes **1** and **21**. We will now consider subsequent ethylene insertion into the palladium-acyl bond employing the same models (Figure 7.1). The results have also allowed us to propose a novel rationale for relative rates of olefin insertion in different systems, involving the participation of trigonal–bipyramidal pre-insertion intermediates.

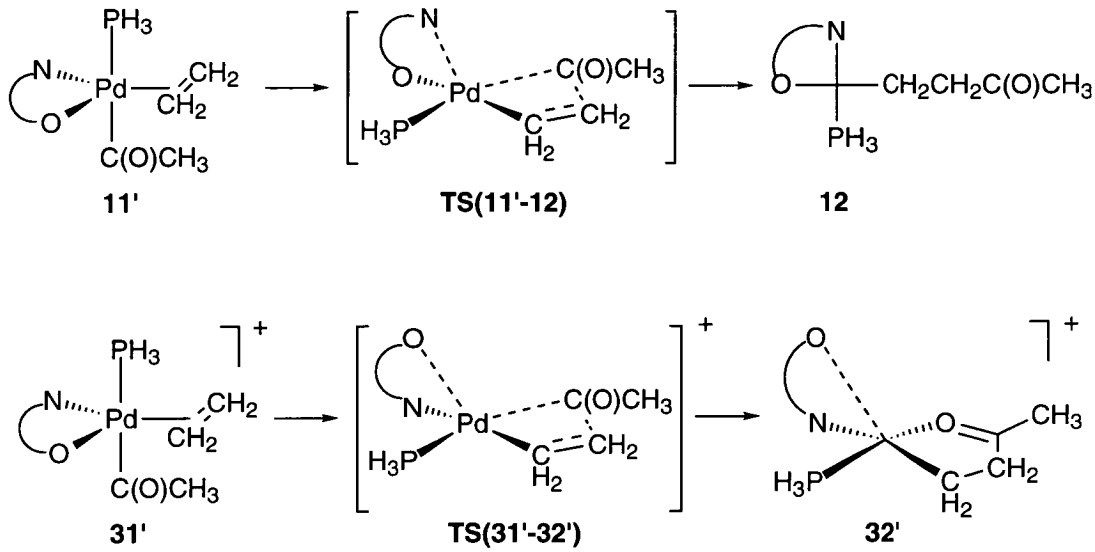

Figure 7.1: *The ethylene "insertion" steps investigated.*

7.2 Overview of the Theoretical Methods

Given the fundamental similarity between the "CO insertion" and "ethylene insertion" transformations, the nature of the ethylene insertion transition structures was assumed to be similar to those proposed for carbonylation of the neutral and cationic systems predicted in Chapters 5 and 6 respectively. Ethylene insertion was assumed to proceed *via* square–pyramidal transition structures in which the Pd-N bond (of the neutral system) or the Pd-O bond (of the cationic system) is elongated (Figure 7.1). Such structures were optimised at the RHF level, and optimisation on the reactant side

of the PES generated square–pyramidal intermediates with the weakly associated chelate arm in the apical position. However, at correlated levels the PES was followed downhill from the reoptimised transition structures to *trigonal–bipyramidal* intermediates (**11'** and **31'** in Figure 7.2). These exhibit features common to experimentally characterised five-coordinate alkene-palladium(II) complexes of bidentate N-N ligands.[76] The bidentate ligand and ethylene occupy positions in the equatorial plane, while the stronger σ-donors (PH_3 and $C(O)CH_3$) are axial. The absence of pre-conceived assumptions regarding the structure of these intermediates again demonstrates the strength of theoretical methods. A related geometry was predicted by Ziegler and coworkers for a pre-insertion intermediate in the stepwise copolymerisation of CO and ethylene catalysed by $[Pd(PH_2CH_2CH_2PH_2)(H)]^+$.[49]

Optimisation of the neutral pre-insertion intermediate was problematic. The calculation oscillated between two closely related structures and a fully optimised geometry was obtained only at the B-LYP level of theory following the adoption of redundant internal coordinates and several hundred optimisation iterations. Consequently, there is no fully optimised MP2 geometry for comparison. However, the MP2 transition structure (**TS(11'-12)**) and product (**12**) compare well with the B-LYP geometries and previous results have indicated that MP2//B-LYP energies are normally reliable (Chapter 4). An exception is observed for the cationic species for which the B-LYP Pd-O bond lengths are significantly longer than those determined at the MP2 level, giving rise to differences in the single-point energies. The favourable comparison between the MP2-optimised metal-ligand bond lengths for **32'** and the experimental X-ray crystal structure parameters[48] verifies the accuracy of this method relative to B-LYP (refer to Table 7.1).

Selected geometric parameters and the relative energies derived at the correlated levels of theory are listed in Table 7.1. Energies were calculated at MP2/[basis set B] and are determined relative to the separated reactants {**1a** + CO + C_2H_4} and

{**21a** + CO + C_2H_4} for the neutral and cationic systems respectively prior to carbonylation. Optimised structures and the PES's are illustrated in Figures 7.2 and 7.3 respectively. The full set of geometric data and total energies at the RHF, B-LYP and MP2 levels of theory is given in Appendix 6.

7.3 Comparison of Ethylene Insertion in the Neutral and Cationic System

Although the reactants and transition structures for the cationic and neutral systems are similar, distinct products are generated. The weakly associated chelate nitrogen of the neutral system recoordinates following insertion to yield a four-coordinate product (**12** in Figure 7.2). In contrast, the donor oxygen of the cationic system remains weakly associated to the metal in the apical position of the pseudo five-coordinate square–pyramidal geometry (**32'** in Figure 7.2). The prediction of such a product is in excellent agreement with the experimental isolation and characterisation of a similar structure in the CO/ethylene stepwise insertions of $[Pd(C_5H_4N(CO_2CH_3)\text{-}2\text{-}N,O)(CH_3)(PPh_3)]^+BF_4^-$.[48] Not only have we reproduced chelation by the alkyl carbonyl group in preference to recoordination of the donor oxygen of the original chelate, but also predicted the correct *cis*(N,P) product isomer. Isolation of this isomer was surprising to experimentalists who previously believed the *trans*(N,P) isomer to be formed.[43,204]

Table 7.1: *Metal-ligand bond lengths (Å), selected bond angles (deg) and relative energies for intermediates, transition structures and products of olefin insertion at B-LYP/[basis set A]. MP2/[basis set A] parameters are in parentheses. Energies were calculated at MP2/[basis set B].*

	Bond lengths (Å)							Angle (deg)	Energy
	$Pd\text{-}C(O)CH_3$	Pd-C1	Pd-C2	Pd-P	Pd-O	Pd-N	$C1\text{-}COCH_3$	$C2\text{-}Pd\text{-}COCH_3$	(kJ/mol)
11'	2.035	2.206	2.221	2.688	2.298	2.350			-108.6
TS(11'-12)	2.263 (2.155)	2.423 (2.314)	2.102 (2.080)	2.336 (2.334)	2.215 (2.178)	2.614 (2.548)	2.002 (1.934)	50.5 (51.1)	-11.2 (-27.2)
12	-	-	2.093 (2.051)	2.287 (2.269)	2.185 (2.147)	2.118 (2.107)	1.515 (1.502)	-	-154.5
31'	2.063 (2.044)	2.298 (2.166)	2.292 (2.190)	2.662 (2.620)	2.851 (2.508)	2.234 (2.256)	3.051 (2.900)	88.6 (87.0)	-110.7 (-141.5)
TS(31'-32')	2.375 (2.236)	2.424 (2.327)	2.096 (2.085)	2.358 (2.366)	3.178 (2.863)	2.218 (2.217)	1.917 (1.855)	47.1 (47.9)	-82.9 (-99.4)
32'	2.913 (2.873)	2.907 (2.811)	2.074 (2.047)	2.294 (2.264)	3.430 (2.766)	2.214 (2.222)	1.510 (1.502)	-	-188.7 (-200.6)
experiment[48]			2.00(1)	2.215(6)	2.78(1)	2.19(1)			

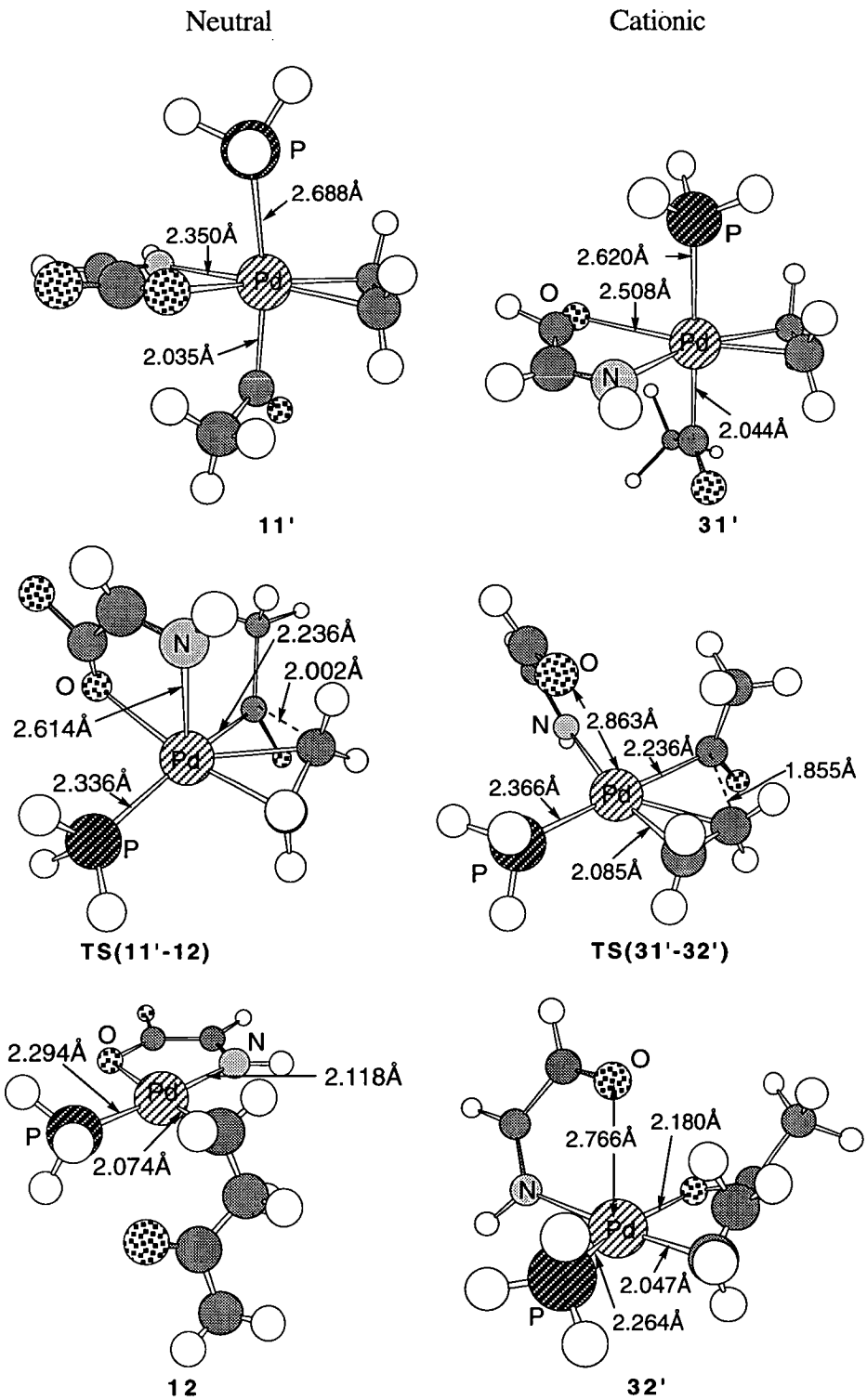

Figure 7.2: *Optimised structures for ethylene insertion. Geometrical parameters were optimised at B-LYP/[basis set A] and MP2/[basis set A] for the neutral and cationic systems respectively.*

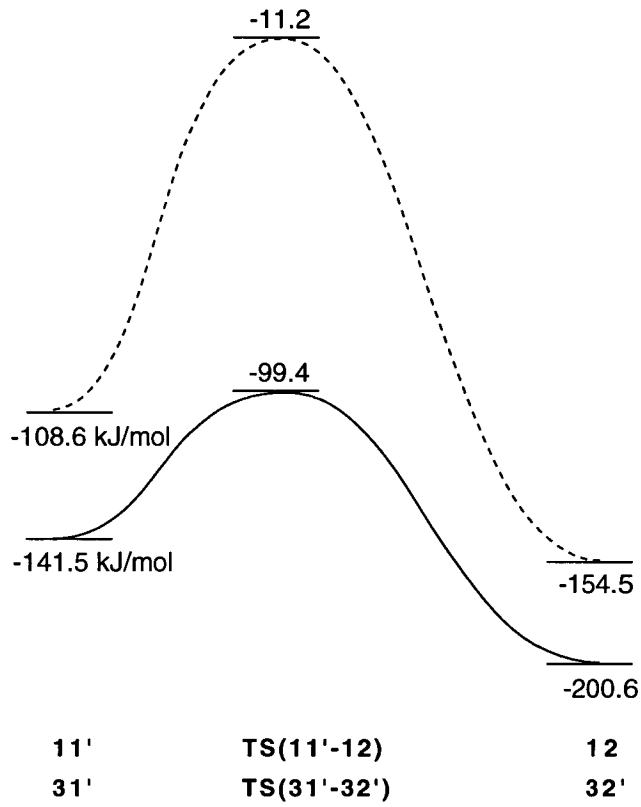

Figure 7.3: *Potential energy surfaces (PES's) for the olefin insertion step. Energies were generated at MP/[basis set B]//MP2/[basis set A] for the cationic system (–) and at MP2/[basis set B]//B-LYP/[basis set A] for the neutral system (--) relative to the pre-carbonylation reactants.*

The low insertion barrier calculated for insertion from the trigonal–bipyramidal intermediate **31'** is contrary to the EHT calculations of Thorn and Hoffmann.[72] This group investigated the 90° rotation of the alkene from coplanar with the equatorial ligands to perpendicular to the plane, which is required for insertion. The high barrier of this rotation apparently precluded olefin insertion from a trigonal–bipyramidal intermediate, whereas the corresponding rotation in a square–planar four-coordinate intermediate is facile. This led them to postulate that olefin insertion preferentially proceeds from a four-coordinate intermediate. However, the isolation of the various

rotations, bond formations/cleavages and bond angle deformations into isolated steps is too simplistic. In the present study, we have found that the geometry of the complex relaxes from trigonal–bipyramidal into square–pyramidal during the insertion step, allowing facile rotation of the alkene. Ziegler reported a similar process for olefin insertion in a cationic P-P chelate complex.[49]

The activation energy associated with ethylene insertion in the neutral system is 55.4 kJ/mol higher than the barrier for the cationic system. This difference is consistent with experimental data which demonstrates a lack of CO/ethylene copolymerisation activity for the neutral N-O complexes despite their facile carbonylation.[62] It therefore appears that the increased reactivity of cationic complexes compared to their neutral counterparts is not merely a result of the provision of an accessible coordination site. It should be noted that the barrier of the olefin insertion step in the cationic system is predicted to be comparable to the barrier determined for methyl migration (44.9 kJ/mol at MP2/[basis set B]//MP2/[basis set A] in Chapter 6).

Natural population analyses were performed on the pre-insertion intermediates and transition structures to delineate the variation in insertion activation energies. The natural charges and orbital populations of selected molecular units are listed in Table 7.2. The most notable difference between the neutral and cationic systems is the electron density on the ethylene group. A negative charge on the olefin is predicted for the neutral system, contrasting the small positive charge in the cationic system.

Classification of the metal orbital populations into σ-donating and π back-donating orbitals is not straightforward for these geometries. There is little variation in the ethylene p_y orbital populations between the pre-insertion intermediates, indicating that ethylene-to-palladium donation is fairly constant. The main difference is observed for the p_x and p_z orbital populations which demonstrates reduced metal-ethylene π back-donation in the cationic intermediate (**31'**), and accounts for the partial positive charge on the ethylene ligand. As discussed in Section 1.5, the olefin

insertion activation energy is governed by interactions between the $\sigma_{M\text{-}C(O)CH_3}$, $\sigma_{M\text{-}C(O)CH_3}$* and alkene π* and π orbitals respectively. Reduced metal-ethylene π back-donation, and a subsequently lower π* orbital population, increases the stabilising interaction with $\sigma_{M\text{-}C(O)CH_3}$, thereby lowering the insertion barrier in the cationic system.

Table 7.2: *Natural charges and orbital populations for the pre-insertion intermediates (11' and 31') and insertion transition structures (TS(11'-12) and TS(31'-32')).*[a]

	Pre-insertion intermediate		Transition Structure	
	11'	**31'**	**TS(11'-12)**	**TS(31'-32')**
Natural Charges				
Pd	0.608	0.478	0.499	0.439
PH_3	0.086	0.117	0.203	0.267
C	0.565	0.544	0.527	0.510
$(C(O)CH_3)$	0.151	0.183	0.118	0.127
CH_2CH_2	-0.126	0.065	-0.029	0.042
	Natural Orbital populations on $\underline{C}H_2\underline{C}H_2$			
p_X	1.056/1.079	1.079/1.103	1.158/1.053	1.109/0.960
p_Y	1.110/1.116	1.114/1.120	1.153/1.169	1.279/1.230
p_Z	1.223/1.218	1.114/1.134	1.125/1.075	1.046/1.102

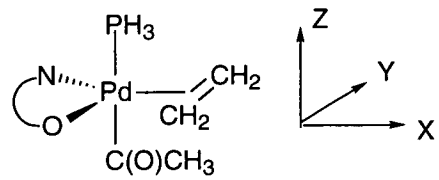

Axes for natural orbitals.

[a] Calculations were performed at MP2/[basis set A]//MP2/[basis set A] for the cationic system and at MP2/[basis set A]//B-LYP/[basis set A] for the neutral system.

The insertion barriers calculated in the present work are compared to the theoretical values of Morokuma *et al.*[46] (insertion from $[Pd(NHCHCHNH)(C(O)CH_3)(CH_2CH_2)]^+$), Ziegler *et al.*[45] (insertion from $[Pd(PH_2CH_2CH_2PH_2)(C(O)CH_2CH_3)(CH_2CH_2)]^+$), and the experimental value of Rix *et al.*[44] Interestingly, the barrier for insertion from **31'** is marginally lower than the barriers determined for other systems. This variation is most likely a result of differences in the coordinated ligands. In particular, the presence of a phosphine ligand has an activating effect on the *trans* metal-acyl bond. This may also explain the relatively low barrier reported by Ziegler for the P-P chelate complex.[45,49] It is also interesting to note the low barrier of insertion into the metal-acyl bond of **31'** compared to the activation energy range reported by Siegbahn for olefin insertion into a metal-alkyl bond (68.6-105.0 kJ/mol).[75]

Table 7.3: *Activation energies (kJ/mol) for olefin insertion.*

System	Pre-insertion Intermediate	Activation Energy
11'	$Pd(NHCHCOO^-)(C(O)CH_3)(PH_3)(CH_2CH_2)$	97.5
31'	$[Pd(NHCHCHO)(C(O)CH_3)(PH_3)(CH_2CH_2)]^+$	42.1
Morokuma *et al.*[46]	$[Pd(NHCHCHNH)(C(O)CH_3)(CH_2CH_2)]^+$	76.1
Ziegler *et al.*[45]	$[Pd(PH_2CH_2CH_2PH_2)(C(O)CH_2CH_3)(CH_2CH_2)]^+$	58
Rix *et al.*[44]	$[Pd(phen)(C(O)CH_3)(CH_2CH_2)]^+$	71

The difference in metal-carbonyl π back-donation between the cationic and neutral pre-methyl migration intermediates is not as marked as the variation in metal-ethylene π back-donation. The presence of an additional π-accepting ligand in the pre-olefin insertion intermediate, namely the migrating acyl group, increases

which also forms σ bonds with the nitrogen and oxygen of the chelate ligand, such that stronger σ-donors in the XY plane will enhance metal-alkene π back-donation. The higher σ-donating ability of the anionic N-O ligand may therefore account for the increased metal-alkene bond strength in **11'** compared to **31'**. This contrasts with the rôle of the palladium π back-donating orbitals in the pre-methyl migration intermediates which are not directly involved with metal-ligand σ bonding.

The prediction of trigonal–bipyramidal pre-insertion intermediates has important consequences when other palladium(II) complexes are considered. The bidentate (N-O) ligand of **31'** lies in the equatorial plane, an orientation which can also be predicted for diimine chelate complexes (refer to Figure 7.4). However, the bidentate phophines of the pre-insertion intermediate optimised by Ziegler *et al.*[49] are coordinated in equatorial and axial positions, which is ideal for insertion due to the *trans* alignment of the phosphine and migrating acyl group. Adoption of this configuration necessarily places the fifth ligand (L) in an equatorial position (Figure 7.4). Replacement of an equatorial weakly π-accepting ligand, such as CH_3CN, by a weak σ-donor, such as Cl^-, has less effect on the other metal-ligand bonds than replacement of an axial ligand due to the absence of a *trans* ligand in the equatorial position. This may therefore account for the observed reactivity of neutral diphosphine complexes (L=Cl^-) towards olefin insertion, while neutral diimine complexes are typically inactive.

Participation of the intermediates in Figure 7.4 also provides a novel rationale for the reported rate-dependencies on the flexibility and bite angle of the bidentate ligand.[11,26,34,205] Increased flexibilty and bite angle of the diphosphine ligand would favour bridging between the axial and equatorial positions, thereby facilitating the formation of an intermediate susceptible to insertion. In contrast, coordination of the diimine ligand in the equatorial plane does not require high flexibility. Decreased flexibility is generally accompanied by increased conjugation yielding a better π-accepting ligand. This effect, together with a smaller bite angle,

diimine ligand in the equatorial plane does not require high flexibility. Decreased flexibility is generally accompanied by increased conjugation yielding a better π-accepting ligand. This effect, together with a smaller bite angle, may allow more efficient competition between the imine nitrogens and ethylene for π back-donation, consequently lowering the insertion barrier.

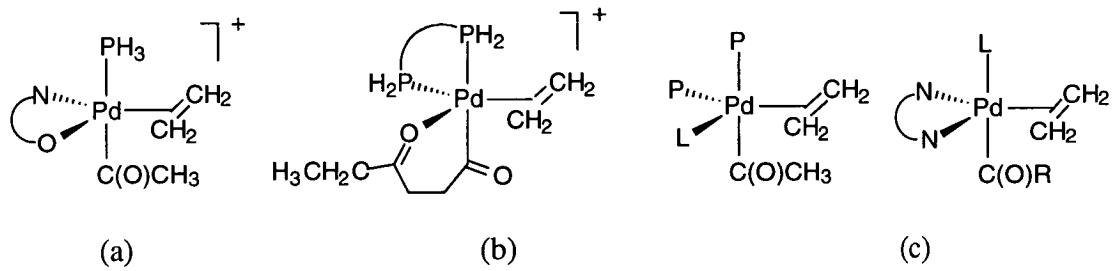

(a) (b) (c)

Figure 7.4: *Proposed pre-insertion intermediates. (a) Intermediate **31'** from the present work; (b) an intermediate optimised by Ziegler et al.;[49] (c) possible pre-insertion intermediates for the experimental diphosphine catalyst of Sen et al.[47] and N-N systems*

Olefin insertion is more exothermic than methyl migration for both the neutral and cationic systems. In contrast to the expected higher exothermicity of the insertion step in the neutral system, it is considerably more exothermic in the cationic system (-78.0 kJ/mol compared to -45.9 kJ/mol at MP2/[basis set B]//B-LYP/[basis set A]). The predicted stability of the cationic product with respect to the reverse reaction is consistent with the experimental isolation of such a structure.[48]

The olefin coordination and rearrangement transformations required to arrive at the pre-insertion intermediates were not considered in this work, and provide a platform for further investigation. Given the dependence of ligand substitutions on the metal-ligand bond strengths, and the relatively facile rearrangements identified for the

carbonylation reaction, we feel that these transformations will have little bearing on the relative PES's for the neutral and cationic systems.

7.4 Conclusions

Together with the results presented in Chapter 6 for the carbonylation reaction, we have demonstrated that carbonylation and subsequent olefin insertion of cationic N-O complexes is a facile process. Comparison of ethylene insertion in neutral and cationic model palladium complexes has revealed a marked difference (55.4 kJ/mol) in the activation energy associated with this step. The high insertion barrier predicted for the neutral system (97.5 kJ/mol) may account for the experimentally observed absence of copolymerisation activity for alkylpalladium(II) complexes of anionic N-O ligands. Natural orbital populations and charges on the ethylene ligand in the pre-insertion intermediates indicate that olefin insertion is favoured in the cationic system due to a reduction in metal-alkene π back-donation. This represents the first theoretical investigation to reproduce and to rationalise the enhanced copolymerisation activity of cationic palladium(II) complexes.

CHAPTER 8

Ligand Effects in the Carbonylation Step

Chapter 8

Ligand Effects in the Carbonylation Step

8.1 Introduction

The carbonylation mechanism and reaction rate of alkyl-palladium(II) complexes has been shown to be highly dependent on the coordinated ligands.[24] Experimental studies of palladium complexes of bidentate N-O ligands have demonstrated their carbonylation behaviour to be particularly sensitive to variations in the phosphine and bidentate ligands.[42,43,61,62] For example, replacement of PPh_3 by the higher trans influencing PCy_3 markedly reduces the reaction rate, presumably due to the loss of lability of the phosphine.[42,61,62] Addition of steric bulk around the donor nitrogen not only facilitates carbonylation but also appears to provide an alternative route.[62] Carbonylation of such complexes is observed even when the phosphine is the highly basic PCy_3 which has been rationalised by initial dissociation of the nitrogen atom.

The π-acidity and σ-basicity of a number of phosphines has been investigated by Pacchioni and Bagus using *ab initio* techniques.[172] They concluded that all phosphines are good σ-donors, and their π-accepting ability increases in the series:

$$P(CH_3)_3 < PH_3 < P(OCH_3)_3 < PF_3$$

such that the π back-bonding interaction is more important than σ-donation in the metal-PH_3 bond. Note that the neglect of correlation effects in this work is likely to have resulted in underestimation of the degree of π back-donation. They also reported the palladium-phosphine bond strength to increase in the order:

$$Pd\text{-}PH_3 < Pd\text{-}P(OCH_3)_3 \sim Pd\text{-}P(CH_3)_3 \sim Pd\text{-}PF_3$$

A spectrum of π-accepting and σ-donating capacities can therefore be studied by replacing PH_3 in **21** by PF_3 (**41**) and $P(CH_3)_3$ (**51**). This allows us to delineate the importance of the π-accepting and σ-donating strength of the phosphine on the mechanism and energetics of carbonylation of alkylpalladium(II) complexes of bidentate N-O ligands.

The use of $P(CH_3)_3$ also provides a better model for triphenylphosphine. Although the majority of *ab initio* studies incorporating phosphine ligands have employed PH_3 as a model for trialkyl- and triaryl-phosphine ligands due to its manageable size, a number of publications have appeared which highlight the need for caution when using PH_3. Häberlen and Rösch investigated the use of PH_3 and $P(CH_3)_3$ as models for PPh_3.[188] They concluded that PH_3 was adequate for the determination of geometries, however reliable energetics required the use of a better model, such as $P(CH_3)_3$. Sargent and Hall showed that the steric and electronic differences between PH_3 and PPh_3 were sufficient to result in incorrect predictions regarding the course of reactions.[189] In particular, PH_3 is a stronger π-acceptor than PPh_3 which may influence the relative stability of five-coordinate transition structures and intermediates with respect to the corresponding four-coordinate species. Conversely, $P(CH_3)_3$ is a slightly poorer π-acceptor than PPh_3.

Experimental studies have demonstrated that the relative rates of carbonylation for neutral and cationic systems is dependent on the chelate (refer to Chapter 6). Following inspection of the available experimental data, it appears that CO insertion into a Pd-alkyl or Pd-aryl is consistently more facile for cationic compared to neutral complexes only when the chelate ligand is symmetrical (diphosphine or dinitrogen).[11,29,31,33,66] Note that this is not the case for CO insertion into a Pd-allene bond.[39] To investigate this proposal further, we have studied the carbonylation of $Pd(NHCHCHNH)(CH_3)(L)$ (L = PH_3 (**61**), L = CH_3 (**71**)), in which the bidentate diimine ligand models diazobutadienes (such as bpy and phen).

Although several theoretical studies of palladium-catalysed carbonylation mechanisms have appeared in the literature, little attention has been paid to competing mechanisms or to the ligand effects. In this final chapter we will present a comparison of the carbonylation reaction for a range of palladium(II) complexes: $Pd(X\text{-}Y)(CH_3)(L)$ (X-Y = NHCHCHO, L = PF_3 (**41**), $P(CH_3)_3$ (**51**); X-Y = NHCHCHNH, L = PH_3 (**61**), CH_3 (**71**). The PES's generated will be compared to those presented in Chapters 5 and 6 for $Pd(NHCHCOO^-)(CH_3)(PH_3)$ and $[Pd(NHCHCHO)(CH_3)(PH_3)]^+$ respectively, imparting a more thorough understanding of the carbonylation process.

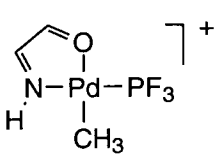

(**41**)

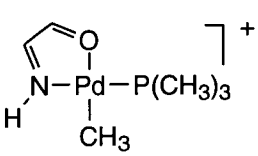

(**51**)

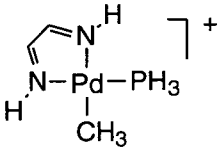

(**61**)

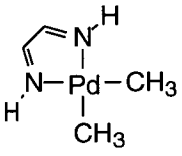

(**71**)

8.2 Overview of the Theoretical Methods

In light of the agreement between MP2 and B-LYP methods with respect to the geometries of stationary points on the PES's for $[Pd(N\text{-}O)(CH_3)(L)]^+$ (L = PH_3 (Chapter 6), PF_3), the PES for L=$P(CH_3)_3$ was probed at the B-LYP level of theory only. Unless otherwise stated, the geometries discussed for the cationic systems $[Pd(N\text{-}O)(CH_3)(L)]^+$ (L = PH_3, PF_3, $P(CH_3)_3$) were optimised at the B-LYP level of theory. Energies have been generated at MP2/[basis set B]//B-LYP/[basis set A] and are presented as relative energies with respect to the separated reactants. Significant geometrical variations between the B-LYP and MP2 optimisations were observed for the diimine systems and will be discussed in Section 8.5. We will first discuss the carbonylation mechanism for each system (Sections 8.3 to 8.5) and then present a comparison of the PES's (Section 8.6).

The metal-ligand bond lengths (Å), natural population analyses and relative energies (kJ/mol) from the correlated calculations are presented in Tables 8.1 - 8.8. The complete set of geometrical data and total energies generated for each system at the correlated and RHF levels of theory are listed in Appendices 7 to 10.

8.3 Carbonylation of $[Pd(N\text{-}O)(CH_3)(PF_3)]^+$ (41)

The migration steps for the two low-energy pathways identified for the cationic system **21** in Chapter 6 were examined for the present system (refer to Figure 8.1). In agreement with carbonylation of **21**, the migration activation energy is marginally lower when proceeding from the pseudo five-coordinate intermediate **44'** to yield a stable four-coordinate product. However, the five-coordinate pre-migration intermediate **44'** is 28.8 kJ/mol lower in energy than **44** (at MP2/[basis set A]//B-LYP/[basis set A]), impeding full dissociation of the oxygen. This contrasts with the PH_3 cationic system for which the related intermediates **25'** and **25** differ by only 10.1 kJ/mol at the same level of theory. Stabilisation of the five-coordinate pathway relative to the four-coordinate pathway may be due to the higher π-accepting capacity of PF_3 compared to PH_3, a factor which is known to favour five-coordinate geometries.[77,80]

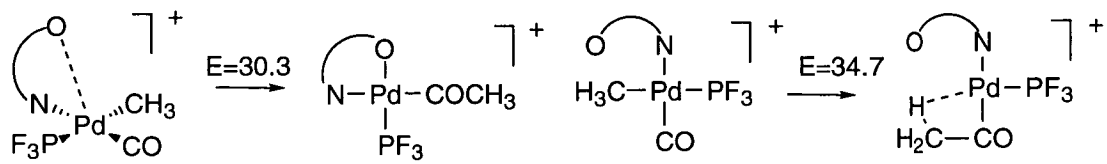

Figure 8.1: *Two low-energy methyl migration steps studied for carbonylation of* ***41****. Relative energies (kJ/mol) were generated at MP2/[basis set A]//B-LYP/[basis set A].*

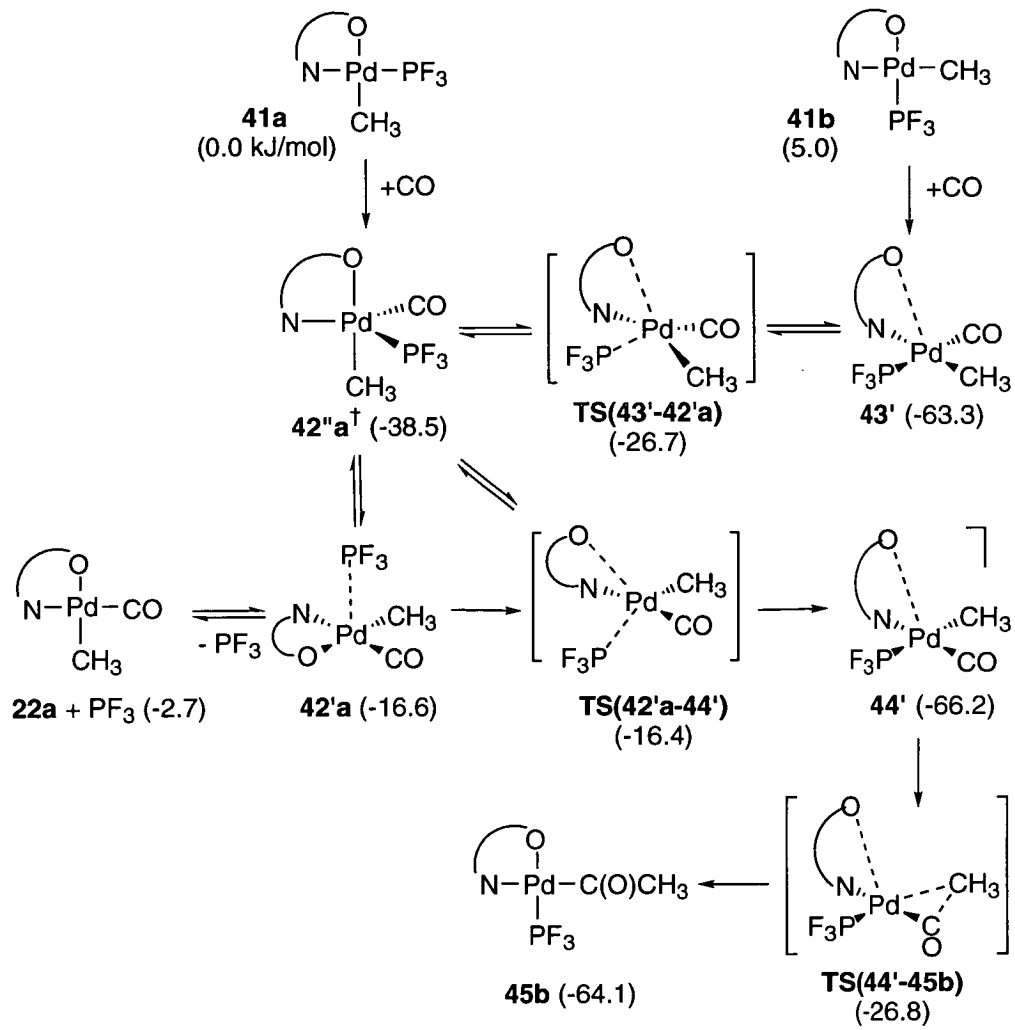

Scheme 8.1: *The lowest energy reaction mechanism for carbonylation of* ***41****. All species have a charge of 1+. Energies have been calculated at MP2/[basis set B]//B-LYP/[basis set A]. †This structure was only optimised at MP2/[basis set A].*

Table 8.1: *Metal-ligand bond lengths (Å) and relative energies (kJ/mol) for intermediates, transition structures, and products of the lowest energy reaction mechanism for carbonylation of [Pd(N-O)(CH_3)(PF_3)]$^+$ (N-O = NHCHCHO) (**41**). Geometries were optimised at B-LYP/[basis set A], and MP2/[basis set A] in parentheses. Energies have been generated at MP2/[basis set B].*

	Metal-ligand bond lengths (Å)					Relative Energy
	Pd-PF_3	Pd-CO	Pd-CH_3	Pd-O	Pd-N	(kJ/mol)
41a	2.264 (2.227)	-	2.068 (2.063)	2.326 (2.311)	2.154 (2.166)	0.0
41b	2.235 (2.206)	-	2.073 (2.072)	2.243 (2.230)	2.240 (2.249)	5.0
42'a	2.833 (2.232)	1.947 (2.222)	2.102 (2.100)	2.333 (2.301)	2.135 (2.291)	-16.6 (-38.5)
42a	-	1.927 (1.912)	2.085 (2.070)	2.348 (2.338)	2.128 (2.140)	-2.7
43'	2.397 (2.360)	1.961 (1.959)	2.127 (2.116)	2.885 (2.759)	2.253 (2.230)	-63.3
TS(43'-42'a)	2.373 (2.331)	1.967 (1.990)	2.131 (2.122)	2.545 (2.441)	2.578 (2.506)	-26.7 (-27.8)
TS(42'a-44')†	2.907 (2.865)	1.927 (1.905)	2.116 (2.101)	2.571 (2.488)	2.115 (2.145)	-16.4
44'	2.505 (2.470)	1.927 (1.901)	2.137 (2.110)	2.896 (2.702)	2.146 (2.156)	-66.2 (-67.5)
TS(44'-45b)	2.364 (2.342)	1.886 (1.861)	2.354 (2.279)	2.757 (2.583)	2.227 (2.256)	-26.8 (-27.3)
45b	2.274 (2.222)	2.038 (2.017)	3.132 (3.191)	2.337 (2.424)	2.288 (2.274)	-64.1

†At basis set A, this transition structure corresponds to **TS({22a+PF_3}-44')** (optimisation on the reactant side of the PES predicted *full* dissociation of PF3 (refer to the text)).

The complete reaction mechanism associated with migration *via* **44'** is illustrated in Scheme 8.1. Metal-ligand bond lengths for each species are listed in Table 8.1, and the PES is depicted in Figure 8.2. The variation in the geometry of **42'a** determined at the MP2 and B-LYP levels is opposite to that discussed in Chapter 6 for **22'a**. In this case, a trigonal–bipyramidal intermediate (**42"a**) is predicted by MP2 methods, whereas B-LYP optimisation yields a square–pyramidal geometry (**42'a**). The single-point MP2/[basis set B] energies indicate that subsequent transformations are likely to proceed directly from **42"a**, in preference to full dissociation of the phosphine (refer to Scheme 8.1). Agreement between the MP2 and B-LYP geometries is adequate for the remaining structures which is demonstrated by the excellent agreement in single-point energies (refer to Table 8.1). Hence, with the exception of **42"a**, we will concentrate on the B-LYP geometries for consistency.

The mechanism deviates from that determined for the PH_3 cationic system in two main respects. First, the PF_3 ligand exhibits an increased lability. At basis set A, both B-LYP and MP2 methods predict that *full* dissociation of PF_3 to yield {**22a** + PF_3} is facile.[‡] However, the single-point MP2/[basis set B] energy of {**22a** + PF_3} is 13.9 kJ/mol higher in energy than **42"a**, disfavouring full dissociation. Notably, the enthalpy for full displacement of PF_3 from **41a** is less than the enthalpy for displacement of PH_3 from **21a**, despite the higher Pd-PF_3 bond strength. We tentatively attribute this to the affinity of PF_3 for π-electrons from the electrophilic metal. The second contrast to the PES of **21** is the absence of a barrier to strong coordination of CO for both **41a** and **41b**. A saddle point corresponding to a transition structure for CO entering the "inner" coordination sphere of **21a** was located.

[‡] MP2/[basis set A]//B-LYP/[basis set A] energies at fixed intermediate Pd-P bond lengths indicate that the PES is fairly flat in this region.

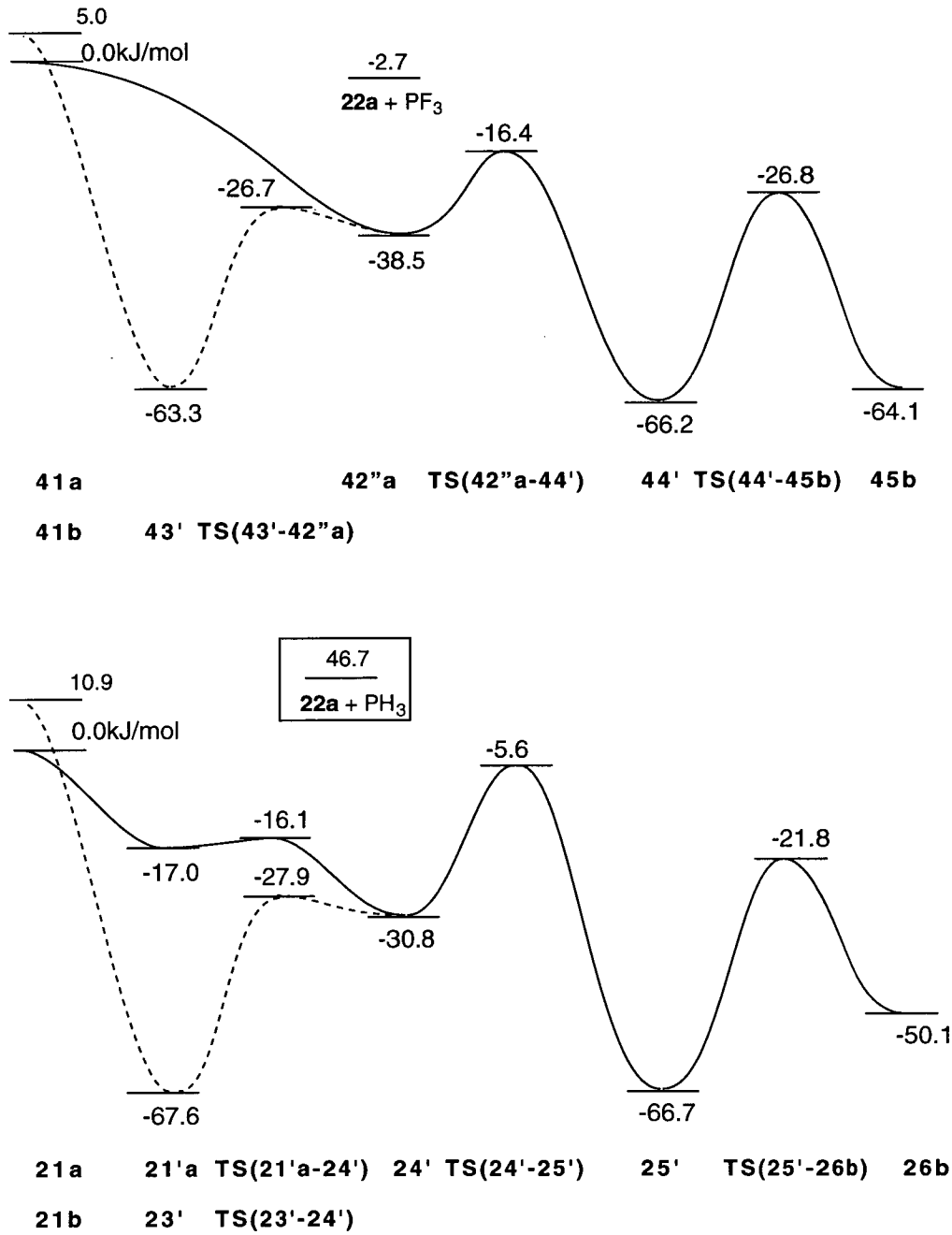

Figure 8.2: *Comparison of the PES's for the lowest energy reaction mechanisms for carbonylation of* ***41*** *and* ***21*** *(Chapter 6) respectively. The PES for the cis(N,P) reactant is dashed. Energies have been calculated at MP2/[basis set B]//B-LYP/[basis set A]. The surfaces for the cis(N,P) reactants are dashed.*

Two rearrangements from the MP2-optimised intermediate **42"a** are illustrated in Scheme 8.1: ligand substitution or concomittant ligand susbstitution and isomerisation to yield **44'** or **43'** respectively. The barrier associated with the formation of **43'** is 10.3 kJ/mol lower than the barrier to the formation of **44'**. Migration from the *cis*(CO,N) intermediate (**43'**) is unlikely due to a high activation energy (60.9 kJ/mol at MP2/[basis set A]//B-LYP/[basis set A]).[†] Consequently, the small barrier to the formation of **43'** from **42"a** and the well-depth associated with its formation (46.9 kJ/mol), produces a "thermodynamic sink" in the PES and can be expected to lower the carbonylation rate.

The activation energy of methyl migration from **44'** is marginally lower than the corresponding migration from **25'** (by 5.4 kJ/mol). Natural orbital analyses of the pre-insertion intermediates (**25'** and **44'** in Tables 8.2 and 8.3) indicate that this difference can be attributed to the higher π-acidity of PF_3 relative to PH_3. Sigma-donation from the methyl group is enhanced by the π-accepting *trans*-PF_3 in **44'**, giving rise to a partial positive charge on the methyl group. In addition, competition between PF_3 and CO for π electrons gives rise to a small decrease in metal-carbonyl π back-donation together with an increase in carbonyl σ-donation. All of these variations facilitate migration from **44'** (as discussed in Section 1.4.2).

[†] Relative energies of various species with respect to other species of similar coordination numbers appear to be reasonably insensitive to the theoretical method employed.

Table 8.2: *Selected natural orbital populations for the pre-migration intermediates of the lowest-energy carbonylation pathways.*

	Intermediate						
	4'[a]	**25'**[a]	**44'**[b]	**53'**[b]	**63'**[a]	**73'**[a]	**81'**[c]
Pd							
d_{xy}	1.863	1.897	1.864	1.856	1.873	1.851	1.871
$d_{x^2-y^2}$	1.438	1.426	1.472	1.482	1.430	1.431	1.377
C							
s	1.304	1.298	1.320	1.304	1.301	1.275	1.277
p_x	0.856	0.844	0.837	0.787	0.856	0.843	0.849
p_y	0.654	0.648	0.649	0.698	0.656	0.677	0.648
p_z	0.710	0.659	0.651	0.656	0.685	0.712	0.704

Calculations were performed at MP2/[basis set A] at the following geometries: [a]MP2/[basis set A]; [b]B-LYP/[basis set A] and [c]non-optimised geometry (refer to the text).

Table 8.3: *Natural charges on molecular units of each pre-migration intermediate for the lowest energy carbonylation route.*

	Pre-migration intermediate						
	4'[a]	**25'**[a]	**44'**[b]	**53'**[b]	**63'**[a]	**73'**[a]	**81'**[c]
Pd	0.555	0.462	0.392	0.446	0.505	0.565	0.573
CO	0.387	0.472	0.464	0.477	0.423	0.404	0.435
ΔC-O[†]	0.774	0.778	0.748	0.794	0.752	0.831	0.827
CH_3	-0.008	-0.021	0.009	-0.075	0.015	-0.312	-0.110
P	0.112	0.073	1.856	0.926	0.083	-	-
PH_3	0.182	0.217	0.225	-	0.216	-	-

Calculations were performed at MP2/[basis set A] at the following geometries: [a]MP2/[basis set A]; [b]B-LYP/[basis set A] and [c]non-optimised geometry (refer to the text). [†]Difference in electron density.

The lability of the phosphine ligand may become important in a solvent medium. In Chapter 6 we showed that migration from **22a** is not feasible. However, if isomerisation to **22b** is facile then migration may take place with a low barrier (+48.4 kJ/mol). As discussed in Section 6.5, the agostic product of migration from **22b** is unstable and activated towards deinsertion or β-hydride elimination in the absence of an additional ligand. Solvent effects may be expected to inhibit recoordination of the phosphine following full dissociation, so that termination of the reaction is likely. This rationalises the inactivity of Pd(pyca)(py)(CH_3) towards carbonylation.[61] Reaction with CO results in displacement of the labile pyridine ligand to yield Pd(pyca)(CO)(CH_3) which fails to react further, presumably due to the lack of a recoordinating ligand of high trans influence.

8.4 Carbonylation of [Pd(N-O)(CH_3)($P(CH_3)_3$)]$^+$ (51)

The reaction mechanism investigated for carbonylation of **51** is illustrated in Scheme 8.2. Relevant geometrical parameters are given in Table 8.4, and the complete PES is illustrated in Figure 8.3. Only the *trans*(N,P) reacting isomer was considered as the *cis*(N,P) isomer of the cationic reactants has been shown in previous sections to be higher in energy, and is not observed experimentally.[42,43]

There are several distinguishing features of carbonylation of **51**. The rearrangements required prior to migration take place in a single transformation (*via* **TS(51'a-53')**) rather than several small steps. The barrier associated with this process is relatively high in energy (+42.1 kJ/mol relative to **51'a**) so that carbonylation of **51** possesses an overall barrier of +23.0kJ/mol with respect to the separated reactants. This contrasts the previously discussed cationic complexes (**21** and **41**) which were shown to carbonylate with no overall activation energy. The high relative energy of **TS(51'a-53')** arises due to the low trans effect of $P(CH_3)_3$ (related

to the reduced π-accepting capacity) and elongation of the strong Pd-$P(CH_3)_3$ bond as discussed in Section 6.4. This transformation therefore accounts for the decrease in carbonylation rate observed when PPh_3 is replaced by PCy_3. Although the Pd-$P(CH_3)_3$ bond length is longer than the Pd-PF_3 bond length in related species, the ratio of σ-donation:π back-donation contributions is higher and favoured by the electrophilic metal.

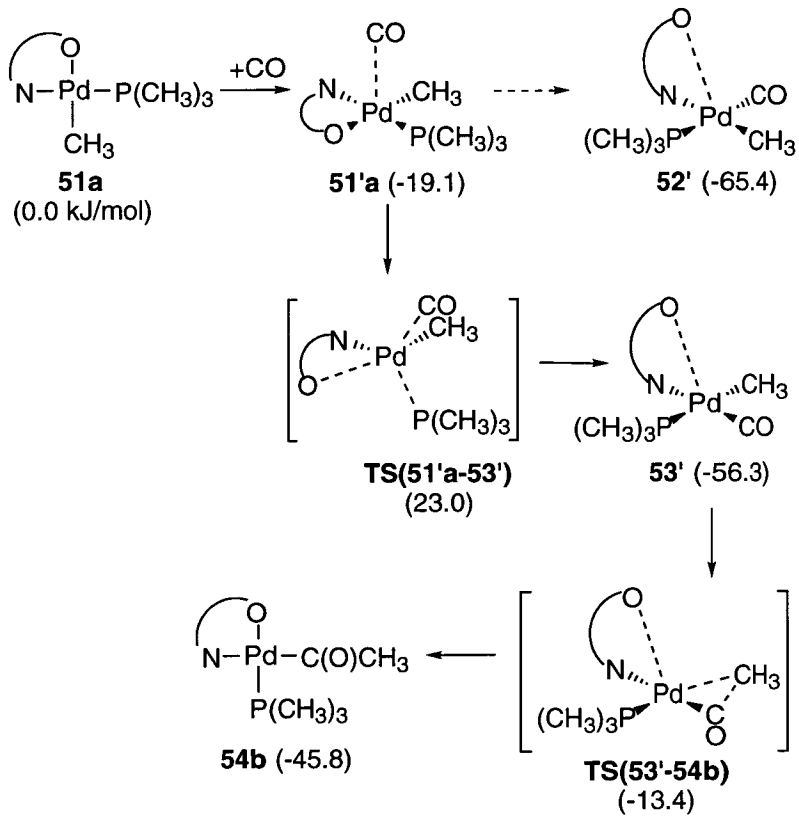

Scheme 8.2: *The reaction mechanism studied for carbonylation of* ***51****. Energies were calculated at MP2/[basis set B]//B-LYP/[basis set A]. Note that a transition structure linking* ***52'*** *to other species was not located in this study.*

Table 8.4: *Metal-ligand bond lengths (Å) and relative energies (kJ/mol) for the reactants, intermediates, transition structures, and products of the lowest energy mechanism for carbonylation of* $[Pd(N\text{-}O)(CH_3)(P(CH_3)_3)]^+$ *(N-O = NHCHCHO)* ***(51)****. Geometries were optimised at B-LYP/[basis set A] and energies have been generated at MP2/[basis set B]//B-LYP/[basis set A].*

	Metal-Ligand bond lengths (Å)					Relative energy
	$Pd\text{-}P(CH_3)_3$	Pd-CO	$Pd\text{-}CH_3$	Pd-O	Pd-N	(kJ/mol)
51a	2.324	-	2.062	2.338	2.158	0.0
51'a	2.324	2.907	2.066	2.354	2.169	-19.1
TS(51'a-53')	2.694	1.923	2.135	2.067	2.420	23.0
53'	2.516	1.900	2.163	2.931	2.128	-56.3
TS(53'-54b)	2.409	1.876	2.369	2.885	2.187	-13.4
54b	2.348	2.030	2.980	2.310	2.317	-45.8
52'	2.426	1.981	2.118	3.050	2.259	-65.4

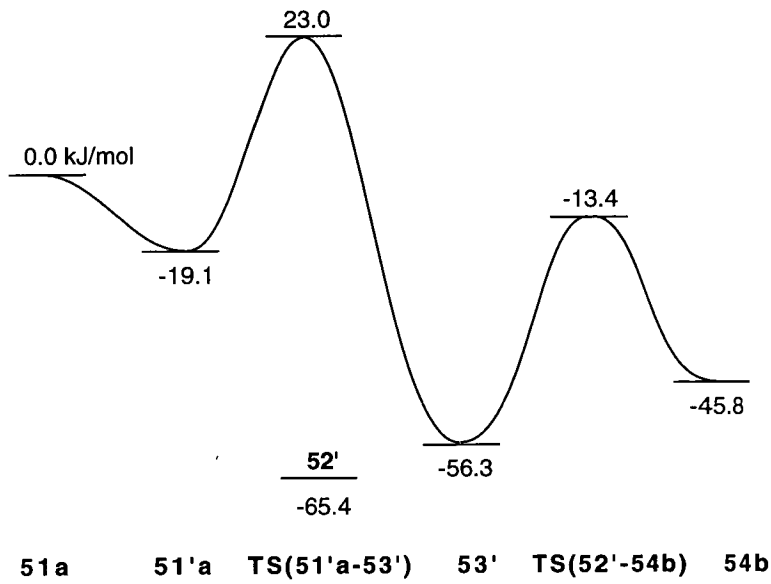

Figure 8.3: *PES for carbonylation of* ***51*** *at MP2/[basis set B]//B-LYP/[basis set A].*

The relatively low-energy of **52'** (-65.4 kJ/mol) suggests that rearrangement to yield this isomer may be favoured over the formation of **53'** and subsequent methyl migration. The related rearrangements for the formation of **24'** and **43'** from **23'** and **42'** respectively have negligible activation energies and we would expect a similar scenario for the formation of **52'**.

The activation energy associated with the methyl migration (+43.0 kJ/mol) is similar to the energies calculated for the related migrations in systems **21** and **41** (+39.4 and +44.9 respectively at MP2/[basis set B]//B-LYP/[basis set A]). The $P(CH_3)_3$ group possesses a stronger trans influence than PH_3 and PF_3 which is reflected by the elongation in the Pd-CH_3 bond of **53'** compared to **25'** and **43'**. Intuitively, we would therefore expect migration from **53'** to be more facile than from the latter intermediates as the metal-methyl bond can be more easily cleaved. The absence of such an observation can be rationalised in terms of the natural population analyses on **53'** (Tables 8.2 and 8.3). Sigma-donation by the methyl group is decreased due to the low π-accepting capacity of $P(CH_3)_3$, resulting in a partial

donation allows a small increase in the Pd-CO π interaction with a synergic increase in σ-donation (only the latter favouring migration). The influence of each of these factors on the migration barrier effectively cancel to produce a barrier close to that obtained for migration from **25'**.

Finally, the contrast between the PES's for the cationic systems **21** and **51** highlights the importance of employing an adequate model for PPh_3. The mechanisms share similar features, such as extension of the Pd-P, Pd-N and Pd-O bonds in the course of the reaction. However, an *intermediate* possessing an elongated Pd-N bond was not located on the PES for the $P(CH_3)_3$ cationic system. Steric factors neglected in the present study may affect this region of the PES. We can predict increased bulk adjacent to the nitrogen to favour formation of an intermediate related to **23'**, and a bulky phosphine to lower the barrier to CO coordination due to a decreased Pd-P bond strength. Note that although $P(CH_3)_3$ appears to satisfactorily model the electrostatic features of PPh_3, it cannot afford an understanding of steric factors.[188]

8.5 Carbonylation of the diimine complexes $[Pd(N\text{-}N)(CH_3)(PH_3)]^+$ (61) and $Pd(N\text{-}N)(CH_3)_2$ (71).

In light of our previous work on the methyl migration steps, for the N-N chelate system the migration barrier was initially assumed to be lowest when proceeding from a square–pyramidal five-coordinate intermediate with a donor nitrogen in the apical position. Species of this type were located at the RHF and B-LYP levels of theory. Reoptimisation of the migration transition structures at the MP2 level, using the B-LYP geometry and force constants generated trigonal–bipyramidal geometries (refer to Figures 8.4 and 8.5). Single-point energies at MP2/[basis set B] predicted increased stability of the trigonal–bipyramidal species relative to the square–pyramidal structures.

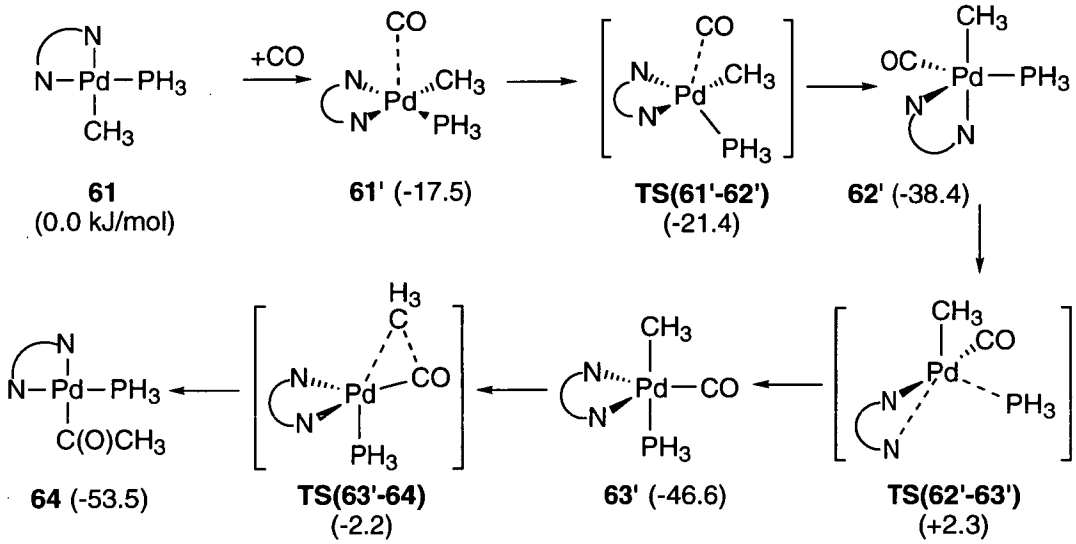

Scheme 8.3: *Reaction mechanism for carbonylation of* ***61*** *at MP2/[basis set B]//MP2/[basis set A].*

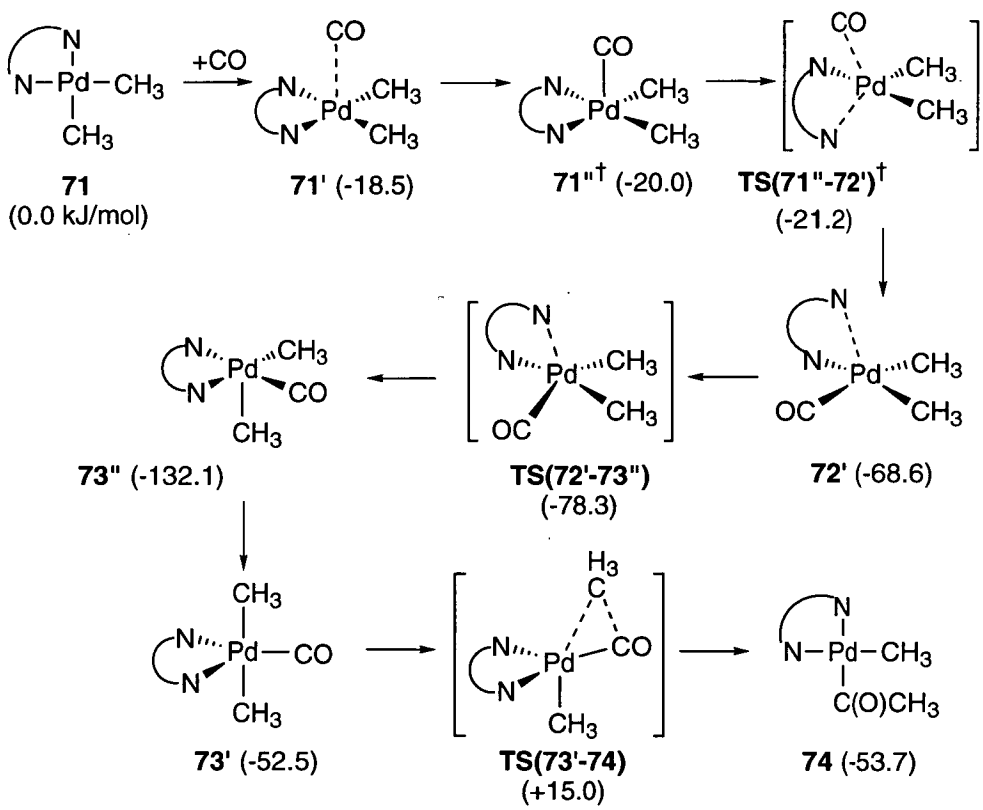

Scheme 8.4: *Reaction mechanism for carbonylation of* ***71*** *at MP2/[basis set B]//MP2/[basis set A]. †Stuctures optimised at B-LYP/[basis set A] .*

Table 8.5: *Metal-ligand bond lengths and relative energies for the reactant, intermediates, transition structures, and product for the lowest energy reaction pathway for carbonylation of [Pd(N-N)(CH_3)(PH_3)]$^+$ (N-N = NHCHCHNH) (**61**). Geometries were optimised at B-LYP/[basis set A], and MP2/[basis set A] in parentheses. Energies have been determined at MP2/[basis set B].*

	Metal-Ligand bond lengths (Å)					Relative energy
	Pd-PH_3	Pd-CO	Pd-CH_3	Pd-N (cis P)	Pd-N	(kJ/mol)
61	2.308 (2.289)	-	2.077 (2.056)	2.235 (2.235)	2.141 (2.145)	0.0
61'	(2.295)	(2.942)	(2.059)	(2.232)	(2.146)	(-17.5)
TS(61'-62')	2.338 (2.293)	2.328 (2.275)	2.101 (2.087)	2.237 (2.227)	2.185 (2.244)	-15.7 (-21.4)
62'	2.684 (2.472)	1.945 (1.909)	2.112 (2.106)	2.230 (2.222)	2.176 (2.329)	(-38.4)
TS(62'-63')	2.799 (2.689)	1.910 (1.872)	2.136 (2.124)	2.527 (2.425)	2.118 (2.145)	(2.3)
63'	2.529 (2.494)	1.909 (1.861)	2.138 (2.119)	2.831 (2.301)	2.156 (2.323)	-34.6 (-46.6)
TS(63'-64)	2.402 (2.403)	1.876 (1.826)	2.358 (2.296)	2.682 (2.363)	2.231 (2.363)	8.7 (-2.2)
64	2.358 (2.341)	2.042 (2.013)	3.049 (2.949)	2.182 (2.182)	2.327 (2.319)	(-53.5)

Table 8.6: *Metal-ligand bond lengths (Å) and relative energies (kJ/mol) for the reactant, intermediates, transition structures, and product of the lowest energy reaction pathway for carbonylation of Pd(N-N)(CH_3)(CH_3) (N-N = NHCHCHNH) (71). Geometries were optimised at B-LYP/[basis set A] and MP2/[basis set A] in parentheses. Energies have been determined at MP2/[basis set B].*

	Metal-Ligand bond lengths (Å)					Relative energy
	Pd-CH_3	Pd-CO	Pd-CH_3	Pd-N	Pd-N	(kJ/mol)
71	2.069 (2.050)	-	2.069 (2.050)	2.197 (2.201)	2.197 (2.201)	0.0
71'	(2.052)	(2.970)	(2.052)	(2.202)	(2.205)	(-18.5)
71"	2.115	2.081	2.117	2.200	2.208	-20.0
TS(71"-72')	2.104	2.085	2.095	2.181	2.609	-21.2
72'	2.113 (2.121)	1.985 (1.920)	2.109 (2.100)	2.212 (2.207)	3.491 (2.816)	-55.4 (-68.6)
TS(72'-73')	(2.172)	(1.900)	(2.113)	(2.143)	(2.217)	(-78.3)
73"	2.173 (2.139)	1.992 (1.935)	2.106 (2.115)	2.144 (2.000)	2.182 (2.080)	-74.9 (-132.1)
73'	2.198 (2.162)	2.187 (1.793)	2.198 (2.162)	2.089 (2.262)	2.963 (2.262)	-31.6 (-52.5)
TS(73'-74)	2.426 (2.327)	1.873 (1.794)	2.128 (2.127)	2.122 (2.319)	3.005 (2.371)	29.3 (15.0)
74	3.135 (3.128)	2.022 (1.968)	2.084 (2.059)	2.336 (2.301)	2.168 (2.189)	(-53.7)

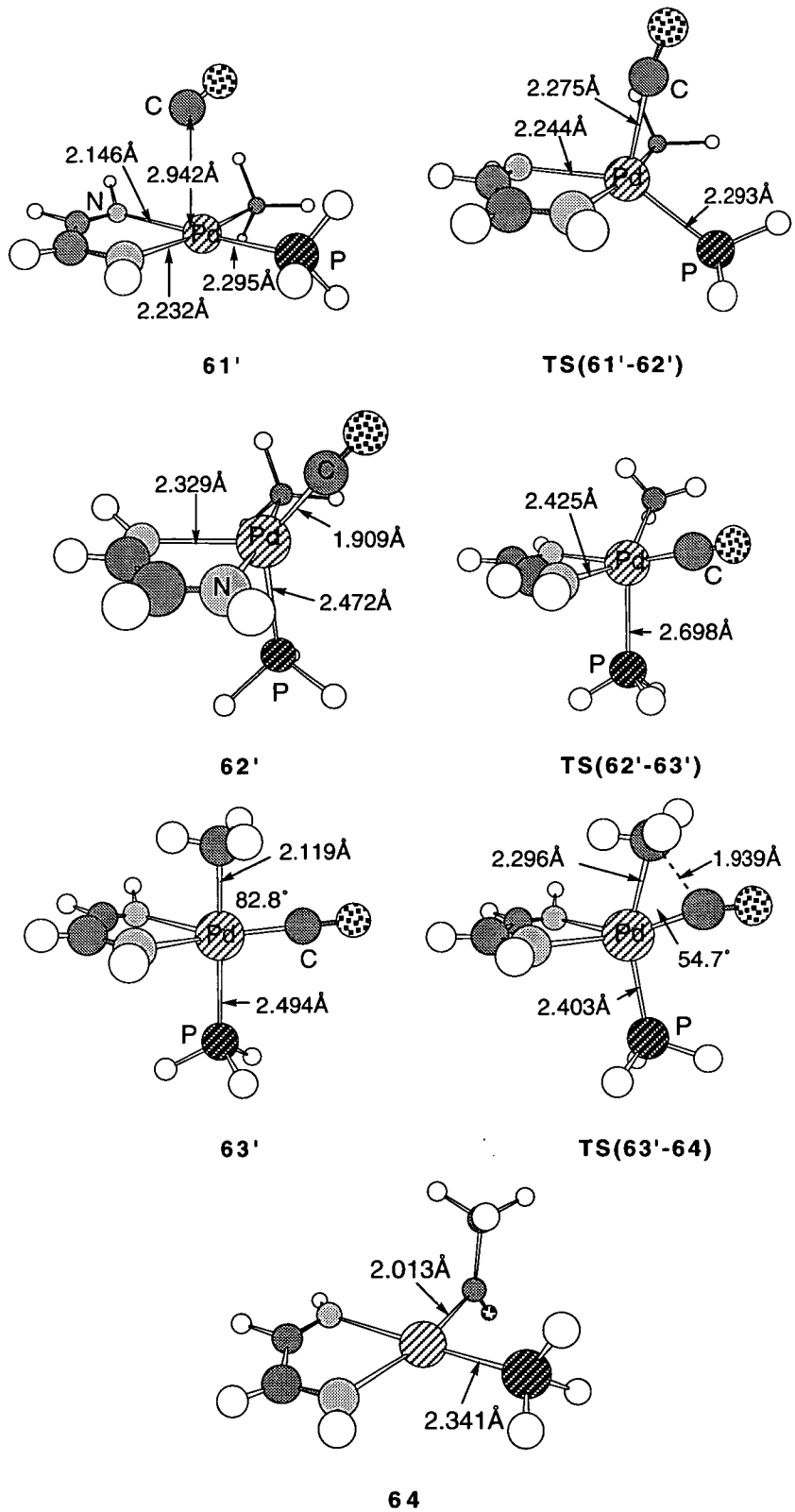

Figure 8.4: *Selected structures in the carbonylation of* ***61*** *at MP2/[basis set A].*

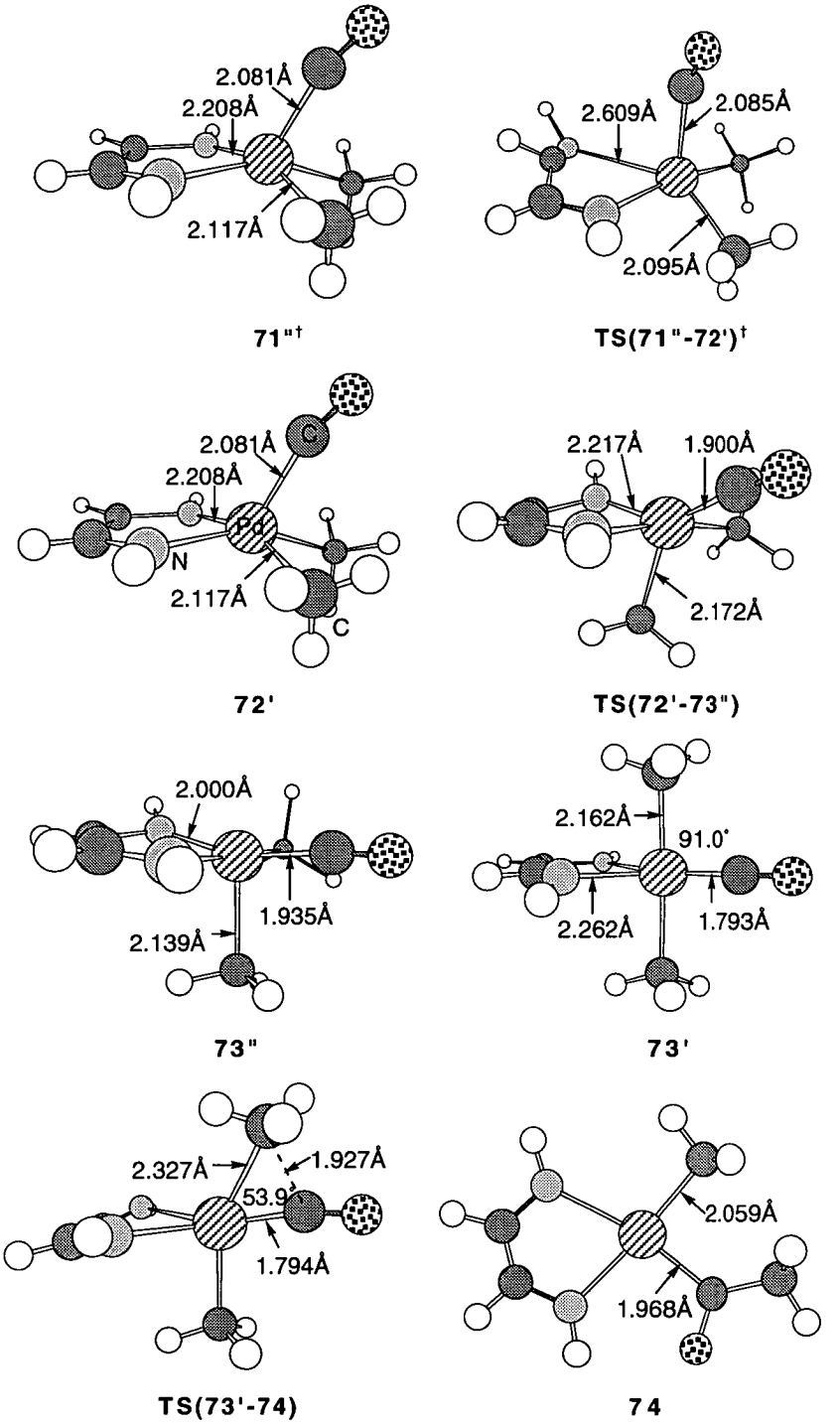

Figure 8.5: *Selected structures in the carbonylation of* ***71*** *at MP2/[basis set A] and* †*B-LYP/[basis set A].*

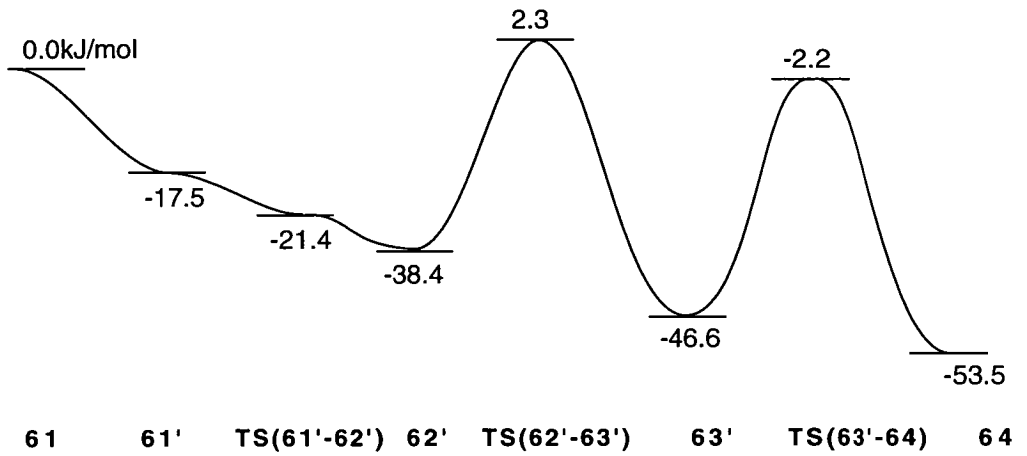

Figure 8.6: *PES for carbonylation of* ***61*** *at MP2/[basis set B]//MP2/[basis set A]*

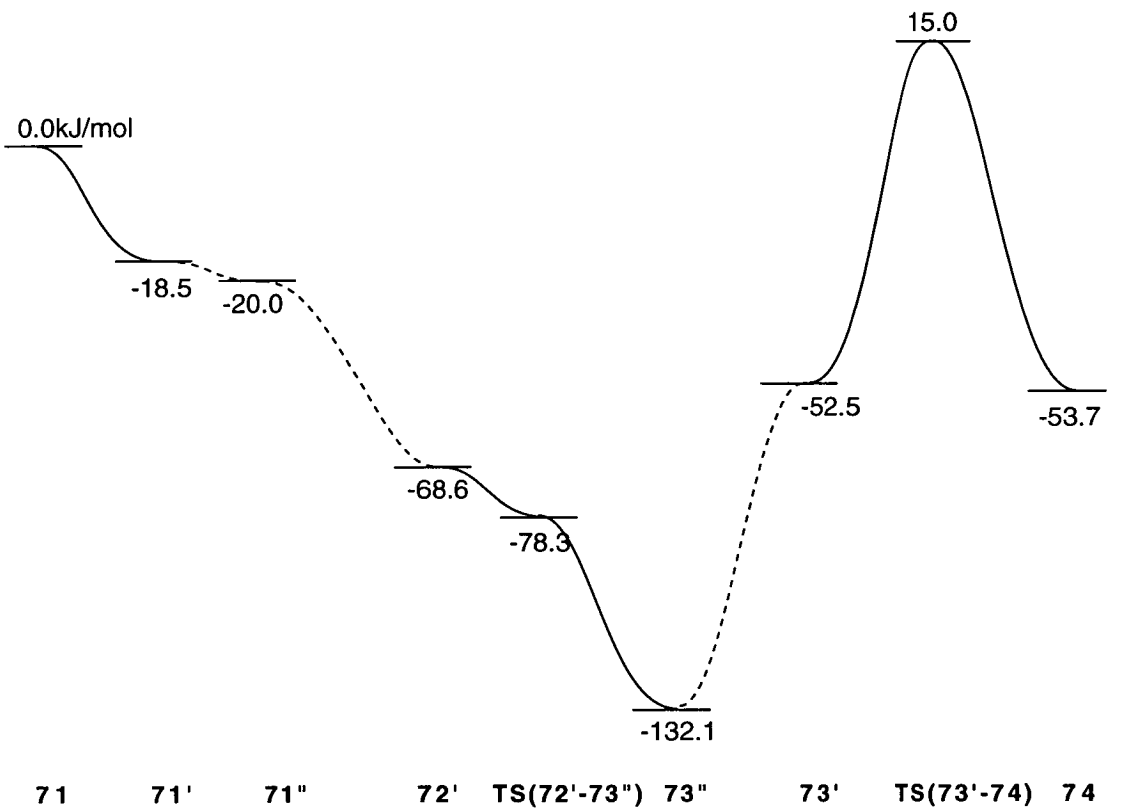

Figure 8.7: *PES for carbonylation of* ***71*** *at MP2/[basis set B]//MP2/[basis set A]. The dashed line signifies a region of the PES which was not confirmed at MP2/[basis set A]. Structure* ***71"*** *was optimised at B-LYP/[basis set A] only.*

This work represents the first investigation of methyl migration from trigonal–bipyramidal intermediates. In fact, few optimisations of trigonal–bipyramidal palladium(II) or platinum(II) species have appeared in the literature to date.[77] Interestingly, the current results contradict the speculations of Vrieze *et al.*[29] that migration from such intermediates would be unlikely. The structures are consistent with experimentally characterised five-coordinate palladium complexes of N-N chelate ligands in which the chelate and π-accepting carbonyl group occupy positions in the equatorial plane.[76,77] The participation of trigonal–bipyramidal geometries in the carbonylation reaction is also consistent with the experimentally observed increase in reactivity with increasing steric bulk adjacent to the chelating nitrogens.[29] Steric interactions are known to destabilise the square–planar geometry of d^8 complexes and favour the formation of five-coordinate species,[76] so that we can predict an enhanced CO binding energy.

The complete reaction mechanisms studied for carbonylation of **61** and **71** are illustrated in Schemes 8.3 and 8.4 respectively. Selected structures are depicted in Figures 8.4 and 8.5 for the cationic and neutral systems respectively. Tables 8.5 and 8.6 list selected geometrical parameters and relative energies, the PES's are given in Figures 8.6 and 8.7.

As a result of the symmetry of the diimine complexes, the pathway is trivial compared to the case of the unsymmetrical N-O ligands. Although the trans influence of CH_3 is greater than that of PH_3, giving rise to a weakened *trans* Pd-N bond in **61**, displacement of the *trans*-P chelating nitrogen is favoured due to the higher trans effect of PH_3 relative to CH_3. Consequently, there is no "thermodynamic sink" in the PES of the cationic diimine system associated with the formation of a low-energy non-productive intermediate (such as **43'** and **52'**). Saddle points *en route* to strong coordination of CO to **61** were located, however single-point energies suggest that no barrier is involved.

Coordination of CO to **71** was predicted to take place without activation energy at the B-LYP level of theory to yield **71"**. Reoptimisation of **71"** at the MP2 level yielded a geometry with CO weakly associated (**71'**). The MP2/[basis set B] energies of **71'** and **71"** (optimised at the MP2 and B-LYP levels respectively) are within 2 kJ/mol, indicating that there would be little or no barrier to full coordination of CO. Transition structure **TS(71"-72')** was optimised at the B-LYP level of theory and corresponds to facile replacement of a donor nitrogen of **71** by CO yielding a low-energy *trans*(CH_3,CO) intermediate (**72'**). Reoptimisation of **TS(71"-72')** at the MP2 level generated a distinct saddle point (**TS(72'-73")**) corresponding to recoordination of the donor nitrogen of **72'** to produce a square–pyramidal intermediate **73"**. The relatively low single-point energy of **TS(72'-73")** highlights small differences between the MP2/[basis set A] and MP2/[basis set B] potential energy surfaces in this relatively flat region. A saddle point linking **73"** and **73'** was not located, however the similarity between the structures implies that the barrier of deformation is likely to be little more than the difference in energy between the structures. The B-LYP and MP2-optimised rearrangements have been combined to formulate the PES illustrated in Figure 8.7. Note that migration from **72'** will be unfavourable due to the increase in metal-CO π back-donation resulting from the "push-pull" interaction between the Pd-CO and *trans* Pd-CH_3 bonds.

The relative energies of the five-coordinate intermediates and transition structures are higher than those presented for the N-O cationic systems due to the relative strength of the Pd-imine bond relative to the Pd-O bond in the latter systems. The activation energy for the methyl migration step for the cationic system (+44.4 kJ/mol) is again similar to that calculated for the other cationic systems. In contrast, the migration barrier for the neutral diimine system is moderately high (+67.5 kJ/mol), particularly if the energy difference between **73"** and **73'** is included (+147.1 kJ/mol). This outcome will be discussed in the following section.

8.6 Comparison of the Energetics of Carbonylation for Systems 1 - 71.

The lowest migration barrier for each system investigated is listed in Table 8.7, together with the results of Morokuma *et al.*[46] (for migration from $[Pd(N\text{-}N)(CO)(CH_3)]^+$), Zeigler *et al.*[49] (for migration from $[Pd(PH_2CH{=}CHPH_2)(CO)(CH_2CH_2OEt)]^+$), and the experimental results of Rix *et al.*[44] (for migration from $[Pd(phen)(CO)(CH_3)]^+$). It can be seen that the barriers associated with the neutral complexes are higher than those of the related cationic systems. While the difference was minor in the case of the N-O complexes (12.4 kJ/mol), migration in the neutral N-N system possesses a barrier 23.1 kJ/mol higher in energy than the corresponding cationic system. This is in agreement with the results of experimental kinetic studies,[11] and represents the first theoretical study to reproduce the increased carbonylation reactivity of cationic complexes of symmetrical N-N ligands compared to the related neutral complexes. It is also important to note the excellent agreement between migration barriers generated from the MP2 and B-LYP geometries, regardless of variations in the geometry (Table 8.7).

With the exception of methyl migration in the neutral diimine system, variations in the migration activation energies are surprisingly small. This demonstrates the relative independence of the migration step on the coordinated ligands. The activation energy determined by Ziegler *et al.* for the P-P system compares well with our values. These are, however, lower than the result of Morokuma and the experimental value. Steric interactions and solvent effects lacking in our models are likely to explain differences in absolute activation energies between the current results and experiment. The discrepancy between our values and those of Morokuma may be ascribed to differences in the ligands. Migration in the cationic diimine system considered here proceeds from a five-coordinate intermediate incorporating a phosphine ligand, which weakens the *trans* metal-methyl bond and reduces the carbonyl π interaction. To ensure

that the variation between our results and those of Morokuma's is not due to the theoretical method used, the transition structure of Morokuma *et al.* was re-optimised employing the B-LYP functional. The migration barrier was 60.3 kJ/mol and 69.2 kJ/mol at MP2/[basis set A] and MP2/[basis set B] respectively, displaying excellent agreement with the result of Morokuma (62.8 kJ/mol). The high migration activation energy coupled with the unfavourable dissociation of the phosphine precludes this migration as a competitive route.

Table 8.7: *Activation energies (kJ/mol) for the methyl migration step of the lowest energy pathway. Energies were determined at MP2/[basis set B]//MP2/[basis set A], and MP2/[basis set B]//B-LYP/[basis set A] in parentheses.*

	Model catalyst system	Activation Energy
1	$Pd(NHCHCOO^-)(PH_3)(CH_3)$	58.7 (55.6)
2 1	$[Pd(NHCHCHO)(PH_3)(CH_3)]^+$	46.3 (44.9)
4 1	$[Pd(NHCHCHO)(PF_3)(CH_3)]^+$	40.2 (39.5)
5 1	$[Pd(NHCHCHO)(P(CH_3)_3)(CH_3)]^+$	(43.0)
6 1	$[Pd(NHCHCHNH)(PH_3)(CH_3)]^+$	44.4 (43.2)
7 1	$Pd(NHCHCHNH)(CH_3)(CH_3)$	67.5 (70.9)
Ziegler *et al.*[45]	$[Pd(PH_2CHCHPH_2)(H)]^+$	49
Morokuma *et al.*[46]	$[Pd(NHCHCHNH)(CH_3)]^+$	62.8
Experiment (-66°C)[44]	$[Pd(phen)(H)]^+$	64.4

Natural population and localised molecular orbital analyses were performed on the migration transition structures and preceding intermediates. Selected orbital populations and charges are given in Tables 8.2, 8.3 and 8.8. Comparison of the natural charges clearly distinguishes the neutral diimine system, consistent with the anomalous value for the migration barrier derived for this system. In particular, while

the charge on the methyl group is fairly constant for the intermediates and transition structures of the other systems, the methyl group of **73'** has a discernible negative charge (-0.312).

Table 8.8: *Natural charges for the methyl migration transition structures determined at MP2/[basis set A].*

Molecular	Transition Structure					
Unit	**TS(4'-5a)**	**TS(25'-26b)**	**TS(44'-45b)**	**TS(53'-54b)**	**TS(63'-64)**	**TS(73'-74)**
Pd	0.519	0.450	0.379	0.417	0.486	0.494
CO	0.475	0.500	0.483	0.485	0.468	0.432
ΔC-O[†]	0.897	0.840	0.789	0.837	0.824	0.907
CH_3	-0.003	0.028	0.057	-0.006	0.040	-0.153
P	0.143	0.099	1.874	0.958	0.105	-

[†]Difference in electron density.

The increased negative charge on the methyl group of **73'**, due to decreased σ-donation, can be rationalised by the absence of a "push-pull" relationship with a *trans* π-acceptor. This decreases polarisation of the metal along the Y axis.[206] To investigate this effect further, a natural population analysis was performed on **81'**, in which the *trans*-methyl group in **73'** is replaced by a chlorine. Geometrical parameters were fixed at values optimised for **73'** and the metal-Cl bond length was taken from experiment.[29] The charge on the methyl group in **81'** (-0.110) was also found to be negative, the reduced magnitude consistent with the low trans influence of Cl^- compared to CH_3^-. Little variation in methyl σ-donation between cationic and neutral N-O pre-migration intermediates is observed as the *trans* ligand is PH_3 in both cases. This contributes to the reduced difference in migration barriers for carbonylation of **1** and **21** compared to the cationic and neutral diimine systems (**61** and **71** respectively).

Another result of the absence of an axial π-acceptor is reduced competition with the carbonyl for metal π back-donation. Consequently, there is a synergic increase in carbonyl π-accepting and σ-donation in both **73'** and **81'**. An increase in π back-donation is manifested by an increase in the carbon p_y and p_z orbital populations, while the decrease in s and p_x orbital populations reflects changes in σ-donation (refer to Table 8.2). Note that the palladium $d_{x^2-y^2}$ orbital population varies little between **63'** and **73'**, indicating that the increased σ-donation from CO in the latter is cancelled by a decrease in σ-donation from other ligands (primarily the methyl group). The polarisation of the carbonyl group of **73'** and **81** is also particularly high. Natural charges on molecular units of the migration transition structures demonstrate an increase in CO polarisation in the transition structure which is inhibited by an already high polarisation.

As discussed in Section 1.4.2, migration is facilitated by low $\sigma_{M\text{-}CO}$, $\sigma_{M\text{-}CH_3}$ populations, CO π* and metal d_{XY} populations. Variations in migration barriers between systems can be clearly rationalised in terms of differences in these populations. The metal-carbonyl π interaction is enhanced in both neutral

pre-migration intermediates compared to their cationic counterparts. This observation accounts for the marginally higher migration activation energy exhibited by the neutral N-O system (**1**).

The Pd-CO π-interaction is optimum in the neutral trigonal–bipyramidal diimine pre-migration intermediate (**73'**), due to the alignment of the imine nitrogens which σ-donate electron density into the metal orbitals participating in Pd-CO π back-donation. In contrast, σ-donation by a *trans* orientated imine in square–pyramidal or square–planar pre-insertion intermediates increases electron density in the Pd-CO σ-orbital, thereby inhibiting CO σ-donation. Furthermore, it is possible that carbonylation of complexes incorporating asymmetrical N-N ligands proceeds *via* square–pyramidal pre-migration intermediates similar to those adopted by the N-O complexes. This may explain the unpredictable relative carbonylation rates of cationic and neutral complexes of asymmetric N-N ligands, a proposal that warrants further study.

8.7 Conclusions

We have investigated the mechanism and energetics for carbonylation of a number of cationic and neutral methyl-palladium complexes. Methyl migration from novel five-coordinate intermediates to yield four-coordinate products is favoured in each case. In particular, migration in the diimine systems was shown to proceed from trigonal–bipyramidal intermediates, representing the first theoretical evidence of such a pathway. In all cases, the experimental trends were consistently reproduced.

Comparison of carbonylation of neutral and cationic alkyl-palladium complexes of bidentate N-O ligands has demonstrated that the dependence of the experimental rate on the ligands is not associated with the methyl migration step. The observed sensitivity of the reaction on the π-basicity of the phosphine ligand originates from the rearrangements required to arrive at the preferred pre-migration

intermediate. A highly basic phosphine inhibits the initial coordination of carbon monoxide due to necessary elongation of the metal-phosphine bond in the transition structure. Conversely, full dissociation of a less basic phosphine in a solvent medium inhibits further rearrangements or stabilisation of a three-coordinate migration product, thereby terminating the reaction.

The migration activation energy for the neutral diimine system was shown to be significantly higher than the energies derived for the other systems. This agrees with the reported increased carbonylation rates of cationic alkyl-palladium complexes of symmetric N-N ligands compared to their neutral counterparts. The main contributors to the high activation energy are the partial negative charge on the migrating group, and increased metal-carbonyl π back-donation.

CHAPTER 9

Summary

&

Conclusions

Chapter 9

SUMMARY AND CONCLUSIONS

The body of work presented provides an understanding of the carbonylation mechanism of organopalladium(II) complexes which is unparalleled by previous theoretical studies. The levels of theory employed have been justified and surpass those generally utilised in theoretical studies of model catalyst systems, yielding physically meaningful results. Agreement between the theoretical results and experimentally reported trends is exceptional. Most importantly, we have provided evidence which supports the participation of novel five-coordinate intermediates and transition structures in these reactions. The proposed rôle of five-coordinate species has important consequences, particularly with respect to the interpretation of ligand effects in CO/olefin copolymerisation.

The relative carbonylation barriers of related cationic and neutral complexes has been shown to be dependent on the system. Cationic and neutral complexes incorporating the asymmetric N-O ligand exhibited similar reaction energetics albeit different pathways. Conversely, the activation energy of methyl migration in the neutral diimine system was significantly higher than the energy predicted for the cationic system. This is rationalised by a decrease in σ-donation from the migrating methyl group together with an increase in metal-olefin π back-donation. With the exception of the latter diimine system, the dependence of the carbonylation rate on the coordinated ligands was shown to result from the ligand substitution reactions rather than the methyl migration step.

We are now in a position to design catalyst systems exhibiting improved reaction rates, with particular emphasis on the synthesis of strictly alternating polyketones. The use of a symmetric ligand avoids the formation of stable

unproductive intermediates which hinder the reaction. In the case of the N-O ligands, the stability of isomers of the type **24'** may be reduced by increasing the lability of the donor nitrogen. This can be achieved by the addition of steric bulk in the *ortho* position of the pyridine ring of pyca. Note that substitution by electron-withdrawing substituents such as NO_2 in the *para* position of the pyridyl ring will have a two-fold effect. The σ-donation component of the Pd-N bond will decrease, while the π back-donation is enhanced. Although this will stabilise *trans*(N,CH_3) intermediates due to an increased Pd-CH_3 bond strength, the lability of the nitrogen is increased. In addition, the increased π-interaction inhibits metal-carbonyl π back-donation which subsequently increases the migration barrier.

Experimental studies have shown that the carbonylation rate of organopalladium complexes of N-N ligands is enhanced by the addition of steric bulk adjacent to the nitrogen. The theoretically predicted involvement of trigonal–bipyramidal intermediates in the reaction therefore has some interesting consequences. We can speculate that the reaction is aided by stabilisation of five-coordinate geometries. Apart from increased steric interactions, the stability of trigonal–bipyramidal structures is enhanced by π-acidic ligands. Addition of electron-withdrawing substituents on the N-N bidentate ligand may therefore facilitate carbonylation by stabilisation of five-coordinate species and reduction of the metal-carbonyl π back-donation.

The cationic diimine complexes studied experimentally generally incorporate a weakly associated ligand, such as CH_3CN, rather than PPh_3. The relatively high activation energy associated with migration from a four-coordinate diimine intermediate and inadequate stabilisation of the agostic product suggests that migration in diimine complexes including phosphine ligands may be favoured. Carbonylation rates would subsequently depend on the activation energies of pre-migration rearrangements. As previously discussed, Vrieze *et al.* recently reported a lack of carbonylation reactivity for cationic allyl-palladium complexes.

The reactivity of such complexes in the presence of quantitative amounts of PPh_3 would be of interest.

We have shown in Chapter 7 that ethylene insertion of the N-O complexes occurs from trigonal-bipyramidal intermediates in which the bidentate ligand and CO occupy equatorial positions. This leads us to postulate that insertion will be facilitated by increasing the π-accepting ability of the bidentate ligand and the *trans*-methyl ligand, and decreasing the σ-donating capacity of the bidentate ligand. Given the previous speculations that insertion from intermediates of this type is unlikely, the predictions of the current work are particularly dramatic. Consequently, we have provided an alternative explanation for the insertion rate dependence on the flexibility and bite angles of N-N and P-P bidentate ligands, based on the participation of such intermediates. The distinct activities of cationic and neutral alkyl-palladium(II) complexes of N-O ligands towards CO/ethylene copolymerisation can be attributed to the olefin insertion step. We have revealed a significant difference in calculated insertion barriers between the cationic and neutral N-O complexes, which can be rationalised by an increase in metal-ethylene π back-donation in the neutral system. This arises due to replacement of the weakly π-accepting/weak donor Pd-O bond in the cationic system by a strong covalent Pd-O bond in the neutral system.

In conclusion, the research presented here exemplifies the burgeoning scope and potential of computational techniques as an elucidative tool in the increasingly important field of organometallic chemistry. The development of more efficient algorithms creates exciting prospects for the future with respect to the design of new catalyst systems with only pivotal experimentation required.

REFERENCES

References

(1) Sen, A. *Acc. Chem. Res.* **1993**, *26*, 303.

(2) Brookhart, M.; Wagner, M. I. *J. Am. Chem. Soc.* **1994**, *116*, 3541.

(3) Jiang, Z.; Adams, S. E.; Sen, A. *Macromol.* **1994**, *27*, 2694.

(4) Bronco, S.; Consiglio, G.; Hutter, R.; Batistini, A.; Suter, V. W. *Macromol.* **1994**, *27*, 4436.

(5) Jiang, Z.; Sen, A. *J. Am. Chem. Soc.* **1995**, *117*, 4455.

(6) Forbes, M. D. E.; Ruberu, S. R.; Nachtigallova, D.; Jordan, K. D.; Barborak, J. C. *J. Am. Chem. Soc.* **1995**, *117*, 3946.

(7) Drent, E.; Arnoldy, P.; Budzelaar, P. H. M. *J. Organomet. Chem.* **1994**, *475*, 57.

(8) Jin, H.; Cavell, K. J. *J. Organomet. Chem.* **1991**, *419*, 259.

(9) Rix, F. C.; Brookhart, M. *J. Am. Chem. Soc.* **1995**, *117*, 1137.

(10) van Leeuwen, P. W. N. M.; Roobeek, C. F.; van der Heijden, H. *J. Am. Chem. Soc.* **1994**, *116*, 12117.

(11) van Asselt, R.; Gielens, E. E. C. G.; Rülke, R. E.; Vrieze, K.; Elsevier, C. J. *J. Am. Chem. Soc.* **1994**, *116*, 977.

(12) Markies, B.; Kruis, D.; Rietveld, M. H. P.; Verkerk, K. A. N.; Boersma, J.; Kooijman, H.; Lakin, M. T.; Spek, A. L.; Koten, G. V. *J. Am. Chem. Soc.* **1995**, *117*, 5263.

(13) Koga, N.; Morokuma, K. *Chem. Rev.* **1991**, *91*, 823.

(14) Anderson, G. K. In *Chemistry of the Platinum Group Metals: Recent Developments*; F. R. Hartley, Ed.; Elsevier Publishing: Amsterdam, Netherlands, 1991.

(15) Sen, A. *Chemtech* **1986**, *43*, 48 and references therein.

(16) Green, M. J.; Lucy, A. R.; Lu, S.-Y.; Paton, M. *J. Chem. Soc., Chem. Commun.* **1994**, 2603.

(17) Brubaker, M. M.; Coffman, D. D.; Hoehn, H. H. *J. Am. Chem. Soc.* **1952**, *74*, 1509.

(18) Drent, E.; van Broekhoven, J. A. M.; Doyle, M. J. *J. Organomet. Chem.* **1991**, *417*, 235.

(19) Drent, E.; Budzelaar, P. H. M. *Chem. Rev.* **1996**, *96*, 663.

(20) Brookhart, M.; Rix, F. C.; DeSimone, J. M.; Barborak, J. C. *J. Am. Chem. Soc.* **1992**, *114*, 5894.

(21) Markies, B. A.; Rietveld, M. H. P.; Boersma, J.; Spek, A. L.; van Koten, G. *J. Organomet. Chem.* **1992**, *424*, C12.

(22) Drent, E.; Eur. Pat. Appl. 121, A., 1984 *Chem. Abstr.* **1985**, *102*, 46423.

(23) Ash, C. E. *J. Mater. Educ.* **1994**, *16*, 1.

(24) Cavell, K. J. *Coord. Chem. Rev.* **1996**, *155*, 209.

(25) van Asselt, R.; Elsevier, C. J. *Organometallics* **1992**, *11*, 1999.

(26) van Asselt, R.; Gielens, E. E. C. G.; Rülke, R. E.; Elsevier, C. J. *J. Chem. Soc., Chem. Commun.* **1993**, 1203.

(27) de Graaf, W.; Boersma, J.; van Koten, G. *Organometallics* **1990**, *9*, 1479.

(28) Markies, B. A.; Wijkens, P.; Dedieu, A.; Boersma, J.; Spek, A.; Vankoten, G. *Organometallics* **1995**, *14*, 5628.

(29) Rülke, R. E.; Delis, J. G. P.; Groot, A. M.; Elsevier, C. J.; van Leeuwen, P. W. N. M.; Vrieze, K.; Goubitz, K.; Schenk, H. *J. Organomet. Chem.* **1996**, *508*, 109.

(30) Anderson, G. K.; Lumetta, G. J. *Organometallics* **1985**, *4*, 1542.

(31) Dekker, G. P. C. M.; Buijs, A.; Elsevier, C. J.; Vrieze, K.; van Leeuwen, P. W. N. M.; Smeets, W. J. J.; Spek, A. L.; Wang, Y. F.; Stam, C. H. *Organometallics* **1992**, *11*, 1937.

(32) Ozawa, F.; Hayashi, T.; Koide, H.; Yamamoto, A. *J. Chem. Soc., Chem. Commun.* **1991**, 1469.

(33) Dekker, G. P. C. M.; Elsevier, C. J.; Vrieze, K.; van Leeuwen, P. W. N. M.; Roobeek, C. F. *J. Organomet. Chem.* **1992**, *430*, 357.

(34) Dekker, G. P. C. M.; Elsevier, C. J.; Vrieze, K.; van Leeuwen, P. W. N. M. *Organometallics* **1992**, *11*, 1598.

(35) de Graaf, W.; Boersma, J.; Grove, D. M.; Spek, A. L.; van Koten, G. *Recl. Trav. Chim. Pays-Bas* **1988**, *107*, 299.

(36) Rülke, R. E.; Han, I. M.; Elsevier, C. J.; Vrieze, K.; van Leeuwen, P. W. N. M.; Roobeek, C. F.; Zoutberg, M. C.; Wang, Y. F.; Stam, C. H. *Inorg. Chim. Acta* **1990**, *169*, 5.

(37) Markies, B. A.; Wijkens, P.; Boersma, J.; Spek, A. L.; van Koten, G. *Recl. Trav. Chim. Pays-Bas* **1991**, *110*, 133.

(38) Rülke, R. E.; Kaasjager, V. E.; Kliphuis, D.; Elsevier, C. J.; van Leeuwen, P. W. N. M.; Vrieze, K. *Organometallics* **1996**, *15*, 668.

(39) Groen, J. H.; Elsevier, C. J.; Vrieze, K.; Smeets, W. J. J.; Spek, A. L. *Organometallics* **1996**, *15*, 3445.

(40) Groen, J. H.; Delis, J. G. P.; van Leeuwen, P. W. N. M.; Vrieze, K. *Organometallics* **1997**, *16*, 68.

(41) Britovsek, G. J. P.; Keim, W.; Mecking, S.; Sainz, D.; Wagner, T. *J. Chem. Soc., Chem. Commun.* **1993**, 1632.

(42) Green, M. J.; Britovsek, G. J. P.; Cavell, K. J.; Gerhards, F.; Skelton, B. W.; White, A. H. **1997**, manuscript in preparation.

(43) Britovsek, G. J. P.; Cavell, K. J.; Green, M. J.; Gerhards, F.; Skelton, B. W.; White, A. H. *J. Chem. Soc., Dalton Trans.*, **1997**, in press.

(44) Rix, F. C.; Brookhart, M.; White, P. S. *J. Am. Chem. Soc.* **1996**, *118*, 4746.

(45) Margl, P.; Ziegler, T. *J. Am. Chem. Soc.* **1996**, *118*, 7337.

(46) Svensson, M.; Matsubara, T.; Morokuma, K. *Organometallics* **1996**, *15*, 5568.

(47) Brumbaugh, J. S.; Whittle, R. R.; Parvez, M.; Sen, A. *Organometallics* **1990**, *9*, 1735.

(48) Green, M. J.; Britovsek, G. J. P.; Cavell, K. J.; Skelton, B. W.; White, A. H. *J. Chem. Soc., Chem. Commun.* **1996**, 1563.

(49) Margl, P.; Ziegler, T. *Organometallics* **1996**, *15*, 5519.

(50) Garrou, P. E.; Heck, R. F. *J. Am. Chem. Soc.* **1976**, *98*, 4115.

(51) Anderson, G. K.; Cross, R. J. *Acc. Chem. Res.* **1984**, *17*, 67.

(52) Johnson, L. K.; Killian, C. M.; Brookhart, M. *J. Am. Chem. Soc.* **1995**, *117*, 6414.

(53) Tóth, I.; Elsevier, C. J. *J. Chem. Soc., Chem. Commun.* **1993**, 529.

(54) van Leeuwen, P. W. N. M.; Roobeek, C. S. *Rec. Trav. Chim. Pays-Bas* **1995**, *114*, 73.

(55) Koga, N.; Morokuma, K. In *Theoretical Aspects of Homogeneous Catalysis: Applications of ab initio Molecular Orbital Theory*; P. W. N. M. van Leeuwan, K. Morokuma and J. H. van Lenthe, Eds.; Kluwer Academic Publishers: Netherlands, 1995; pp 93-113.

(56) Koga, N.; Morokuma, K. *J. Am. Chem. Soc.* **1985**, *107*, 7230.

(57) Coffield, T. H.; Kozikowski, J.; Closson, R. D. *J. Org. Chem.* **1957**, *22*, 598.

(58) Anderson, G. K.; Cross, R. J. *J. Chem. Soc., Dalton Trans.* **1979**, 1246.

(59) Cross, R. J.; Gemmill, J. *J. Chem. Soc., Dalton Trans.* **1981**, 2317.

(60) Jin, H.; Cavell, K. J. *J. Chem. Soc., Dalton Trans.* **1994**, 415.

(61) Jin, H.; Cavell, K. J.; Skelton, B. W.; White, A. H. *J. Chem. Soc., Dalton Trans.* **1995**, 2159.

(62) Hoare, J. L.; Cavell, K. J.; Hecker, R.; Skelton, B. W.; White, A. H. *J. Chem. Soc., Dalton Trans.* **1996**, 2197.

(63) van Leeuwen, P. W. N. M.; Roobeek, C. F.; Frijns, J. H. G. *Organometallics* **1990**, *9*, 1211.

(64) Sakaki, S.; Kitaura, K.; Morokuma, K.; Ohkubo, K. *J. Am. Chem. Soc.* **1983**, *105*, 2280.

(65) Koga, N.; Morokuma, K. *J. Am. Chem. Soc.* **1986**, *108*, 6136.

(66) Yamamoto, A. *J. Organomet. Chem.* **1995**, *500*, 337 and references therein.

(67) Berke, H.; Hoffmann, R. *J. Am. Chem. Soc.* **1978**, *100*, 7224.

(68) Koga, N.; Morokuma, K. *New. J. Chem.* **1991**, *15*, 749.

(69) Tchougreeff, A. L.; Gulevich, Y. V.; Misurkin, I. A.; Beletskaya, I. P. *J. Organomet. Chem.* **1993**, *455*, 261.

(70) Sen, A.; Lai, T.-W. *J. Am. Chem. Soc.* **1982**, *104*, 3520.

(71) Koga, N.; Morokuma, K. In *Theoretical Aspects of Homogeneous Catalysis: Applications of ab initio Molecular Orbital Theory*; P. W. N. M. van Leeuwan, K. Morokuma and J. H. van Lenthe, Eds.; Kluwer Academic Publisher: Netherlands, 1995; pp 65-93.

(72) Thorn, D. L.; Hoffmann, R. *J. Am. Chem. Soc.* **1978**, *100*, 2079.

(73) Samsel, E. G.; Norton, J. R. *J. Am. Chem. Soc.* **1984**, *106*, 5505.

(74) Koga, N.; Morokuma, K. *J. Am. Chem. Soc.* **1985**, *107*, 7109.

(75) Siegbahn, P. E. M.; Strömberg, S.; Zetterberg, K. *Organometallics* **1996**, *15*, 5542.

(76) Albano, V. G.; Natile, G.; Panunzi, A. *Coord. Chem. Rev.* **1994**, *133*, 67 and references therein.

(77) Albano, V. G.; Castellari, C.; Cucciolito, M. E.; Panunzi, A.; Vitagliano, A. *Organometallics* **1990**, *9*, 1269.

(78) Albano, V. G.; Demartin, F.; DeRenzi, A.; Morelli, G.; Saporito, A. *Inorg. Chem.* **1985**, *24*, 2032.

(79) Cucciolito, M. E.; DeFelice, V.; Panunzi, A.; Vitagliano, A. *Organometallics* **1989**, *8*, 1180.

(80) Fanizzi, F. P.; Maresca, L.; Natile, G.; Lanfranchi, M.; Tiripicchio, A.; Pacchioni, G. *J. Chem. Soc., Chem. Commun.* **1992**, 333.

(81) Rossi, A. R.; Hoffmann, R. *Inorg. Chem.* **1975**, *14*, 365.

(82) der Heyde, T. A. *Angew. Chem. Int. Ed. Engl.* **1994**, *33*, 823.

(83) Lin, Z.; Hall, M. B. *Inorg. Chem.* **1991**, *30*, 646.

(84) Muguruma, C.; Koga, N.; Kitaura, K.; Morokuma, K. *J. Chem. Phys.* **1995**, *103*, 9274.

(85) Hückel, E. *Z. Physik* **1930**, *60*, 423.

(86) Hoffmann, R. *J. Chem. Phys.* **1963**, *39*, 1397.

(87) Sandorfy, C. *Can. J. Chem.* **1955**, *33*, 1337.

(88) Fukui, K.; Kato, H.; Yonezawa, T. *Bull. Chem. Soc. Japan* **1960**, *33*, 1197.

(89) Fukui, K.; Kato, H.; Yonezawa, T. *Bull. Chem. Soc. Japan* **1960**, *33*, 1201.

(90) Kealy, T. J.; Pauson, P. L. *Nature* **1951**, *168*, 1039.

(91) Miller, S. A.; Tebboth, J. A.; Tremaine, J. F. *J. Chem. Soc.* **1952**, 632.

(92) Dewar, M. J. S. *Bull. Soc. Chim. Fr.* **1951**, *18*, C79.

(93) Chatt, J.; Duncanson, L. A. *J. Chem. Soc.* **1953**, 2939.

(94) Hoffmann, R. *Angew. Chem.* **1982**, *94*, 725.

(95) For example, ZINDO (Anderson, W. P.; Cundari, T. R.; Drago, R. S.; Zerner, M. C. *Inorg. Chem.,* 1990, 1, 29) and SINDO (Li, J.; de Mello, P. C.; Jug, K., *J. Comp. Chem.*, 1992, 13, 85).

(96) Li, J.; Schreckenbach, G.; Ziegler, T. *J. Am. Chem. Soc.* **1995**, *117*, 486.

(97) Szabo, A.; Ostlund, N. S. *Modern Quantum Chemistry;* 1 ed.; McGraw-Hill Publishing Company: USA, 1982.

(98) Durand, P.; Malrieu, J. In *Ab initio methods in Quantum Chemistry-1*; K. P. Lawley, Ed.; John Wiley and Sons Ltd.: 1987.

(99) Frenking, G.; Antes, I.; Böhme, M.; Dapprich, S.; Ehlers, A. W.; Jonas, V.; Neuhaus, A.; Otto, M.; Stegmann, R.; Veldkamp, A.; Vyboishchikov, S. F. In *Reviews in Computational Chemistry*; K. B. Lipkowitz and D. B. Boyd, Eds.; VCH Publishers, Inc.: New York, 1996; Vol. 8; pp 63-130.

(100) Cundari, T. R.; Benson, M. T.; Lutz, M. L.; Sommerer, S. O. In *Reviews in Computational Chemistry*; K. B. Lipkowitz and D. B. Boyd, Eds.; VCH Publishers, Inc.: New York, 1996; Vol. 8; pp 145-193.

(101) Jones, R. O. In *Ab initio Methods in Quantum Chemistry - Part 1*; K. P. Lawley, Ed.; Wiley, Chichester: New York, 1987.

(102) Salahub, D. R.; Zerner, M. C. *The Challenge of d and f Electrons*; ACS: Washington, D.C., 1989.

(103) Parr, R. G.; Yang, W. *Density-functional theory of atoms and molecules*; Oxford Univ. Press: Oxford, 1989.

(104) Pople, J. A.; Head-Gordon, M.; Raghavachari, K. *J. Chem. Phys.* **1987**, *87*, 5968.

(105) Bohme, M.; Frenking, G. *Chem. Phys. Lett.* **1994**, *224*, 195.

(106) Gill, P. M. W.; Radom, L. *Chem. Phys. Lett.* **1986**, *132*, 16.

(107) Neuhaus, A.; Frenking, G.; Huber, C.; Gauss, J. *Inorg. Chem.* **1992**, *13*, 5355.

(108) Marsden, C. J.; Wolynec, P. P. *Inorg. Chem.* **1991**, *30*, 1681.

(109) Davidson, E. R.; Feller, D. *Chem. Rev.* **1986**, *86*, 681.

(110) Poirier, R.; Kari, R.; Csizmadia, I. G. *Handbook of Gaussian Basis Sets*; Elsevier Science Publishers B.V.: Amsterdam, The Netherlands, 1985.

(111) The most commonly used are those developed by Pople and coworkers (Stewart, R. F. *J. Chem. Phys.*, **1969**, *50*, 2485; Hehre, W. J.; Stewart, R. F.; Pople, J. A. *J. Chem. Phys.*, **1969**, *51*, 2657; Stewart, R. F. *J. Chem. Phys.* **1970**, *52*, 431; Hehre, W. J.; Ditchfield, R.; Stewart, R. F.; Pople, J. A. *J. Chem. Phys.*, **1970**, *52*, 2769 (STO-NG for Na-Ar); Pietro, W. J.; Levi, B. A.; Hehre, W. J.; Stewart, R. F. *Inorg. Chem.*, **1980**, *19*, 2225 (STO-NG for K, Ca, Ga-Kr); Pietro, W. J.; Blurock, E. S.; Hout, R. F.; Hehre, W. J.; Defrees, D. J.; Stewart, R. F. *Inorg Chem.*, **1981**, *20*, 3650 (STO-NG for Rb, Sr, In-Xe); Pietro, W. J.; Hehre, W. J. *J. Comp. Chem.*, **1983**, *4*, 241.

(112) For example, the 3-21G (H-Ne: Binkley, J. S.; Pople, J. A.; Hehre, W. J. *J. Am. Chem. Soc.*, **1980**, *102*, 939; Na-Ar: Gordon, M. S.; Binkley, J. S.; Pople, J. A.; Pietro, W. J.; Hehre, W. J. *J. Am. Chem. Soc.*, **1982**, *104*, 2797) and 6-31G (Hehre, W. J.; Ditchfield, R.; Pople, J. A. *J. Chem. Phys.* **1972**, *56*, 2257) basis sets.

(113) Davidson, E. R.; Chakravorty, S. J. *Chem. Phys. Lett.* **1994**, *217*, 48.

(114) Jansen, H. B.; Ros, P. *Chem. Phys. Lett.* **1969**, *3*, 140.

(115) Boys, S. F.; Bernardi, F. *Mol. Phys.* **1970**, *19*, 553.

(116) Das, M. P. In *Lectures on Methods of Electronic Structure Calculations*; V. Kumar, O. K. Anderson and A. Mookerjee, Eds.; World Scientific Publishing Company Pte. Ltd.: Singapore, 1994; pp Part 1.

(117) Hohenberg, P.; Kohn, W. *Phys. Rev. B* **1964**, *136*, 864.

(118) von Barth, U. *In Lectures on Methods of Electronic Structure Calculations*; World Scientific Publishing Co. Pte. Ltd.: Singapore, 1994 and references therein.

(119) Stanton, R. V.; Merz, K. M. J. *J. Chem. Phys.* **1994**, *100*, 434.

(120) Langreth, D. C.; Perdew, J. P. *Phys. Rev. B* **1980**, *21*, 5469.

(121) Langreth, D. C.; Mehl, M. J. *Phys Rev. B* **1983**, *29*, 2310.

(122) Perdew, J. P. *Phys. Rev. B* **1981**, *33*, 8822.

(123) Perdew, J. P.; Wang, Y. *Phys. Rev. B* **1992**, *45*, 13244.

(124) Becke, A. D. *Int. J. Quantum Chem.* **1983**, *23*, 1915.

(125) Becke, A. D. *Phys. Rev. A* **1986**, *33*, 2786.

(126) Becke, A. D. *Phys. Rev. A* **1988**, *38*, 3098.

(127) Lee, C.; Yang, W.; Parr, R. G. *Phys. Rev. B* **1988**, *37*, 785.

(128) Becke, A. D. *J. Chem. Phys.* **1993**, *98*, 1372.

(129) Pople, J. A.; Head-Gordon, M.; Fox, D. J.; Raghavachari, K.; Curtiss, L. A. *J. Chem. Phys.* **1989**, *90*, 5622.

(130) Curtiss, L. A.; Jones, C.; Trucks, G. W.; Raghavachari, K.; Pople, J. A. *J. Chem. Phys.* **1990**, *93*, 2537.

(131) Ziegler, T. *Chem. Rev.* **1991**, *91*, 651.

(132) Johnson, B. G.; Gill, P. M.; Pople, J. A. *J. Chem. Phys.* **1993**, *98*, 5612.

(133) Andzelm, J.; Wimmer, E. *J. Chem. Phys.* **1992**, *96*, 1280.

(134) Delley, B.; Wrinn, M.; Lüthi, H. P. *J. Chem. Phys.* **1994**, *100*, 5785.

(135) Smith, B. J.; Radom, L. *Chem. Phys. Lett.* **1994**, *231*, 345.

(136) Csonka, G. I.; Sztraka, L. *Chem. Phys. Lett.* **1995**, *233*, 611.

(137) Curtiss, L. A.; Raghavachari, K.; Trucks, G. W.; Pople, J. A. *J. Chem. Phys.* **1991**, *94*, 7221.

(138) Sosa, C.; Andzelm, J.; Elkin, B. C.; Wimmer, E.; Dobbs, K. D.; Dixon, D. A. *J. Phys. Chem.* **1992**, *96*, 6630.

(139) Barone, V.; Adamo, C.; Mele, F. *Chem. Phys. Lett.* **1996**, *249*, 290.

(140) Barone, V.; Adamo, C. *J. Phys. Chem.* **1996**, *100*, 2094.

(141) Jursic, B. S. *Int. J. Quantum Chem.* **1997**, *61*, 93.

(142) Nguyen, M. T.; Creve, S.; Vanquickenborne, L. G. *J. Phys. Chem.* **1996**, *100*, 18422.

(143) Stevens, W. J.; Krauss, M.; Basch, H.; Jasien, P. G. *Can. J. Chem.* **1992**, *70*, 612.

(144) Balasubramanian, K.; Pitzer, K. S. In *Ab Initio Methods in Quantum Chemistry - I*; K. P. Lawley, Ed.; John Wiley and Sons Ltd.: 1987; pp 287-319 and references therein.

(145) Almlöf, J.; Gropen, O. In *Reviews in Computational Chemistry*; K. B. Lipkowitz and D. B. Boyd, Eds.; VCH Publishers, Inc.: New York, 1996; Vol. 8; pp 203-240 and references therein.

(146) Hay, P. J.; Wadt, W. R. *J. Chem. Phys.* **1985**, *82*, 270.

(147) Wadt, W. R.; Hay, P. J. *J. Chem. Phys.* **1985**, *82*, 284.

(148) Hay, P. J.; Wadt, W. R. *J. Chem. Phys.* **1985**, *82*, 299.

(149) Dolg, M.; Wedig, U.; Stoll, H.; Preuß, H. *J. Chem. Phys.* **1987**, *86*, 866.

(150) Andrae, D.; Häußermann, U.; Dolg, M.; Stoll, H.; Preuß, H. *Theor. Chim. Acta* **1990**, *77*, 123.

(151) van Wüllen, C. *Int. J. Quantum Chem.* **1996**, *58*, 147.

(152) Baker, J.; Hehre, W. J. *J. Comp. Chem.* **1991**, *12*, 606.

(153) Schlegel, H. B. *Int. J. Quant. Chem. Symp.* **1992**, *26*, 243.

(154) Pulay, P.; Fogarasi, G.; Pang, F.; Boggs, J. E. *J. Am. Chem. Soc.* **1979**, *101*, 2550.

(155) Pulay, P.; Fogarasi, G. *J. Chem. Phys.* **1992**, *96*, 2856.

(156) Fogarasi, G.; Zhou, X.; Taylor, P.; Pulay, P. *J. Am. Chem. Soc.* **1992**, *114*, 8191.

(157) Baker, J. *J. Comp. Chem.* **1993**, *14*, 1085.

(158) Frisch, M. J.; Trucks, G. W.; Schlegel, H. B.; Gill, P. M. W.; Johnson, B. G.; Robb, M. A.; Cheeseman, J. R.; Keith, T.; Petersson, G. A.; Montgomery, J. A.; Raghavachari, K.; Al-Laham, M. A.; Zakrzewski, V. G.; Ortiz, J. V.; Foresman, J. B.; Peng, C. Y.; Ayala, P. Y.; Chen, W.; Wong, M. W.; Andres, J. L.; Replogle, E. S.; Gomperts, R.; Martin, R. L.; Fox, D. J.; Binkley, J. S.; Defrees, D. J.; Baker, J.; Stewart, J. P.; Head-Gordon, M.; Gonzalez, C.; Pople, J. A., GAUSSIAN 94, Gaussian, Inc., Pittsburgh, PA 1995

(159) Frisch, M. J.; Trucks, G. W.; Head-Gordon, M.; Gill, P. M. W.; Wong, M. W.; Foresman, J. B.; Johnson, B. G.; Schlegel, H. B.; Robb, M. A.; Replogle, E. S.; Gomperts, R.; Andres, J. L.; Raghavachari, K.; Binkley, J. S.; Gonzalez, C.; Martin, R. L.; Fox, D. J.; Defrees, D. J.; Baker, J.; Stewart, J. J. P.; Pople, J. A., GAUSSIAN 92, Gaussian, Inc. 1992

(160) Baker, J. *J. Comp. Chem.* **1986**, *7*, 385.

(161) Baker, J. *J. Comp. Chem* **1987**, *8*, 563.

(162) Slater, J. C. *Quantum Theory of Molecules and Solids, Vol. 4: The Self-Consistent Field for Molecules and Solids* McGraw-Hill: New York, **1974**.

(163) Vosko, S. H.; Wilk, L.; Nusair, M. *Can. J. Phys.* **1980**, *58*, 1200.

(164) Analytic second derivatives for pseudopotentials are, however, available in some comercial packages, such as GRADSCF

(165) Foster, J. P.; Weinhold, F. *J. Am. Chem. Soc.* **1980**, *102*, 7211.

(166) Reed, A. E.; Curtiss, L. A.; Weinhold, F. *Chem. Rev.* **1988**, *88*, 899.

(167) Reed, A. E.; Weinhold, F. *J. Chem. Phys.* **1983**, *78*, 4066.

(168) Reed, A. E.; Weinstock, R. B.; Weinhold, F. *J. Chem. Phys.* **1985**, *83*, 735.

(169) Glendening, E. D.; Reed, A. E.; Carpenter, J. E.; Weinhold, F. *NBO 3.0 Program Manual*.

(170) Langhoff, S. R.; Petterson, L. G.; Bauschlicher, J., C. W.; Partridge, H. J. *J. Chem. Phys.* **1987**, *86*, 268.

(171) Pacchioni, G.; Koutecky, J.; Fantucci, P. *Chem. Phys. Lett.* **1982**, *92*, 486.

(172) Pacchioni, G.; Bagus, P. S. *Inorg. Chem.* **1992**, *31*, 4391.

(173) Rohlfing, C. M.; Hay, P. J. *J. Chem. Phys.* **1985**, *83*, 4641.

(174) Dedieu, A.; Sakaki, S.; Strich, A.; Siegbahn, P. E. M. *Chem. Phys. Lett.* **1987**, *133*, 317.

(175) Maseras, F.; Lledós, A.; Duran, M.; Bertrán, J. *J. Chem. Soc., Faraday Trans.* **1992**, *88*, 1111.

(176) Ehlers, A.; Frenking, G. *J. Am. Chem. Soc.* **1994**, *116*, 1514.

(177) Frankcombe, K. E.; Cavell, K. J.; Yates, B. F.; Knott, R. B. *J. Phys. Chem.* **1996**, *100*,18363.

(178) Blomberg, M. R. A.; Lebrilla, C. B.; Siegbahn, P. E. M. *Chem. Phys. Lett.* **1988**, *150*, 522.

(179) Koutecky, J.; Pacchioni, G.; Fantucci, P. *Chem. Phys.* **1985**, *99*, 87.

(180) Pacchioni, G.; Koutecky, J. *J. Phys. Chem.* **1987**, *91*, 2658.

(181) Schwerdtfeger, P.; McFeaters, J. S.; Moore, J. J.; McPherson, D. M.; Cooney, R. P.; Bowmaker, G. A.; Dolg, M.; Andrae, D. *Langmuir* **1991**, *7*, 116.

(182) Ehlers, A. W.; Böhme, M.; Dapprich, S.; Gobbi, A.; Höllwarth, A.; Jonas, V.; Köhler, K. F.; Stegmann, R.; Veldkamp, A.; Frenking, G. *Chem. Phys. Lett.* **1993**, *208*, 111.

(183) Schäfer, A.; Horn, H.; Ahlrichs, R. *J. Chem. Phys.* **1992**, *97*, 2571.

(184) Refer to Section 2.4 for a discussion of BSSE. For the present system, too many basis functions of the ligands with respect to the metal results in a contraction of the metal-ligand bond lengths as the metal uses the ligand valence orbitals to lower the energy of the metal valence electrons (as illustrated by basis sets 26 and 27). In particular, for the present system, the augmentation of basis set 24 with a set of polarisation functions on the main group elements favours the formation of the Pd-CO bond with respect to the Pd-PH_3 bond, due to the nature of the metal-carbonyl bond. The metal can employ the polarisation functions of both the carbon and the oxygen to lower the energy of the metal valence electrons.

(185) Jonas, V.; Frenking, G.; Reetz, M. T. *J. Comput. Chem.*, **1992**, *13*, 919.

(186) Curtiss, L. A.; Raghavachari, K.; Pople, J. A. *J. Chem. Phys.* **1993**, *98*, 1293.

(187) Frankcombe, K. E.; Cavell, K. J.; Yates, B. F.; Knott, R. B. *J. Phys. Chem.* **1995**, *99*, 14316.

(188) Häberlen, O. D.; Rösch, N. *J. Phys. Chem.* **1993**, *97*, 4970.

(189) Sargent, A. L.; Hall, M. B. *Inorg. Chem.* **1992**, *31*, 317.

(190) Hambley, T. W.; Frankcombe, K. E.; Yates, B. F.; Cavell, K. J.; Knott, R. B. to be published.

(191) Pietro, W. J.; Francl, M. M.; Hehre, W. J.; Defrees, D. J.; Pople, J. A.; Binkley, J. S. *J. Am. Chem. Soc.* **1982**, *104*, 5039.

(192) Desmarais, N.; Adamo, C.; Panunzi, B.; Barone, V.; Giovannitti, B. *Inorg. Chim. Acta* **1995**, *238*, 159.

(193) Geometry optimisation at MP2/LANL2:6-31G(d) restricting the carbonyl group to adopt a linear association to the metal generated an intermediate with an energy of -1.1 kJ/mol relative to **1** + CO. The BSSE associated with this structure (4.5 kJ/mol) are reduced in comparison to the BSSE associated with **1'** (9.2 kJ/mol), however the energy of the BSSE-corrected linear structure remains higher than **1'** by 3.6 kJ/mol.

(194) Abu-Hasanayn, F.; Krogh-Jespersen, K.; Goldman, A. S. *J. Am. Chem. Soc.* **1994**, *116*, 5979.

(195) Blomberg, M. A.; Karlsson, C. A. M.; Siegbahn, P. E. M. *J. Phys. Chem.* **1993**, *97*, 9341.

(196) Frankcombe, K. E.; Cavell, K. J.; Knott, R. B.; Yates, B. F. *J. Chem. Soc., Chem. Commun.* **1996**, 781.

(197) Frankcombe, K. E.; Cavell, K. J.; Knott, R. B.; Yates, B. F. *Organometallics*, **1997**, in press.

(198) Jordan, R. F. *Adv. Organomet. Chem.* **1991**, *32*, 325.

(199) Marks, T. J. *Acc. Chem. Res.* **1992**, *25*, 57.

(200) Möhring, P. C.; Coville, N. J. *J. Organomet. Chem.* **1994**, *479*, 1.

(201) Cotton, F. A. *Inorg. Chem.* **1964**, *3*, 702.

(202) Horrocks, W. D., Jr.; Taylor, R. C. *Inorg. Chem.* **1963**, *2*, 723.

(203) Maseras, F.; Morokuma, K. *Chem. Phys. Lett.* **1992**, *195*, 500.

(204) Britovsek, G. J. P. **1996**, personal communication.

(205) Rülke, R. E.; Kliphuis, D.; Elsevier, C. J.; Fraanje, J.; Goubitz, K.; van Leeuwen, P. W. N. M.; Vrieze, K. *J. Chem. Soc., Chem. Commun.* **1994**, 1817.

(206) An effect which cannot be illustrated by NBO analyses unless the unoccupied 5p orbitals are defined as valence, rather than Rydberg orbitals (Maseras, F.; Morokuma, K. *Chem. Phys. Lett.* **1992**, *195*, 500).